Doctoral Dissertation

Study on the self-growing materials in response to mechanical stimuli using double-network system

（ダブルネットワークシステムを用いた

力学応答自己成長材料に関する研究）

Takahiro Matsuda

Laboratory of Soft and Wet Matter

Graduate School of Life Science, Hokkaido University, Japan

December 2019

Content

Content i

List of important abbreviations vii

List of important symbols viii

Chapter 1: General Introduction 1

Chapter 2: Background 4

2.1. Mechanoresponsive living tissues 4

2.2. Polymer mechanochemistry for mechanoresponsive materials 5

2.2.1. Mechanoradicals 6

2.2.2. Mechanochemistry using mechanophores. 7

2.2.3. Mechanochemistry for self-strengthening or related objectives 8

2.3. Core issues on the self-growing materials and the strategy of this work 9

References 11

Figures 20

Chapter 3: Synthesis and Characterization of DN Gels 22

3.1. Introduction 22

3.2. Experiment 23

3.2.1. Materials 23

3.2.2. Synthesis of PNaAMPS SN hydrogels 23

3.2.3. Synthesis of PAAm SN gels 24

3.2.4. Synthesis of PNaAMPS/PAAm DN hydrogels 24

3.2.5. Characterization of the weight fraction of each component in gels 25

3.2.6. Uniaxial tensile test 26

3.3. Results and Discussion 26

3.3.1. Weight fraction of each component in gels 26

3.3.2. Mechanical properties characterized by uniaxial tensile test 27

3.4. Summary 27

References 28

Figures and Tables 29

Chapter 4: Quantification of Polymer Strand Scission in DN Gels 34

4.1. Introduction 34

4.2. Experiments 36

4.2.1. Materials 36

4.2.2. Visualization of oxidized ferrous ions in stretched gels (visual demonstration) 37

4.2.3. Quantification of oxidized ferrous ions in stretched gels 37

4.2.4. Calibration procedure for the quantification of Fe^{3+} concentration 38

4.2.5. Quantification of radicals generated by small-molecular radical initiators from the oxidation of Fe^{2+} 39

4.2.6. Cyclic uniaxial tensile test 40

4.3. Results and Discussion 41

4.3.1. Visualization of internal fracturing in stretched DN gels 41

4.3.2. Kinetics of the color change of Fenton reaction 42

4.3.3. Concentration of the ferrous oxidation in various stretched DN and SN gels

..... 44

4.3.4. Concentration of the mechanoradicals 46

4.3.5. Quantitative comparison of the chemical evidence to previous mechanical evidence of the internal fracturing..... 48

4.4. Conclusion..... 53

References 54

Figures and Tables 58

Chapter 5: Mechanoradical Polymerization in DN gels 81

5.1. Introduction 81

5.2. Experiments..... 81

5.2.1. Materials..... 81

5.2.2. Mechanoradical polymerization of AMPS in a DN gel..... 82

5.2.3. Characterization of monomer conversion by near-infrared light absorption spectroscopy 83

5.2.4. Spatially controlled mechanoradical polymerization 83

5.3. Results and Discussion..... 84

5.3.1. Mechanoradical polymerization of AMPS in DN gels..... 84

5.3.2. Spatially controlled mechanoradical polymerization 87

5.4. Conclusion..... 89

References 90

Figures and Table..... 93

Chapter 6: Self-Strengthening/Growing DN Gels 99

6.1. Introduction 99

6.2. Experiments 100
6.2.1. Materials 100
6.2.2. Mechanoradical network-polymerization in DN gel using MBAA crosslinker (preliminary experiment) 100
6.2.3. Self-strengthening of DN gel using TADETA crosslinker characterized by stress−strain behavior 101
6.2.4. Characterization of polymer weight fraction 103
6.2.5. Characterization of the kinetics of the self-strengthening 103
6.2.6. Self-stiffening of DN gel using TADETA crosslinker 104
6.2.7. Self-growing of DN gel 105
6.3. Results and Discussion 106
6.3.1. Mechanoradical network-polymerization in DN gel using MBAA crosslinker (preliminary experiment) 106
6.3.2. Self-strengthening of DN gel using TADETA crosslinker 110
6.3.3. Kinetics of mechanoradical network-polymerization 112
6.3.4. Self-stiffening of the DN gels by the mechanoradical polymerization 114
6.3.5. Self-growing of the DN gels through repetitive stretching 115
6.3.6. Demonstration of the self-growing DN gel 119
6.4. Conclusion 120
References 121
Figures and Table 125

Chapter 7: Fabrication of Hybrid Double-Network Elastomers 145
7.1. Introduction 145

7.2. Experiments 147
7.2.1. Materials 147
7.2.2. Measurement of dielectric constant of solvent and solution 148
7.2.3. Synthesis of polyelectrolyte gels for the first network 148
7.2.4. Measurement of swelling ratio of PNaAMPS gel in various solvent 149
7.2.5. Measurement of elastic shear modulus μ of (1-3) PNaAMPS gel swollen with solutions 150
7.2.6. Synthesis of PEA organogels and elastomers 150
7.2.7. Fabrication of DN elastomers 151
7.2.8. Characterization of volume fraction of each component 152
7.2.9. Uniaxial tensile test and the cyclic test 153
7.2.10. Fracture test with single-edge notched geometry 154
7.2.11. Fracture test with trouser shaped geometry 155
7.3. Results and Discussion 156
7.3.1. Swelling behavior of a PNaAMPS network in pure organic solvents 156
7.3.2. Miscibility of high dielectric solvent with a monomer for the second network 158
7.3.3. Swelling behavior of a PNaAMPS network in EA/NMF binary mixture .. 158
7.3.4. Effect of salt on swelling, and elastic modulus of the swollen gels 160
7.3.5. Compatibility of PEA with NMF 162
7.3.6. Synthesis and characterization of a PNaAMPS/PEA DN organogel 163
7.3.7. Fabrication and uniaxial tensile test of a PNaAMPS/PEA DN elastomer.. 164
7.3.8. Cyclic tensile test of a PNaAMPS/PEA DN elastomer to confirm internal fracturing 166

7.3.9. Toughness (crack resistance) of a PNaAMPS/PEA DN elastomer 167

7.3.10. Mechanical properties of PNaAMPS/PEA DN elastomers with various formulations under uniaxial tensile test 169

7.3.11. Fracture energy of PNaAMPS/PEA DN elastomers with various formulations 172

7.3.12. DN elastomers with various polymer combinations 173

7.4. Conclusion 175

References 176

Figures and Tables 181

Chapter 8: General Conclusion and Outlook 210

List of Publications 213

Original papers related to doctoral dissertation 213

Other original papers 213

Other written works 214

Presentations in conferences related to doctoral dissertation 215

Presentations in conferences (others) 218

Presentations in conferences related to doctoral dissertation (presented by co-authors) 219

Presentations in conferences (other reports contributed as a co-author) 220

Acknowledgement 221

List of important abbreviations

4EGDA	Tetraethylene glycol diacrylate
AIBN	2,2'-Azobis(isobutyronitrile)
DN	Double-network
(FT-)NIR	(Fourier transform) near infrared
MBAA	*N*,*N'*-Methylenebisacrylamide (crosslinker)
NMF	*N*-Methylformamide
(P)AAm	(Poly) acrylamide
(P)AMPS	(Poly) 2-acrylamido-2-methylpropane sulfonic acid
(P)EA	(Poly) ethyl acrylate
(P)NaAMPS	(Poly) 2-acrylamido-2-methylpropane sulfonic acid sodium salt
(P)NIPAAm	(Poly) *N*-isopropylacrylamide
QN	Quadruplet-network
SN	Single-network
TADETA	*N*,*N'*,*N''*-Triacryloyl diethylenetriamine (crosslinker)
TN	Triple-network
UV	Ultraviolet
Vis	Visible (light)
XO	Xylenol orange

List of important symbols

A	Absorbance
C	Molar concentration
- C_1	- Feed monomer concentration for the first network
- C_2	- Feed monomer concentration for the second network
- C_m	- Feed monomer concentration for mechanoradical polymerization
- C_x	- Feed crosslinker concentration for mechanoradical polymerization
c_0	Initial notch length
D_b	Bond dissociation energy
E	Young's modulus
F	Force, load
f	Weight fraction
- f_1	- Weight fraction of the first network
- f_2	- Weight fraction of the second network
- f_{EA}	- Weight fraction of feed EA monomer for the second network
- f_c	- Weight fraction of feed crosslinker (for the second network)
- f_i	- Weight fraction of feed initiator (for the second network)
G_c	Fracture energy characterized by single-edge notched geometry
k_B	Boltzmann constant
L	Sample gauge length
M	Molar mass
N_b	(Average) number of covalent bonds in the backbone of a polymer strand
N_m	(Average) polymerization degree of a network strand ($N_m = 2N_b$ when vinyl monomer is used.)
R	(Average) end-to-end distance of a strand

[R·]	Radical concentration
T	Absolute temperature
T_c	Fracture energy characterized by trouser-shaped tearing test
t	Thickness
U_{hys}	Mechanical hysteresis area on cyclic tensile test
U_{total}	Energy theoretically required for the fracture of all the first network chains within a unit volume
U_b	Mechanical energy required to break one covalent bond
V	Volume
- V/V_0	- Volumetric swelling ratio
W	Input mechanical energy density (or, Strain energy density)
- W_b	Input mechanical energy density until the material breakage
- W_c	Strain energy density at critical point on fracture test
W_{strand}	Average (strain) energy per strand
w	Weight
x	Feed crosslinker molar ratio with respect to the monomer (mol%)
- x_1	- x of the first network at preparation
- x_2	- x of the second network at preparation
ε	Nominal strain
ε_r	Dielectric constant
λ	Elongation ratio
- λ_y	- Elongation ratio at yield
- λ_b	- Elongation ratio at break
μ	Shear modulus
ν	Number density of polymer strands of network in unit volume

ρ	Specific density
σ	Nominal stress
- σ_y	- Nominal stress at yield
- σ_b	- Nominal stress at break
σ_T	True stress
Φ_c	Fraction of the broken strands obtained by the chemical ferrous oxidation
Φ_b	Fraction of the broken strands obtained from the mechanical hysteresis
ϕ	Volume fraction
- ϕ_{1st}	- Volume fraction of the first network
- ϕ_{2nd}	- Volume fraction of the second network

Chapter 1: General Introduction

Biological tissues are open and dynamic systems that alter their properties to grow and adapt to surrounding environments. Some load-bearing tissues have an ability to upgrade (or sometimes positively reduce) their size and properties to adapt to the mechanical environment. If you work out in a gym, your skeletal muscles may get strength with increase of size. Bones also change their strength, density and structure under the mechanical stressing to optimize the overall mechanical property to support the applied load. Such mechano-adaptive growing, i.e. enhancement of mechanical properties induced by mechanical stress, is intriguing character of the biological materials in our body. On the contrary, man-made materials are usually static materials without changing their property under their environment that may change from moment to moment. When gigantic or repetitive mechanical stress is applied to typical synthetic materials, their mechanical properties deteriorate, and the materials finally get broken or become no longer usable. To extend the working lifetime of materials, strengthening and toughening to make the materials endurable to larger force and tolerant to crack are the typical approaches for the structural materials. In recent tens years, self-healing materials have been intensely pursued to extend the working lifetime of materials. On the self-healing materials, the goal is to recover to the original state after being damaged. These strategies —strengthening, toughening and self-healing— are no doubt crucially important in the materials science for our daily lives to be safety and happily; however, these strategies are namely *passive* approaches for the materials to fight against mechanical force. Can we create materials, in analogous to muscles and bones, that *positively* use the mechanical force to alter their properties with the time? How such materials will change our life?

This research devotes to find such new class “mechano-responsive” material. I have investigated to create the materials that increase their size and mechanical properties such as strength, using mechanical stress applied to the materials’ body. Considering living tissues grow step by step with a time in the life, the growing properties in a repetitive way will put broader values both for the scientific and engineering fields. In this work, I call the new stuff as “self-growing materials” because the term “grow” essentially includes the repetitive enhancement with the time. Considering the inspiration from the muscles and bones, I focused on the growth of size and mechanical performances in response to a repetitive mechanical stressing; even though the “growing” is not limited in the mechanical features but also includes other various activation ways (temperature, electromagnetic waves, magnetic force, electric potential, sound waves, …) and various properties changes (shape, color, intelligence, …).

As described above, the main goal of this dissertation is to create a self-growing material that repetitively increases strength and size in response to repetitive mechanical stressing. This dissertation comprises eight chapters including this general introduction as **Chapter 1**.

In **Chapter 2**, the background of this research is summarized especially from the aspects of scientific research including recent progresses. At first, the previous researches on the mechanoresponsive materials or molecular mechanisms related to self-growing materials is overviewed. Considering the research history, the fundamental issues that block achieving the creation of self-growing material are extracted. To overcome the issues, I employed a double-network (DN) gels in this research. The major strategic hypothesis here is: “A lot of mechanoradicals are generated in a stressed DN gel owing

to the internal fracturing. The mechanoradicals can induce radical polymerization in the DN gels, which can increase the strength and size of the materials."

In **Chapter 3**, before describing the main result and discussion on the self-growing DN gels, synthetic procedure and fundamental properties of these DN gels used in this research are summarized.

In **Chapter 4**, plenty of mechanoradical generation in stressed DN gels is confirmed. By using ferrous ion oxidation triggered by radicals in an aqueous media, mechanoradical generation in the DN gels are investigated systematically and quantitatively. In **Chapter 5**, radical polymerization in the stressed DN gels initiated by the mechanoradicals is described. Efficient mechanoradical polymerization is found in the stressed DN gels. In **Chapter 6**, by using the efficient polymerization in the DN gels, self-growing DN gel is demonstrated. First, one-shot self-strengthening owing to the mechanoradical network-polymerization is systematically investigated. Afterwards, such self-strengthening effect is improved from one-shot event to repetitive way, to achieve the self-growing phenomenon. Repetitive size increase is also demonstrated. In consequence, the self-growing material is successfully developed.

The self-growing strategy essentially roots in the unique internal fracturing nature of the DN gel which generates abundant mechanoradicals. Looking ahead the widespread future applicability of the discovered growing system, not only a hydrogel but also other various materials to exhibit internal fracturing are required. Hence, in **Chapter 7**, strategy to fabricate solvent-free DN elastomers with intrinsic internal fracturing nature is reported.

Finally, in **Chapter 8**, the conclusion and contributions of this research are summarized along with outlooks.

Chapter 2: Background

2.1. Mechanoresponsive living tissues

As described in **Chapter 1**, some biological tissues have a function to change their properties in response to mechanical force. Most famous example is skeletal muscles. When the muscles experience mechanical stress through daily life or active physical training, the power of the muscles become bigger along with the hypertrophy, i.e., size increase of the muscles through a growth in size of its component cells.[1] The muscle strengthening is often called as muscle adaptation because the muscle adapts to the applied load. The muscle growth effect depends on the training type such as training volume, intensity and frequency.[2,3] In molecular biological point of view, such muscle growth is initiated by potential primary messengers, such as mechanical stretch, calcium flux, redox state, phosphorylation state and/or others, followed by multiple signaling transductions, and finally new proteins are formed from a series of generated amino acids.[1,2]

Bones are one of the most intensely investigated tissues that remodel in response to mechanical stress. The bone remodeling is often referred to as “Wolff’s law”, which roots in the term “over time, the mechanical load applied to living bone influences the structure of bone tissue” by Julius Wolff, a German anatomist and surgeon in 19th Century.[4] Nowadays, the bone remodeling effect has been experimentally confirmed and detail mechanisms are getting unveiled gradually.[5–9] For example, it has been proposed that, mechanosensory osteocyte could detect the stimuli such as bone deformation, load-induced flow of canalicular fluid and/or electrical streaming potentials.[8]

As well as the muscles and bones, other various biological tissues sense the mechanical stress: skin feels “pain”; vascular responds to blood shear flow;[10] tumor

growth can be inhibited by mechanical stress;[11] tissue feels and responds stiffness of substrate *in vitro*,[12] and so on. Some possible mechanosensing molecular mechanisms, such as membrane protein that opens Ca^{2+} channel responding to force,[13] have also been investigated.

As shown above, various mechanoresponsive phenomena and inherent possible mechanisms are widely investigated on the living tissues; however, truly-important mechanoreceptor(s), mechanotransduction pathway and overall mechanisms are still big open questions on this research field.[14] Anyway, the transduction process from mechanical stress through biological signals to biological functionalization is considered to be complicated process.[14] Therefore, direct mimic of the biological phenomena for application for the synthetic materials would be difficult.

2.2. Polymer mechanochemistry for mechanoresponsive materials

To change the materials' properties, a direct way is inducing chemical reaction in the materials. A research field for inducing/activating chemical reaction by mechanical force/stress/energy is called as "mechanochemistry". It has known that mechanical energy can activate chemical potential, which induces chemical reaction for organic synthesis, inorganic synthesis, ceramics phase transition and polymer reaction. There are various ways to apply mechanical energy to the molecule: Stretch, compression, grinding, milling, rubbing, fracturing of solid materials; ultrasound irradiation (sonication), mastication, vigorous stirring, elongational shear flow of the liquid materials and solutions, and so on.[15–20] One effective way to transmit the bulk mechanical force to the molecular level is using polymers due to the easiness in transferring the external mechanical force to the molecular chains.[20,21] Hence, polymer mechanochemistry get increasing attention

recently. The historical overview, current progress and issues of the polymer mechanochemistry are summarized below.

2.2.1. Mechanoradicals

The history of polymer mechanochemistry dates back to more than half century ago. In 1930s, several researchers including Staudinger found that polymer chain can break during the sonication of polymer solution or mastication of rubbery polymer.[22,23] Melville and Murray considered that when a polymer chain that are jointed with C−C covalent bonds is broken, radical species, now called as *mechanoradicals*, would be generated at the ends of the broken polymer (**Figure 2-1**). They found that the mechanoradical might be generated in the sonicated polymer solution from several weak evidences.[24] Afterwards, such mechanoradical was successfully confirmed by such as mechanoradical-initiated radical polymerization.[25,26] Since the polymerization starts from the broken end of the polymer, block copolymer was synthesized using the mechanoradical polymerization. The bond breaking-initiated radical polymerization has been also used to form graft polymer on the broken surface of a solid polymer.[27] Around 1960−1970s, mechanoradical generation by polymer chain fracture was clearly confirmed by using electron paramagnetic resonance (EPR or ESR).[28] Because EPR detects unpaired electrons (including radicals) that usually do not exist in normal polymers and organic molecules, EPR is the powerful technique to detect and quantify the mechanoradicals. Sohma et al. have systematically worked on the polymer mechanoradicals using various tools such as ball milling, sonication, strong stirring and radical trapping method, combined with ESR technique.[28] Most recently, Baytekin et al. found that mechanoradicals can react with water to generate hydrogen peroxide to induce subsequent chemical reactions,[29] and can

induce deposition of metal nanoparticles from metal salts in a solution.[30] As shown above, there are abundant historical knowledges and techniques on the mechanoradicals and some recent fascinating researches; however, the number of current researches on the mechanoradicals is quite few. This may be because progressed techniques of controlled polymerization are better way than breaking-induced mechanoradical copolymerization to synthesize block copolymer or grafting polymer, and human interests on the mechanochemistry have shifted to designed mechanophores described in **section 2.2.2**.[21]

2.2.2. Mechanochemistry using mechanophores.

Mechanochemistry is getting much attention in these 10–20 years. Specifically, the concept of *mechanophore* that change their structure against mechanical stimuli opens the wide possibilities of the mechanochemical reactions. Various mechanophores have been designed and incorporated to polymers to realize various functions such as force-responsive color change,[31,32] luminescence,[33] biasing reaction pathway,[34] isomerization[35], catalyst,[36,37] small molecule release[38] and cross-linking.[39,40] To activate the mechanophore in polymer, sonication of a polymer solution is widely used because effective force transmittance is typically observed. Such mechanophores are also incorporated in polymer materials to realize the new functional materials that response to mechanical force. Recently, mechanophore to change color or emit photon/fluorescence such as spiropyran, dioxetane and Diels–Alder adducts of π-extended anthracene are used for not only demonstrating the mechanochromic property but also analyzing the materials' mechanics and fracture behavior.[41–46]

2.2.3. Mechanochemistry for self-strengthening or related objectives

Most recently, mechanophores for the self-strengthening of the materials, which relate to the objective of my work, have been also reported. The first report for the mechanophore-based self-strengthening is a force-induced crosslinking reaction using *gem*-dibromocyclopropanes (*g*DBCs) (**Figure 2-2a**).[39] When the *g*DBCs polymer is mechanically stretched, ring opening reaction occurs, which subsequently leads crosslinking reaction with dicarboxylate. They achieved to detect the reaction progress and solidification (gelation) from the polymer solution; however, strengthening of the bulk solid materials by incorporating the polymer in the solid materials was never tested (or not succeeded). The other examples of the self-strengthening or mechano-crosslinking reactions are using latent olefin methathesis catalyst bearing two polymeric N-heterocyclic carbene (NHC) ligands[47] or spirothiopyran[40] (**Figures 2-2b** and **2-2c**). In these researches, the cross-linking reaction in the stressed bulk solid polymer as well as in the sonicated soliton was detected. However, even though reaction was observed, the increase of mechanical property of the solid materials was not observed. Other related works to report mechanochemical crosslinking reactions achieved the gelation or solidification from solution, but they also did not report self-strengthening of the bulk material.[48–52] Such situation implies that many researchers working on mechanochemistry want to create a self-strengthening (or self-growing) materials in response to mechanical activation, but that is difficult to achieve.

In addition, other material scientists have created self-stiffening composite materials without using mechanochemical reaction.[53–56] In these examples, internal structure of the materials are orientated or are biased to the other stable state by single or repetitive stressing, resulting the stiffness increases. Considering that these researches

were reported in the recent decade, not only mechanochemists but also many material scientists are trying to create self-adaptive materials that evolve their properties in response to applied mechanical force, which would become a new stream of materials science.

2.3. Core issues on the self-growing materials and the strategy of this work

Given the long history of the researches on mechanoradicals including mechanoradical polymerization and current distinctive progress of the mechanochemistry using mechanophores, it is surprising that no one has achieved to create the self-strengthening, self-growing or self-adaptive materials that positively respond to mechanical stress using mechanochemical reaction. The expected reason is that the efficiency of the mechanochemical reaction in a material is not enough to strengthen it. Such possible poor reaction efficiency is divided into two reasons.

First, the reaction efficiency in solid state materials is usually poorer than solution environment. This is because low mobility of the polymers and/or small molecular reactants. It is reasonable that mechanochemical crosslinking reaction occurred in sonicated solution because high mobility of the polymers and good diffusivity of the small molecular reactants enable high reaction efficiency.

Next, importantly, the amount of the activated mechanophores may be very low. According to a previous research on quantitative investigation of the *g*DBC mechanophore-embedded poly(butadiene), the activated mechanophores are only 0.3% in a compressed polymer, and it was even less effective under the uniaxial stretching.[57,58] The other group (Otsuka *et al.*) has reported that, for radical-type mechanochromic

polymers incorporated with e.g. diarylbibenzofuranone (DABBF), the fraction of activated mechanophores in *stretched* polymer is less than 0.1% (e.g. 0.03%,[59] 0.05%,[60] and 0.02%[61]) even though the activation has reached more than 10% in *ground* polymer (e.g. 14%,[60] and 42%[62]). The ground polymer powders are probably break into rather smaller pieces. The low efficiency of the activation without breakage of bulk materials could be explained by the mechanics of the polymeric materials. Considering the deformation of soft polymeric materials, the strong chain extension in the materials occurs first on relatively short chains or chains closed to the defects. Mechanophores in the chain would be activated, then the chain reaches the extension limit and eventually breaks. When a polymer chain is ruptured, a microcrack would initiate auto-accelerated crack propagation to cause catastrophic failure of the materials. Given such a failure mechanism, the amount of activated mechanophores would be too few to perform efficient mechanochemical reaction in the materials.

To solve these possible essential issues on the creation of self-growing material, I here employed double-network (DN) hydrogel.[63] A polymer gel, consisting of cross-linked polymer network solvated with abundant of solvent, is liquid at the scale smaller than the network size (typically several to hundreds nm) and elastic solid at scale larger than the network size. Given such a unique property, the reactant molecules have good solubility and diffusion ability in a gel for efficient chemical reaction.[64,65] Accordingly, polymer gels are potential good mechanochemical reactors to solve the first issue. Furthermore, it is also possible to continuously feed the reactant to the DN gels, which would enable growing property with repetitive mechanical activation along with freshly supplied reactant.

A conventional hydrogel, however, is much more brittle than the other polymeric

materials, so that the amount of activated mechanophores would be much lower. Therefore, I use tough DN gel that have a unique internal fracture mechanism.[66–69] A mechanically tough DN gel, containing large amount of solvent (typically 80–90 wt.%), consists of two interpenetrated polymer networks with contrasting structure and mechanical properties. The first network, given very short and prestretched strands, is rigid and brittle; and the second network, given very long and coiled strands, is soft and ductile. When the DN gel is deformed, the load bearing first network strands break, transferring the load to the second network that maintains the integrity of the gel without breaking. As a result, the auto-accelerated crack propagation of the first network is avoided, and the amount of strand scissions of the first network gradually increases with increasing strain and finally reaches quite large. The massive strand scission of the first network generates abundant of mechanoradicals, which possibly trigger mechanoradical polymerization in the DN gels with high efficiency.

In summary, the strategy of this research is, by using possible large amount of mechanoradical generation in the DN gels due to its internal fracture, mechanoradical polymerization in the stressed DN gels is used to reconstruct the network structure that stiffen and strengthen the gel. Furthermore, with such mechanoradical polymerization, repetitive growth in size and strength may also be granted.

References

(1) B. J. Schoenfeld, The mechanisms of muscle hypertrophy and their application to resistance training. *J. Strength Cond. Res.* **24,** 2857–2872 (2010).

(2) V. G. Cofey, J. A. Hawley, The molecular bases of training adaptation. *Sports Med.* **37,** 737–763 (2007).

(3) M. Izquierdo, J. Ibáñez, K. Häkkinen, W. J. Kraemer, M. Ruesta, E. M. Gorostiaga, Maximal strength and power, muscle mass, endurance and serum hormones in weightlifters and road cyclists. *J. Sports Sci.* **22,** 465–478 (2004).

(4) C. Ruff, B. Holt, E. Trinkaus, Who's afraid of the big bad Wolff?: ''Wolff's law'' and bone functional adaptation. *Am. J. Phys. Anthropol.* **129,** 484–498 (2006).

(5) S. J. Warden, R. K. Fuchs, C. H. Turner, Steps for targeting exercise towards the skeleton to increase bone strength. *Euro. Med. Phys.* **40,** 223–232 (2004).

(6) A. G. Robling, F. M. Hinant, D. B. Burr, C. H. Turner, Improved bone structure and strength after long-term mechanical loading is greatest if loading is separated into short bouts. *J. Bone Mineral Res.* **17,** 1545–1554 (2002).

(7) A. G. Robling, A. B. Castillo, C. H. Turner, Biomechanical and molecular regulation of bone remodeling. *Annu. Rev. Biomed. Eng.* **8,** 455–498 (2006).

(8) S. L. Dallas, M. Prideaux, L. F. Bonewald, The Osteocyte: An endocrine cell … and more. *Endocr Rev.* **34,** 658–690 (2013).

(9) L. Ren, P. Yang, Z. Wang, J. Zhang, C. Ding, P. Shang, Biomechanical and biophysical environment of bone from the macroscopic to the pericellular and molecular level. *J. Mech. Behav. Biomed. Mater.* **50,** 104–122 (2015).

(10) P. F. Davies, Flow-mediated endothelial mechanotransduction. *Physiol Rev.* **75,** 519–560 (1995).

(11) G. Helmlinger, P. A. Netti, H. C. Lichtenbeld, R. J. Melder, R. K. Jain, Solid stress inhibits the growth of multicellular tumor spheroids. *Nat. Biotechnol.* **15,** 778–783 (1997).

(12) D. E. Discher, P. Janmey, Y.-L. Wang, Tissue cells feel and respond to the stiffness of their substrate. *Science* **310,** 1139–1143 (2005).

(13) S. S. Ranade, R. Syeda, A. Patapoutian, Mechanically activated ion channels. *Neuron (Cambridge)* **87,** 1162–1179 (2015).

(14) 佐藤正明（編）『細胞のマルチスケールメカノバイオロジー』森北出版（2017）.

(15) E. Boldyreva, Mechanochemistry of inorganic and organic systems: what is similar, what is different? *Chem. Soc. Rev.* **42,** 7719–7738 (2013).

(16) G.-W. Wang, Mechanochemical organic synthesis. *Chem. Soc. Rev.* **42,** 7668–7700 (2013).

(17) C. F. Burmeister, A. Kwade, Process engineering with planetary ball mills. *Chem. Soc. Rev.* **42,** 7660–7667 (2013).

(18) G. Cravotto, E. C. Gaudinoa, P. Cintas, On the mechanochemical activation by ultrasound. *Chem. Soc. Rev.* **42,** 7521–7534 (2013).

(19) D. Crawford, J. Casaban, Recent developments in mechanochemical materials synthesis by extrusion. *Adv. Mater.* **28,** 5747–5754 (2016).

(20) M. M. Caruso, D. A. Davis, Q. Shen, S. A. Odom, N. R. Sottos, S. R. White, J. S. Moore, Mechanically-induced chemical changes in polymeric materials. *Chem. Rev.* **109,** 5755–5798 (2009).

(21) J. Li, C. Nagamani, J. S. Moore, Polymer mechanochemistry: from destructive to productive. *Acc. Chem. Res.* **48,** 2181–2190 (2015).

(22) E. W. Flosdorf, L. A. Chambers, The chemical action of audible sound. *J. Am. Chem. Soc.* **55,** 3051–3052 (1933).

(23) H. Staudinger, W. Heuer, Über hochpolymere Verbindungen, 93. Mitteil.: Über das Zerreißen der Faden-Moleküle des Poly-styrols. *Ber. Dtsch. Chem. Ges.* **67,** 1159–1164 (1934).

(24) H. W. Melville, A. J. R. Murray, The ultrasonic degradation of polymers. *Trans.*

Faraday Soc. **46,** 996–1009 (1950).

(25) G. Ayrey, C. G. Moore, W. F. Watson, Mastication. Part III. Chemical verification of the mechanical degradation mechanism of cold mastication. *J. Polym. Sci.* **19,** 1–15 (1956).

(26) D. J. Angier, W. F. Watson, Mastication of rubber. IV. Polymerization of vinyl monomers by the cold mastication of rubber. *Rubber Chem. Tech.* **29,** 1140–1153 (1956).

(27) M. Sakaguchi, J. Sohma, Copolymerizations initiated by mechano-radicals on particle surfaces of poly(tetrafluoroethylene), *J. appl. Polym. Sci.* **22,** 2915–2924 (1978).

(28) J. Sohma, Mechanochemistry of polymers. *Prog. Polym. Sci.* **14,** 451–596 (1989).

(29) H. T. Baytekin, B. Baytekin, B. A. Grzybowski, Mechanoradicals created in "polymeric sponges" drive reactions in aqueous media. *Angew. Chem. Int. Ed.* **51,** 3596–3600 (2012).

(30) H. T. Baytekin, B. Baytekin, S. Huda, Z. Yavuz, B. A. Grzybowski, Mechanochemical activation and patterning of an adhesive surface toward nanoparticle deposition. *J. Am. Chem. Soc.* **137,** 1726–1729 (2015).

(31) D. A. Davis, A. Hamilton, J. Yang, L. D. Cremar, D. V. Gough, S. L. Potisek, M. T. Ong, P. V. Braun, T. J. Martínez, S. R. White, J. S. Moore, N. R. Sottos, Force-induced activation of covalent bonds in mechanoresponsive polymeric materials. *Nature* **459,** 68–72 (2009).

(32) K. Imato, A. Irie, T. Kosuge, T. Ohishi, M. Nishihara, A. Takahara, H. Otsuka, Mechanophores with a reversible radical system and freezing-induced mechanochemistry in polymer solutions and gels. *Angew. Chem. Int. Ed.* **54,** 6168–

6172 (2015).

(33) Y. Chen, A. J. H. Spiering, S. Karthikeyan, G. W. M. Peters, E. W. Meijer R. P. Sijbesma, Mechanically induced chemiluminescence from polymers incorporating a 1,2-dioxetane unit in the main chain. *Nat. Chem.* **4,** 559–562 (2012).

(34) C. R. Hickenboth, J. S. Moore, S. R. White, N. R. Sottos, J. Baudry, S. R. Wilson, Biasing reaction pathways with mechanical force. *Nature* **446,** 423–427 (2007).

(35) J. M. Lenhardt, M. T. Ong, R. Choe, C. R. Evenhuis, T. J. Martinez, S. L. Craig, Trapping a diradical transition state by mechanochemical polymer extension. *Science* **329,** 1057–1060 (2010).

(36) A. Piermattei, S. Karthikeyan, R. P. Sijbesma, Activating catalysts with mechanical force. *Nat. Chem.* **1,** 133–137 (2009).

(37) C. E. Diesendruck, B. D. Steinberg, N. Sugai, M. N. Silberstein, N. R. Sottos, S. R. White, P. V. Braun, J. S. Moore, Proton-coupled mechanochemical transduction: a mechanogenerated acid. *J. Am. Chem. Soc.* **134,** 12446–12449 (2012).

(38) M. B. Larsen, A. Boydston, “Flex-activated” mechanophores: using polymer mechanochemistry to direct bond bending activation. *J. Am. Chem. Soc.* **135,** 8189–8192 (2013).

(39) A. L. B. Ramirez, Z. S. Kean, J. A. Orlicki, M. Champhekar, S. M. Elsakr, W. E. Krause, S. L. Craig, Mechanochemical strengthening of a synthetic polymer in response to typically destructive shear forces. *Nat. Chem.* **5,** 757–761 (2013).

(40) H. Zhang, F. Gao, X. Cao, Y. Li, Y. Xu, W. Weng, R. Boulatov, Mechanochromism and mechanical-force-triggered cross-linking from a single reactive moiety incorporated into polymer chains. *Angew. Chem. Int. Ed.* **55,** 3040–3044 (2016).

(41) Y. Lin, M. H. Barbee, C.-C. Chang, S. L. Craig, Regiochemical Effects on

mechanophore activation in bulk materials. *J. Am. Chem. Soc.* **140,** 15969–1597 (2018).

(42) E. Ducrot, Y. Chen, M. Bulters, R. P. Sijbesma, C. Creton, Toughening elastomers with sacrificial bonds and watching them break. *Science* **344,** 186–189 (2014).

(43) M. Stratigaki, C. Baumann, L. C. A. van Breemen, J. P. A. Heuts, R. P. Sijbesma, R. Göstl, Fractography of poly(*N*-isopropylacrylamide) hydrogel networks crosslinked with mechanofluorophores using confocal laser scanning microscopy. *Polym. Chem.* (2019) DOI: 10.1039/C9PY00819E

(44) Z. Qiu, W. Zhao, M. Cao, Y. Wang, J. W. Y. Lam, Z. Zhang, X. Chen, B. Z. Tang, Dynamic visualization of stress/strain distribution and fatigue crack propagation by an organic mechanoresponsive AIE luminogen. *Adv. Mater.* **30,** 1803924 (2018).

(45) A. N. Celestine, B. A. Beiermann, P. A. May, J. S. Moore, N. R. Sottos, S. R. White, Fracture-induced activation in mechanophore-linked, rubber toughened PMMA. *Polymer* **55,** 4164–4171 (2014).

(46) A. N. Celestine, N. R. Sottos, S. R. White, Strain and stress mapping by mechanochemical activation of spiropyran in poly(methyl methacrylate). *Strain* **55,** e12310 (2019).

(47) R. T. M. Jakobs, S. Ma, R. P. Sijbesma, Mechanocatalytic polymerization and cross-linking in a polymeric matrix. *ACS Macro Lett.* **2,** 613–616 (2013).

(48) Z. S. Kean, Z. Niu, G. B. Hewage, A. L. Rheingold, S. L. Craig, Stress-responsive polymers containing cyclobutane core mechanophores: reactivity and mechanistic insights. *J. Am. Chem. Soc.* **135,** 13598–13604 (2013).

(49) J. Wang, I. Piskun, S. L. Craig, Mechanochemical strengthening of a multi-mechanophore benzocyclobutene polymer. *ACS Macro Lett.* **48,** 834–837 (2015).

(50) F. Verstraeten, R. Göstl, R. P. Sijbesma, Stress-induced colouration and crosslinking of polymeric materials by mechanochemical formation of triphenylimidazolyl radicals, *Chem. Commun.* **52,** 8608–8611 (2016).

(51) M. B. Gordon, S. Wang, G. A. Knappe, N. J. Wagner, T. H. Epps, C. J. Kloxin, Force-induced cleavage of a labile bond for enhanced mechanochemical crosslinking. *Polym. Chem.* **8,** 6485–6489 (2017).

(52) M. H. Barbee, J. Wang, T. Kouznetsova, M. Lu, S. L. Craig, Mechanochemical ring-opening of allylic epoxides. *Macromolecules* **52,** 6234–6240 (2019).

(53) B. J. Carey, P. K. Patra, L. Ci, G. G. Silva, P. M. Ajayan, Observation of dynamic strain hardening in polymer nanocomposites. *ACS Nano* **5,** 2715–2722 (2011).

(54) B. S. Chang, R. Tutika, J. Cutinho, S. Oyola-Reynoso, J. Chen, M. D. Bartlett, M. M. Thuo, Mechanically triggered composite stiffness tuning through thermodynamic relaxation (ST3R). *Mater. Horiz.* **5,** 416–422 (2018).

(55) A. Agrawal, A. C. Chipara, Y. Shamoo, P. K. Patra, B. J. Care, P. M. Ajayan, W. G. Chapman, R. Verduzco, Dynamic self-stiffening in liquid crystal elastomers. *Nat. Commun.* **4,** 1739 (2013).

(56) P. Dong, A. C. Chipara, P. Loya, Y. Yang, L. Ge, S. Lei, B. Li, G. Brunetto, L. D. Machado, L. Hong, Q. Wang, B. Yang, H. Guo, E. Ringe, D. S. Galvao, R. Vajtai, M. Chipara, M. Tang, J. Lou, P. M. Ajayan, Solid−liquid self-adaptive polymeric composite. *ACS Appl. Mater. Interfaces* **8,** 2142–2147 (2016).

(57) C. L. Brown, S. L. Craig, Molecular engineering of mechanophore activity for stress-responsive polymeric materials. *Chem. Sci.*, **6,** 2158–2165 (2015).

(58) J. M. Lenhardt, A. L. Black, B. A. Beiermann, B. D. Steinberg, F. Rahman, T. Samborski, J. Elsakr, J. S. Moore, N. R. Sottos, S. L. Craig, Characterizing the

mechanochemically active domains in gem-dihalocyclopropanated polybutadiene under compression and tension. *J. Mater. Chem.* **21,** 8454–8459 (2011).

(59) K. Imato, T. Kanehara, S. Nojima, T. Ohishi, Y. Higaki, A. Takahara, H. Otsuka, Repeatable mechanochemical activation of dynamic covalent bonds in thermoplastic elastomers. *Chem. Commun.* **52,** 10482–10485 (2016).

(60) T. Kosuge, K. Imato, R. Goseki, H. Otsuka, Polymer−inorganic composites with dynamic covalent mechanochromophore. *Macromolecules* **49,** 5903–5911 (2016).

(61) K. Ishizuki, D. Aoki, R. Goseki, H. Otsuka, Multicolor mechanochromic polymer blends that can discriminate between stretching and grinding. *ACS Macro Lett.* **7,** 556–560 (2018).

(62) H. Oka, K. Imato, T. Sato, T. Ohishi, R. Goseki, H. Otsuka, Enhancing mechanochemical activation in the bulk state by designing polymer architectures. *ACS Macro Lett.* **5,** 1124–1127 (2016).

(63) J. P. Gong, Y. Katsuyama, T. Kurokawa, Y. Osada, Double-network hydrogels with extremely high mechanical strength. *Adv. Mater.* **15,** 1155–1158 (2003).

(64) R. Yoshida, Self-oscillating gels driven by the Belousov–Zhabotinsky reaction as novel smart materials. *Adv. Mater.* **22,** 3463–3483 (2010).

(65) D. D. Díaz, D. Kühbeck, R. J. Koopmans, Stimuli-responsive gels as reaction vessels and reusable catalysts. *Chem. Soc. Rev.* **40,** 427–448 (2011).

(66) J. P. Gong, Why are double network hydrogels so tough? *Soft Matter* **6,** 2583–2590 (2010).

(67) T. Nakajima, T. Kurokawa, S. Ahmed, W. -L. Wu, J. P. Gong, Characterization of internal fracture process of double network hydrogels under uniaxial elongation. *Soft Matter* **9,** 1955–1966 (2013).

(68) Y. -H. Na, Y. Tanaka, Y. Kawauchi, H. Furukawa, T. Sumiyoshi, J. P. Gong, Y. Osada, Necking phenomenon of double-network gels. *Macromolecules* **39,** 4641–4645 (2006).

(69) R. E. Webber, C. Creton, H. R. Brown, J. P. Gong, Large strain hysteresis and Mullins effect of tough double-network hydrogels. *Macromolecules* **40,** 2919–2927 (2007).

Figures

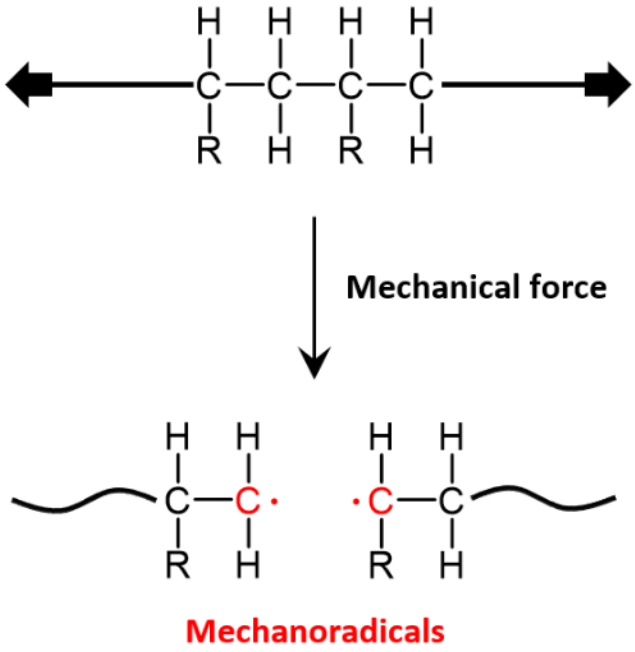

Figure 2-1. An example of mechanoradical generation by cleavage of polymer backbone.

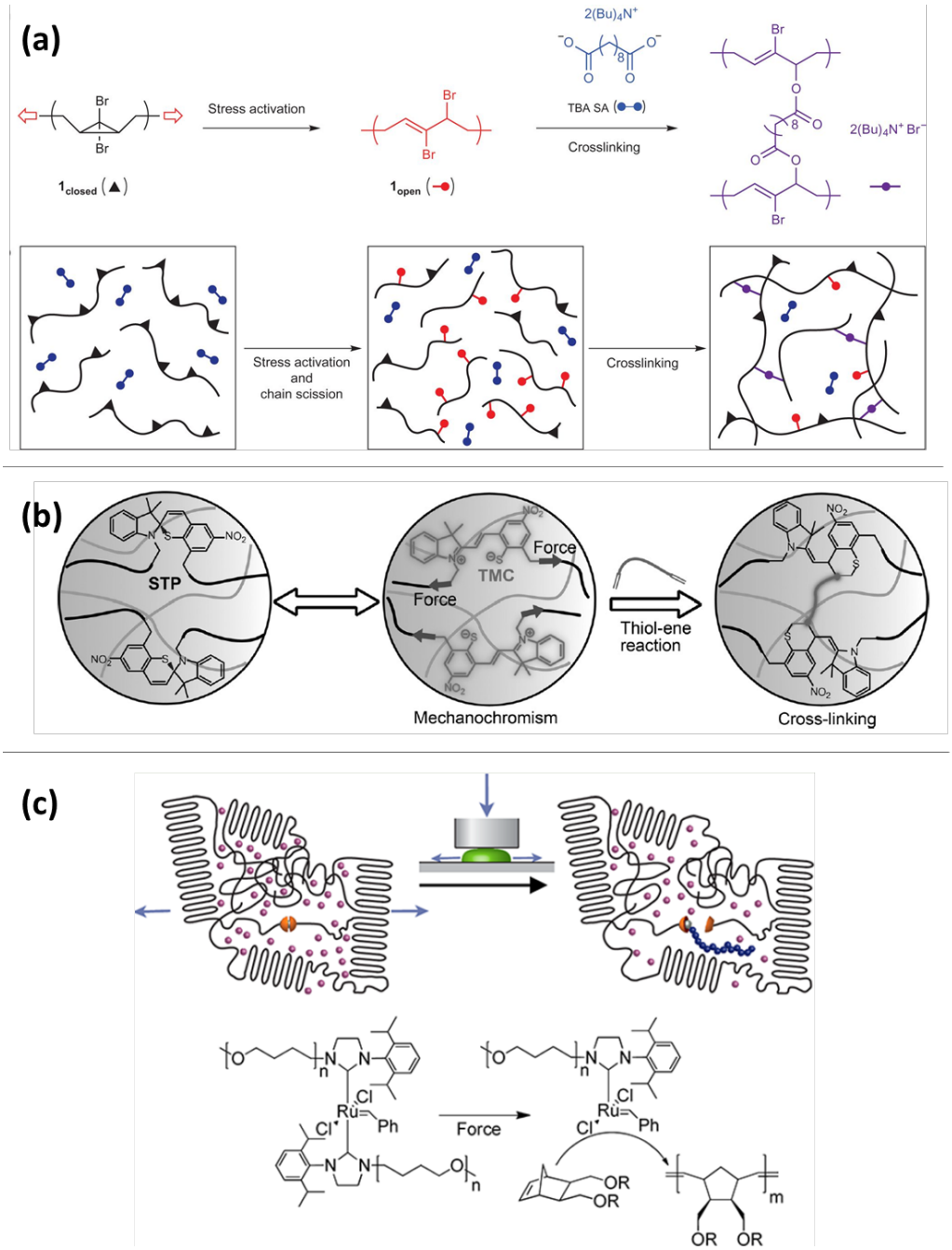

Figure 2-2. Some reported mechanochemical crosslinking reactions using **(a)** *gem*-dibromocyclopropane,[39] **(b)** spirothiopyran,[40] and **(c)** latent olefin methathesis catalyst bearing two polymeric NHC ligands.[47] These figures are from **(a)** *Nature Chemistry* 5, 757–761 (2013), **(b)** *Angewandte Chemie International Edition* 55, 3040–3044 (2016), **(c)** *ACS Macro Letters* 2, 613–616 (2013). Reprinted with permissions. Copyright 2013 Springer Nature Customer Service Centre GmbH, 2016 Wiley-VCH Verlag GmbH & Co. KGaA, and 2013 American Chemical Society, respectively.

Chapter 3: Synthesis and Characterization of DN Gels

3.1. Introduction

In this research described in **Chapters 4–6**, I used single-network (SN) and double-network (DN) hydrogels synthesized by reported procedure.[1,2] By using this procedure in which relatively high concentration of the initiator (1 mol%) is used at the first network synthesis, the first and second network are virtually not connected each other because most or all of the covalent bonds of the crosslinker was reacted. The DN gels are called as *truly independent* DN gels.[1] The DN hydrogels used here are composed of poly(2-acrylamido-2-methylpropane sulfonic acid sodium salt) (PNaAMPS) first network and polyacrylamide (PAAm) second network. The chemical structure and schematic illustration of this DN hydrogel are shown in **Figure 3-1**. Many previous researches on DN hydrogels, including the first paper to report a DN gel and the truly independent DN gels, have used poly(2-acrylamido-2-methylpropane sulfonic acid) (PAMPS) as the first network.[1–6] In this research, not PAMPS but neutralized sodium salt PNaAMPS was used for the first network because of following two reasons: (1) In this research, several kinds of chemical reactions are carried out inside of the gel as shown in the following chapters. Considering chemical reaction, neutral condition is more normal situation than acidic condition. (2) The polymer networks in the hydrogels are crosslinked with *N*,*N*'-methylenebisacrylamide (MBAA) that contains amide bonds. In acidic condition, hydrolysis of amide bonds is faster than that in neutral condition.[7] In order to reduce the possible hydrolysis event, neutralized PNaAMPS was used.

In this chapter, synthetic procedure and fundamental properties of the hydrogels are described, including water content and mechanical properties.

3.2. Experiment

3.2.1. Materials

Deionized water (Milli-Q) was used. 2-Acrylamido-2-methylpropanesulfonic acid sodium salt (NaAMPS) (49.7 wt.% aqueous solution) was provided by Toa Gosei. Acrylamide (AAm) was purchased from Junsei Chemical. *N*,*N*′-Methylenebisacrylamide (MBAA) and 2-oxoglutaric acid were purchased from Wako Pure Chemical Industries. Chloroform was purchased from Kanto Chemical. All the materials except AAm were used as received. The purchased AAm was recrystallized from chloroform before use. The abbreviations and chemical structures of some important compounds are listed in **Table 3-1**.

3.2.2. Synthesis of PNaAMPS SN hydrogels

Aqueous solutions of C_1 = 1.0 M NaAMPS monomer, x_1 (mol%) MBAA as a crosslinker, and 1.0 mol% 2-oxoglutaric acid as a photo-induced radical initiator were prepared. The crosslinker and the initiator concentration (mol%) are denoted as respected to the monomer. The crosslinker concentration x_1 was varied from 1.0 to 4.0 mol%. Each precursor solution containing NaAMPS, MBAA and 2-oxoglutaric acid was moved to an argon glovebox (MBRAUN, oxygen concentration <100 ppm in typical). Then, the solution was poured into a cuboid mold comprising two flat soda-lime glass plates (3-mm thickness, 10 cm × 10 cm) separated by a silicone rubber (0.5−10.0 mm; typically, 0.5 or 1.0 mm) as a spacer in the argon glovebox. Each solution was irradiated with ultraviolet (UV) light (365 nm, 4 mW cm^{-2}) from both sides of the glass mold for 8–9 hours in the glovebox. The as-prepared PNaAMPS gels were used for the next step (**section 3.2.4**) to synthesize DN gels. When the SN gel was used as the control SN gel, the as-prepared

PNaAMPS SN gel was immersed in large amount of water to swell the gel and to extract unreacted molecules from the gel. Each PNaAMPS gel is coded as (C_1-x_1) PNaAMPS SN gel, where C_1 and x_1 are the monomer concentration (C_1 = 1.0 M) and the cross-linker concentration molar ratio (mol%) respective to C_1 (x_1 = 1.0−4.0 mol%), respectively.

3.2.3. Synthesis of PAAm SN gels

An aqueous solution of C_2 = 2.0−4.0 M AAm monomer, x_2 = 0.01 mol% MBAA and 0.01 mol% 2-oxoglutaric acid was prepared. The crosslinker and the initiator concentration (mol%) are denoted as respected to the monomer. The precursor solution was moved to the argon glovebox. Then, the solution was poured into a cuboid mold comprising the two flat soda-lime glass plates separated by a silicone rubber (1.0 mm) as a spacer in the argon glovebox. Each solution was irradiated with UV light (365 nm, 4 mW cm^{-2}) from both sides of the glass mold for 9 hours in the glovebox. The as-prepared PAAm SN gel was immersed in large volume of water to swell the gel and to extract unreacted molecules from the gel. Each PAAm gel is coded as (C_2-x_2) PAAm SN gel, where C_2 and x_2 are the monomer concentration (C_2 = 2.0−4.0 M) and the cross-linker concentration molar ratio (%) respective to C_2 (x_2 = 0.01 mol%), respectively.

3.2.4. Synthesis of PNaAMPS/PAAm DN hydrogels

Each as-prepared PNaAMPS SN gel (**section 3.2.2**) was immersed in a second network precursor aqueous solution containing C_2 (M) AAm (C_2 = 2.0, 3.0 or 4.0 M), x_2 = 0.01 mol% MBAA and 0.01 mol% 2-oxoglutaric acid for more than 1 day at 5–10°C. Then, the gels swollen with the second network precursor solution was sandwiched between the two flat soda-lime glass plates. Air bubbles between the gel and each glass plate were

removed as possible. Each gel sandwiched between glass plates was moved to the argon glovebox and irradiated with the UV light for 9 hours in the glovebox to synthesize the second PAAm network in the presence of the PNaAMPS first network. The synthesized DN gels were immersed in large volume of water for more than 1 day to swell the gel and to remove any unreacted reagents. Each DN gel is coded as (C_1-x_1/C_2-x_2) DN gel, where C_1 and C_2 are the feed monomer (NaAMPS and AAm, respectively) concentration for the first and second network, respectively, and x_1 and x_2 are the cross-linker concentration molar ratio (%) respective to the corresponding monomer concentration, respectively.

3.2.5. Characterization of the weight fraction of each component in gels

The weight fractions of the polymer and water in each gel, f_p and f_w, respectively, were calculated from the weights of the gel before and after drying, w_{wet} and w_{dry}, respectively, using the following equations:

$$f_p = \frac{w_{dry}}{w_{wet}} \quad (3.1)$$

$$f_w = 1 - f_p \quad (3.2)$$

The water-swollen gel samples (approximately 5–10 g gel for PNaAMPS SN gels and approximately 1−2 g gel for PAAm SN gels and DN gels) were dried at 120 °C for 7 h *in vacuo* (< 20 mbar). The polymer weight fraction of a DN gel, $f_{p,DN}$, is the sum of the weight fractions of the brittle first network and the stretchable second network. The weight fractions of the brittle first network and the stretchable second network of the DN gel, $f_{1,DN}$ and $f_{2,DN}$, respectively, were approximately calculated as follows:

$$f_{1,DN} = f_{1,SN}\left(\frac{t_{1,SN}}{t_{DN}}\right)^3 \quad (3.3)$$

$$f_{2,DN} = f_{p,DN} - f_{1,DN} \quad (3.4)$$

where $f_{1,SN}$ is the polymer weight fraction of the original PNaAMPS SN gel at swollen state and t_{DN} and $t_{1,SN}$ are the thicknesses of the swollen DN gel and the original PNaAMPS SN gel, respectively. In equation (3.3), I assumed density (g/cm^3) of the swollen PNaAMPS SN gels is identical to that of the swollen DN gels.

3.2.6. Uniaxial tensile test

Various DN gels and SN gels, 3.0–4.1 mm thick, were cut into dumbbell-shaped pieces following the IEC-540(S) standard (17 mm gauge length and 4 mm width, **Figure 3-2**) by using sample cutter with razor blade (Dumbbell Co.). The cut gels were immersed in water for at least 3 days. Uniaxial tensile tests of these gels were then carried out using a commercial tensile tester (Instron 5965, Instron Co.) at a crosshead velocity of 300 mm min^{-1} in typical. The strain (ε) was measured using a noncontacting video extensometer (AVE, Instron Co.), and the nominal stress (σ) was calculated as the measured load divided by the original cross-sectional area vertical to the load.

3.3. Results and Discussion

3.3.1. Weight fraction of each component in gels

The weight fraction of each component (first network, second network or water) in the SN gels and DN gels is summarized in **Table 3-2**. The sample codes are also shown in the Table. On this measurement, the weight of three individual gels (n = 3) for each sample were measured before and after drying. Observed as standard deviation of polymer weight fraction f_p, the error range is quite small even for high water content samples. For example, f_p of the (1-1) PNaAMPS SN gel was measured as f_p = 0.200 ± 0.005 wt.% (3% error). Note that, although the analyzed polymer weight might contain small amount of bounded

water, it seems that most of water was removed from the gel at the drying condition (120°C, < 20 mbar, 7–8 hours).

As seen in **Table 3-2**, water content of the PNaAMPS SN gels, PAAm SN gels and PNaAMPS/PAAm DN gels are 97.5–99.8 wt.%, 91–93 wt.% and 81–93 wt.%, respectively.

3.3.2. Mechanical properties characterized by uniaxial tensile test

The stress (σ)–strain (ε) curves of some of the synthesized SN and DN gels are shown in **Figure 3-3**. Note that swollen PNaAMPS SN gels were too brittle to stretch with the tensile tester. The σ–ε curves are varied with the composition, similar as previous PAMPS/PAAm DN gels.[2] Yielding stress was increased with the crosslinker concentration of the first network x_1 because yielding stress is proportional to the areal chain density of the first network.[8] Briefly, the volumetric chain density of the first network in a DN gel, ν_1, is related to the first network concentration f_1 and the average polymerization degree of the first network strands between crosslinking point $N_{m,1}$, as $\nu_1 \sim f_1 N_{m,1}^{-1}$. At higher x_1, higher f_1 is observed (**Table 3-2**) because swelling degree of the first network is restricted by the high crosslinking density. $N_{m,1}$ should be smaller at higher x_1. Therefore, ν_1 is higher at higher x_1, so yielding stress is larger with increasing x_1.

3.4. Summary

I prepared PNaAMPS/PAAm DN gels with various mechanical properties. The water content of the DN gels are from 81 to 93 wt.%. As reference samples, PNaAMPS SN gels and PAAm SN gels are also prepared. The DN and SN hydrogels are used in **Chapters 4–6**.

References

(1) T. Nakajima, H. Furukawa, Y. Tanaka, T. Kurokawa, Y. Osada, J. P. Gong, True chemical structure of double network hydrogels. *Macromolecules* **42,** 2184–2189 (2009).

(2) S. Ahmed, T. Nakajima, T. Kurokawa, M. A. Haque, J. P. Gong Brittle–ductile transition of double network hydrogels: Mechanical balance of two networks as the key factor. *Polymer* **55,** 914–923 (2014).

(3) J. P. Gong, Y. Katsuyama, T. Kurokawa, Y. Osada Double-network hydrogels with extremely high mechanical strength. *Adv. Mater.* **15,** 1155–1158 (2003).

(4) T. Nakajima, T. Kurokawa, S. Ahmed, W. -L. Wu, J. P. Gong, Characterization of internal fracture process of double network hydrogels under uniaxial elongation. *Soft Matter* **9,** 1955–1966 (2013).

(5) Y. Tanaka, Y. Kawauchi, T. Kurokawa, H. Furukawa, T. Okajima, J. P. Gong, Localized yielding around crack tips of double-network gels. *Macromol. Rapid Commun.* **29,** 1514–1520 (2008).

(6) Y. -H. Na, Y. Tanaka, Y. Kawauchi, H. Furukawa, T. Sumiyoshi, J. P. Gong, Y. Osada, Necking phenomenon of double-network gels. *Macromolecules* **39,** 4641–4645 (2006).

(7) R. M. Smith, D. E. Hansen, The pH-rate profile for the hydrolysis of a peptide bond. *J. Am. Chem. Soc.* **120,** 8910–8913 (1998).

(8) T. Matsuda, T. Nakajima, Y. Fukuda, W. Hong, T. Sakai, T. Kurokawa, U. Chung, J. P. Gong, Yielding criteria of double network hydrogels. *Macromolecules* **49,** 1865–1872 (2016).

Figures and Tables

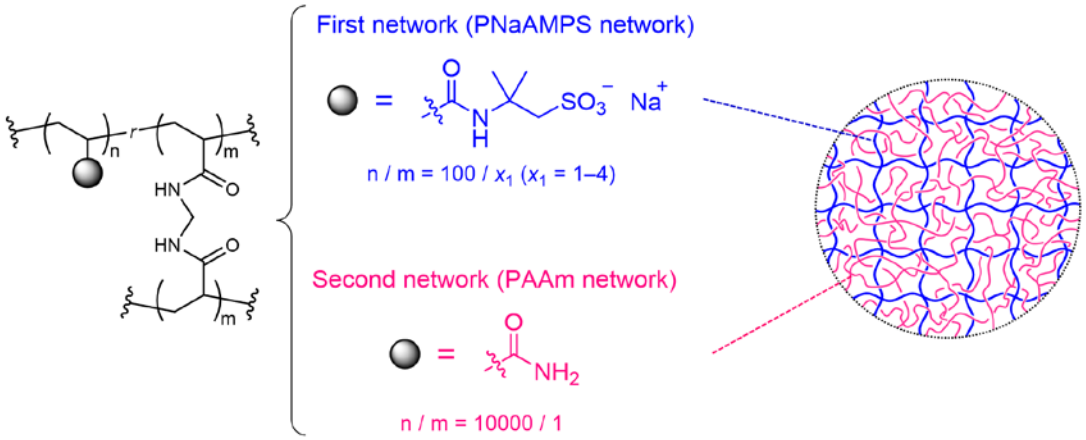

Figure 3-1. Chemical structure and schematic representation of the polymeric network structure of the DN gel. The first network (PNaAMPS, blue) and the second network (PAAm, pink), both covalently crosslinked by MBAA, are interpenetrated and ideally not connected with each other. The ratio n/m corresponds to the molar ratio of the monomer (NaAMPS or AAm) and crosslinker (MBAA) in feed. This figure is from *Science* 363, 504–508 (2019). Reprinted with permission from AAAS.

Table 3-1. Abbreviations and structures of the chemical compounds

Chemical name	Abbreviation	Chemical structure
2-Acrylamido-2-methylpropanesulfonic acid sodium salt	NaAMPS	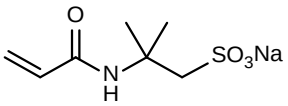
Acrylamide	AAm	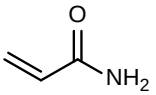
N,N′-Methylenebisacrylamide	MBAA	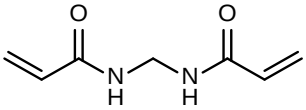
Poly(2-acrylamido-2-methylpropanesulfonic acid) sodium salt	PNaAMPS	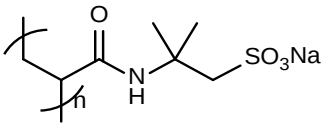
Poly(acrylamide)	PAAm	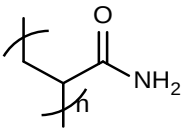

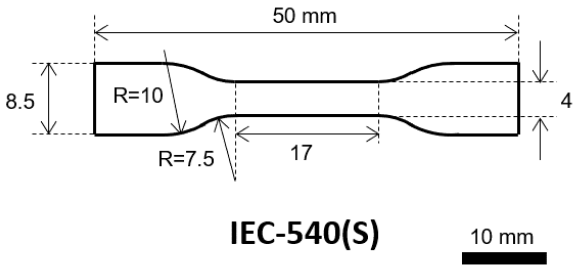

Figure 3-2. The dumbbell-shaped geometry (IEC-540(S) standard) of the sample used for the uniaxial tensile test.

Table 3-2. Sample codes and formulations of the SN and DN gels and the weight fraction of each component at the equilibrium swollen state in water.

Sample code (C_1-x_1/C_2-x_2)	Composition in feed				Composition of swollen gel			
	First network		Second network		First network	Second network	Polymer	Water
	C_1 (M) (NaAMPS)	x_1 (mol%) (MBAA)	C_2 (M) (AAm)	x_2 (mol%) (MBAA)	f_1 (wt.%)	f_2 (wt.%)	f_p (wt.%) (=f_1+ f_2)	f_w (wt.%)
(1-4) PNaAMPS SN gel	1	4	-	-	2.5	-	2.49 (±0.02)	97.5
(1-3) PNaAMPS SN gel	1	3	-	-	1.6		1.60 (±0.01)	98.4
(1-2.5) PNaAMPS SN gel	1	2.5	-	-	1.2		1.16 (±0.01)	98.8
(1-2) PNaAMPS SN gel	1	2	-	-	0.8		0.800 (±0.006)	99.2
(1-1.5) PNaAMPS SN gel	1	1.5	-	-	0.5		0.491 (±0.015)	99.5
(1-1) PNaAMPS SN gel	1	1	-	-	0.2		0.200 (±0.05)	99.8
(4-0.01) PAAm SN gel	-	-	4	0.01	-	8.2	8.18 (±0.08)	91.8
(3-0.01) PAAm SN gel	-	-	3	0.01	-	7.4	7.4 (±0.21)	92.6
(1-4/4-0.01) DN gel	1	4	4	0.01	1.6	17.3	18.90 (±0.05)	81.1
(1-3/2-0.01) DN gel	1	3	2	0.01	1.2	10.3	11.45 (±0.10)	88.6
(1-2.5/2-0.01) DN gel	1	2.5	2	0.01	0.9	9.5	10.36 (±0.03)	89.6
(1-2/2-0.01) DN gel	1	2	2	0.01	0.5	8.9	9.44 (±0.21)	90.6
(1-1.5/2-0.01) DN gel	1	1.5	2	0.01	0.3	8.2	8.46 (±0.16)	91.5
(1-1/2-0.01) DN gel	1	1	2	0.01	0.1	7.7	7.80 (±0.08)	92.2
(1-3/3-0.01) DN gel	1	3	3	0.01	1.0	13.1	14.63 (±0.16)	86.9
(1-4/2-0.01) DN gel	1	4	2	0.01	2.0	10.9	12.82 (±0.11)	87.2

The concentrations of monomer (C) and cross-linker (x; molar percentage given with respect to the monomer) during gel synthesis and the weight fraction of each component in the swollen gels (f) are shown. The subscripts 1, 2 and w denote the first network, the second network and water, respectively. Standard deviation (n = 3) are shown for f_p. Only average values are shown for f_1, f_2 and f_w.

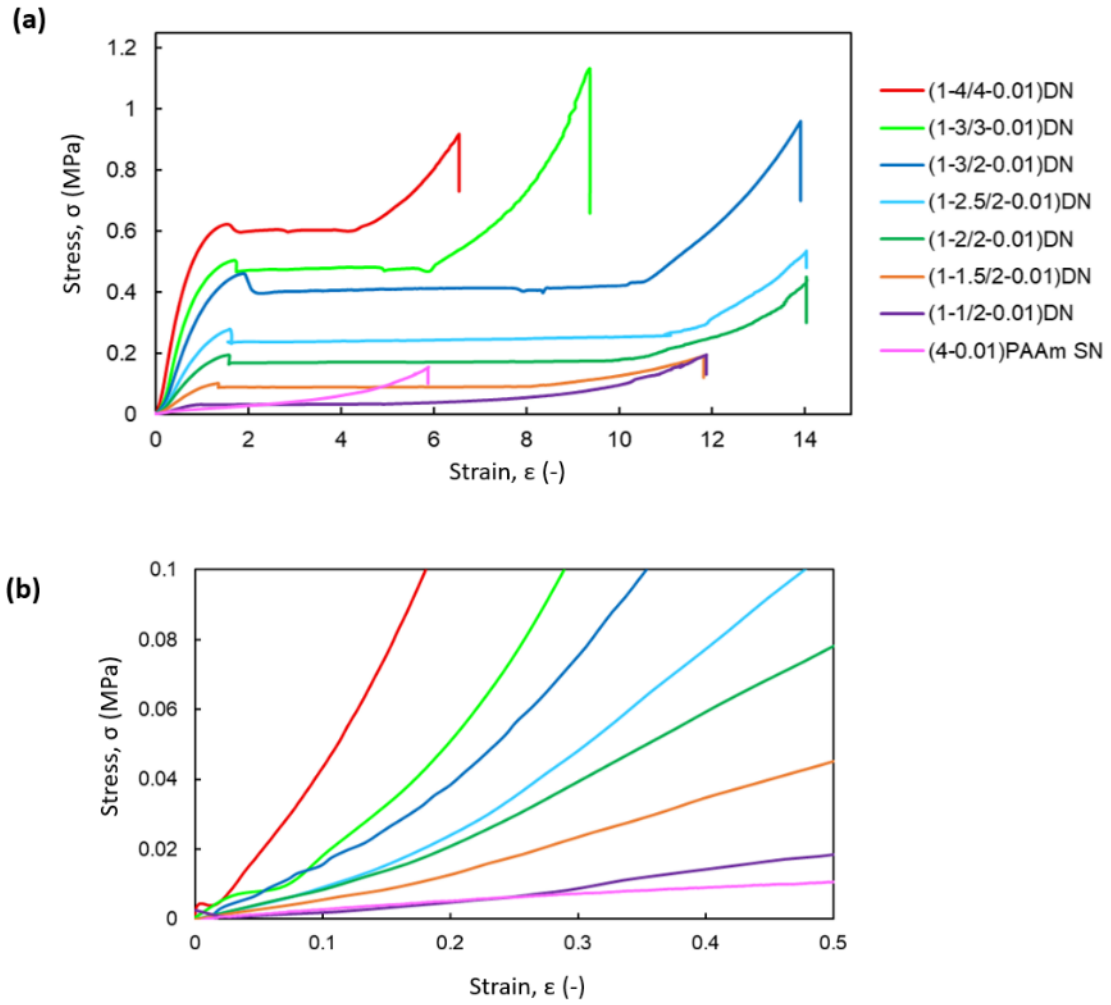

Figure 3-3. Stress–strain curves of DN gels and a PAAm SN gel at equilibrium swollen state with water. **(a)** Full view and **(b)** expanded view at small strain region of the curves. The sample codes (C_1-x_1/C_2-x_2) denote feed crosslinker concentration of the first network x_1 and the feed monomer concentration of the second network C_2 (see **Table 3-2**).

Chapter 4: Quantification of Polymer Strand Scission in DN Gels

4.1. Introduction

The double-network (DN) structure is the state-of-the-arts strategy to toughen soft materials.[1–6] The DN structure contains two interpenetrating polymer networks: one is brittle and sparse network and the other is stretchable and dense network. Currently, it is well known that toughening mechanism of DN gels are based on energy dissipation originated from polymer strands scission of the brittle first network[2,4,6]. To understand why the DN gels are tough, we should first understand why conventional gels are so weak and brittle. Once a conventional hydrogel (i.e. single-network gel) is deformed, some strands of the polymer network are broken. The polymer strand to be broken is usually at the weakest part in the network, for example, shortest chains in the network or sparse region due to the spatial inhomogeneity of the polymeric network in the gels. Such polymer strand scission creates microcrack in the network structure, which easily propagates to neighbor chains because of stress concentration at the microscale. Finally, the crack propagation goes through the global scale; that is, the gel material breaks into two pieces. Therefore, the conventional gels are weak and brittle.[7] On the other hand, such microcrack propagation is restricted in the DN gels. Once a DN gel is deformed, some strands of the brittle first network are broken as same as in the conventional gels. However, the microcrack does not propagate due to the existence of the stretchable second network. As the result, the DN gel can be deformed to higher level accompanying with large amount of strands scission of the brittle network. The strands scission in the DN gel is called as *internal fracture*.[8] Since the DN gels are insensitive to the microcrack propagation, or in other word insensitive to weakest link, the DN gel shows high strength and toughness. The internal fracture dissipates plenty of mechanical energy during the

deformation, which also toughen the DN gels.[2,4,9]

The internal fracture of the DN gels has been confirmed by mechanical characterization. Na *et al.* reported that a DN gel showed mechanical hysteresis under cyclic tensile testing, and the stretched DN gels got soften as the soft second network single-network (SN) gels.[10] This explains the hard and brittle first network is broken in the deformed DN gel. Webber *et al.* clearly showed the mechanical hysteresis of DN gels is originated from network fracture.[11] They observed the hysteresis of DN gels is completely irreversible even after waiting for two weeks. Since (reversible) mechanical hysteresis is also observed on the other soft materials due to such as viscoelastic dissipation, the irreversible hysteresis is the clear evidence that there is irreversible fracture of polymer strands scission. After these reports, irreversible hysteresis is used as the evidence of the internal fracturing (and the evidence of the "DN gels") and to characterize the amount of internal fracture and/or energy dissipation in the DN gels.[8,11–13] Nakajima *et al.* quantitatively considered the amount of fractured strand from the hysteresis.[8] They concluded that 9% of all first network chains broke in a DN gel. The hysteresis characterization has been the only method to detect and quantify the internal fracturing of DN gels; however, the quantification still includes some difficulties such as network inhomogeneity and estimating the energy to break one polymer strand.

In this chapter, detection and quantification of the internal fracture by chemical approach are reported, which is contrasting to the mechanical approach (hysteresis analysis). Considering the polymer strand breakage, I focused on "mechanoradicals". As shown in **Chapter 2**, radical species are usually generated at the both ends of a broken polymer chain when the polymer chain is fractured because the polymer strand is connecting by covalent bonds such as carbon−carbon bond (**Figure 4-1**).[14–17] The radical

species generated by mechanical scission are called as mechanoradicals. Since radical is chemically active, the mechanoradicals can induce chemical reactions[15–21]. According to a report from Baytekin *et al.* in 2012, mechanoradical generated in aqueous system induces generation of hydrogen peroxide (H_2O_2) from water and oxygen.[19] In their report, they quantified the concentration of H_2O_2 generated at the interface of water and stressed polymeric sponge by using Fenton reaction in which ferrous ion (Fe^{2+}) is oxidized to ferric ion (Fe^{3+}) induced by H_2O_2.[22–24]

Herein, I applied the Fenton reaction induced by mechanoradicals in the DN gel system to confirm that (1) the internal fracture is originated from covalent bond rupture accompanying with mechanoradical generation; (2) the mechanoradical is chemically active to induce chemical reaction; and (3) to quantify the concentration of the mechanoradicals (i.e. ruptured polymer strands). The result gives insights of the internal fracture in the chemical quantitative aspect, which must be a complementary way to the mechanical hysteresis approach.

4.2. Experiments

4.2.1. Materials

DN gels and SN gels were fabricated by following the method described in **section 3.2**. Amonium iron(II) sulfate ($(NH_4)_2Fe^{II}(SO_4)_2$) hexahydrate, sulfuric acid (H_2SO_4), 2,2'-azobis[2-(2-imidazolin-2-yl)propane]dihydrochloride (VA-044), 2,2'-azobis(2-methylpropionamidine)dihydrochloride (V-50), 2,2'-azobis[2-methyl-*N*-(2-hydroxyethyl)propionamide] (VA-086) and hydrogen peroxide (30–35.5%) were purchased from Wako Pure Chemical Industries. Ammonium iron (III) sulfate ($NH_4Fe^{III}(SO_4)_2$) dodecahydrate was purchased from Sigma-Aldrich. 3'-Bis[*N*,*N*-

bis(carboxymethyl)aminomethyl]-*o*-cresolsulfonphthalein disodium salt (xylenol orange (XO)) was purchased from Dojindo Laboratories. 1-[4-(2-Hydroxyethoxy)-phenyl]-2-hydroxy-2-methyl-1-propane-1-one (I-2959) was purchased from Ciba Specialty Chemicals. The abbreviations and chemical structures of some important compounds used here are listed in **Table 4-1**.

4.2.2. Visualization of oxidized ferrous ions in stretched gels (visual demonstration)

A (1-4/4-0.01) DN gel (~4 mm-thick) at equilibrium swollen state in water was cut into dumbbell-shaped pieces standardized to the IEC-540(S) (17 mm gauge length and 4 mm width, **Figure 4-2**). The cut gels were immersed in water for at least 1 day to quench the mechanoradicals at the cut surface. Next, each gel was immersed in aqueous solution of 100 μM $(NH_4)_2Fe^{II}(SO_4)_2$ 250 μM XO and 20 mM H_2SO_4 for 4 days. The concentration was appropriate for observing color change by naked eye. The gel was stretched to the strain of $\varepsilon = 3.5$ with hands (nominal stretching rate of roughly 100s mm/min). The stretched gel was put on a desk and covered with plastic film (Saranwrap, Asahikasei Co.) to avoid drying. The color change was observed by naked eye and with video camera (Sony Co.).

4.2.3. Quantification of oxidized ferrous ions in stretched gels

Various DN gels or SN gels at equilibrium swollen state in water were cut into dumbbell-shaped pieces standardized to the JIS K6251-2 (20 mm gauge length and 10 mm width, **Figure 4-2**). The thicknesses of the gels were set as 3.0±0.5 mm that is appropriate for the following light absorption measurement by controlling the initial thickness of the first network (0.5−1.5 mm). The cut gels were immersed in water for at least 1 day to quench

the mechanoradicals at the cut surface. Next, each gel was immersed in aqueous solution of typically 100 μM $(NH_4)_2Fe^{II}(SO_4)_2$, 100 μM XO and 20 mM H_2SO_4 for 4 days. Each gel was then stretched to a prescribed strain with commercial tensile tester (Instron 5965, Instron Co.) at a crosshead velocity of 500 mm min^{-1}. The strain of the gel was measured using a non-contacting video extensometer (AVE, Instron Co.). Once the strain was reached to the prescribed strain, the gel was immediately unloaded and cut with scissor to obtain cuboid-shaped gel with length of 15 mm (**Figure 4-3**). After 30 minutes, each gel was placed in a quartz optical cell (45 mm × 10 mm × 10 mm), and ultraviolet−visible light (UV-Vis) absorption spectroscopic measurement was performed (UV-1800, Shimadzu Co.). The spectrum of DN gels swollen with pure water, which is almost no light absorption at observation wavelength range (350–800 nm), was used as the reference. The time 30 minutes is the period when the color change was completed (discussed in **section 4.3.2**). As the control experiment, the same procedure was performed with an unstretched and uncut gel. To quantify the Fe^{3+} concentration that was oxidized from Fe^{2+}, the ratio of the absorbance at 580 and 440 nm, A_{580}/A_{440}, was compared with that observed in a calibration experiment (see **section 4.2.4**).

4.2.4. Calibration procedure for the quantification of Fe^{3+} concentration

To calibrate Fe^{3+} concentration on the UV-Vis absorption spectroscopy, aqueous solutions of 0−40 μM $NH_4Fe^{III}(SO_4)_2$ (as an Fe^{3+} source), 100 μM $(NH_4)_2Fe^{II}(SO_4)_2$, 100 μM XO and 20 mM H_2SO_4 were prepared. After 30 minutes, UV-Vis absorption spectroscopy of each solution was carried out with a quartz optical cell (45 mm × 3 mm optical path length × 10 mm). The spectrum of pure water, which is almost no light absorption at observation wavelength range (350–800 nm), was used as the reference. A calibration curve was made

using the ratio of the absorbance at 580 and 440 nm, A_{580}/A_{440}, versus the Fe^{3+} concentration.

4.2.5. Quantification of radicals generated by small-molecular radical initiators from the oxidation of Fe^{2+}

To quantitatively determine the concentration of radicals required to oxidize the certain concentration of Fe^{2+}, similar Fe^{2+} oxidation experiment was performed by using conventional small-molecular radical generators. In the DN gels used here, I assumed that carbon-centered mechanoradicals are generated (discussed in **section 4.3.4**). As models of carbon-centered radicals, three thermoresponsive radical generators, V-50, VA-044 and VA-086;[25] and a photoresponsive radical generator I-2959[26] were used. When the thermoresponsive radical generators were used, aqueous solutions of 100 μM $(NH_4)_2Fe^{II}(SO_4)_2$, 100 μM XO, 20 mM H_2SO_4 and specified concentration (C_0 = 0–100 μM) of each radical generator were heated at its 10 h half-life temperature (56, 44 and 86 ℃ for the V-50, VA-044 and VA-086, respectively)[27] for 10 h. When the photoresponsive radical generator I-2959 was used, aqueous solutions of 100 μM $(NH_4)_2Fe^{II}(SO_4)_2$, 100 μM XO, 20 mM H_2SO_4 and specified concentration (C_0 = 0–20 μM) of I-2959 were irradiated with UV light (314 nm, 3 mW cm^{-2}) for 90 s during which virtually all of I-2959 was decomposed to generate radicals (see **section 4.3.4**). Thirty minutes after the end of excitation by heating or irradiation, UV-Vis absorption spectroscopy was performed with a quartz optical cell (45 mm × 3 mm optical path length × 10 mm) to quantify the Fe^{3+} concentration. The concentrations of generated radicals were calculated as $[R\cdot] = 2\ C_0\ r$, where the factor of 2 means two radicals are generated from one radical generator molecule decomposition, C_0 is the feed concentration of the

radical initiator and *r* is the decomposition ratio of each radical generator. To obtain the decomposition ratio *r*, each radical generator (50 mM for each azo-type initiator and 200 μM for I-2959) was excited by heating or photoirradiation at the same condition above in a 20 mM H_2SO_4 (without $(NH_4)_2Fe^{II}(SO_4)_2$ and XO) aqueous solution, and then UV-Vis absorption spectroscopy was carried out.

4.2.6. Cyclic uniaxial tensile test

Various DN gels and SN gels, 3.0–4.1 mm thick, were cut into dumbbell-shaped pieces following the IEC-540(S) standard (17 mm gauge length and 4 mm width, **Figure 4-2**) by using sample cutter (Dumbbell Co.). Uniaxial cyclic tensile tests of these gels were carried out using a commercial tensile tester (Instron 5965, Instron Co.). Each sample was first stretched to a certain strain at a crosshead velocity of 300 mm min^{-1}, and then immediately unloaded at ~1000 mm min^{-1}. Subsequently, the gel was stretched to an increased maximum strain and unloaded again. The cyclic test was repeated with increasing the maximum strain each time until the gel broke. The strain (ε) was measured using a noncontacting video extensometer (AVE, Instron Co.), and the nominal stress (σ) was calculated as the measured load divided by the original cross-sectional area vertical to the load. The strain and stress were measured only during the loading process because mechanical hysteresis of DN gel is known to be irreversible. The mechanical hysteresis area U_{hys} corresponding to the applied strain (ε_{app}) was calculated as follows:[8]

$$U_{\mathrm{hys}} = \int_0^{\varepsilon_{\mathrm{app}}} (\sigma_1 - \sigma_2)\mathrm{d}\varepsilon \qquad (4.1)$$

where σ_1 and σ_2 are the nominal stresses during the first cycle (maximum strain of ε_{app})

and the second cycle, respectively.

4.3. Results and Discussion

4.3.1. Visualization of internal fracturing in stretched DN gels

After a (1-4/4-0.01) DN gel was immersed in aqueous solution of 100 μM $(NH_4)_2Fe^{II}(SO_4)_2$ 250 μM XO and 20 mM H_2SO_4 for 4 days, the DN gel showed yellow color as same as the original solution of Fe^{2+} and XO (**Figure 4-4(i)**). The result suggests that the molecules were fed in the DN gel at the same concentration as external solution, and no ferrous oxidation happened in the unstretched DN gels. When the DN gel (containing Fe^{2+} and XO) was stretched to the strain $\varepsilon = 3.5$, the DN gel showed necking phenomenon, which is often observed on DN gels with high stretchability and toughness accompanied with yielding (**Figure 4-4(ii)**).[10,28,29] Since the applied strain $\varepsilon = 3.5$ was between yielding strain ($\varepsilon_y \approx 1.9$) and the strain of yielding completion to start strain hardening ($\varepsilon_h \approx 4.2$), necked region and un-necked region coexist in the narrow part of the dumbbell shaped DN gel under stretched state ($\varepsilon = 3.5$). Afterwards, the gel was immediately unloaded. Just after unloading, negligible color change was observed; however, the color at the necked region gradually get brownish color within few 10s minutes. The kinetics is discussed in the following section (**section 4.3.2**). Thirty minutes after the stretching, obvious color change was observed only at the necked region (**Figure 4-4(iii)**). On the other hand, when the gel was not stretched, negligible color change was observed. Since the color change is originated from the Fe^{3+}, this is the evidence that the ferrous ion was oxidized into ferric ions by the mechanical stretching. Considering my original idea based on a previous paper,[19] the ferrous oxidation must be triggered by mechanoradicals originated by internal fracturing of the first network which generates

H_2O_2. The reason why the obvious color change was observed only in the necked region is explained by internal fracturing insight based on previous literatures. Previous researches based on elastic modulus measurement, hysteresis analysis and re-swelling experiment have shown that much larger amount of the first network strands are fractured in the necked region than in un-necked region, even though partial internal fracturing is also happen in the un-necked region.[2,8,10,29] My result here is consistent with these previous researches.

Importantly, this is the first chemical evidence of the internal fracturing in DN gels, even though internal fracturing in multiple-network elastomers has detected using chemoluminescent cross-linking molecules as mechanophores.[30] The result also clearly indicates that covalent bonds in the polymer backbone (including crosslinker) are ruptured during the internal fracturing, and the ruptured polymer strands generate mechanoradicals that is chemically active to induce following chemical reaction.

4.3.2. Kinetics of the color change of Fenton reaction

To observe and understand the ~10s minutes delay of the color change of the Fenton reaction (i.e. ferrous oxidation by generated H_2O_2) in the DN gels, time-laps UV-Vis absorption spectroscopy was carried out. In this preliminary experiment, I used 1.55 mm-thick (1-3/2-0.01) DN gel of IEC-540(S)-standardized dumbbell shape (4 mm-width). On the quantification described in following section (**section 4.3.2**), I used ~3 mm-thick and 10-mm width gels because I found that wider and thicker sample is better for the UV-Vis spectroscopic measurement to reduce the experimental error. Nevertheless, the small sample used in this section was enough to understand the kinetics of the color change. **Figure 4-5a** shows the UV-Vis spectra of the stretched (1-3/2-0.01) DN gel containing

100 μM $(NH_4)_2Fe^{II}(SO_4)_2$ 100 μM XO and 20 mM H_2SO_4 at different time after the stretching. The spectrum of the unstretched gel was also shown. The absorbance value are normalized by thickness (~1.6 mm). A peak at around 440 nm gradually decreased with the time, whereas shoulder at around 580 nm appeared and gradually increased. The former decreasing peak corresponds to the bare XO, and the latter increasing peak corresponds to the [Fe^{3+}-XO] complex.[31] Next, the absorbance values at 440 nm and 580 nm are plotted as a function of time (**Figure 4-5b**). The absorbance values rapidly changed during the initial 15–20 mins and became stable after 25–30 mins, indicating the color reaction was completed in 30 mins.

What the color reaction kinetics is dominated? Taking into account the previous literature,[19] the color reaction progress is divided into four major components, (1) mechanoradical generation; (2) H_2O_2 generation by the mechanoradical; (3) Fe^{2+} oxidation by H_2O_2; and (4) formation of [Fe^{3+}-XO] complex:

(1) ≈R—R≈ —force→ ≈R· ·R≈ mechanoradical generation

(2) H_2O, O_2 —≈R·→ H_2O_2 hydrogen peroxide generation

(3) Fe^{2+} —H_2O_2→ Fe^{3+} ferrous oxidation

(4) Fe^{3+} + XO → [Fe^{3+}-XO] complex formation

Note that step (1) (mechanical bond cleavage) must happen at the moment of the stretching. To check which step is rate-limiting, I performed two control experiments. One is that Fe^{3+} ion solution was added into the aqueous solution of Fe^{2+} and XO. As the

result, the color was immediately changed (within seconds or less), indicating step (4) is enough fast process in the overall reaction. The other control experiment was H_2O_2 solution was added into the aqueous solution of Fe^{2+} and XO (resulting H_2O_2 concentration was 12 μM). As shown in **Figure 4-6**, the kinetics of the color reaction is quite similar as that observed in the stretched DN gel. The result implies that step (3) is slower than step (1) and (2). Therefore, I concluded that ferrous oxidation by H_2O_2 in step (3) is the rate-limiting process of the overall reaction, even though the kinetics of step (2) is still less-known. The conclusion tells us the limitation of this visualization method using the Fenton reaction. That is, we may not be able to observe the degree of chain scission in short time scale (e.g. seconds or less) by using this method, which might be of benefit to the analysis of inhomogeneous deformation such as deformation around crack tip. In addition, as the reacted small molecules can easily diffuse in the hydrogels, local measurement (e.g. mm-scale or less) may be difficult with this method. Nevertheless, the method using Fenton reaction is useful to quantify the degree of chain scission under homogeneous deformation discussed in the following sections.

4.3.3. Concentration of the ferrous oxidation in various stretched DN and SN gels

In this section, the concentration of the ferrous oxidation is quantified by using UV-Vis absorption spectroscopy. Before characterizing the UV-Vis spectra of the stretched DN gels, a calibration curve was made to determine the concentration of Fe^{3+} from UV-Vis spectra. The UV-Vis spectra of 0−40 μM $NH_4Fe^{III}(SO_4)_2$ (as an Fe^{3+} source), 100 μM $(NH_4)_2Fe^{II}(SO_4)_2$, 100 μM XO and 20 mM H_2SO_4 are shown in **Figure 4-7a**. Then a calibration curve on the plot of the ratio of the absorbance at 580 and 440 nm, A_{580}/A_{440} as a function of the Fe^{3+} concentration was produced. In this analysis for characterizing

the UV-Vis spectrum of a gel, not the absolute absorbance value but absorbance ratio was used in order to reduce the experimental error from thickness of the gels. **Figure 4-8** shows the calibration curve. The curve was not linear because absorbance ratio was used. The curve was well fitted by second-order fitting. The calibration fitting is used for the following quantification.

Next, UV-Vis spectra of stretched (1-4/4-0.01) DN gel was measured and quantified. In the **section 4.3.1**, we have confirmed that color change in the necked region is much more significant than that in the un-necked region where internal fracturing also occurs. Here, I obtained the UV-Vis spectra of the unstretched DN gel ($\varepsilon = 0.0$), stretched but un-necked DN gel ($\varepsilon = 1.6$), and stretched and necked DN gel ($\varepsilon = 4.7$) (**Figure 4-7b**). The shapes of these spectra correspond to those of calibration spectra (**Figure 4-7a**), indicating desired reaction occurred. I confirmed that the ferrous oxidation also occurred in the un-necked DN gel ($\varepsilon = 1.6$) because the absorbances at around 440 and 580 nm decreased and increased, respectively. By using the calibration curve, the concentrations of the generated Fe^{3+} in the un-necked DN gel ($\varepsilon = 1.6$) and the necked DN gel ($\varepsilon = 4.7$) were characterized as 7.2 and 25.5 μM, respectively (**Figure 4-9**).

As control experiments, same experiments for (1-4) PNaAMPS SN gel and (4-0.01) PAAm SN gel were also carried out. In contrast to the DN gels, almost no ferrous oxidation was detected in the stretched single-network (SN) gels (**Figures 4-7c, 7d and 4-9**). The concentration of them is less than few μM which is approximately detection limit of the current experimental condition. These results show that the DN gel is a unique hydrogel to generate abundant mechanoradicals by deformation.

4.3.4. Concentration of the mechanoradicals

As shown in the previous section, the concentration of ferrous oxidation in stretched DN gels is determined as high as 25 μM which is much higher than that in SN gels. The question here is that how many mechanoradicals are generated in the gels. To solve this question, conventional low-molecular radical generators were used as a model experiment to oxidize ferrous ions. Because the decomposed ratio of the radical generators is measurable, the quantitative analysis can be performed.

Before discussing the model radical generators, I consider which covalent bonds are broken in the DN gel in order to select the appropriate model radical generators (**Figure 4-10**). In DN gels, the brittle first network is fractured under the deformation.[2,10] In this work, PNaAMPS network crosslinked with MBAA was used for the first network. When this PNaAMPS network is mechanically broken, the C−C bond of the PNaAMPS main chain and/or the any bonds on the MBAA crosslinker should be broken because these bonds are directly stressed by the mechanical stretching (**Figure 4-10**). In the former case (main chain rupture), a pair of carbon-centered radical should be generated (**Figure 4-10a**). In the latter case (crosslinker rupture), a weakest bond is expected to be broken. In a previous paper of computational study based on density functional theory (DFT) with constrained geometry optimization calculation, the authors have concluded that α-C−C bond (C−C bond on $-CH_2-CONH-$) is mechanically weakest bond in diglycine because the C−N bond in the amide bond has considerable double-bond character which weaken the opposite α-C−C bond.[32] Given such consideration, I assumed that α-C−C bond is broken to generate a pair of radicals when the MBAA crosslinker was broken (**Figure 4-10b**).

As the models of the normal-carbon-radical generators, thermoresponsive azo-

type radical initiators V-50, VA-044 and VA-086 were selected. As the model of the radical generators by α-C−C bond cleavage, a photoresponsive Norrish type I radical initiator I-2959 was selected. The cleavage reactions are shown in **Figure 4-11**.[25–27] Excitation conditions were chosen as heating for 10 hours at 56, 44 and 86 ℃ for V-50, VA-044 and VA-086, respectively, and UV light (314 nm) irradiation for 90 seconds for I-2959. At these conditions, approximately half of the feed azo-type radical generators and all I-2959 were decomposed. The actual decomposition ratios r in 20 mM H_2SO_4 is r = 0.50, 0.41, 0.44 and 1.0 that are determined by UV-Vis spectroscopy (**Figure 4-12**). Therefore, the concentration of the generated radicals from the model radical generators can be calculated as:

$$[R\cdot] = 2\, C_0\, r \qquad (4.2)$$

where C_0 is the feed concentration of the radical generators and the factor of 2 means that two radicals are generated from one radical generator. **Figure 4-13** shows the UV-Vis spectra of the XO and Fe^{3+} aqueous solution added with each initiator with different concentration after excitation (heating or UV-irradiation). The spectra shape was identical with the calibration curve added with Fe^{3+} (**Figure 4-7**), indicating Fe^{3+} oxidation occurred by the radicals. Even after heating or UV-irradiation, almost no oxidation was observed when no initiator was added. Note that a little oxidation was observed when the solution was heated at 86℃ in the VA-086 data set, which is possibly due to oxidation by oxygen in air accelerated by the high temperature. **Figure 4-14a** shows the oxidized ferrous ion concentration $[Fe^{3+}]$ as a function of the generated radical concentration from the model radical generators $[R\cdot]$. It is found that $[Fe^{3+}]$ is proportional to $[R\cdot]$ when using same radical generator, and the slopes are varied around 1−3 that are not identical among the radical generators. The difference may originate from reactivity of the generated

radicals, recombination of the radicals (that relates to initiator efficiency) and/or excitation condition difference such as temperature. In addition, it should be noted that the slopes of more than one mean one radical oxidized more than one ferrous ion. The fact implies the radical reaction pathway is more complicated than stoichiometric reaction, for example, radical OH· that is possibly generated during Fenton reaction (ferrous oxidation by H_2O_2) may react with water and/or Fe^{2+}.[24] In summary, it is difficult to determine the exact mechanoradical concentration from the ferrous oxidation. Nonetheless, it can be concluded from these results that the Fe^{3+} concentration is in the same order of the generated radicals within numerical factor (**Figure 4-14b**). Therefore, the order of the mechanoradicals generated in the necked (1-4/4-0.01) DN gels is determined as ~10^{-5} M, whereas that in the stretched SN gels is ~10^{-6} M or less. A recent report demonstrated a fluorescence change in mechanically compressed polyethylene glycol (PEG) single-network hydrogels to detect a covalent bond scission.[33] Although the actual concentration of the mechanoradicals was not determined in the report, the activated fluorescent concentration, 10^{-8}–10^{-7} M, was approximately consistent with my result for SN gels (10^{-6} M or less).

4.3.5. Quantitative comparison of the chemical evidence to previous mechanical evidence of the internal fracturing

When the same chemical component is used in the first network, the concentration of ferrous oxidation should be proportional to the concentration of mechanoradicals because same mechanoradical is expected to be generated. Since the concentration of the mechanoradicals directly correlates with the degree of covalent bond scission in the stretched DN gel, the concentration of the ferrous oxidation correlates with the degree of

strand scission. In previous researches, many researchers have characterized mechanical hysteresis on cyclic tensile test to estimate the degree of the strand scission in DN gel.[8,11,12] In this section, the concentration of the ferrous oxidation is quantitatively compared to the mechanical hysteresis. Here I characterized the generated Fe^{3+} concentration in (1-4/4-0.01) DN gel stretched to various strains (ε = 0, 1.0, 1.6, 4.7, 6.0) and in various DN gels ((1-x_1/2-0.01) DN gels; x_1 = 1.0–3.0 mol%) stretched to the strain at which necking was completed in all narrow part of the dumbbell shaped gel. The cyclic stress−strain curves to characterize the mechanical hysteresis are shown in **Figures 4-15 and 4-16**. **Figure 4-17** summarizes the generated Fe^{3+} concentration as a function of the mechanical hysteresis area for various DN and SN gels. The data points are dropped on one master curve that is virtually straight line through the (0,0) point. In contrast, the Fe^{3+} concentration did not exhibit good correlation with either input stress or strain (**Figure 4-18**). Therefore, in mechanical point of view, the DN gels must exhibit large (irreversible) hysteresis to generate large amount of chain scissions and mechanoradicals, which agrees with the previous consideration for the DN gels[8,11,12] and a research on multiple-network elastomers in which bond breaking was observed by a chemiluminescence mechanophore.[30] The insight supports my statement, that is, DN gel is a unique hydrogel to generate large amount of mechanoradicals because most of chemically crosslinked hydrogels do not show mechanical hysteresis, except for the hysteresis due to viscoelastic dissipation due to polymer chain friction/flow or transient/dynamic bonds.

Here, the physical meaning of the correlation between Fe^{3+} concentration and mechanical hysteresis is discussed. From linear fitting in **Figure 4-17**, the slope and its inverse were obtained as:

$$\text{slope} = [Fe^{3+}]/U_{hys} = 10\ (\mu\text{mol L}^{-1} / \text{MJ m}^{-3}) = 10^{-8}\ \text{mol J}^{-1} \qquad (4.3)$$

$$(\text{slope})^{-1} = 10^8 \text{ J mol}^{-1} \quad (4.4)$$

where $[Fe^{3+}]$ and U_{hys} are the Fe^{3+} concentration and mechanical hysteresis, respectively. Note that the mechanical hysteresis obtained from stress−strain curve is the dissipated energy in unit gel volume (J m^{-3}).[8,11,30] Given the Fe^{3+} concentration is in the same order of the mechanoradical concentration, the inverse of slope indicates that ~10^8 J of energy was dissipated when one mole polymer strands were ruptured.

Theoretically, the dissipated energy per mole of strands of the first network was estimated based on the consideration reported by Lake and Thomas.[34] According to their paper that explains a model of the fracture energy (i.e. crack resistance) of crosslinked network polymers, the mechanical energy required to break one polymer strand in the network, U_{strand}, is:

$$U_{strand} = N_b U_b \quad (4.5)$$

where N_b and U_b are the number of covalent bonds (e.g. C−C bonds) in the backbone of the polymer strands and the mechanical energy required to break one covalent bond, respectively. The N_b is estimated by the total number density of covalent bonds of main chain divided by the number density of strands. Assuming all feed monomers were incorporated in the elastic effective strands, the total number density of covalent bonds at the preparation state of the first network is defined as $2C_1$, where C_1 is the feed monomer concentration (1.0 M) and the factor of 2 means one repeat unit of monomer contains two C−C bonds in backbone. To estimate the average number density of strands in unit volume, general rubber elastic theory based on affine network model was applied. According to the theory,[35] the Young's modulus, E, is determined as:

$$E = 3\nu k_B T \quad (4.6)$$

where ν, k_B and T are the number density of the network strands, Boltzmann constant and

absolute temperature, respectively. Therefore, average N_b of the first network is calculated as:

$$N_{b,1} = 2C_1 \nu_1^{-1} = 6C_1 k_B T E_{1,as\text{-}p}^{-1} \quad (4.7)$$

The elastic moduli $E_{1,as\text{-}p}$ for the first networks at their preparation state were characterized as 9−26 kPa, depending on the crosslinker concentration (**Figure 4-19** and **Table 4-2**). Therefore, average N_1 is estimated to be in the range of 500–1800 (**Table 4-2**). Note that the value is much (~10-times or more) larger than the $N_{b,1}$ estimated from the feed crosslinker ratios to the monomer (x_1 = 1.0−4.0%; hence $N_{b,1}$ = 25−100), which may be due to the crosslinking reaction is not ideally efficient. Bond dissociation energy D_b is typically used as a represent of U_b as the first approximation. However, some papers including the original paper by Lake and Thomas suggest that U_b (the "mechanical" energy required to break one covalent bond) is 15–30% of the bond dissociation energy D_b.[34,36–38] Therefore, I assumed a factor of one-fourth and D_b is the bond dissociation energy of C−C bond (approximately 350 kJ mol^{-1}):

$$U_b = (1/4)D_b = 88 \text{ kJ mol}^{-1} \quad (4.8)$$

Consequently, U_{strand} was approximately obtained as:

$$U_{strand} = N_b U_b = (0.5\text{−}1.5) \times 10^8 \text{ J mol}^{-1} \approx 10^8 \text{ J mol}^{-1} \quad (4.9)$$

Even though the calculations above are rough estimation, the obtained result corresponds well with the experimental result from the slope in **Figure 4-17** that ~10^8 J of energy was dissipated when 1 mole polymer strands were ruptured.

From the other aspect, the fraction of the broken strands in the total first network strands can be estimated. The fraction of the broken strands estimated by the chemical ferrous oxidation, Φ_c, is calculated by:

$$\Phi_c = \nu_{broken}/\nu_{1,DN} \quad (4.10)$$

where ν_{broken} is the number density of the broken strands per unit volume in DN gel after stretched, and $\nu_{1,DN}$ is the number density of the total first network strands per unit volume in DN gel before stretching. According to the affine network theory shown above, $\nu_{1,DN}$ is calculated as:

$$\nu_{1,DN} = \nu_{1,as\text{-}p} (V_{DN}/V_0)^{-1} = E_{1,as\text{-}p} (3k_BT)^{-1} (t_{DN}/t_0)^{-3} \qquad (4.11)$$

where $\nu_{1,as\text{-}p}$ and $E_{1,as\text{-}p}$ are the number density of strands and elastic modulus of the first network at the preparation state, respectively, and $V_{DN}/V_0 = (t_{DN}/t_0)^3$ is the volumetric swelling ratio of the first network from the as-prepared state of the first network to the swollen state of the first network in the DN gel (**Table 4-3**). On the other hand, here I assumed that the ν_{broken} corresponds to the concentration of generated Fe^{3+}:

$$\nu_{broken} \approx [Fe^{3+}] \qquad (4.12)$$

Note that it is order estimation so that there may be numerical prefactor. Therefore, the fraction of the broken strands is approximately calculated as:

$$\Phi_c = \nu_{broken}/\nu_{1,DN} \approx 3k_BT\, E_{1,as\text{-}p}^{-1} (t_{DN}/t_0)^3 [Fe^{3+}] \qquad (4.13)$$

The $\nu_{1,DN}$, ν_{broken} and Φ_c are summarized in **Table 4-4**. For (1-4/4-0.01) DN gel, ~5% and ~16% of the first network chains are fractured at $\varepsilon = 1.6$ (un-necked) and $\varepsilon = 4.7$ (necked), respectively. Even though it is rough estimation, approximately ~10% of the first network strands is expected to be fractured in the necked region. In addition, the fraction Φ_b obtained from the mechanical hysteresis proposed by Nakajima *et al*. is also shown in the Table.[8] Briefly, the fraction Φ_b is the fractured first network chains out of all nominally first network chains, which can be calculated from the mechanical hysteresis and the feed monomer concentration.[8]

$$\Phi_b = U_{hys}/U_{total} = U_{hys}/(2C_{1,DN}U_b) \qquad (4.14)$$

where U_{total} is energy theoretically required for the fracture of all the first network chains

within a unit volume, $C_{1,DN}$ is the concentration of the monomer component of the first network in the DN gel, and U_b is the energy required to break one C−C bond. Note that Nakajima *et al*. used U_b = 347 kJ mol^{-1} that is the bond dissociation energy D_b; however, considering current scientific progress, here I used U_b = 1/4 D_b = 88 kJ mol^{-1} (see discussion above around **equation 4.8**). Therefore, Φ_b value with my calculation is 4 times larger than that estimated by Nakajima *et al.*. As the result, interestingly, even though both methods include rough estimations, Φ_c from chemical evidence gives similar value of Φ_b for each gel (**Table 4-4**).

4.4. Conclusion

By using the Fenton color reaction, in which ferrous ion was oxidized to ferric ions, triggered by mechanoradicals generated at the ends of the mechanically ruptured covalent bonds, I have visualized and (semi-)quantified the degree of internal fracturing in the DN gels. The concentration of the generated Fe^{3+} was well-characterized by UV-visible light absorption spectroscopy of the gels. Radical concentration has found to be in the same order as the generated Fe^{3+} concentration, though the exact quantification of the mechanoradicals is still difficult. Therefore, the concentration of the mechanoradicals in largely-stretched DN gels was defined as ~10^{-5} M (≈ 10^{22} m^{-3}), which is 10 times or more larger than that in SN gels. I also found that ~10^8 J of the mechanical energy are released when 1 mole of strands are ruptured, and ~10s % of the first network strands may be broken when the DN gels are largely deformed up to necking deformation, which are consistent with the consideration based on the mechanical hysteresis and Lake−Thomas theory. The result verified the mechanoradical concentration estimated from the ferrous oxidation.

These findings clearly indicate that the DN gel is the unique hydrogel to generate abundant mechanoradicals by the mechanical stressing, and the mechanoradicals can trigger chemical reaction as demonstrated by the Fenton reaction.

References

(1) J. P. Gong, Y. Katsuyama, T. Kurokawa, Y. Osada, Double-network hydrogels with extremely high mechanical strength. *Adv. Mater.* **15,** 1155–1158 (2003).

(2) J. P. Gong, Why are double network hydrogels so tough? *Soft Matter* **6,** 2583–2590 (2010).

(3) Q. Chen, H. Chen, L. Zhua, J. Zheng, Fundamentals of double network hydrogels. *J. Mater. Chem. B* **3,** 3654–3676 (2015).

(4) C. Creton, M. Ciccotti, Fracture and adhesion of soft materials: a review. *Rep. Prog. Phys.* **79,** 046601 (2016).

(5) C. Creton, 50th anniversary perspective: networks and gels: soft but dynamic and tough. *Macromolecules* **50,** 8297–8316 (2017).

(6) T. Nakajima, Generalization of the sacrificial bond principle for gel and elastomer toughening. *Polym. J.* **49,** 477–485 (2017).

(7) S. Naficy, H. R. Brown, J. M. Razal, G. M. Spinks, P. G. Whitten, Progress toward robust polymer hydrogels. *Aust. J. Chem.* **64,** 1007–1025 (2011).

(8) T. Nakajima, T. Kurokawa, S. Ahmed, W. -L. Wu, J. P. Gong, Characterization of internal fracture process of double network hydrogels under uniaxial elongation. *Soft Matter* **9,** 1955–1966 (2013).

(9) Y. Tanaka, Y. Kawauchi, T. Kurokawa, H. Furukawa, T. Okajima, J. P. Gong, Localized yielding around crack tips of double-network gels. *Macromol. Rapid*

Commun. **29,** 1514–1520 (2008).

(10) Y. -H. Na, Y. Tanaka, Y. Kawauchi, H. Furukawa, T. Sumiyoshi, J. P. Gong, Y. Osada, Necking phenomenon of double-network gels. *Macromolecules* **39,** 4641–4645 (2006).

(11) R. E. Webber, C. Creton, H. R. Brown, J. P. Gong, Large strain hysteresis and Mullins effect of tough double-network hydrogels. *Macromolecules* **40,** 2919–2927 (2007).

(12) T.-T. Mai, T. Matsuda, T. Nakajima, J. P. Gong, K. Urayama, Distinctive characteristics of internal fracture in tough double network hydrogels revealed by various modes of stretching. *Macromolecules*, **51,** 5245–5257 (2018).

(13) T.-T. Mai, T. Matsuda, T. Nakajima, J. P. Gong, K. Urayama, Damage cross-effect and anisotropy in tough double network hydrogels revealed by biaxial stretching, *Soft Matter*, **15,** 3719–3732 (2019).

(14) H. W. Melville, A. J. R. Murray, The ultrasonic degradation of polymers. *Trans. Faraday Soc*. **46,** 996–1009 (1950).

(15) D. J. Angier, W. F. Watson, Mastication of rubber. II. Interpolymerization of natural rubber and neoprene on cold milling. *J. Polym. Sci.* **18,** 129–140 (1955).

(16) J. Sohma, Mechanochemistry of polymers. *Prog. Polym. Sci.* **14,** 451–596 (1989).

(17) G. Kaupp, Mechanochemistry: the varied applications of mechanical bond-breaking. *CrystEngComm*, **11,** 388–403 (2009).

(18) D. J. Angier, W. F. Watson, Mastication. V. Separation and structural investigation of natural rubber–polymethyl methacrylate interpolymers formed by mastication. *J. Polym. Sci*. **25,** 1–18 (1957).

(19) H. T. Baytekin, B. Baytekin, B. A. Grzybowski, Mechanoradicals created in

"polymeric sponges" drive reactions in aqueous media. *Angew. Chem. Int. Ed.* **51,** 3596–3600 (2012).

(20) H. T. Baytekin, B. Baytekin, S. Huda, Z. Yavuz, B. A. Grzybowski, Mechanochemical activation and patterning of an adhesive surface toward nanoparticle deposition. *J. Am. Chem. Soc.* **137,** 1726–1729 (2015).

(21) B. Baytekin, H. T. Baytekin, B. A. Grzybowski, Retrieving and converting energy from polymers: deployable technologies and emerging concepts. *Energy Environ. Sci*. **6,** 3467–3482 (2013).

(22) H. J. H. Fenton, LXXIII.—Oxidation of tartaric acid in presence of iron. *J. Chem. Soc., Trans.* **65,** 899–910 (1894).

(23) W. H. Koppenol, The centennial of the Fenton reaction, *Free Rad. Biol. Med.* **15,** 645–651 (1993).

(24) C. Walling, Fenton's reagent revisited. *Acc. Chem. Res*. **8,** 125–131 (1975).

(25) Y. Yoshida, N. Itoh, Y. Saito, M. Hayakawa, E. Niki, Application of water-soluble radical initiator, 2,2'-azobis-[2-(2-imidazolin-2-yl)propane] dihydrochloride, to a study of oxidative stress. *Free Rad. Res.* **38,** 375–384 (2004).

(26) S. Jockusch, M. S. Landis, B. Freiermuth, N. J. Turro, Photochemistry and photophysics of α-hydroxy ketones. *Macromolecules* **34,** 1619–1626 (2001).

(27) FUJIFILM Wako Pure Chemical Corporation, "Azo polymerization initiators comprehensive catalog" nodate, Retrieved September 2, 2019, from https://labchem-wako.fujifilm.com/us/category/docs/azo%20initiators%20catalog.pdf.

(28) S. Ahmed, T. Nakajima, T. Kurokawa, M. A. Haque, J. P. Gong, Brittle–ductile transition of double network hydrogels: mechanical balance of two networks as the key factor. *Polymer* **55,** 914–923 (2014).

(29) T. Matsuda, T. Nakajima, Y. Fukuda, W. Hong, T. Sakai, T. Kurokawa, U.-I. Chung, J. P. Gong, Yielding criteria of double network hydrogels. *Macromolecules* **49,** 1865–1872 (2016).

(30) E. Ducrot, Y. Chen, M. Bulters, R. P. Sijbesma, C. Creton, Toughening elastomers with sacrificial bonds and watching them break. *Science* **344,** 186–189 (2014).

(31) C. Gay, J. Collins, J. M. Gebicki, Determination of iron in solutions with the ferric–xylenol orange complex. *Anal. Biochem.* **273,** 143–148 (1999).

(32) H. S. Smalø, E. Uggerud, Breaking covalent bonds using mechanical force, which bond breaks? *Mol. Phys.* **111,** 1563–1573 (2013).

(33) K. R. Fitch, A. P. Goodwin, Mechanochemical reaction cascade for sensitive detection of covalent bond breakage in hydrogels. *Chem. Mater*. **26,** 6771–6776 (2014).

(34) G. J. Lake, A. G. Thomas, The strength of highly elastic materials. *Proc. R. Soc. London, Ser. A* **300,** 108–119 (1967).

(35) P. J. Flory, Principles of Polymer Chemistry Ch. 11 (Cornell University Press, 1953).

(36) A. Ghatak, K. Vorvolakos, H. She, D. L. Malotky, M. K. Chaudhury, Interfacial rate processes in adhesion and friction. *J. Phys. Chem. B* **104,** 4018–4030 (2000).

(37) A. M. Saitta, M. L. Klein, Polyethylene under tensil load: Strain energy storage and breaking of linear and knotted alkanes probed by first-principles molecular dynamics calculations. *J. Chem. Phys.* **111,** 9434–9440 (1999).

(38) S. Wang, S. Panyukov, M. Rubinstein, S. L. Craig, Quantitative adjustment to the molecular energy parameter in the Lake–Thomas theory of polymer fracture energy. *Macromolecules* **52,** 2772–2777 (2019).

Figures and Tables

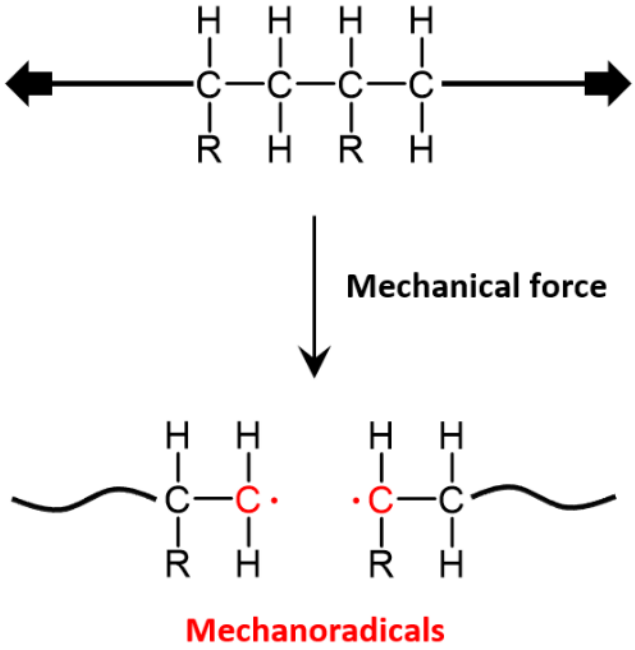

Figure 4-1. An example of mechanoradical generation by cleavage of polymer backbone.

Table 4-1. Abbreviations and structures of the chemical compounds used in this chapter.

Chemical name	Abbreviation	Chemical structure
N,N'-Methylenebisacrylamide	MBAA	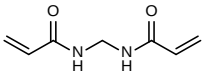
Poly(2-acrylamido-2-methylpropanesulfonic acid) sodium salt	PNaAMPS	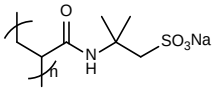
Poly(acrylamide)	PAAm	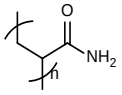
3,3'-Bis[*N,N*-bis(carboxymethyl) aminomethyl]-*o*-cresolsulfonphthalein disodium salt (xylenol orange)	XO	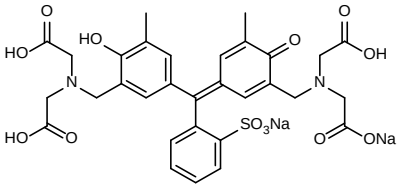
2,2'-Azobis(2-methylpropionamidine)dihydrochloride	V-50	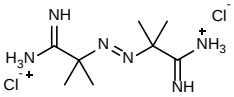
2,2'-Azobis[2-(2-imidazolin-2-yl)propane]dihydrochloride	VA-044	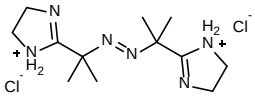
2,2'-Azobis[2-methyl-*N*-(2-hydroxyethyl)propionamide]	VA-086	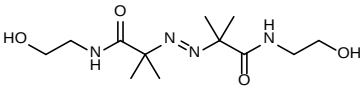
1-[4-(2-Hydroxyethoxy)-phenyl]-2-hydroxy-2-methyl-1-propane-1-one	I-2959	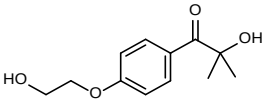

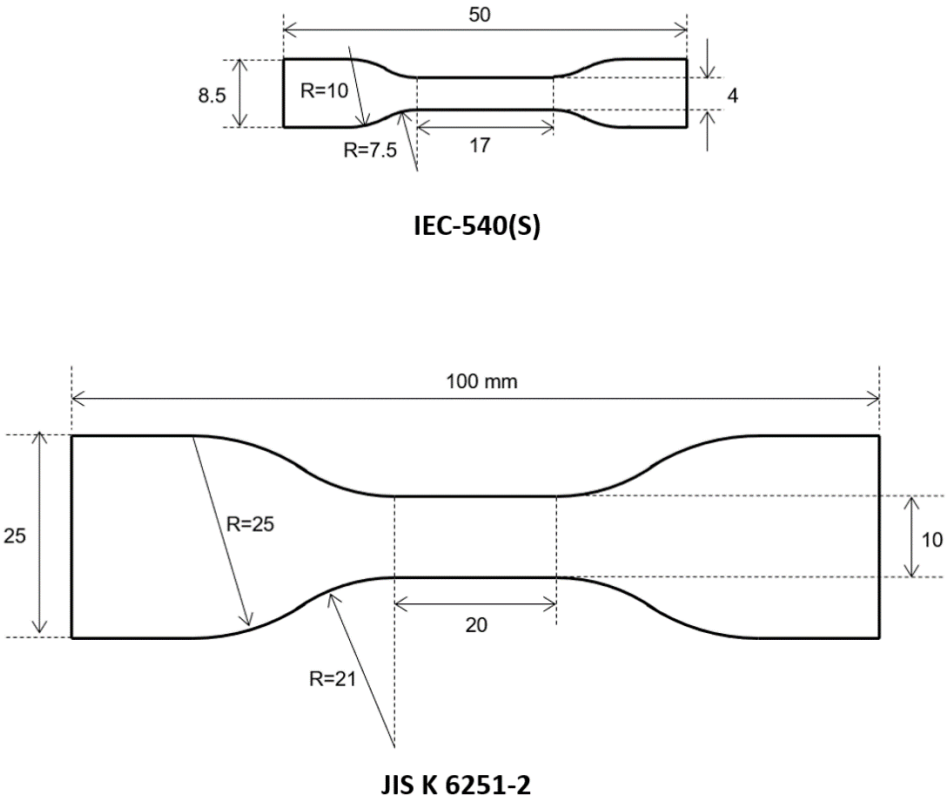

Figure 4-2. Dumbbell shapes (IEC-540(S) and JIS K 6251-2 standards) used in this chapter for tensile test.

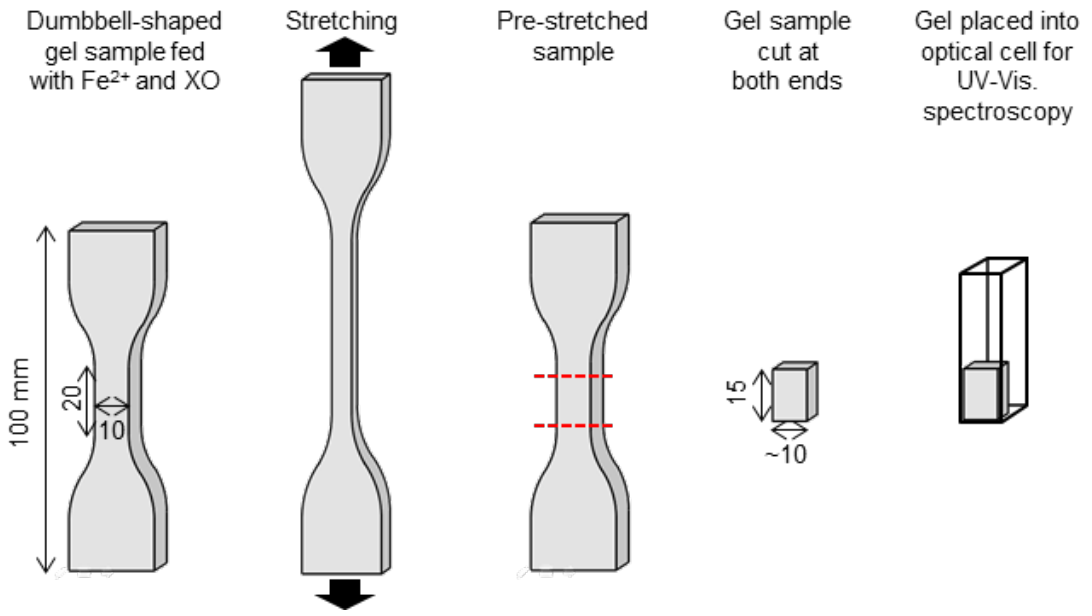

Figure 4-3. Schematic illustration of procedure of UV-Vis light absorption spectroscopy for stretched DN gels. Dumbbell shape of JIS K 6251-2 standard was used. This figure is from *Science* 363, 504–508 (2019). Reprinted with permission from AAAS.

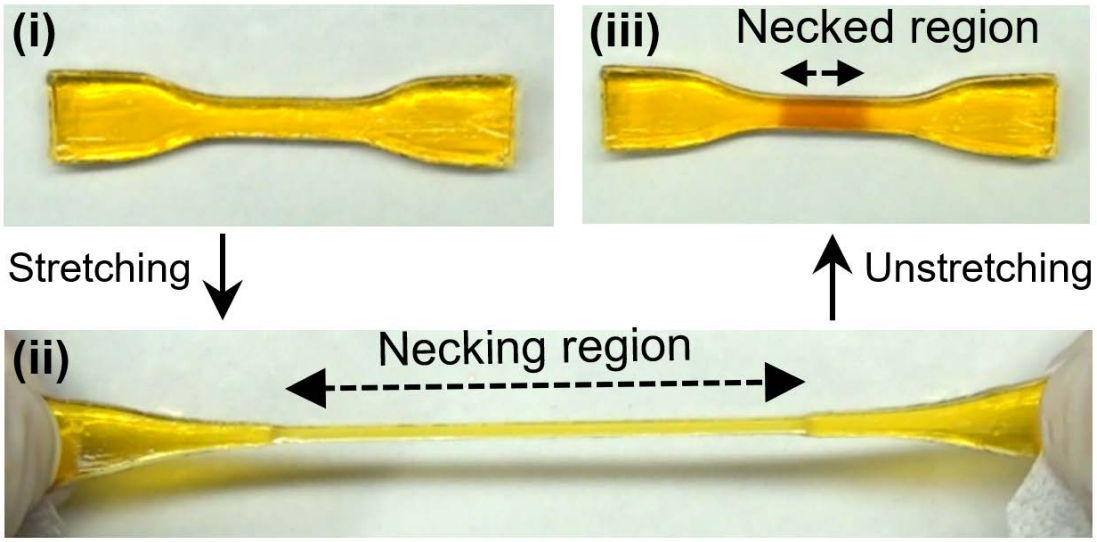

Figure 4-4. Optical images of a (1-4/4-0.01) DN gel fed with 100 μM $(NH_4)_2Fe^{II}(SO_4)_2$ 250 μM XO and 20 mM H_2SO_4 **(i)** before, **(ii)** during, and **(iii)** 30-min after the stretching (strain ε = 3.5). A distinct color change from yellow to brown only in the necked region was visually observed. This figure is from *Science* 363, 504–508 (2019). Reprinted with permission from AAAS.

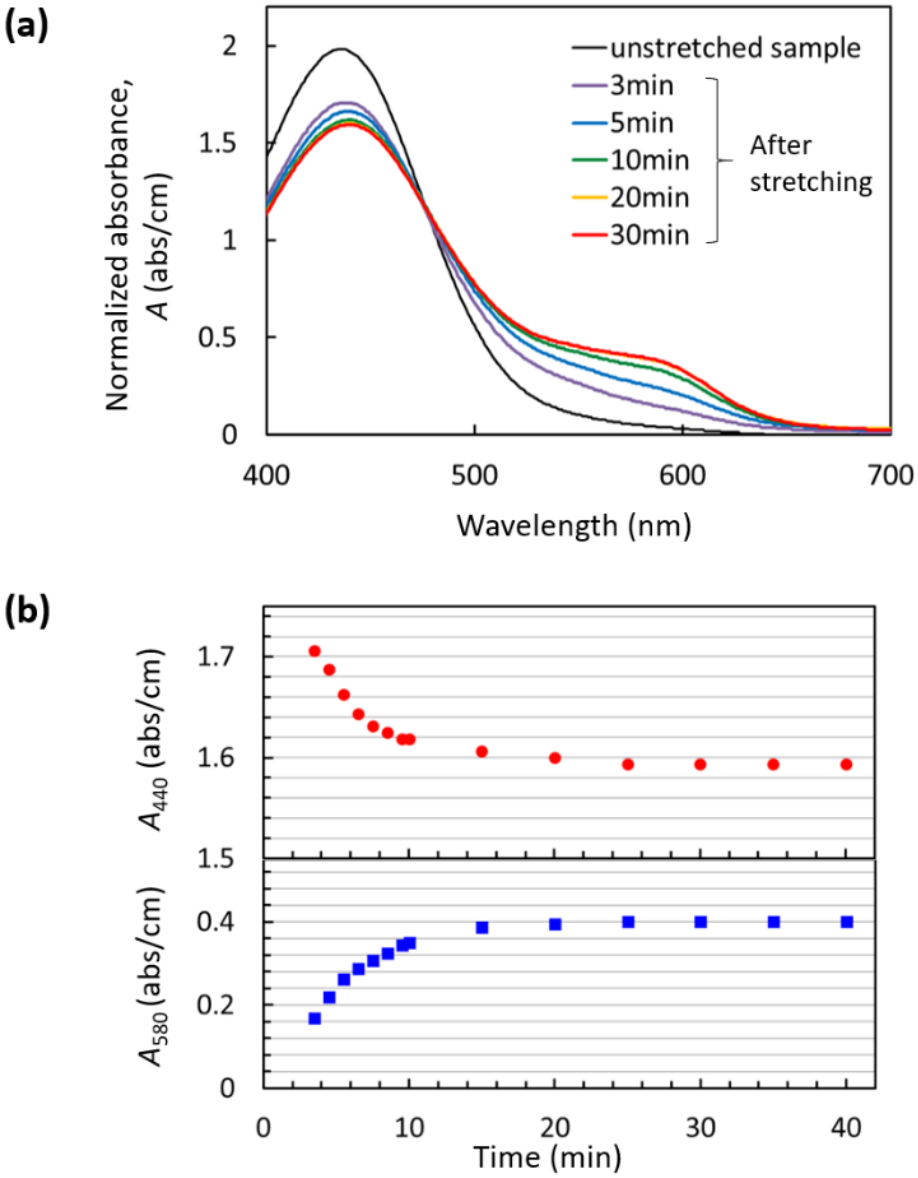

Figure 4-5. Kinetics of Fenton color reaction in a stretched DN gel. **(a)** UV-Vis spectra and **(b)** absorbance value at 440 and 580 nm (A_{440} and A_{580}, respectively) as the function of time after the stretching. Absorbance value was normalized by the gel thickness (~1.6 mm).

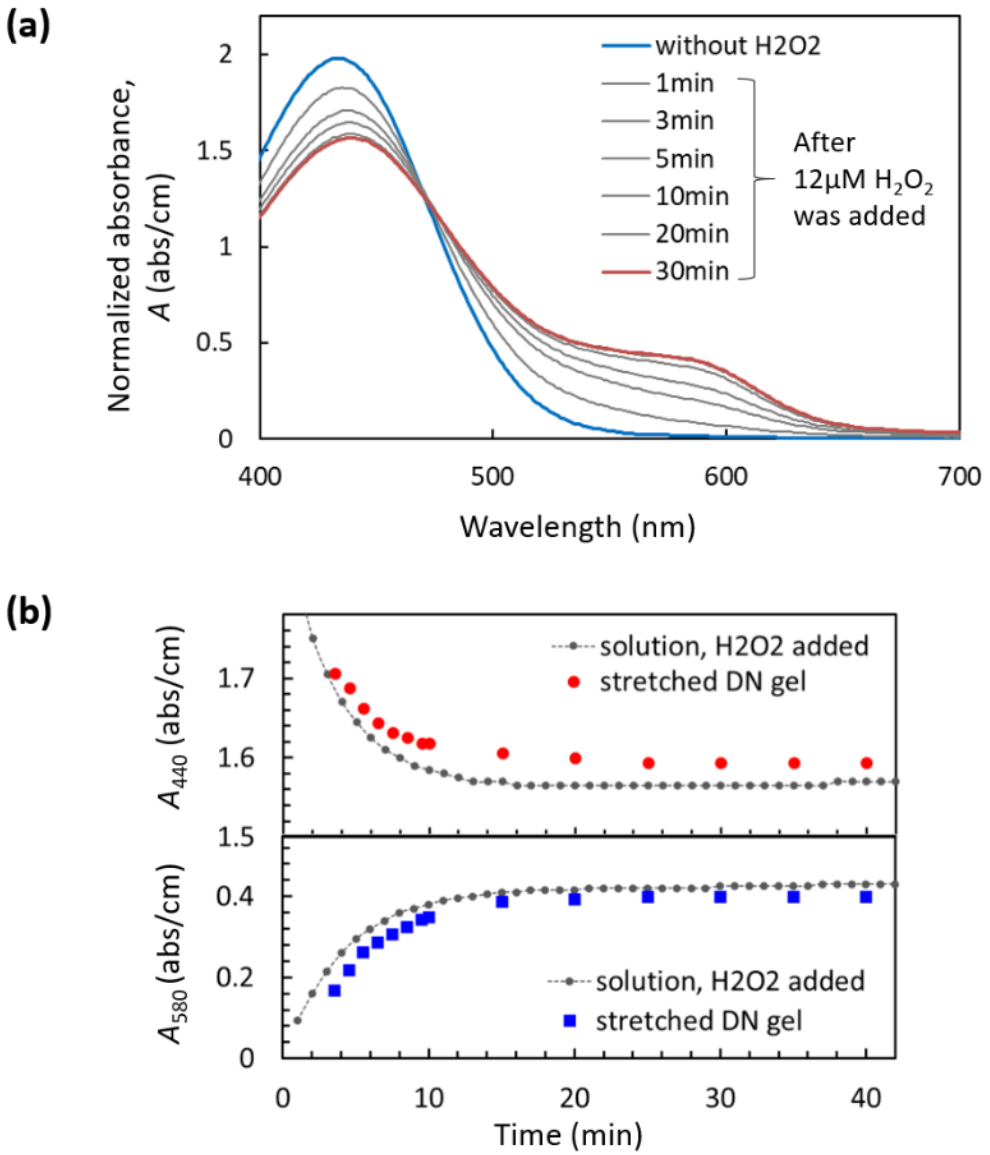

Figure 4-6. Kinetics of Fenton color reaction in a solution. Into the aqueous solution of Fe^{2+} and XO, H_2O_2 solution was added. **(a)** UV-Vis spectra and **(b)** absorbance value at 440 and 580 nm (A_{440} and A_{580}, respectively) as the function of time after the H_2O_2 addition. In (b), the data observed in stretched DN gel shown in **Figure 4-5** are also shown. Absorbance value was normalized by the optical pass length.

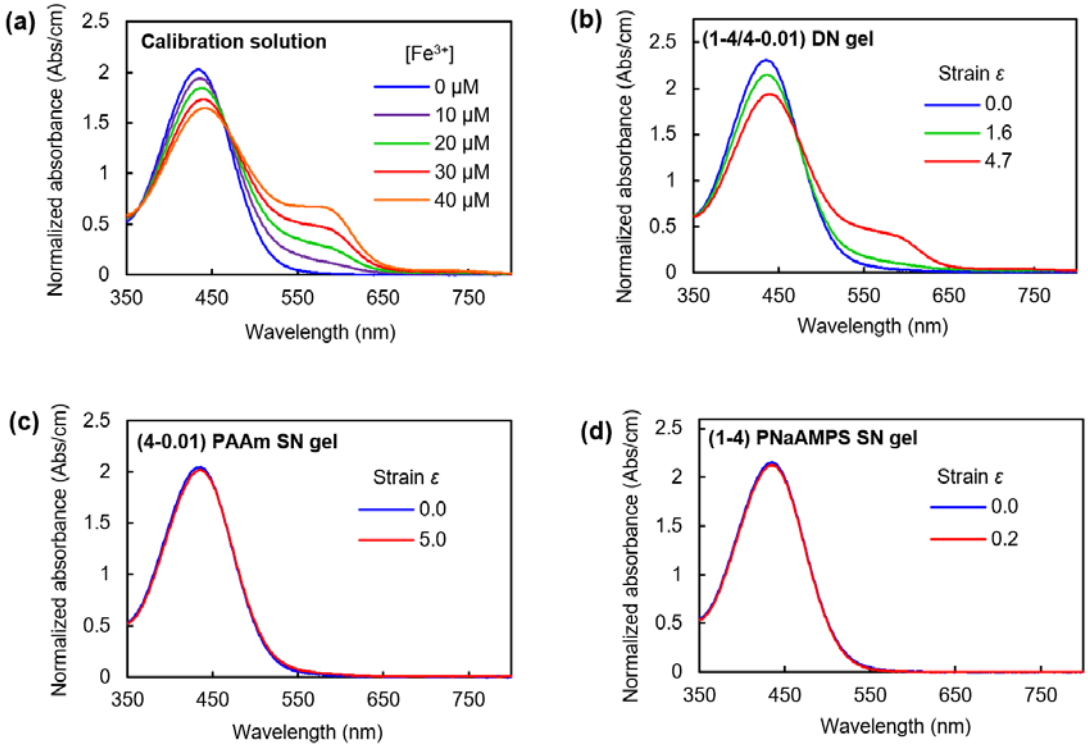

Figure 4-7. (a) UV-Visible light absorption spectra of aqueous calibration solutions loaded with a specified concentration of $NH_4Fe^{III}(SO_4)_2$, 100 μM $(NH_4)_2Fe^{II}(SO_4)_2$, 100 μM XO and 20 mM H_2SO_4. **(b–d)** UV-Visible spectra of unstretched and stretched gels fed with ferrous ions and XO: **(b)** (1-4/4-0.01) DN gel, **(c)** (1-4) PNaAMPS SN gel, and **(d)** (4-0.01) PAAm SN gels. All gels were fed with 100 μM $(NH_4)_2Fe(SO_4)_2$, 100 μM XO and 20 mM H_2SO_4. The peaks at approximately 440 and 580 nm correspond to unbound XO and XO complexed with Fe^{3+}, respectively. Absorbance value was normalized by the optical pass length. This figure is from *Science* 363, 504–508 (2019). Reprinted with permission from AAAS.

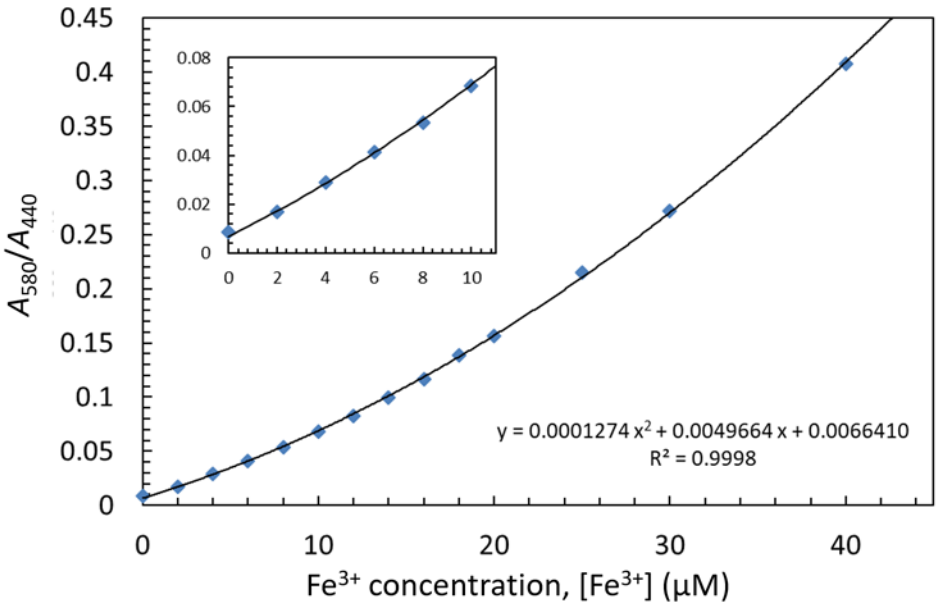

Figure 4-8. Calibration curve to determine the Fe^{3+} concentration from the absorbance value. The data points (blue dots) are obtained from aqueous calibration solutions loaded with a specified concentration of $NH_4Fe^{III}(SO_4)_2$ as well as 100 μM $(NH_4)_2Fe^{II}(SO_4)_2$, 100 μM XO and 20 mM H_2SO_4. Some spectra are shown in **Figure 4-7(a)** as examples. Black curve is the fitted curve by second-order fitting with Microsoft Excel. The inset figure is the expanded view of the low concentration regime where the curve fitted well too.

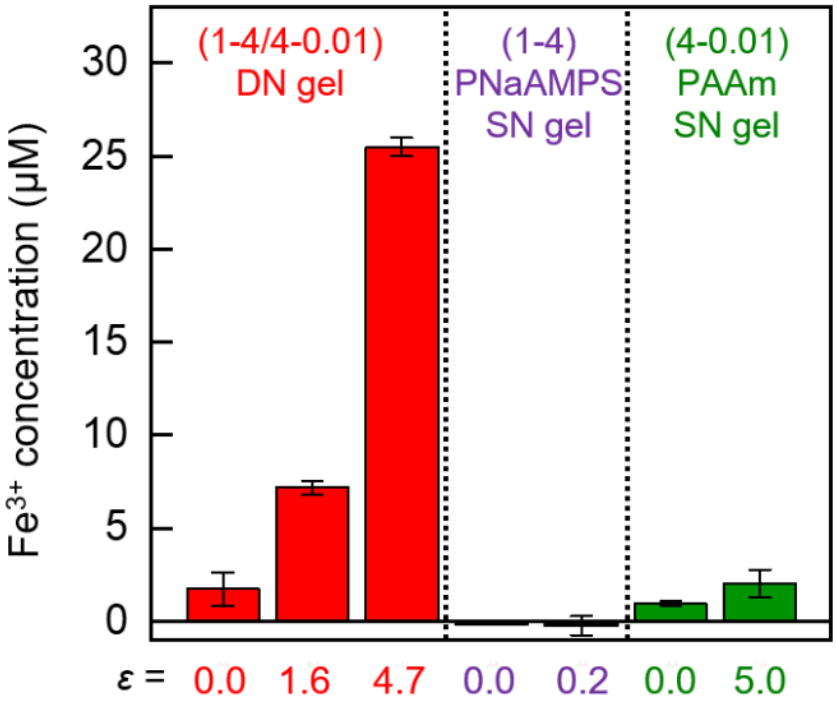

Figure 4-9. Estimated Fe^{3+} concentration from ferrous oxidation induced by mechanoradicals in the stretched and unstretched gels. The error bars represent standard deviations among three measurements. This figure is from *Science* 363, 504–508 (2019). Reprinted with permission from AAAS.

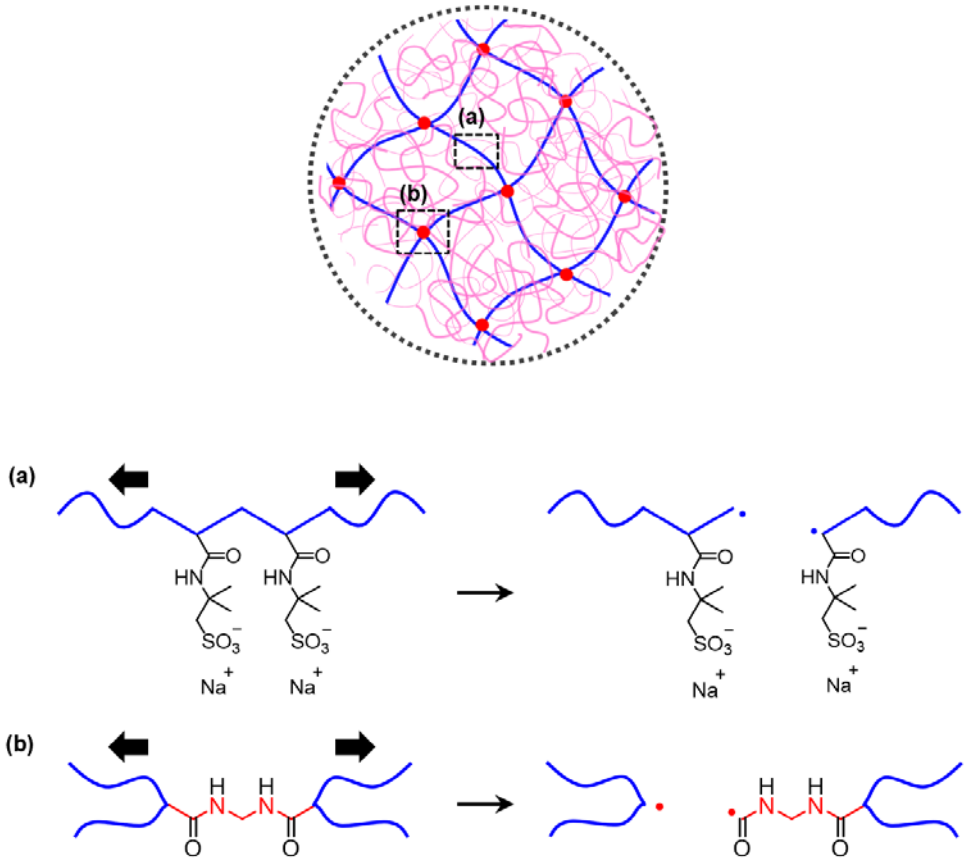

Figure 4-10. Assumed bond cleavages and radical generation in the PNaAMPS first network of a deformed DN gel. The PNaAMPS polymer backbone and the MBAA cross-linker backbone are represented by blue and red colors, respectively. **(a)** The C–C bonds of the PNaAMPS main chains and/or **(b)** the α-C–C bonds of the MBAA cross-linker are expected to break under a mechanical force. The black arrows indicate the direction of the mechanical force to the molecules. This figure is from *Science* 363, 504–508 (2019). Reprinted with permission from AAAS.

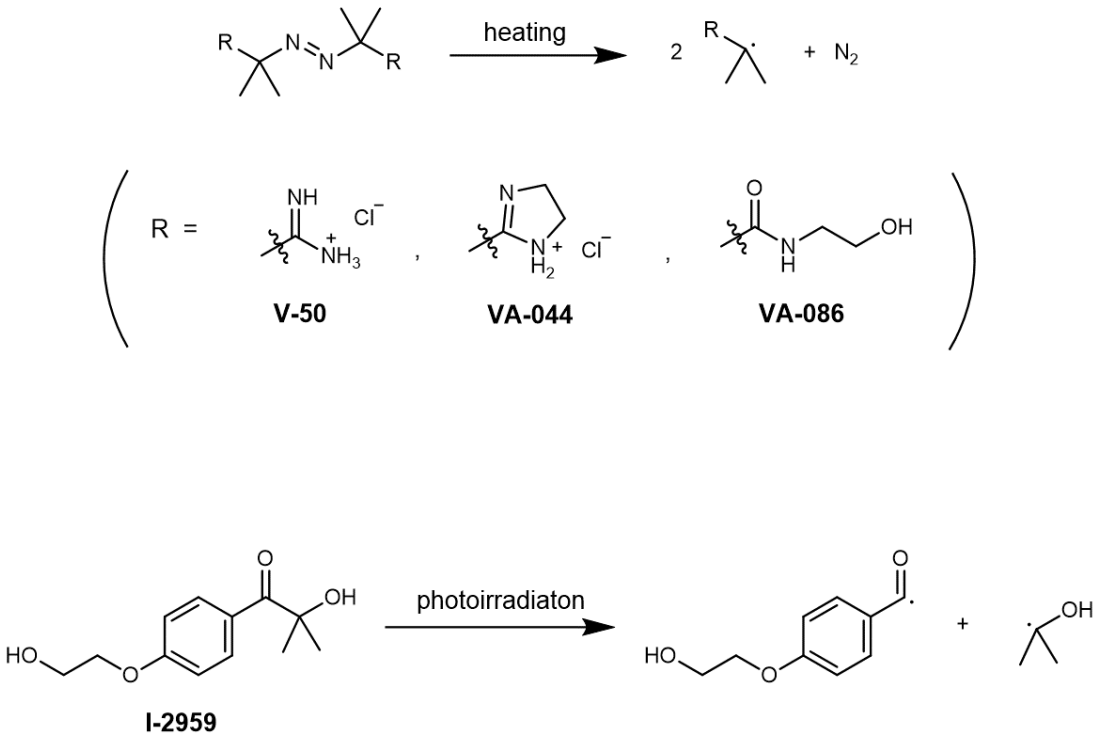

Figure 4-11. Thermal and photo-cleavage reactions of V-50, VA-044, VA-086 and I-2959, which are model compounds for generating certain concentrations of the carbon-centered radicals by scission of the C–C or α-C–C bonds.

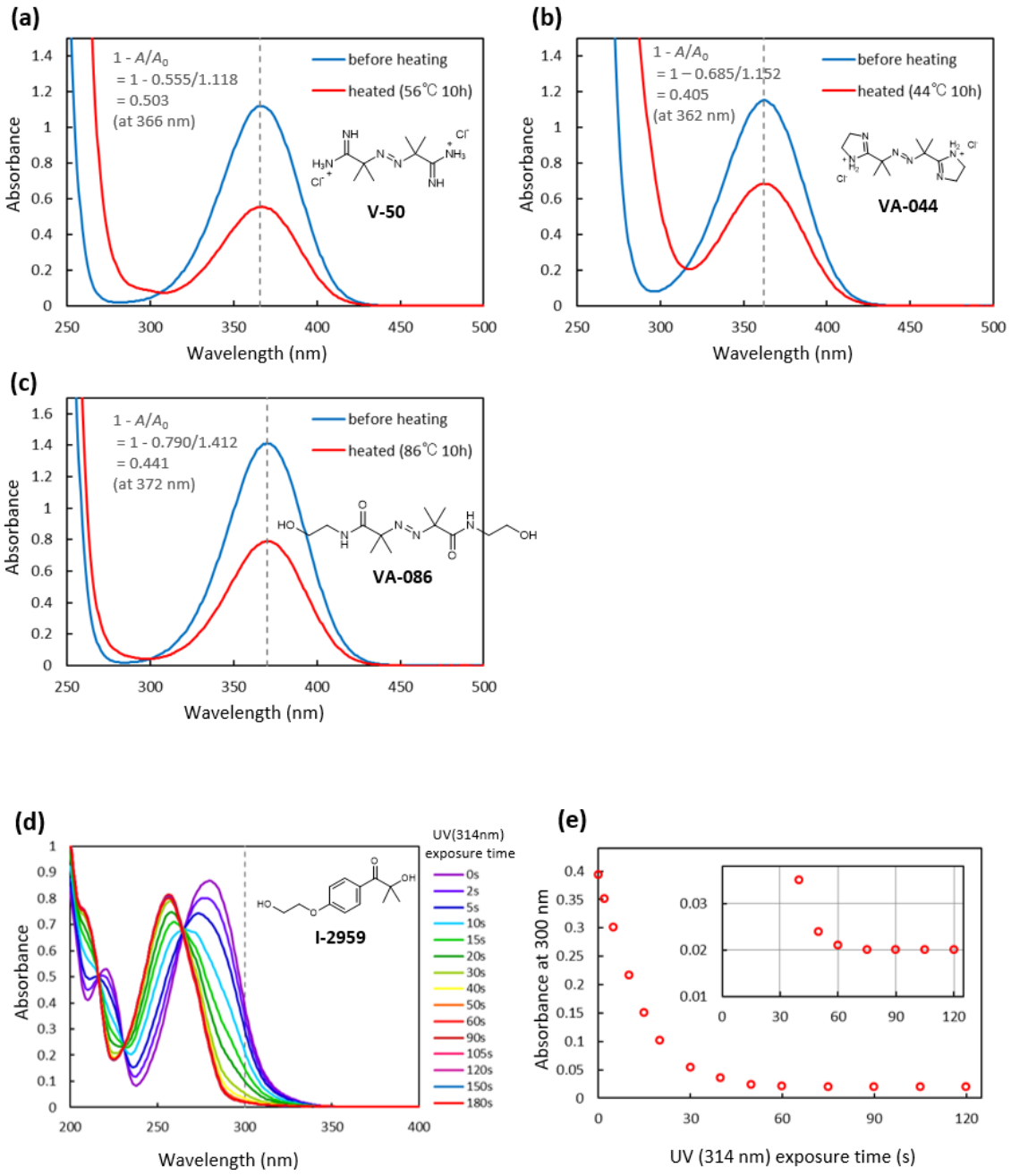

Figure 4-12. (a-d) UV-visible spectra of the aqueous solution of low-molecular radical generators in 20 mM H_2SO_4 before and after excitation to detect the decomposition degree. Note that neither Fe^{2+} nor XO was added, so that the absorption originates in each radical generator. For the azo-type initiator, 50 mM initiator was used. For I-2959, 200 μM initiator was used. **(e)** Absorbance at 300 nm for the I-2959 shown in **d** as the function of UV irradiation time. Relatively short wavelength UV (314 nm) was used. As shown in **e**, the initiator seems to be almost completely decomposed at the time more than 90 seconds.

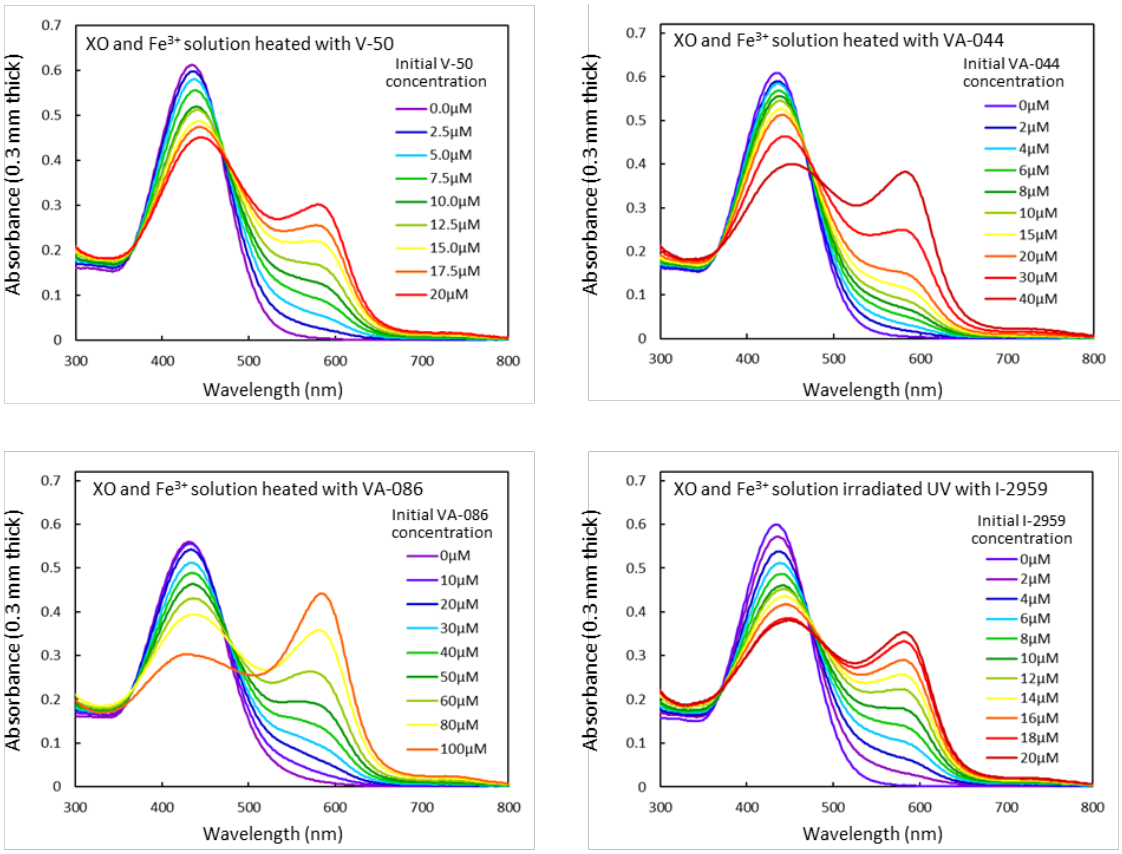

Figure 4-13. UV-Vis spectra of 100 μM $(NH_4)_2Fe^{II}(SO_4)_2$, 100 μM XO and 20 mM H_2SO_4 along with certain concentrations of the low-molecular radical generators after excitation. In all cases, lager amount of Fe^{3+} generation (degreasing the peak at around 440 nm and increasing the peak at around 580 nm) was observed at larger concentration of generated radical.

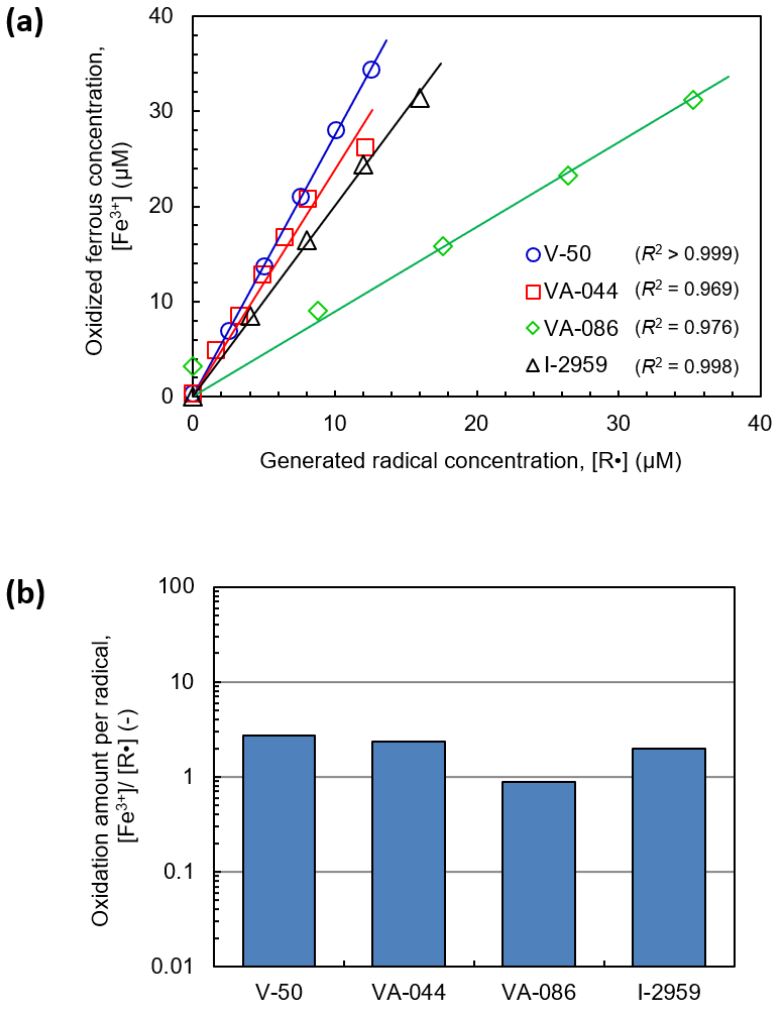

Figure 4-14. (a) The concentrations of generated Fe^{3+} ions as a function of the concentration of generated radicals. In this experiment, 100 μM $(NH_4)_2Fe(SO_4)_2$, 100 μM XO, 20 mM H_2SO_4 and 0–40 μM of radical generators were used. The generated radical concentration, [R·], was determined as $[R\cdot] = 2C_0r$, where C_0 is feed concentration of radical generator and r is the decomposition ratio determined from **Figure 4-12** (see also main text). The straight lines represent the fitted curves through the origin. The generated Fe^{3+} concentration is linearly proportional to the radical concentration in each radical generator system. **(b)** The number of generated Fe^{3+} ions per radical, as obtained from the slopes of the fitted curves in (a). The proportional constants, which indicate the number of Fe^{2+} ions oxidized per a radical, vary only within the order of unity for the different radicals. This figure is from *Science* 363, 504–508 (2019). Reprinted with permission from AAAS.

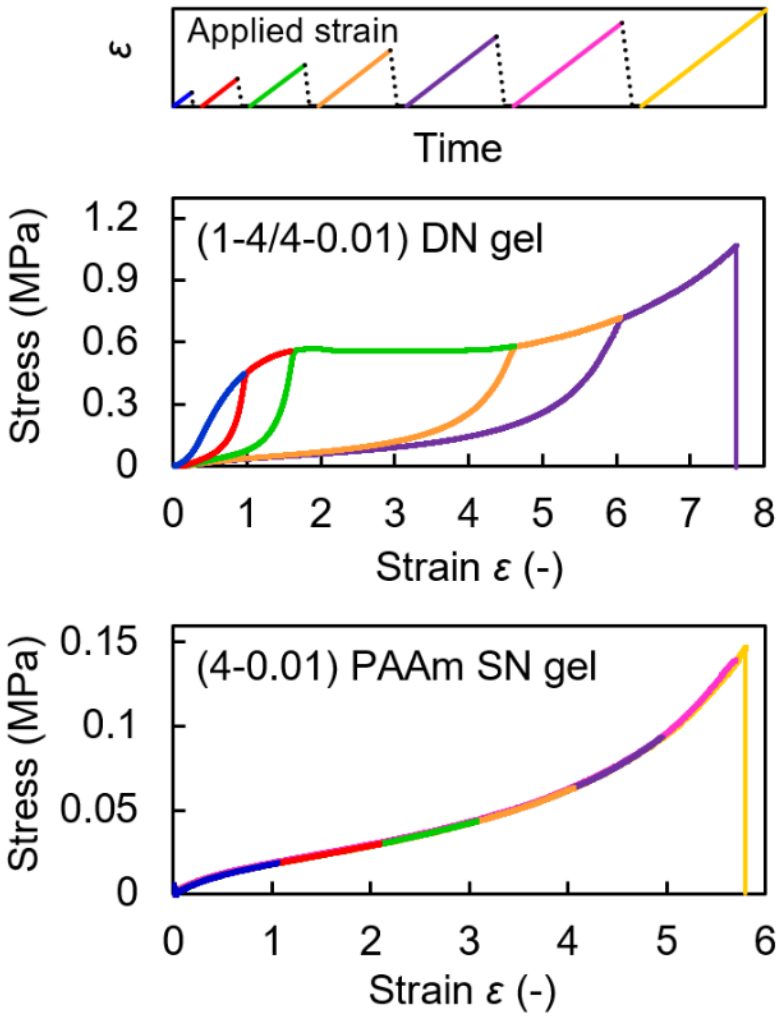

Figure 4-15. Cyclic tensile loading curves of (1-4/4-0.01) DN gels and (4-0.01) PAAm SN gels. This figure is from *Science* 363, 504–508 (2019). Reprinted with permission from AAAS.

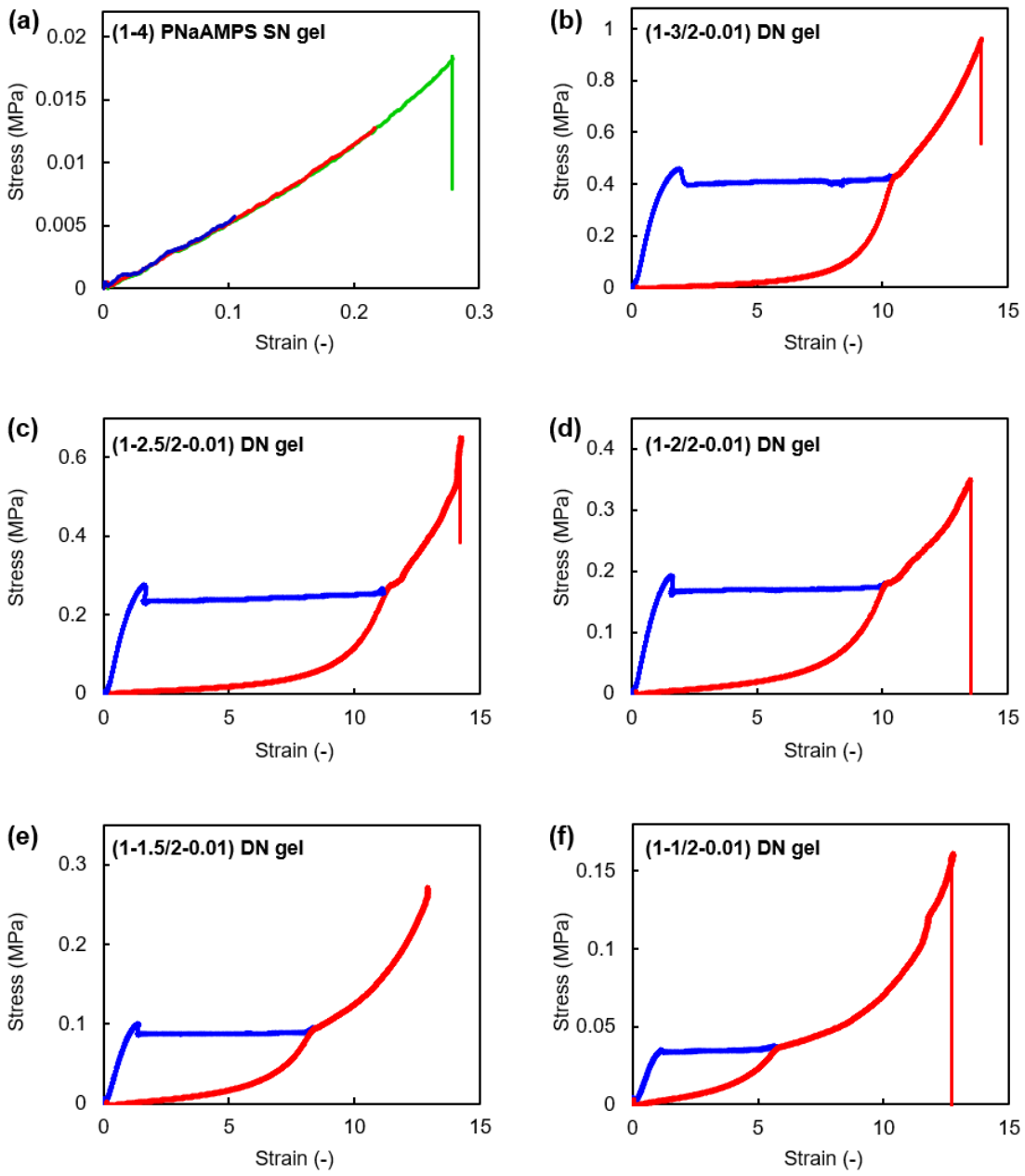

Figure 4-16. Cyclic tensile loading curves of (1-4) PNaAMPS SN gel and (1-x_1/2-0.01) DN gels (x_1 = 1, 1.5, 2, 2.5, 3). For the DN gels, each gel was stretched up to the strain where necking of the sample was completed in the all narrow part of the dumbbell-shaped sample. This figure is from *Science* 363, 504–508 (2019). Reprinted with permission from AAAS.

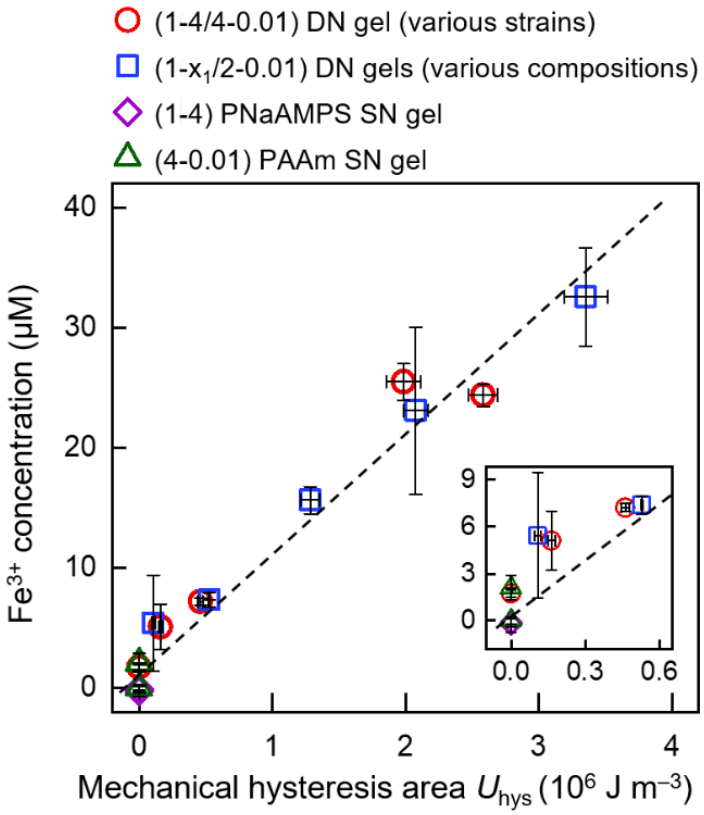

Figure 4-17. Correlation between the mechanical hysteresis areas and the Fe^{3+} concentrations in the stretched gels: (1-4/4-0.01) DN gels stretched to various strains (ε = 0, 1.0, 1.6, 4.7, 6.0); (1-x_1/2-0.01)DN gels of various compositions (x_1 = 1, 1.5, 2, 2.5, 3) stretched until the completion of necking; the (1-4) PNaAMPS SN gel (ε = 0, 0.2); and the (4-0.01) PAAm SN gel (ε = 0, 5.0). The dashed line is a guide for the eye. The error bars represent standard deviations among three measurements. This figure is from *Science* 363, 504–508 (2019). Reprinted with permission from AAAS. The gel codes were modified to fit to this dissertation.

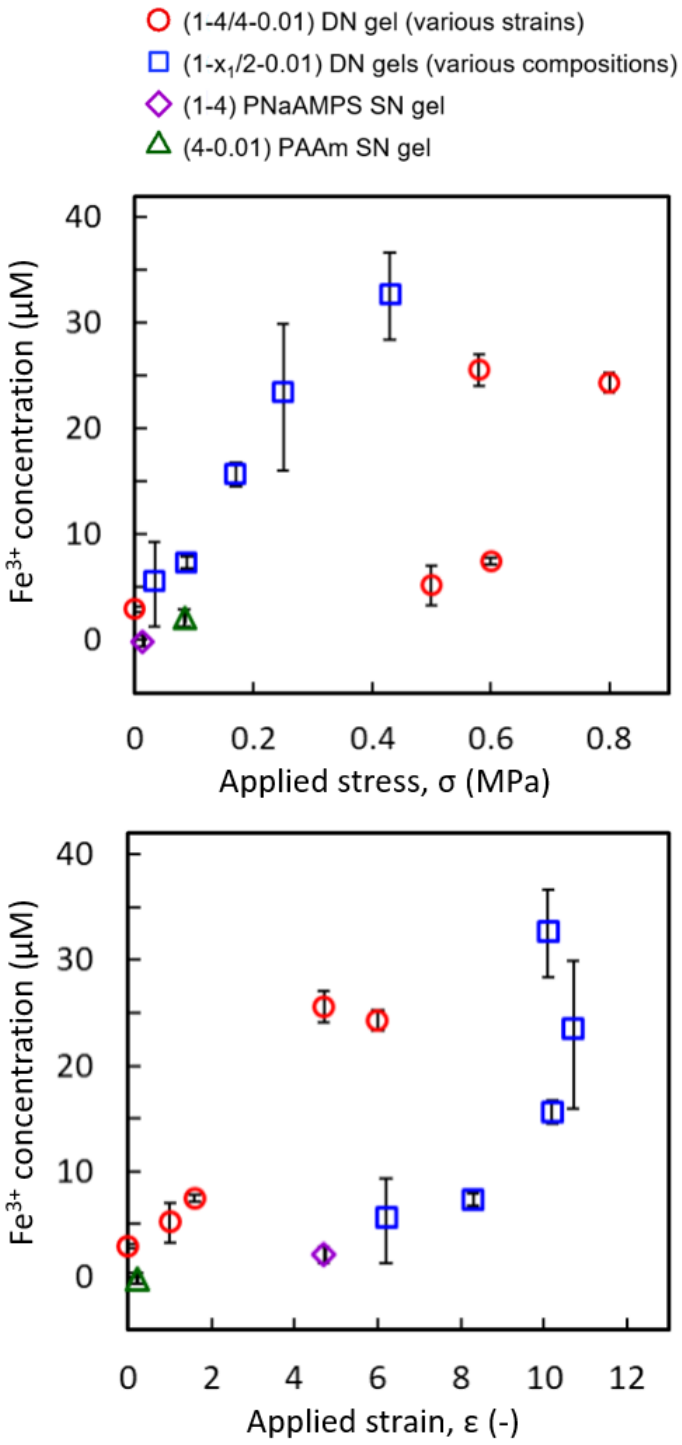

Figure 4-18. Correlation between the applied stress or strains and the generated Fe^{3+} concentrations in the stretched gels, corresponding to **Figure 4-17**. The error bars represent standard deviations among three measurements.

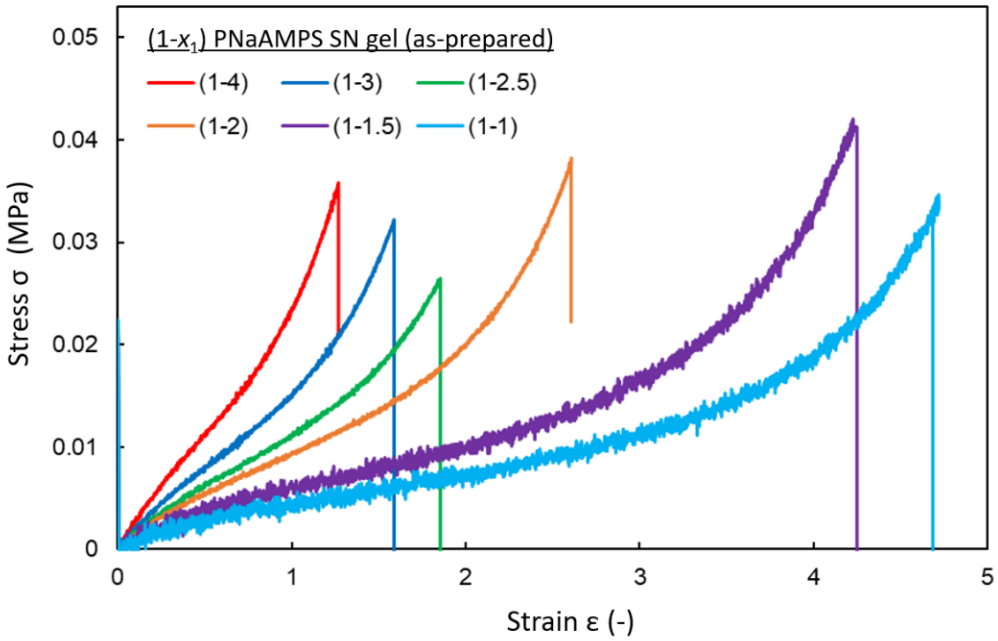

Figure 4-19. Stress–strain curves of (1-x_1) PNaAMPS SN gel at their as-prepared state. Strain were measured by video extensometer. JIS-K 6251-7 sample geometry (12 mm length and 2 mm width) with the thickness of 1.5 mm (x_1 = 2, 2.5, 3, 3.5) or 0.5 mm (x_1 = 1, 1.5) was used.

Table 4-2. Young's modulus E of the as-prepared (1-x_1) PNaAMPS SN gels and the structural parameters calculated from E.

gel code	(1-4)	(1-3)	(1-2.5)	(1-2)	(1-1.5)	(1-1)
E (kPa)	25.7	19.1	16.4	14.1	8.5	8.5
$\nu_{1,\text{as-p}}$ (mol m^{-3})	3.5	2.6	2.2	1.9	1.1	1.1
$N_{b,1}$ (-)	578	776	906	1054	1743	1746

E: elastic modulus of each as-prepared PNaAMPS SN gel characterized from uniaxial stress–strain curve of the gel (**Figure 4-19**). Slope at the small deformation was obtained. $\nu_{1,\text{as-p}}$: estimated number density of polymer strands of the first network at the as-prepared state of the PNaAMPS SN gel, calculated by $\nu_{1,\text{as-p}} = E/3k_BT$. $N_{b,1}$: estimated number of covalent C−C bonds in the backbone of a first network polymer strand on average, calculated by $N_{b,1} = 2C_1\nu_{1,\text{as-p}}^{-1}$, where C_1 is the feed monomer (NaAMPS) concentration (C_1 = 1.0 M).

Table 4-3. Number density of polymer strands of the first network in the DN gels estimated from elastic modulus and swelling ratio.

gel code	(1-4/4-0.01)	(1-3/2-0.01)	(1-2.5/2-0.01)	(1-2/2-0.01)	(1-1.5/2-0.01)	(1-1/2-0.01)
$\nu_{1,as\text{-}p}$ (mM)	3.5	2.6	2.2	1.9	1.1	1.1
t_{DN}/t_0 (-)	2.8	3.2	3.6	4.0	4.5	6.3
$\nu_{1,DN}$ (mM)	0.16	0.081	0.049	0.030	0.013	0.005

$\nu_{1,as\text{-}p}$: number density of polymer strands of the first network at the as-prepared state of the PNaAMPS SN gel; t_{DN}/t_0: one-dimensional swelling ratio characterized by thickness change; $\nu_{1,DN}$: number density of the first network polymer strands in the DN gels, calculated by $\nu_{1,DN} = \nu_{1,as\text{-}p} (t_{DN}/t_0)^{-3}$.

Table 4-4. Estimation of fraction of broken chains in the first network.

	$\nu_{1,DN}$ (μM)	$[Fe^{3+}]$ (μM)	Φ_c (%)	U_{total} (MJ m^{-3})	U_{hys} (MJ m^{-3})	Φ_b (%)
(1-4/4-0.01) DN gel, ε = 1.6	158	8	4.7	8.0	0.46	6
(1-4/4-0.01) DN gel, ε = 4.7	158	26	16	8.0	2.0	25
(1-3/2-0.01) DN gel, ε = 10.1	81	33	40	5.5	3.4	61
(1-2.5/2-0.01) DN gel, ε = 10.7	49	24	48	3.9	2.1	54
(1-2/2-0.01) DN gel, ε = 10.2	30	16	53	2.8	1.3	47
(1-1.5/2-0.01) DN gel, ε = 8.3	13	7	58	1.9	0.53	27
(1-1/2-0.01) DN gel, ε = 6.2	5	6	124	0.7	0.11	16

$\nu_{1,DN}$: number density of the first network polymer strands in the DN gels. $[Fe^{3+}]$: oxidized ferrous concentration in the stretched DN gel. Φ_c: fraction of broken strands in the total strands of the first network, characterized as $\Phi_c = [Fe^{3+}]/\nu_{1,DN}$. U_{total}: energy theoretical required for the fracture of all the first network strands within a unit volume, calculated by $U_{total} = 2C_{1,DN}U_b$. Here I used U_b = 88 kJ mol^{-1} (see main text). Φ_b: fraction of broken strands in the total strands of the first network, characterized as $\Phi_b = U_{hys}/U_{tot}$.

Chapter 5: Mechanoradical Polymerization in DN gels

5.1. Introduction

As shown in the general introduction, the goal of my research is to create a "self-growing" materials that respond to mechanical stressing to upgrade their "mechanical" properties. For hydrogels composed of polymer network and water, the mechanical properties such as elastic modulus and strength rely on the structure of the polymer network, specifically on the polymer concentration and crosslinking density. Therefore, a direct strategy to enhance the mechanical properties of hydrogels is creating a new polymer network structure and/or increase the crosslinking density of a polymer network.

In the previous chapter (**Chapter 4**), I have found that plenty of mechanoradicals is generated in stretched DN gels compared to in conventional hydrogels. In general, radicals can initiate/trigger various chemical reactions especially on organic synthesis.[1,2] Here, I chose radical polymerization initiated by the mechanoradicals because radical polymerization can induce creation of new polymer or new polymeric network, which can directly enhance the mechanical property of the DN gels. However, the mechanoradical concentration in the DN gels found as ~10^{-5} M is not as high as the concentration of radical initiator that is typically used for conventional radical polymerization (10^{-3}–10^{-1} M).[3] Hence in this chapter, I show, quantify and discuss the mechanoradical polymerization initiated by the mechanoradicals when the DN gel is deformed.

5.2. Experiments

5.2.1. Materials

DN gels and SN gels were fabricated by following the method described in **section 3.2**.

2-Acrylamido-2-methylpropanesulfonic acid (AMPS) was provided by Toa Gosei. *N*-Isopropylacrylamide (NIPAAm) was purchased from Wako Pure Chemical Industries. The abbreviations and chemical structures of some important compounds used in this work are listed in **Table 5-1**.

5.2.2. Mechanoradical polymerization of AMPS in a DN gel

A (1-4/4-0.01) DN gel, 1.4–1.5 mm thick, was cut into dumbbell-shaped pieces standardized to JIS K6251-2 (20 mm gauge length and 10 mm width) (**Figure 5-1**). The cut gels were immersed in water for 1 day to quench radicals on the cut surface. The gels were then immersed in large amount of aqueous solution of 2.0 M AMPS. The gels in the solutions were settled in an argon glovebox (O_2 concentration < 50 ppm) for two days to remove oxygen. Afterwards, the gels were stretched by hands up to $\varepsilon \approx 5$ where necking was completed in the whole narrow part of the dumbbell shaped sample, and then unloaded immediately and cut with scissors for separating the narrow part and the grip to avoid residual monomer diffusion from the grip (unstressed region) to the narrow part (objective region). The samples were wrapped in plastic film (Saran wrap) and covered with aluminum foil to avoid drying and photo-polymerization, respectively, and stored in the glovebox for 12 hours to proceed the polymerization. To prepare a control sample in which no monomer was polymerized, the same procedure was carried out with an unstretched and uncut (1-4/4-0.01) DN gel. Another control sample in which all monomers were assumed to be polymerized was prepared as following procedure. A cuboid-shaped (1-4/4-0.01) DN gel, ~1.5 mm × ~10 mm × ~10 mm, was immersed in an aqueous solution of 2.0 M AMPS and 0.01 M (0.5 mol% to the monomer) 2-oxoglutaric acid (photo-radical initiator) for two days. The DN gel was sandwiched between two glass

plates, placed in argon glovebox and irradiated with UV light (365 nm, 4 mW cm^{-2}) for ~8 hours to polymerize the AMPS monomer in the DN gel by conventional photo-radical polymerization.

5.2.3. Characterization of monomer conversion by near-infrared light absorption spectroscopy

The monomer conversion was characterized by Fourier transform transmittance near-infrared (FT-NIR) light absorbance spectroscopy. A gel sample was sandwiched between two CaF_2 plates, and FT-NIR light absorbance spectroscopy was carried out with commercial spectrometer (FT/IR-6100, Jasco Co.) at transmittance mode.

According to a previous paper on NIR spectroscopy monitoring polymerization of AMPS in water, a peak at around 6173 cm^{-1} corresponds to C−H stretching overtone at the C=C double bond of AMPS.[4] To quantify the residual monomer concentration, the half-band peak integral at 6173–6265 cm^{-1} in the difference absorbance spectrum was calculated following the previous paper.[4] In my analysis, the error of gel thickness may affect the quantification. Therefore, The difference absorbance A_{diff} is modified as $A_{diff} = aA_{sample} - A_{standard}$, where A_{sample} is the absorbance value of the stretched or unstretched sample, $A_{standard}$ is that of the standard sample with photopolymerized AMPS, and a is the correlation factor that is closed to 1.0 to calibrate the error on the gel thickness. The factor a is determined by assuming the absorbance at 6265 cm^{-1} does not change during the polymerization of AMPS in water.[4]

5.2.4. Spatially controlled mechanoradical polymerization

A (1-4/4-0.01) DN gel, 1.3 mm thick, was cut into a 70 mm × 40 mm sheet, and immersed

in water for 1 day. The sample was then immersed in aqueous solution containing 1.0 M NIPAAm and the sample in the solution was placed in an argon glovebox at 5℃ for two days to remove oxygen. Cool condition was chosen because NIPAAm polymerization may be suppressed at high temperature (room temperature or higher) due to phase separation of growing PNIPAAm. After two days, the gel was picked up from the solution and sandwiched between a polyacrylic resin mold with the convex letters “LSW” (1.5 mm-convex height) and a flat plate in the argon atmosphere (**Figure 5-2**). The mold was fabricated using a commercial 3D printer (Agilista-3100, Keyence Co.). Compression was applied to the DN gel to induce internal fracturing in the regions in contact with the convex letters. Afterwards, the compressed DN gel was wrapped with plastic film (Saran wrap) and left in the glovebox for 8 hours to allow NIPAAm polymerization. After the 8 hours, the DN gel was observed in air at the temperature of 5 and 50℃ to see the reversible microscopic phase separation behavior of the synthesized PNIPAAm.

5.3. Results and Discussion

5.3.1. Mechanoradical polymerization of AMPS in DN gels

The monomer conversion was characterized by using near-infrared (NIR) light absorption spectroscopy at the wavenumber ranged around 6000−7000 cm^{-1}. With this method, the conversion of the C=C double bond to C−C single bond is directly observed.[4–6] Compared to normal infrared (IR) spectroscopy (400–3000 cm^{-1}), bulk information in the gel can be obtained appropriately. Since organic compounds and water is sensitive to the IR absorption (i.e. having high molar absorption coefficient), the sample thickness <10–100 μm should be used for the transmittance mode of normal IR range in usual case. However, synthesizing thin DN gels (<100 μm) is technically difficult.[7] If using normal IR,

reflection mode such as attenuated total reflection (ATR) method would be applicable; however, the method measures only thin surface (e.g. few μm for ATR-IR) in which the conversion and/or composition of the gel might be different from the bulk. Therefore, here I used NIR spectroscopy at transmittance mode.

Figure 5-3 shows the FT-NIR spectra of the stretched, unstretched and photopolymerized DN gels that had initially contained 2.0 M AMPS monomer. The peak at around 6173 cm^{-1} of the stretched sample was almost disappeared as well as that of the photopolymerized sample. This peak corresponds to the C−H stretching overtone at the C=C double bond of AMPS.[4] Therefore, the results clearly indicate that the AMPS was polymerized in the DN gel when it was stretched. Since mechanoradicals are generated in the stretched DN gel, the polymerization should be initiated by them. Such mechanoradical polymerization has also found in previous researches in polymer solutions, melts and polymer surfaces,[8–10] though mechanoradical polymerization in a bulk material has never found before. Next, the monomer conversion was quantified. Assuming all monomers were polymerized in the photopolymerized sample, the spectra of unstretched and stretched samples are subtracted by the spectrum of photopolymerized sample (see method section for detail) (**Figure 5-4**). Note that the peak at around 6173 cm^{-1} is asymmetric that is also found in a reference,[4] because there is other peak corresponding to C−H stretching at the C=C bond at the lower wavenumber.[6] To quantify the monomer conversion, the half-band peak integral values at 6173–6265 cm^{-1} was calculated, resulting 0.15±0.08 and 1.57±0.07 cm^{-1} for the stretched and unstretched samples, respectively. The errors represent standard deviation among three individual measurements for each sample. Assuming no monomer was reacted in the unstretched sample, the monomer conversion in the stretched sample was obtained as high as

90.3±5.1%. The high conversion dramatically increases the weight fraction of polymer in the gel. Before stretching, the DN gels with monomers contained approximately 20 wt.% polymer, 30 wt.% AMPS monomer and 50 wt.% water because water content of (1-4/4-0.01) DN gel without monomer is 81 wt.% and weight fraction of AMPS in 2.0 M aqueous solution is about 37 wt.%. After stretching at which 90% of monomer were converted, the DN gel compositions turned into 47 wt.% polymer, 3 wt.% residual monomer and 50 wt.% water. Hence the polymer fraction was increased by more than double, from 20 wt.% to 47 wt.%.

Considering the estimated radical concentration (~10^{-5} M) and the reacted monomer concentration (~10^{0} M), the degree of polymerization and the molecular weight of each new polymer chain on average is calculated to be ~10^{5} (dimensionless) and ~10^{7} g/mol, respectively, assuming chain transfer reaction is negligible. The values are comparably high in the synthetic polymers, but such high molecular weight (in the order of 10^{6}–10^{7} g/mol) of polymers has been reported when polyacrylamide derivatives was synthesized by free-radical polymerization in aqueous media.[4,11–13] One possible reason of the high efficiency is due to the small transfer constant to water. As an example, for polymerization of methyl methacrylate, the transfer constant to water at 60℃ is (0−0.03) × 10^{-4}, whereas those to organic solvents at 60℃ are 0.394 × 10^{-4} to butyl alcohol, (0.45−1.77) × 10^{-4} to chloroform, (0.1−0.46) × 10^{-4} to ethyl acetate, 0.583 × 10^{-4} to isopropyl alcohol and (0.17–0.45) × 10^{-4} to toluene.[14] When a radical is transferred to a solvent molecule, the diffusivity of the transferred small-molecular radical is much higher than that of mechanoradical and propagating radical both of which are at the end of a polymer chain. Hence the possibility of the termination reaction become high when the radical is transferred to the solvent. Therefore, such high efficiency of mechanoradical

polymerization in DN gels may depend on the solvent.

It should be noted that almost no polymerization was observed when the stretching experiment was carried out not in an argon glovebox but in air. This is because oxygen quenched radical, which is well-known phenomenon in radical chemistry.[15] The solubility of oxygen in fresh water at atmospheric condition (under 1 atm air with 0.21 atm O_2) at 25℃ is 2.6×10^{-4} M,[16,17] that is one-order larger than the estimated mechanoradical concentration (~10^{-5} M). Therefore, the mechanoradical polymerization is quenched by the oxygen. The result supports that the polymerization was driven by the mechanoradicals generated by the mechanicals stressing. On the other hand, the oxygen will be one problem on this system for future applications because the mechanoradical polymerization in our DN gels can perform only in inert atmosphere for now. To solve the problem to open broad applications, one will be possible to use oxygen trapping/quenching agent or oxygen tolerant techniques in the DN gels.[15,18]

5.3.2. Spatially controlled mechanoradical polymerization

Since the mechanoradical polymerization in the DN gels is triggered by mechanical stressing, monomer can be polymerized only at the stressed region. To demonstrate that, local patterning of the polymerization by local compression was performed. It has been known that not only stretching but also compression can induce internal fracturing.[19,20] Because a hydrogel is “incompressible” material, i.e. material’s volume is constant under deformation, the gel expands to lateral direction when the gel is compressed. Therefore, in a compressed DN gel, polymer strands are stretched to lateral direction, and ruptured when they are stretched until their stretching limit.

Here a DN gel sheet containing *N*-isopropyl acrylamide (NIPAAm) monomer

were locally compressed by a mold with a convex letter “LSW” (abbreviation of the name of our laboratory: laboratory of soft and wet matter) (**Figures 5-2** and **5-5a**). The photographical images of the locally compressed DN gel at 5 and 50℃ are shown in **Figure 5-5b**. At low temperature, whole of the DN gel sheet was transparent. When the gel sheet was heated to 50℃, the locally compressed region became untransparent (white) and the letters “LSW” appeared. The thermal response was reversible. The result demonstrates that the monomer NIPAAm was polymerized by mechanoradical polymerization only at the compressed region. The corresponding polymer poly(*N*-isopropyl acrylamide) (PNIPAAm) is known to show thermo-responsive phase separation at around 35℃ because of lowest critical solution temperature (LSCT) phenomenon.[21] At low temperature, PNIPAAm is soluble in aqueous phase, so the gel is totally transparent at 5℃. On the other hand, because PNIPAAm is insoluble in aqueous phase at high temperature, the mechanically synthesized PNIPAAm showed micro-phase separation and hence the compressed region became opaque at 50℃. The uncompressed region kept transparent because the monomer in the gel was not polymerized without stressing. Even after 1 year during which the gel had been stored in water at room temperature, the embedded letters “LSW” were clearly observed by naked eyes, suggesting the mechanically synthesized PNIPAAm could not diffused out from the compressed part. The result implies that the mechanoradical polymerization was mainly or totally initiated from the broken ends of polymer strands that are connected to the infinite network. If plenty of radical transfer reaction to small molecule had happen, the PNIPAAm would have diffused.

These results explain that the mechanoradical polymerization in DN gels can be triggered at a desired position by applying spatially programmed deformation. Moreover,

as demonstrated by the reversible thermo-response of the letter appearance by PNIPAAm, desired function will be embedded at the desired position by the mechanical stressing/stamping using appropriate monomer, which may be used in a fabrication process and/or for recording mechanical history under usage.

5.4. Conclusion

I found that mechanoradicals generated in stressed DN gels can initiate radical polymerization of vinyl monomers, AMPS and NIPAAm. For the mechanoradical polymerization of 2.0 M AMPS in a stretched and necked (1-4/4-0.01) DN gel, the conversion was quantified as high as 90% (1.8 M) by NIR spectroscopy. The high conversion significantly increased the polymer concentration in the gel from 20% to 47% as an example. The high conversion essentially roots in radical polymerization. Since estimated oxygen concentration in DN gel at atmospheric condition is much higher than mechanoradical concentration, the mechanoradical polymerization could not induced under atmospheric condition. Additional solution to reduce oxygen concentration will be required for future applications.

The mechanoradical polymerization in a DN gel can induced by both stretching and compression. By applying local deformation such as local compression, selective pattern is imprinted only at the stressed region. As exemplified by imparting thermoresponsive property by stress-induced NIPAAm polymerization, diverse functions can be imparted on demand by applying programmed mechanical stimuli to DN gels with using appropriate functional monomers.

References

(1) H. Togo, Advanced Free Radical Reactions for Organic Synthesis (Elsevier Science, 2004).

(2) P. Renaud, M. P. Sibi, Radicals in Organic Synthesis (Wiley-VCH, 2001).

(3) M. Kamigaito, K. Satoh, Radical polymerization. *Network Polymer* (in Japanese) **30,** 234–249 (2009).

(4) S. Beuermann, M. Buback, P. Hesse, T. Junkers I. Lacík, Free-radical polymerization kinetics of 2-acrylamido-2-methylpropanesulfonic acid in aqueous solution. *Macromolecules* **39,** 509–516 (2006).

(5) H.Wang, T. Hirano, M. Seno, T. Sato, Radical polymerization behavior of 3-(*N*-2-methacryloyloxyethyl-*N,N*-dimethyl)ammonatopropanesulfonate in water, *Eur. Polym. J.* **39**, 2107–2114 (2003).

(6) P. Drawe, M. Buback, I. Lacík, Radical polymerization of alkali acrylates in aqueous solution. *Macromol. Chem. Phys.* **216,** 1333–1340 (2015).

(7) S. Liang, Q. M. Yu, H. Yin, Z. L. Wu, T. Kurokawa, J. P. Gong, Ultrathin tough double network hydrogels showing adjustable muscle-like isometric force generation triggered by solvent. *Chem. Commun.* **48,** 7518–7520 (2009).

(8) D. J. Angier, W. F. Watson, Mastication. V. Separation and structural investigation of natural rubber–polymethyl methacrylate interpolymers formed by mastication. *J. Polym. Sci.* **25,** 1–18 (1957).

(9) J. Sohma, Mechanochemistry of polymers. *Prog. Polym. Sci.* **14,** 451–596 (1989).

(10) M. Sakaguchi, T. Ohura, T. Iwata, S. Takahashi, S. Akai, T. Kan, H. Murai, M. Fujiwara, O. Watanabe, M. Narita, Diblock copolymer of bacterial cellulose and poly(methyl methacrylate) initiated by chain-end-type radicals produced by

mechanical scission of glycosidic linkages of bacterial cellulose. *Biomacromolecules* **11,** 3059–3066 (2010).

(11) T. Ishige, A. E. Hamielec, Solution polymerization of acrylamide to high conversion. *J. App. Polym. Sci.* **17,** 1479–1506 (1973).

(12) F. Mabire, R. Audebert, C. Quivoron, Synthesis and solution properties of water soluble copolymers based on acrylamide and quaternary ammonium acrylic comonomer. *Polymer* **25,** 1317–1322 (1984).

(13) H. Tsukeshiba, M. Huang, Y.-H. Na, T. Kurokawa, R. Kuwabara, Y. Tanaka, H. Furukawa, Y. Osada, J. P. Gong, Effect of polymer entanglement on the toughening of double network hydrogels. *J. Phys. Chem. B* **109,** 16304–16309 (2005).

(14) J. Brandrup, E. H. Immergut, E. A. Grulke (editors), *Polymer Handbook*, 4th ed. (Wiley-Interscience, 1999).

(15) S. C. Ligon, B. Husár, H. Wutzel, R. Holman, R. Liska, Strategies to reduce oxygen inhibition in photoinduced polymerization. *Chem. Rev.* **114,** 557–589 (2014).

(16) Engineering ToolBox. *Oxygen - Solubility in Fresh Water and Sea Water.* (2005) Available at: https://www.engineeringtoolbox.com/oxygen-solubility-water-d_841.html (Accessed on 23rd August 2019).

(17) W. Xing, G. Yin, J, Zhang, Rotating Electrode Methods and Oxygen Reduction Electrocatalysts (Elsevier, 2014).

(18) J. Yeow, R. Chapman, A. J. Gormley, C. Boyer, Up in the air: oxygen tolerance in controlled/living radical polymerization. *Chem. Soc. Rev*. **47,** 4357–4387 (2018).

(19) R. E. Webber, C. Creton, H. R. Brown, J. P. Gong, Large strain hysteresis and Mullins effect of tough double-network hydrogels. *Macromolecules* **40,** 2919–2927 (2007).

(20) T. Matsuda, T. Nakajima, Y. Fukuda, W. Hong, T. Sakai, T. Kurokawa, U. Chung, J. P. Gong, Yielding criteria of double network hydrogels. *Macromolecules* **49,** 1865–1872 (2016).

(21) H. G. Schild, Poly(*N*-isopropylacrylamide): experiment, theory and application. *Prog. Polym. Sci.* **17,** 163–249 (1992).

Figures and Table

Table 5-1. Abbreviations and structures of the chemical compounds used in this chapter.

Chemical name	Abbreviation	Chemical structure
Poly(2-acrylamido-2-methylpropanesulfonic acid) sodium salt	PNaAMPS	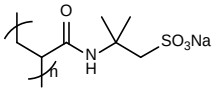
Poly(acrylamide)	PAAm	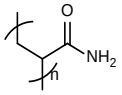
2-Acrylamido-2-methylpropanesulfonic acid	AMPS	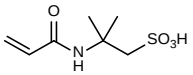
Poly(2-acrylamido-2-methylpropanesulfonic acid)	PAMPS	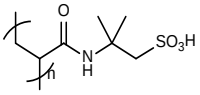
N-Isopropylacrylamide	NIPAAm	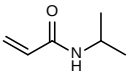
Poly(*N*-isopropylacrylamide)	PNIPAAm	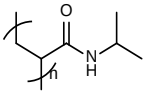

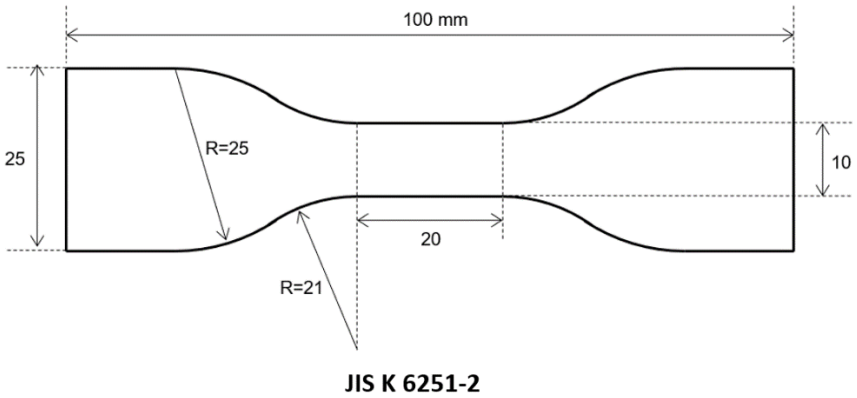

Figure 5-1. Dumbbell shape (JIS K 6251-2 standard) used in this chapter for tensile experiment.

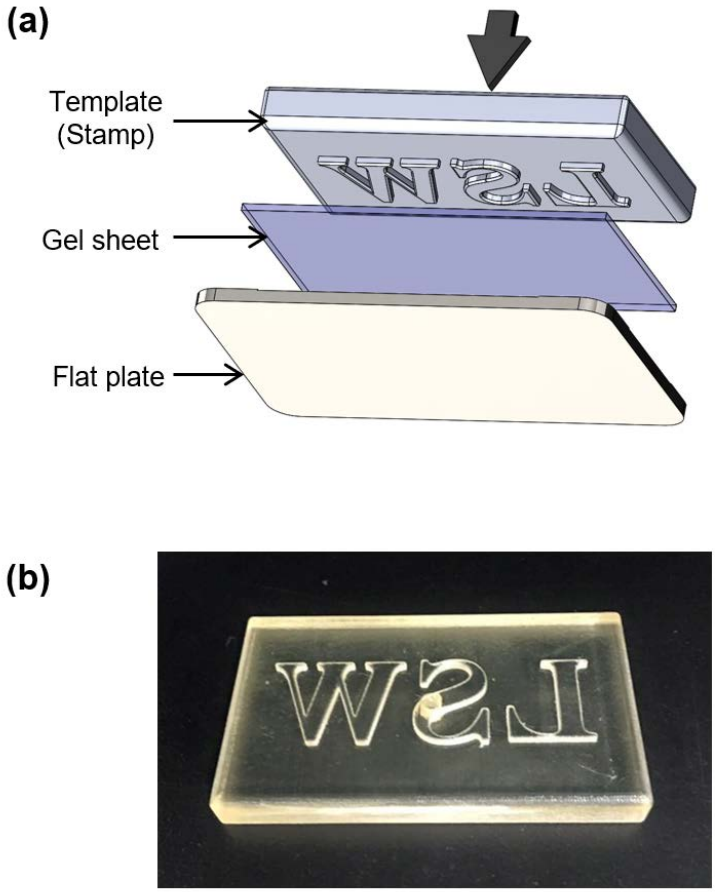

Figure 5-2. (a) Experimental set-up for inducing spatially controlled internal damage in a DN gel to achieve space-selective mechanoradical polymerization. A stamp with the convex letters "LSW" was pressed onto the DN gel. **(b)** A photographic image of the stamp made of 3D-printed acrylic resin. This figure is from *Science* 363, 504–508 (2019). Reprinted with permission from AAAS.

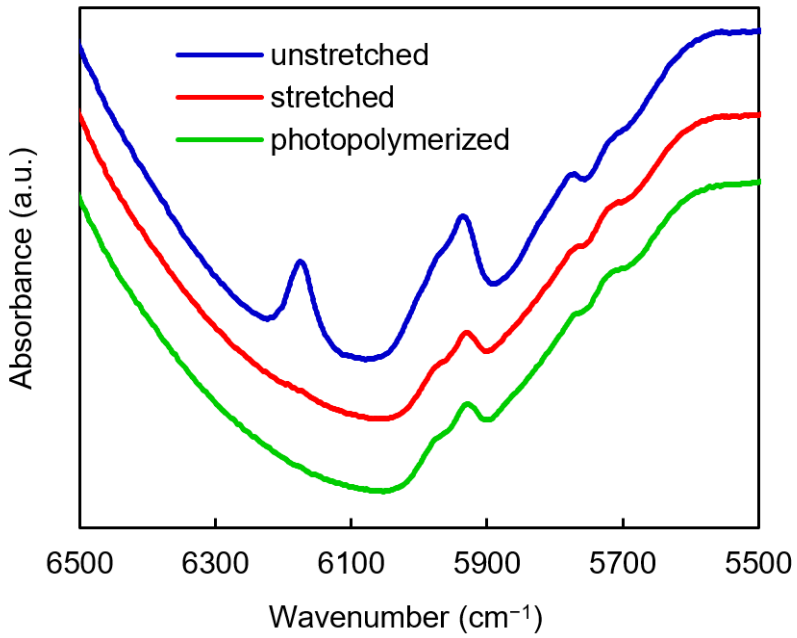

Figure 5-3. Fourier transform near-infrared (FT-NIR) transmittance spectra of unstretched (blue) and stretched (red) (1-4/4-0.01) DN gels fed with a 2.0 M aqueous solution of vinyl monomer AMPS. In addition, the spectrum of a photoirradiated, unstretched DN gel loaded with 2.0 M AMPS and 0.01 M 2-oxoglutaric acid (photoradical initiator) is also shown as a control (green). The peak at approximately 6,173 cm^{-1} corresponds to C–H overtone stretching at the C=C double bond of AMPS. This figure is from *Science* 363, 504–508 (2019). Reprinted with permission from AAAS.

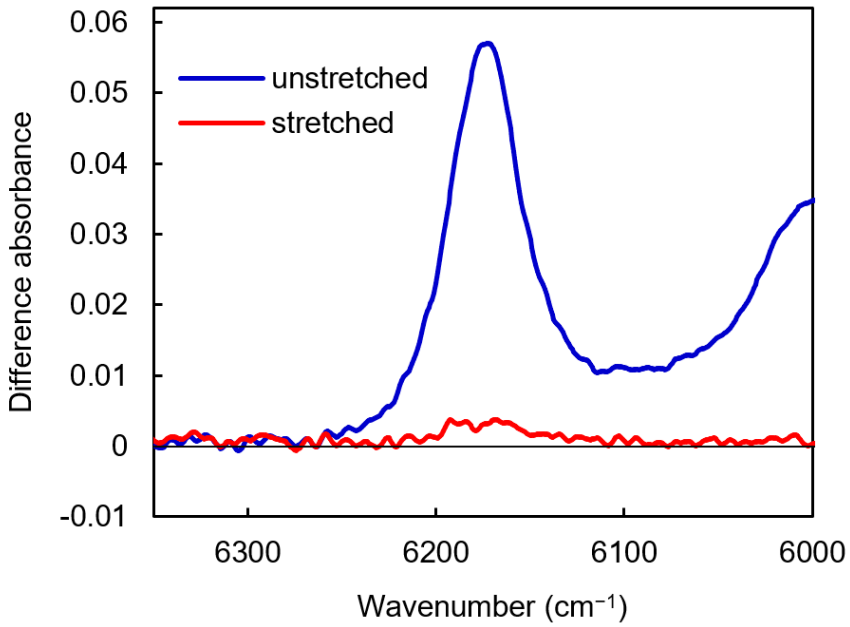

Figure 5-4. Difference spectra of the unstretched and stretched (up to the completion of necking) (1-4/4-0.01) DN gels loaded with 2.0 M AMPS monomer obtained by subtracting the spectra of the photoirradiated DN gels (see also **Figure 5-3**). This figure is from *Science* 363, 504–508 (2019). Reprinted with permission from AAAS.

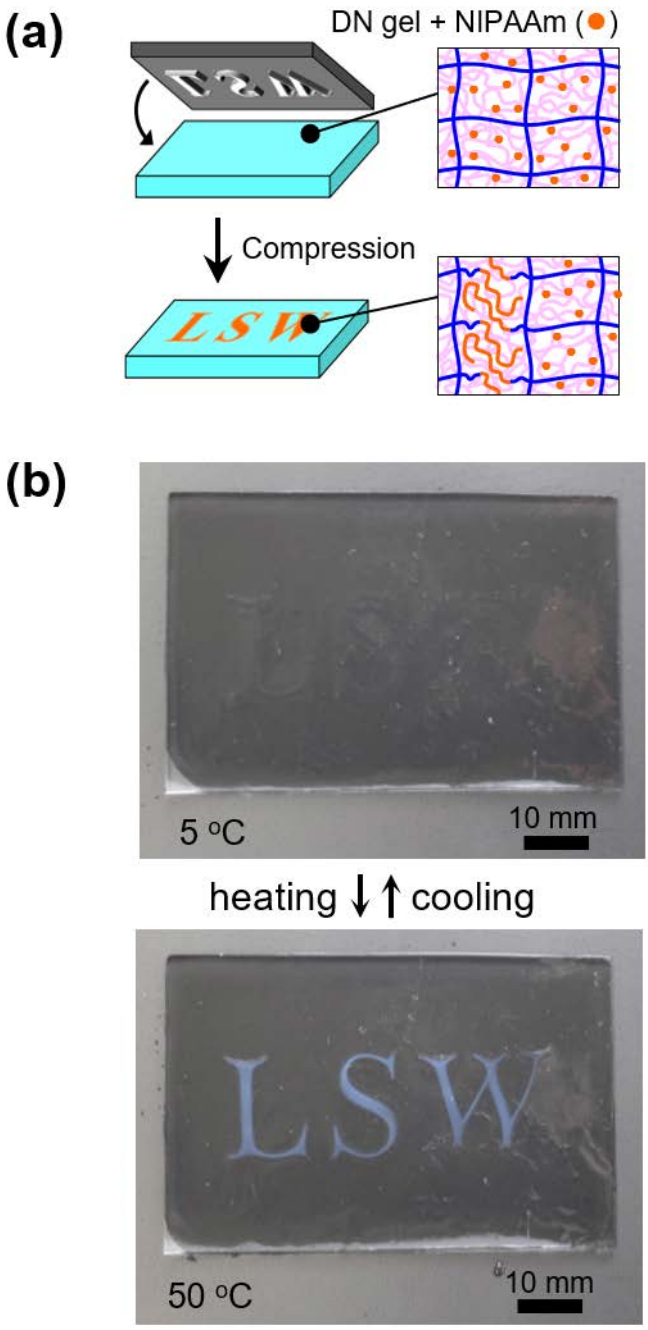

Figure 5-5. (a) Illustration of space-selective mechanoradical polymerization in a DN gel fed with NIPAAm monomer under compression with a stamp embossed with the raised letters "LSW". **(b)** Optical images of the (1-4/4-0.01) DN gel after compression with the stamp at 5°C and 50°C. The letters "LSW" were reversibly displayed or erased by changing the temperature. This figure is from *Science* 363, 504–508 (2019) (rearranged). Reprinted with permission from AAAS.

Chapter 6: Self-Strengthening/Growing DN Gels

6.1. Introduction

Until the previous chapter, it has been revealed that plenty of mechanoradicals generated in a stressed DN gel due to its internal fracturing has an ability to induce efficient mechanoradical polymerization, which dramatically increases the polymer weight fraction in the gels. Because mechanical properties of a polymer gel essentially root in polymeric network structure, such mechanoradical polymerization possibly upgrades the mechanical property of the DN gels which is one of the main goals of my research. On covalently crosslinked hydrogels including a DN gel, the number density of crosslinkers affects strongly to their mechanical properties. Hence, adding crosslinker as well as monomer for the mechanoradical polymerization is a direct approach to positively change the mechanical properties of a hydrogels effectively. In this research, both “self-strengthening” and “self-growing” have been investigated. Here, self-strengthening means the upgrade of stiffness, stress at break and/or the stress−strain behavior. Besides, self-growing means *repetitive* upgrade of the mechanical properties and/or the size of the materials.

In this chapter, at first, self-strengthening of the DN gels is investigated. The effect of the concentrations of monomer and crosslinker on the self-strengthening is systematically discussed. The extent of the self-strengthening is characterized by stress−strain curve and elastic modulus change (self-stiffening). Afterwards, the experiment and discussion are shifted to the self-growing of the DN gels, i.e. repetitive upgrade of the properties such as strength and size in response to the repetitive mechanical stimuli. To achieve the self-growing phenomenon, several issues should be solved. The issues are found from the results and discussion of the self-strengthening experiment. The

strategy and solution to solve the issues are discussed, and finally the self-growing hydrogels is demonstrated.

6.2. Experiments

6.2.1. Materials

DN gels and SN gels were fabricated by following the method described in **section 3.2**. 2-Acrylamido-2-methylpropanesulfonic acid sodium salt (NaAMPS) (49.7 wt.% aqueous solution) was provided by Toa Gosei. *N*,*N*′-Methylenebisacrylamide (MBAA) was purchased from Wako Pure Chemical Industries. *N*,*N*′,*N*″-Triacryloyl diethylenetriamine (TADETA) was provided by Fujifilm. 4-Hydroxy-2,2,6,6-tetramethylpiperidine 1-oxyl (TEMPOL) was purchased from Tokyo Chemical Industry. The abbreviations and chemical structures of some important compounds used in this chapter are listed in **Table 6-1.**

6.2.2. Mechanoradical network-polymerization in DN gel using MBAA crosslinker (preliminary experiment)

A (1-4/4-0.01) DN gel, 2.8 mm-thick, was cut into dumbbell-shaped pieces standardized to IEC-540(S) (17 mm gauge length and 4 mm width, **Figure 6-1**). The cut gels were immersed in water for 1 day to quench radicals on the cut surface. The gels were then immersed in large amount of aqueous solution of NaAMPS and MBAA of which concentrations were varied at 0–1.0 M and 0–0.1 M, respectively. The gels in the solutions were settled in an argon glovebox (O_2 concentration < 100 ppm) for 2–4 days to remove oxygen. Afterwards, the gels were stretched by hands up to $\varepsilon \approx 6$ where necking was completed in the whole narrow part of the dumbbell shaped sample, and then unloaded

immediately. The samples were wrapped in plastic film (Saran wrap) and covered with aluminum foil to avoid drying and photo-polymerization, respectively, and stored in the glovebox for half day to proceed the polymerization.

After the half-day incubation, the gel samples were taken out from the glovebox and uniaxial tensile test of the samples was carried out using a commercial tensile tester (Instron 5965, Instron Co.) at a crosshead velocity of 100 mm min^{-1}. The strain (ε) was measured using a noncontacting video extensometer (AVE, Instron Co.), and the nominal stress (σ) was calculated as the measured load divided by the original cross-sectional area vertical to the load. Because the gel exhibits small residual strain, the stress and strain were normalized to the state of original (unstretched) DN gel. The procedure is shown in the results and discussion section.

6.2.3. Self-strengthening of DN gel using TADETA crosslinker characterized by stress−strain behavior

A (1-3/3-0.01) DN gel, 1.5 mm-thick, was cut into dumbbell-shaped pieces standardized to JIS K 6251-2 (20 mm gauge length and 10 mm width, **Figure 6-1**). The cut gels were immersed in water for 1 day to quench radicals on the cut surface. The gels were then immersed in large amount of aqueous solution of 0.3 M NaAMPS and 0.3 M TADETA. The gels in the solutions were settled in an argon glovebox (O_2 concentration < 100 ppm) for 2 days to remove oxygen. Afterwards, the gels were stretched to the point at which the necking of the sample was complete (ε ≈ 6) and then were unloaded in an argon atmosphere with a commercial tensile tester (MCT-2150, A&D Co.) operating at a crosshead velocity of 300 mm min^{-1}. The samples were wrapped in plastic film (Saran wrap) and covered with aluminum foil to avoid drying and photo-polymerization,

respectively, and stored in the glovebox for one day to proceed the polymerization.

After the one-day incubation, the gel samples were taken out from the glovebox. Then necked part of each samples was cut into smaller dumbbell-shaped piece (JIS K 6251-7; 12 mm gauge length and 2 mm width, **Figures 6-1 and 6-2**). Uniaxial tensile test of the small dumbbell gel pieces was carried out using a commercial tensile tester (Instron 5965, Instron Co.) at a crosshead velocity of 300 mm min^{-1}. The strain (ε) was measured using a noncontacting video extensometer (AVE, Instron Co.), and the nominal stress (σ) was calculated as the measured load divided by the original cross-sectional area vertical to the load. Because the gel exhibits small residual strain, the stress and strain were normalized to the state of original (unstretched) DN gel. The procedure is shown in the results and discussion section.

In addition to the (1-3/3-0.01) DN gels fed with 0.3 M NaAMPS and 0.3 M TADETA, four control samples were also prepared, and their stress−strain curves were characterized. The same experimental procedure above was carried out for these control samples except as mentioned below. The first control sample is a (1-3/3-0.01) DN gel immersed in water, which is a sample without feeding any monomer or crosslinker. The second control sample is a (1-3/3-0.01) DN gel fed with 1.2 M NaAMPS, which is a sample with monomer but without feeding any crosslinker. The NaAMPS concentration was selected as 1.2 M to match the concentration of vinyl group of the fed chemicals. The third control sample is a (1-3/3-0.01) DN gel fed with 0.01 M TEMPOL as well as 0.3 M NaAMPS and 0.3 M TADETA, which is a sample with radical trapping agent TEMPOL. The fourth control sample is a (3-0.01) PAAm SN gel (1.4-mm thick) fed with 0.3 M NaAMPS and 0.3 M TADETA, which is a sample of a conventional SN (single-network) gel. Only for the control experiment using an SN gel, the pre-stretching strain in the argon

glovebox was set as $\varepsilon \approx 4$ because $\varepsilon \approx 5$–6 is the stretching limit of the gel.

6.2.4. Characterization of polymer weight fraction

Related to the self-strengthening experiment shown in the previous section (**section 6.2.2**), polymer weight fractions of the pre-stretched/unstretched gels fed with/without monomer and crosslinker were also characterized. The DN and SN gel samples were prepared as described in **section 6.2.2**. Briefly, each gel fed with/without monomer and/or crosslinker was stretched (or not stretched) in the argon glovebox, stored in the glovebox for 1 day, and then picked out from the glovebox.

The weight fraction of polymer for each gel sample was characterized. First, the weight of each gel, w_{wet}, was measured. The gel is composed of polymer, monomer, crosslinker and water. Next, the gel was immersed in large amount of water for 2 days in order to extract the unreacted monomer and crosslinker from the gel. After the immersion, each gel composed of polymer and water was dried at 120℃ for 8 h *in vacuo*. The weight of each dried gel, w_{dry}, was measured. The weight fraction of polymer for each gel, f_p, was characterized as $f_p = w_{dry}/w_{wet}$.

6.2.5. Characterization of the kinetics of the self-strengthening

A (1-3/3-0.01) DN gel, 1.5 mm-thick, was cut into dumbbell-shaped pieces standardized to JIS K 6251-7 (12 mm gauge length and 2 mm width, **Figure 6-1**). The cut gels were immersed in water for 1 day, and then were immersed in large amount of aqueous solution of 0.2 M NaAMPS and 0.2 M TADETA. The gels in the solution were placed in an argon glovebox (O_2 concentration < 100 ppm) for 2 days to remove oxygen. Afterwards, each gels was stretched to the point at which the necking of the sample was complete ($\varepsilon = 6$)

and then was unloaded in an argon atmosphere with a commercial tensile tester (MCT-2150, A&D Co.) operating at a crosshead velocity of 300 mm min^{-1}. The sample was wrapped in plastic film (Saran wrap) and covered with aluminum foil to avoid drying and photo-polymerization, respectively. After waiting for certain time (1–720 min), each sample was stretched again in the argon glovebox with the tensile tester. The reloading stress−strain curve for each waiting time was characterized.

6.2.6. Self-stiffening of DN gel using TADETA crosslinker

A (1-3/3-0.01) DN gel, 1.5 mm-thick, was cut into dumbbell-shaped pieces standardized to IEC-540(S) (17 mm gauge length and 4 mm width, **Figure 6-1**). The cut gels were immersed in water for 1 day, and then were immersed in large amount of aqueous solution of 0–0.8 M NaAMPS and 0–1.0 M TADETA. The gels in the solution were placed in an argon glovebox (O_2 concentration < 100 ppm) for 2 days to remove oxygen. Afterwards, the gels were stretched to the point at which the necking of the sample was complete ($\varepsilon \approx 6$) and then were unloaded in an argon atmosphere with a commercial tensile tester (MCT-2150, A&D Co.) operating at a crosshead velocity of 300 mm min^{-1}. The samples were wrapped in plastic film (Saran wrap) and covered with aluminum foil to avoid drying and photo-polymerization, respectively, and stored in the glovebox for one day to proceed the polymerization.

After the one-day incubation, the gel samples were taken out from the glovebox, and Young's moduli of the gel samples were characterized. The Young's modulus was characterized by indentation test with a spherical metal indenter (1-mm radius) and a commercial mechanical testing machine (Autograph AG-X 20 kN, Shimadzu Co.) operating at a crosshead velocity of 1 mm min^{-1}. Silicone oil was thinly applied on the

gel to avoid the friction effect. The Young's modulus E was determined by fitting to Hertzian equation for an incompressible isotropic soft material:[1–3]

$$P = \frac{9}{16} E R^{1/2} h^{3/2} \quad (6.1)$$

where P is the loading force, R is the radius of the spherical indenter, and h is the indentation depth. Fitting range $0 < h < 0.2$ mm was used.

6.2.7. Self-growing of DN gel

A (1-3/3-0.01) DN gel, 1.5 mm-thick, was cut into dumbbell-shaped pieces (15 mm gauge length and 2 mm width, **Figure 6-1**). The cut gels were immersed in water for 1 day, and then were immersed in large amount of aqueous solution of 0.08 M NaAMPS and 0.08 M MBAA. The gels in the solution were placed in an argon glovebox (O_2 concentration < 100 ppm) for at least 1 day to remove oxygen. For a "open system" sample, the gel was stretched to a displacement of 75 mm ($\varepsilon \approx 5$) and then was unloaded in an monomer solution (0.08 M NaAMPS and 0.08 M MBAA, ~500 mL) with a commercial tensile tester (MCT-2150, A&D Co.) operating at a crosshead velocity of 300 mm min^{-1}. The experimental setup is described in **Figure 6-3**, in which home-made polymethylmethacrylate box (*ca.* 5 × 5 × 25 cm) was used as a solution bath. After remaining in the monomer solution for 60 min after the first stretching, the gel was stretched to 75 mm (same displacement as before) and unloaded again with the same manner as described above. The stretching, unstretching and incubation process was repeated for four times. For the "closed system" sample, the monomer-fed gel was repetitively stretched, unloaded and incubated following procedure above, except that the experiment was performed not in the monomer solution but under the argon atmosphere. During the 60-min incubation, the gel was wrapped with plastic film (Saran wrap) to

avoid drying. As a reference experiment, a dumbbell-shaped (1-3/3-0.01) DN gel without monomer nor crosslinker was repetitively stretched, unstretched and incubated in water. The procedure was same for the “open system” sample, except that not monomer solution but water was used.

6.3. Results and Discussion

6.3.1. Mechanoradical network-polymerization in DN gel using MBAA crosslinker (preliminary experiment)

First, *N*,*N*′-methylenebisacrylamide (MBAA) crosslinker as well as NaAMPS monomer was fed in a DN gel for the mechanoradical network-polymerization. The MBAA having two acryloyl groups in a molecule is commonly used as the chemical crosslinker to prepare hydrogels. The (1-4/4-0.01) DN gels fed with NaAMPS and MBAA were stretched in the argon glovebox, and the stress−strain curves of the stretched DN gels were characterized. As the DN gel exhibits small residual strain after stretching, the residual strain should be considered when the stress−strain curve of the stretched sample is compared to the original unstretched sample. When the residual strain appeared, the sample length increased and the cross-sectional area decreased for the pre-stretched sample at their load free state compared to the original unstretched state. In this preliminary experiment described in this **section 6.3.1**, the stretched dumbbell shaped gel was restretched as it was. Therefore, normalized stress σ_n is calculated as:

$$\sigma_n = F/A_{0,\text{unstretched}} \tag{6.2}$$

where F is the applied force and $A_{0,\text{unstretched}}$ is the original cross-sectional area *before* pre-stretching. On the other hand, normalized strain ε_n is calculated as:

$$\varepsilon_n = \lambda_n - 1 = \lambda_{obs} \times \lambda_{res} - 1 = (\varepsilon_{obs} + 1)(\varepsilon_{res} + 1) - 1 \tag{6.3}$$

where λ and ε are the elongation ratio and strain ($\lambda \equiv \varepsilon + 1$), respectively, and the subscribed “n”, “obs” and “res” denotes the normalized, observed and residual, respectively. In this preliminary experiment, I briefly assumed that the residual strain is $\varepsilon_{res} = 10\%$. (In the following **section 6.3.2**, the residual strain was individually measured for each sample).

The normalized stress−strain curves of the pre-stretched DN gels fed with NaAMPS and MBAA are shown in **Figure 6-4**. The concentration of NaAMPS C_m was varied from 0, 0.25, 0.5 to 1.0 M, and that of MBAA C_x was varied from 0, 0.025, 0.05 to 0.1 M. Note that 0.1 M is close to the solubility limit of MBAA in water. In **Figure 6-4**, the data are summarized both same C_m varied with C_x, and same C_x varied with C_m. When only NaAMPS was fed in the DN gel (i.e. no MBAA was fed; **Figure 6-4(d)**), the stress−strain curves are almost overlapped with the curve of the control sample in which neither monomer nor crosslinker was fed (discussed in **section 6.3.2**). In contrast, when the MBAA crosslinker was fed as well as NaAMPS, the enhanced mechanical properties were observed compared to the control stretched sample. The strain hardening began at small strain when higher C_x was used. When the C_x was fixed, the stress value at certain strain level is larger for the sample of higher NaAMPS concentration. The result indicates that new polymer network was synthesized by the mechanoradical polymerization because the MBAA acted as the crosslinker of the new network.

Even though the stress−strain curve was changed due to the newly formed network, the stresses at break observed in this experiment were almost constant around 1.4 MPa. However, the result does not reflect the actual strength of the self-strengthened gel but originates in the experimental setup. When the gel broke into two pieces on this re-tensile test, the breaking point was not the narrow part of the dumbbell-shaped sample

where new network polymerization occurred but the un-necked part at the edge of the narrow part. In the un-necked part, few mechano-polymerization should have occurred because the amount of the mechanoradicals in the un-necked region is much fewer than in the necked region (see **Chapter 4** especially **Figures 4-4 and 4-9**). Hence, even if the necked part became stronger than the original DN gel, the dumbbell-shaped gel would break at the un-necked part which has similar strength as the original DN gel. Therefore, the result does not mean that mechanoradical polymerization does not affect to the stress at break of the DN gels. In order to characterize the actual strength of the necked region, small sample specimen must be cut off from the necked region, which is performed in the following **section 6.3.2**.

Young's moduli of the stretched DN gels are also characterized (**Figure 6-5**). To characterize the Young's modulus, slope of the normalized stress−strain curve at small deformation range (10% strain except for the initial noisy region and residual strain; $0.02 < \varepsilon < 0.10$ for the unstretched DN gel and $0.12 < \varepsilon < 0.20$ for the stretched DN gels), was obtained by linear fitting. As shown in **Figure 6-5**, the moduli of the stretched DN gels fed with monomer and crosslinker are higher than that of the stretched DN gel without feeding monomer and crosslinker. The modulus was virtually increased when higher concentration of monomer and crosslinker was used. In the series of this experiment, the highest modulus reached as 0.13 MPa at C_m = 1.0 M NaAMPS and C_x = 0.1 M MBAA, which is 2.1 times higher than the stretched DN gel. However, the modulus was still much lower than the virgin DN gels (0.6 MPa). Therefore, self-stiffening effect was not observed in this series of experiment, even though stress-induced mechanoradical network-polymerization occurred. The modulus of chemically-crosslinked hydrogels essentially roots in two terms: one is the number density of the network strands which is

virtually proportional to the number density of the crosslinking point, and the other is the elastic stored energy of each chain which relates to the stretching degree of the polymer strands by swelling. The Young's modulus of the DN gels is quite high (10^5–10^6 Pa) compared to the other hydrogels (10^3–10^5 Pa) because the first network strands are highly stretched state due to the dense crosslinking and high swelling of the polyelectrolyte first network.[3–5] Because the strands of newly formed network at the as-polymerized state are virtually unstretched and coiled state, it is not easy to form enough stiff network in order to achieve the self-stiffening effect on DN gel. One would be possible to achieve if much larger amount of crosslinker is fed in the DN gel; however, it is technically difficult when using MBAA because the current best condition using C_x = 0.1 M MBAA is close to the solubility limit of MBAA in water. In the followed **section 6.3.2**, the other crosslinker is used to solve the issue.

In **Figure 6-4**, interestingly, yielding-like phenomenon was observed on some stretched DN gels such as a sample fed with C_m = 0.25 M NaAMPS and C_x = 0.1 M MBAA. Such yielding-like behavior is the sign of structure destruction in the gel.[6–8] On a cyclic tensile test for the sample, mechanical hysteresis was also observed (**Figure 6-6**). Since the yielding and hysteresis was observed at the strain less than the pre-stretching strain ($\varepsilon \approx 6$), the newly formed network must be broken during the deformation. Conventionally, the sacrificial bond mechanism (i.e. internal fracturing) of DN gels is used only at first mechanical stressing because covalent bond is irreversible. Hence, the mechanoradical network formation at proper condition have a potential to recover the sacrificial bond mechanism.

As short summary for this **section 6.3.1**, mechanoradical network-polymerization was achieved by feeding crosslinker as well as monomer in the DN gel.

The new network formation was characterized by re-tensile test of the pre-stretched DN gels. During the experiment and characterization, two issues were found for achieving and characterizing distinct self-strengthening; (1) small sample specimen should be cut off from the necked region to characterize the actual strength of the self-strengthen region and (2) appropriate crosslinker which has high solubility in water should be used instead of MBAA to achieve distinct self-stiffening.

6.3.2. Self-strengthening of DN gel using TADETA crosslinker

Given the issues shown above, the experimental procedure was changed as follows. (1) As shown in **Figures 6-2** and **6-7,** bigger dumbbell-shaped specimen (20-mm gauge length and 10-mm width) was used for the pre-stretching to induce mechanoradical network-polymerization, and small dumbbell-shaped specimen (12-mm gauge length and 2-mm width) was cut off from the necked part of the big dumbbell-shaped specimen. (2) A crosslinker *N*,*N*′,*N*″-triacryloyl diethylenetriamine (TADETA, **Table 6-1**) was used instead of MBAA. The solubility of TADETA in water is more than 50 wt.% (supplier information) that corresponds to > 1.8 M which is much higher than that of MBAA (0.1–0.2 M) or the other conventional water-soluble crosslinkers (typically <0.1 M). The crosslinker TADETA may also have an advantage for the self-strengthening experiment, that is, TADETA has three acryloyl groups in one molecule which can enhance the crosslinking efficiency per molecule. The experimental changes (1) and (2) are the essential modifications to solve the issues found in **section 6.3.1**. The experimental details and the other small modifications of the experimental condition are described in the method section.

In this experiment described in **section 6.3.2**, stress and strain are normalized

similar to that described in **section 6.3.1**. Here, residual strain of each sample was individually measured assuming that DN gel is incompressible soft material. Considering the materials incompressibility, the inverse of residual elongation ratio, λ_{res}^{-1}, is corresponding to the change ratio of cross-sectional area. Hence, by measuring the width and thickness of each sample before and after the pre-stretching, the residual strain ε_{res} (= $\lambda_{res} - 1$) is obtained. With the residual elongation ratio λ_{res}, the normalized stress σ_n and strain ε_n are calculated as:

$$\sigma_n = \sigma_{obs}\,\lambda_{res}^{-1} \tag{6.4}$$

$$\varepsilon_n = \lambda_n - 1 = \lambda_{obs} \times \lambda_{res} - 1 \tag{6.5}$$

where σ, λ and ε are the nominal stress, elongation ratio and strain ($\lambda \equiv \varepsilon + 1$), respectively, and the subscribed “n”, “obs” and “res” denotes the normalized, observed and residual, respectively.

Figure 6-8 shows the stress−strain curves of the stretched and un-stretched (1-3/3-0.01) DN gels fed with 0.3 M NaAMPS and 0.3 M TADETA. In this figure, the curves for control samples are also shown. As another control, the experiment using PAAm was also shown in **Figure 6-9**. For these samples, polymer weight fractions in the gel was also characterized (**Figure 6-10**). First, comparison of two *virgin* DN gels fed with/without monomer and crosslinker indicates that fed monomer does not affect to the mechanical property of the DN gel when the monomer is not reacted still. Second, most importantly, the Young’s modulus, yield stress and stress at break of the pre-stretched DN gel fed with NaAMPS and TADETA are 1.1, 1.6 and 1.8 times larger than those corresponding of the virgin DN gel, respectively. This demonstrates the self-strengthening and self-stiffening of the DN gel triggered by mechanical stressing. The distinctive increase of the polymer weight fraction was also observed from 14 wt.% to 26 wt.% (**Figure 6-10**) because of the

efficient mechanoradical polymerization. Third, the stress−strain curve of a pre-stretched DN gel fed only with 1.2 M NaAMPS (but without crosslinker) was almost overlapped with that of a pre-stretched DN gel without feeding of monomer and crosslinker. Even though the polymer weight fraction was increased from 13 wt.% to 36 wt.% (**Figure 6-10**), the newly formed polymer chains do not almost affect to the mechanical property of the DN gels. Since crosslinker was not fed, each newly formed polymer chain is virtually grafted dangling chain of which one end is connected to the ruptured first network strand and the other end is free end. Even if some of the newly formed chains are recombined at their propagation ends, the small amount of coiled long strands may less effective to the mechanical properties on the strong DN gel. Note that such concentrated grafted chains may affect to the mechanical properties of the DN gel if the much faster strain rate was applied to the gel. Fourth, no self-strengthening was observed when 0.01 M TEMPOL (radical trapping agent) was added as well as NaAMPS and TADETA to the DN gel, indicating the self-strengthening definitely originates from (mechano)radical polymerization. Fifth, neither strength nor polymer weight fraction increased in a prestretched PAAm SN gel fed with 0.3 M NaAMPS and 0.3 M TADETA (**Figures 6-9 and 6-10**). The result indicates that the mechanoradical concentration generated in stretched SN gels is too low to induce effective polymerization. Therefore, a material to generate plenty of the mechanoradicals, here this is the DN gel, acts the essential role for this strategy using mechanoradical polymerization in the material.

6.3.3. Kinetics of mechanoradical network-polymerization

Kinetics of the mechanoradical network-polymerization was also investigated briefly. On this experiment, pre-stretching and re-stretching were carried out with different waiting

time between the two stretching (**Figure 6-11a**). Both the first stretching (pre-stretching) and the second stretching (re-stretching) are carried out in an argon atmosphere. The (1-3/3-0.01) DN gels fed with 0.2 M NaAMPS and 0.2 M TADETA were used. **Figure 6-11b** shows the stress−strain curves of the pre-stretching and the second stretchings with different waiting time. The stress curve changed with the time especially at the first 60 minutes. To analyze the data quantitatively, the input mechanical work on the second stretching from strain 0 to 6, $W_{0\to6}$, was characterized (**Figure 6-11c**):

$$W_{0\to6} = \int_0^6 \sigma \, d\varepsilon \qquad (6.6)$$

As shown in the **Figure 6-11d**, $W_{0\to6}$ significantly increased at the first 60 minutes, and it was gradually increased for few hours. The result indicates that the mechanoradical network-polymerization took 1 hour or more, implying some radicals are alive during the period. Considering the *so-called* short lifetime of radicals (e.g. $\ll 1$ second),[9,10] the relatively long-term stability of the mechanoradicals is surprising. However, it has also known that half-life of macro-radical (i.e. radical on a polymer chain) such as mechanoradical in solid polymer is a few-tens minutes, hours, or more than days because of the poor mobility of the macro-radical in the solid.[11–15] Note that such researches on radical decay in solid polymer are mostly focused on glassy or crystalline polymers (e.g. polyethylene and polymethylmethacrylate).[11–15] On my research for hydrogels, the mobility of radical in DN gels is expected to be slower than low-molecular radical in solution and faster than the macro-radical in solid polymers because the propagating macro-radical connected to the ruptured strand is trapped in the polymeric network in solution-like environment. Therefore, it is possibly reasonable to consider the macro-radicals in the DN gel are alive during ~1 hour. To further investigate the issue, other techniques such as electron paramagnetic resonance (EPR) measurement will be required.

6.3.4. Self-stiffening of the DN gels by the mechanoradical polymerization

In **section 6.3.2**, self-stiffening of a DN gel was achieved using tri-functional TADETA crosslinker at high concentration. In this section, the effect of the concentration of the monomer and/or crosslinker on self-stiffening was systematically investigated. The Young's modulus of the stretched (1-3/3-0.01) DN gels fed with various concentration of NaAMPS and TADETA was characterized by the indentation test. Note that only Young's modulus was characterized because of the technical limitation of the amount of TADETA. **Figure 6-12** shows the Young's modulus of stretched DN gels fed with fixed concentration (0.3 M) of NaAMPS and varied concentration (0.0001–1.0 M) of TADETA. The moduli of the virgin DN gel (0.37 MPa) and the stretched DN gel (0.07 MPa) with no feeding of the monomers are also shown. For these controls, the stretched DN gel exhibits low modulus compared to the virgin DN gel because the stiff first network was fractured by the pre-stretching. When the concentration of TADETA was less than ~0.01 M, the elastic modulus was almost constant as similar as the modulus of the stretched DN gels without feeding the monomers. When the concentration was higher than ~0.01 M, the modulus was linearly increased. At high concentration of TADETA (>0.3 M), the modulus was higher than that of virgin DN gel. The modulus reached 0.76 MPa when the TADETA concentration was 1.0 M, which is 2.1 times higher than that of virgin DN gel. The critical concentration of ~0.01 M suggest that percolate network formed at the concentration, or the modulus of the newly formed network was much less than that of the un-damaged second network of the DN gel.

The self-stiffening experiment using various concentration of NaAMPS and TADETA at fixed molar ratio of them (NaAMPS:TADETA = 1:1 mol/mol) was also characterized. As shown in **Figure 6-13**, the modulus was comparable when 0.2 M

NaAMPS and TADETA was used, and the modulus was significantly increased by the factor of 10 and 23 when 0.4 M and 0.8 M monomers were used, respectively. Note that the modulus of virgin sample was slightly decreased from 0.37 to 0.19 MPa at the concentrations from 0 M to 0.8 M, which is because the gel slightly shrunk in the high concentration monomer solution typically with high concentration TADETA. Compared to the previous result, the significant modulus increase indicates that not only crosslinker concentration but also monomer concentration also plays important role on the self-stiffening, even though the number of crosslinking points essentially affect to the modulus of a hydrogel according to a conventional rubber elastic theory.[16] The expected reasons are that the high monomer concentration can increase the overall conversion of the C=C double bonds of the crosslinker, and/or the number of trapped entanglements of polymer strands is larger when higher monomer concentration was used.

6.3.5. Self-growing of the DN gels through repetitive stretching

In this section, the target of the research shift from the one-shot strengthening to the repetitive strengthening. As described in the **sections 6.3.1–6.3.4**, self-strengthening and stiffening after the first stretching were achieved using mechanoradical network-polymerization in a DN gel. However, considering the high conversion of the monomers described in **section 5.3.1**, repetitive mechanoradical strengthening would not happen effectively because the most of monomers were reacted at the first mechanical activation. One idea to solve the issue is continuous supplying of the monomer and crosslinker to the DN gels. Because hydrogel enables permeability to small molecules dissolved in aqueous solution, the monomer and crosslinker can be continuously supplied if the gel is kept immersed in the monomer solution. Hence, in this research to achieve the repetitive

strengthening, repetitive stretching of a DN gel was performed in the solution of monomer and crosslinker so that the monomers can continuously diffuse in the gel. The experimental system with continuous monomer supply is called as “open system” (**Figure 6-14a**). As comparison, the repetitive stretching of a DN gel fed with monomer operated under argon atmosphere was also carried out, which is called as “closed system” because no additional monomer was supplied during the repetitive stretching. As a reference experiment, repetitive stretching of a DN gel in water was also performed.

In addition to the monomer supply, concentration of the feeding monomer and crosslinker is also important issue to achieve the repetitive strengthening of the DN gel. Because the brittle network is fractured at the first stretching, the first network is no more fractured at the second or following stretchings when same or smaller strain is repetitively applied. Therefore, the newly formed network synthesized by the mechanoradical polymerization must be fractured to generate mechanoraticals that initiate the polymerization at the second or following stretchings. Therefore, the newly formed network should be brittle as similar as the original first network. To synthesize the brittle network, low monomer concentration but high crosslinker molar ratio to the monomer should be selected. After several trials to find the appropriate concentrations, I selected the use of 0.08 M NaAMPS and 0.08 M MBAA.

In this experiment, (1-3/3-0.01) DN gels was stretched from an initial sample gauge length (15 mm) to a preset length (90 mm), and then unloaded to the initial position. Such loading−unloading process was repetitively performed with a 60-minute waiting time between two consecutive cycles (**Figure 6-14b, top**). Here, the force curves were described as not stress–strain curves but force–length curves because the load-free length and cross-sectional area changed with increasing the number of cycles. The result is

shown in **Figures 6-14b (bottom)** and **6-14c**. First, on the reference sample, mechanical hysteresis was observed only in the first cycle, and the loading and unloading curves in the second to fourth cycles were overlapped with the first unloading curve. The irreversible hysteresis, a typical character of the DN gel, explains that the first network is fractured only at the first cycle. Second, on the closed system sample in which monomers were supplied only at the beginning, self-strengthening in terms of stress upturn was observed at the second loading due to the mechanoradical network-polymerization. Mechanical hysteresis was exhibited on the second cycle, indicating the newly formed network was fractured at the second stretching because the network is enough brittle. On the third and fourth cycles, the force in loading curve was slightly larger than that in the previous unloading curve and small hysteresis was observed in the cycle. The result suggests that repetitive mechanoradical network-polymerization was occurred even in the closed system. The possible reason is that some residual monomers and crosslinkers were polymerized at the second and third stretching. Nevertheless, the force did not increase with the cycles after the third cycle because the monomers in the closed system was almost depleted. Third, importantly, on the open system sample to which monomers were continuously supplied, the self-strengthening was continuously observed on every cycle. In the open system, large hysteresis was exhibited in every cycle, suggesting the newly formed network was fractured during the subsequent stretching. The network fracture generates mechanoradicals in the DN gel, which induced subsequent radical polymerization of the freshly supplied monomers from the external solution.

Interestingly, the second stretching curve in the open system exhibits higher force compared to that of the second stretching curve in the closed system, even though initial concentration of the monomers in the DN gels were identical. The result suggests

that, during the 60-minute waiting time, the fresh monomer supplied from the external solution were also polymerized. This discussion is consistent with the possible long-term radical stability in this system considered in **section 6.3.3**. If the lifetime of the radicals in our system were a second or less, the force curves of the open system would almost overlap with the closed system with considering the diffusion kinetics of the monomers.

Furthermore, not only strength but also size was increased with the cycles. Equilibrium gauge length of the gel at the beginning of each cycle are shown in **Figure 6-15**. Stiffness and mechanical hysteresis in each cycle are also shown. In the open system, the equilibrium gauge length increased from 15 mm at the first cycle to 41 mm at the fourth cycle. The size increment originates from two reasons. One is the residual strain due to the anisotropic internal fracture.[7,17] The other is the re-swelling of the DN gel. Once the first network is fractured, DN gels swell more due to release of elastic pressure of the first network.[5,18] In addition to the elastic pressure release, the newly formed network increases the osmotic pressure in the gels in case of this self-growing experiment. The two factors shifted the swelling equilibrium of the DN gel, therefore the DN gel swelled more so that the size of the gel increased.

As shown above, the repetitive strengthening and size growth was achieved when the DN gel was repetitively stretched with the continuous supply of monomers. Note that the DN gel was finally broke at fifth or sixth cycle at this condition because the newly formed network became so strong that the second network could not stop the microcrack propagation of the newly formed network. Given this result, the maximum number of cycles can be controlled by changing the concentration of the monomers; however, the extent of the self-growing, such as maximum strength, has the intrinsic upper limit that is essentially dominated by the second network property. If new soft

networks like the second network is also synthesized at some steps in the repetitive cycle, the upper limit may be increased.

6.3.6. Demonstration of the self-growing DN gel

Finally, two examples of the self-growing DN gel are demonstrated to visually exhibit the research concept. Corresponding movies are found in reference 19. In the first example, a (1-3/3-0.01) DN gel connected to a weight (200 g) was repeatedly lifted to a fixed height in an aqueous solution of 0.08 M NaAMPS and 0.08 M MBAA. The waiting time between two consecutive cycles was 60 minutes. The photographical images and force–length curves are shown in **Figures 6-16** and **6-17**, respectively. In the first cycle, the gel was just stretched because it was relatively soft at the beginning. During the first stretching, mechanoradical network-polymerization was occurred which strengthen the DN gel. Therefore, the DN gel lifted the weight in the second cycle. In the force–length curve, the force was kept at ~1.7 N when the gel was lifting the weight. Note that the 1.7 N corresponds to the force originating from 200 g weight with considering buoyancy. In the second cycle, the hysteresis was exhibited again; hence the gel further got stronger at the third cycle. In consequence, the gel lifted the weight up to higher level with increasing the stretching cycles. In the third cycle, only a few hysteresis was observed because the gel got strong enough for the prescribed force (1.7 N). Therefore, few mechanoradical polymerization was happen in the gel, resulting force curve and lifting height in the fourth cycle were similar as those in the third cycle (photographical images of the fourth cycle are not shown in **Figure 6-16**).

As like the muscle training in our body, heavier load is required when the substance get stronger. In the second example, (1-3/3-0.01) DN gels connected to a weight

was repeatedly lifted similar as previous example; except that heavier weight was used at the third and latter cycles, and monomer concentrations were increased as 0.3 M NaAMPS and 0.15 M MBAA. The results are shown in **Figures 6-18** and **6-19**. In the second cycle, the gel lifted the 200 g weight to higher level than that observed in the previous example because higher monomer concentrations were used. In this second cycle, almost no hysteresis was observed because the 200 g weight is too light to train the grown DN gel. Hence, the weight was changed to 500 g weight. In the third cycle connected to the 500 g weight, the gel hardly lifted the weight. Instead, large hysteresis was observed so that the gel was strengthen by the training with 500 g weight. As the result, the gel finally lifted the 500 g weight in the fourth cycle.

6.4. Conclusion

By using a mechanoradical polymerization with crosslinking agent, DN gels get stiffer and stronger after mechanical stressing. The degree of such self-strengthening effect can be tuned by the concentration of feeding monomer and crosslinker. In this research, increase of stress at break by the factor of 1.5 times and increase of Young's modulus by the factor of up to 23 times are demonstrated. Such effective self-strengthening has never been found in the previous research using mechanochemical reaction in sold-state materials,[20–23] which can be mainly attributed to the difficulty of achieving high-level activation of mechanophores.[24,25] Thanks to the efficiency of the mechanoradical polymerization, the weight fraction of polymer was also significantly increased by the factor of 2 times for example. The success of the self-strengthening in this research is hiring the DN gels with internal fracturing mechanism to generate abundant mechanoradicals. The statement was supported by the fact that no self-strengthening was

observed on conventional single-network hydrogels. We also observed that the mechanoradical network-polymerization takes about 1 hour after the stretching. When the monomers are continuously supplied, the self-strengthening occurs repeatedly. In this research, such continuous monomer supply is achieved by stretching a DN gel in the monomer solution. Size of the gels also increases with the repetitive training. The co-authors and I call the repetitive strengthening and size increase as “self-growing”.

The self-strengthening and self-growing properties will find some applications. As an example, the mechanism will be used to strengthen the materials only at the point where huge mechanical stress is applied. The practical application is to use such technology to strengthen only around a crack tip, which enables to toughen materials while keeping overall flexibility. Moreover, the self-growing property by mechanical activation is brand-new concept in the field of materials science. Therefore, it would find more broad applications such as self-growing soft robotics in response to mechanical attack or training.

References

(1) M. -G. Zhang, Y. -P. Cao, G. -Y. Li, X. -Q. Feng, Spherical indentation method for determining the constitutive parameters of hyperelastic soft materials. *Biomech. Model Mechanobiol.* **13,** 1–11 (2014).

(2) M. Czerner, L. S. Fellay, M. P. Suárez, P. M. Frontini, L. A. Fasce, Determination of elastic modulus of gelatin gels by indentation experiments. *Procedia Mater. Sci.* **8,** 287–296 (2015).

(3) K. Hoshino, T. Nakajima, T. Matsuda, T. Sakai, J. P. Gong, Network elasticity of a model hydrogel as a function of swelling ratio: from shrinking to extreme swelling

states. *Soft Matter* **14,** 9693–9701 (2018).

(4) J. P. Gong, Why are double network hydrogels so tough? *Soft Matter* **6,** 2583–2590 (2010).

(5) T. Nakajima, T. Kurokawa, S. Ahmed, W. -L. Wu, J. P. Gong, Characterization of internal fracture process of double network hydrogels under uniaxial elongation. *Soft Matter* **9,** 1955–1966 (2013).

(6) Y. -H. Na, Y. Tanaka, Y. Kawauchi, H. Furukawa, T. Sumiyoshi, J. P. Gong, Y. Osada, Necking phenomenon of double-network gels. *Macromolecules* **39,** 4641–4645 (2006).

(7) S. Ahmed, T. Nakajima, T. Kurokawa, M. A. Haque, J. P. Gong, Brittle–ductile transition of double network hydrogels: mechanical balance of two networks as the key factor. *Polymer* **55,** 914–923 (2014).

(8) T. Matsuda, T. Nakajima, Y. Fukuda, W. Hong, T. Sakai, T. Kurokawa, U. Chung, J. P. Gong, Yielding criteria of double network hydrogels. *Macromolecules* **49,** 1865–1872 (2016).

(9) W. A. Pryor, Oxy-radicals and related species: Their formation, lifetimes, and reactions. *Ann. Rev. Physiol.* **48,** 657–667 (1986).

(10) G. B. Watts, K. U. Ingold, Kinetic applications of electron paramagnetic resonance spectroscopy. V. Self-reactions of some group IV radicals. *J. Am. Chem. Soc.* **94,** 491–494 (1972).

(11) S. Ohnishi, I. Nitta, Rate of formation and decay of free radicals in γ-irradiated polymethyl methacrylate by means of electron spin resonance absorption measurements. *J. Polym. Sci.* **38,** 451–458 (1959).

(12) S. Nara, S. Shimada, H. Kashiwabara, J. Sohma, Relation of the decay of free

radicals in irradiated polyethylene to the molecular motion of the polymer and the configurations of the free radicals. *J. Polym. Sci. A-2: Polym. Phys.* **6,** 1435–1449 (1968).

(13) P. J. Butiagin, The decay of free radicals in polymer media. *Chemical Transformations of Polymer* (Elsevier), 57–76 (1972).

(14) S. Shimada, H. Kashiwabara, Decay reactions of free radicals in irradiated polyethylene and diffusion-controlled processes. *Polym. J.* **6,** 448–450 (1974).

(15) S. Shimada, ESR studies on molecular motion and chemical reactions in solid polymers in relation to structure. *Prog. Polym. Sci.* **17,** 1045–1106 (1992).

(16) P. J. Flory, Principles of Polymer Chemistry Ch. 11 (Cornell University Press, 1953).

(17) T.-T. Mai, T. Matsuda, T. Nakajima, J. P. Gong, K. Urayama, Distinctive characteristics of internal fracture in tough double network hydrogels revealed by various modes of stretching, *Macromolecules* **51,** 5245–5257 (2018).

(18) T.-T. Mai, T. Matsuda, T. Nakajima, J. P. Gong, K. Urayama, Damage cross-effect and anisotropy in tough double network hydrogels revealed by biaxial stretching, *Soft Matter*, **15,** 3719–3732 (2019).

(19) Hokkaido Uni, Mechanoresponsive self-growing hydrogels inspired by muscle training, Youtube. https://www.youtube.com/watch?time_continue=4&v=0_MIYHgK_8w (Accessed on 2nd September 2019).

(20) A. L. B. Ramirez, Z. S. Kean, J. A. Orlicki, M. Champhekar, S. M. Elsakr, W. E. Krause, S. L. Craig, Mechanochemical strengthening of a synthetic polymer in response to typically destructive shear forces. *Nat. Chem.* **5,** 757–761 (2013).

(21) R. T. M. Jakobs, S. Ma, R. P. Sijbesma, Mechanocatalytic polymerization and cross-linking in a polymeric matrix. *ACS Macro Lett.* **2,** 613–616 (2013).

(22) H. Zhang, F. Gao, X. Cao, Y. Li, Y. Xu, W. Weng, R. Boulatov, Mechanochromism and mechanical-force-triggered cross-linking from a single reactive moiety incorporated into polymer chains. *Angew. Chem. Int. Ed.* **55,** 3040–3044 (2016).

(23) F. Verstraeten, R. Göstl, R. P. Sijbesma, Stress-induced colouration and crosslinking of polymeric materials by mechanochemical formation of triphenylimidazolyl radicals. *Chem. Commun.* **52,** 8608–8611 (2016).

(24) C. L. Brown, S. L. Craig, Molecular engineering of mechanophore activity for stress-responsive polymeric materials. *Chem. Sci.* **6,** 2158–2165 (2015).

(25) R. Adhikari, D. E. Makarov, Mechanochemical kinetics in elastomeric polymer networks: heterogeneity of local forces results in nonexponential kinetics. *J. Phys. Chem. B* **121,** 2359–2365 (2017).

Figures and Table

Table 6-1. Abbreviations and structures of the chemical compounds used in this chapter.

Chemical name	Abbreviation	Chemical structure
Poly(2-acrylamido-2-methylpropanesulfonic acid) sodium salt	PNaAMPS	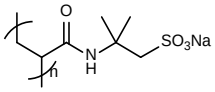
Poly(acrylamide)	PAAm	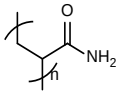
(2-Acrylamido-2-methylpropanesulfonic acid) sodium salt	NaAMPS	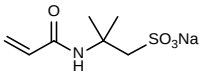
N,N′-Methylenebisacrylamide	MBAA	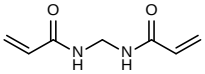
N,N′,N″-Triacryloyl diethylenetriamine	TADETA	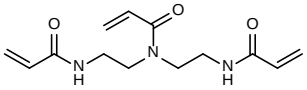
4-Hydroxy-2,2,6,6-tetramethylpiperidine-1-oxyl	TEMPOL	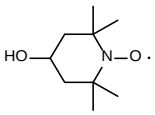

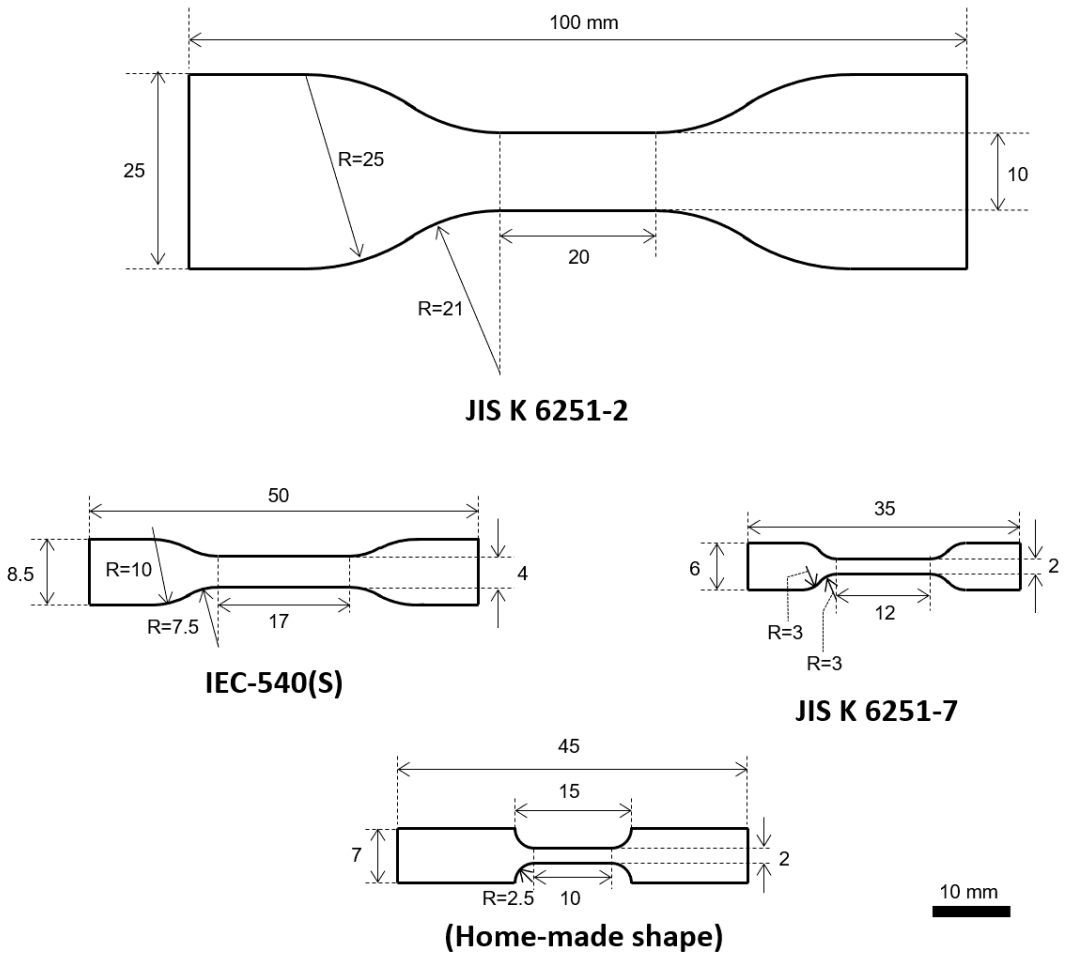

Figure 6-1. Dumbbell shapes used in this chapter for tensile test.

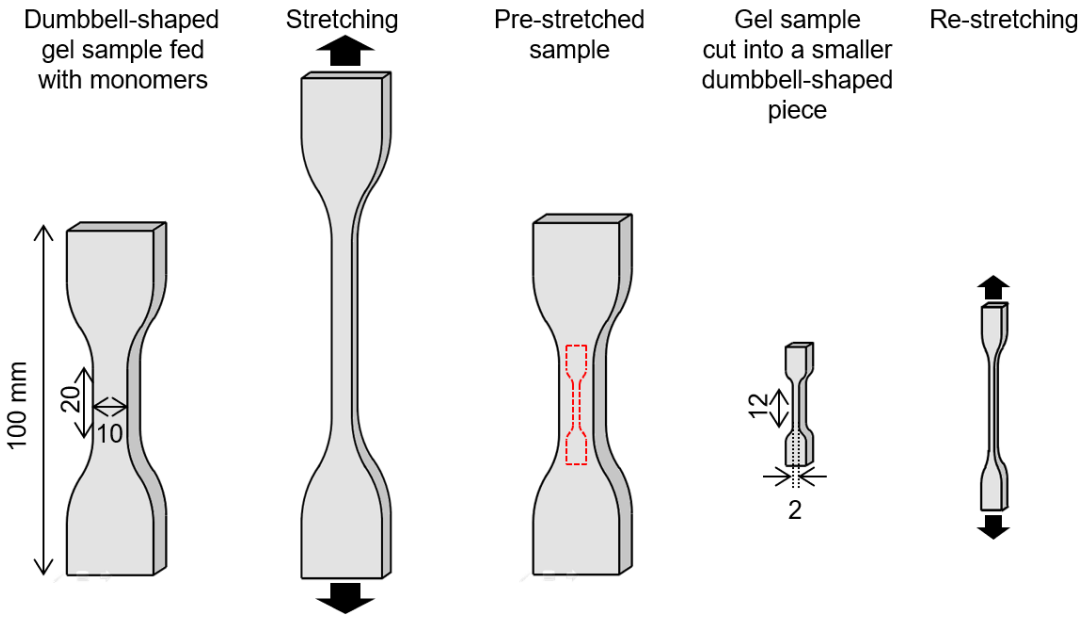

Figure 6-2. Illustration of the procedure for characterizing the self-strengthening due to mechanoradical polymerization in a pre-stretched DN gel by tensile testing described in **sections 6.2.3** and **6.3.2**. The corresponding photographic images of the result are shown in **Figure 6-7**. This figure is from *Science* 363, 504–508 (2019). Reprinted with permission from AAAS.

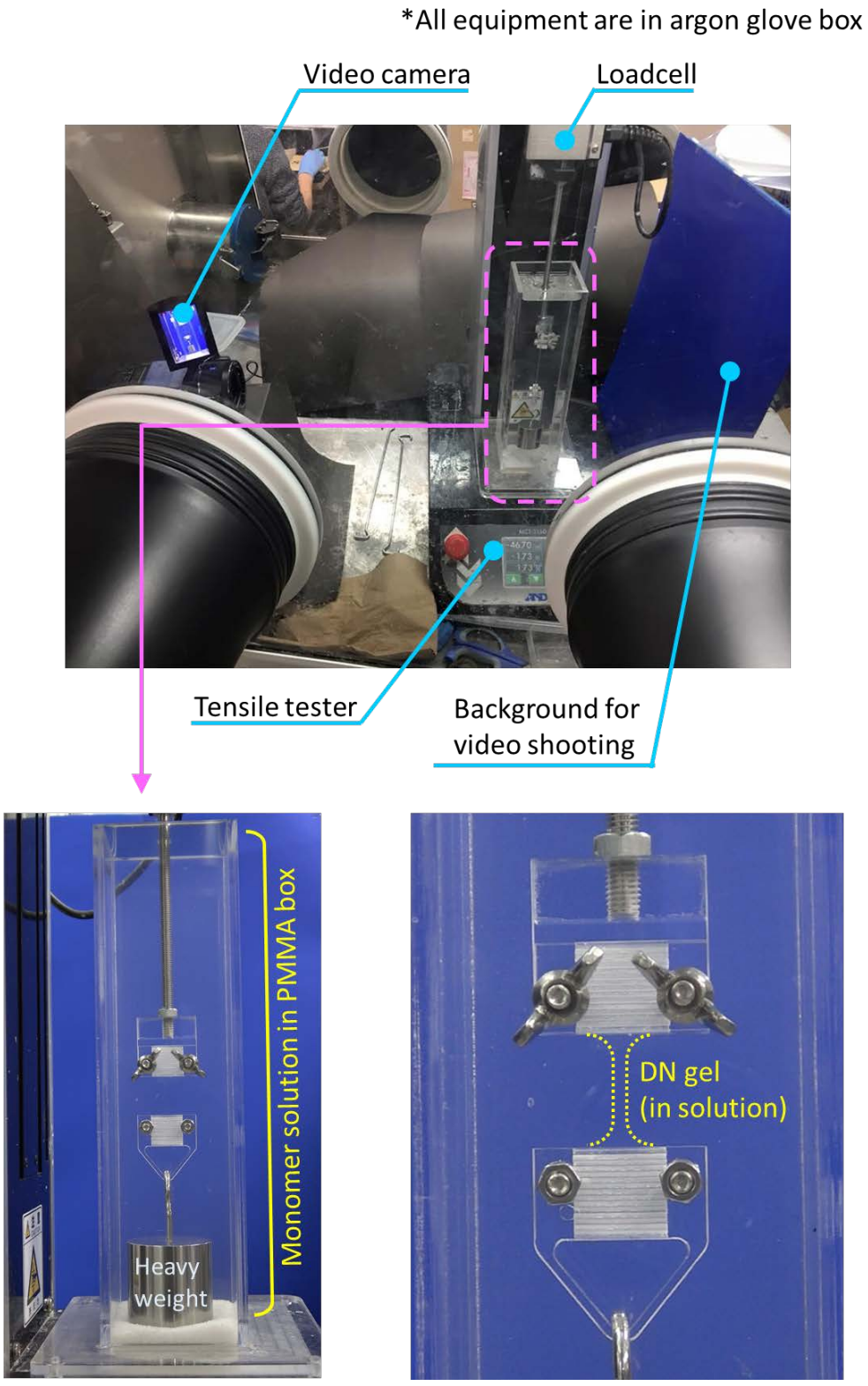

Figure 6-3. Experimental setup of self-growing experiment. A dumbbell-shaped DN gel is repetitively stretched in monomer solution with tensile tester in an argon glovebox.

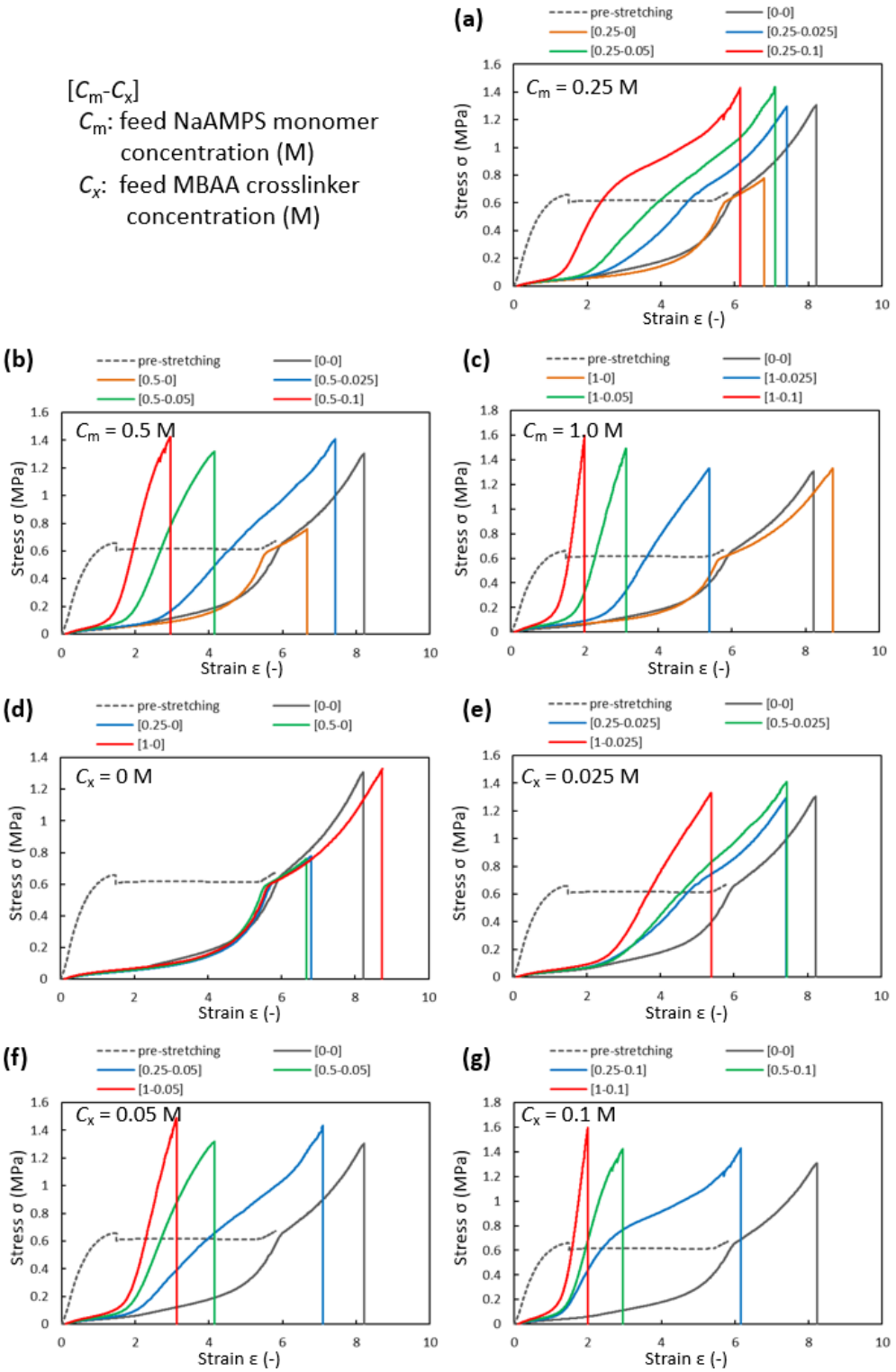

Figure 6-4. Stress–strain curves of virgin and pre-stretched (1-4/4-0.01) DN gels fed with or without NaAMPS (concentration C_m) and/or MBAA (concentration C_x). **(a)–(c)** are summarized by C_m, and **(d)–(g)** are summarized by C_x. The stress and strain were normalized by residual strains induced by pre-stretching (see main text).

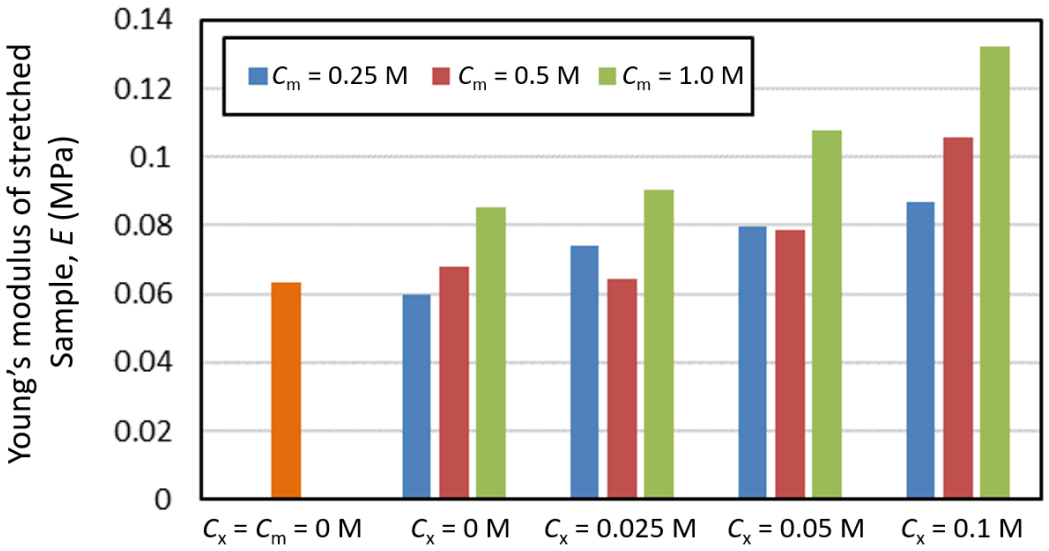

Figure 6-5. Young's moduli of virgin and pre-stretched (1-4/4-0.01) DN gels fed with or without NaAMPS (concentration C_m) and/or MBAA (concentration C_x). The moduli were characterized from the normalized stress−strain curves shown in **Figure 6-4**.

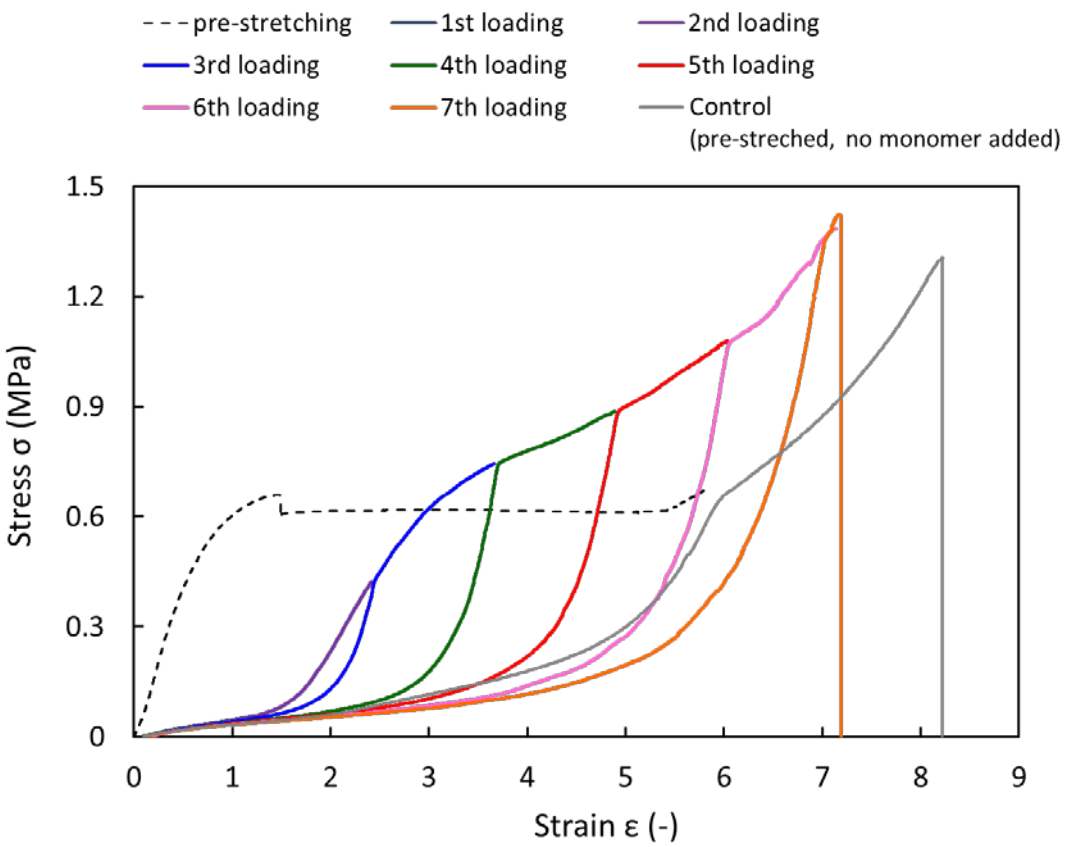

Figure 6-6. Cyclic stress–strain curves of pre-stretched (1-4/4-0.01) DN gel fed with 0.25 M NaAMPS and 0.1 M MBAA. The stress and strain were normalized by residual strains induced by pre-stretching (see main text).

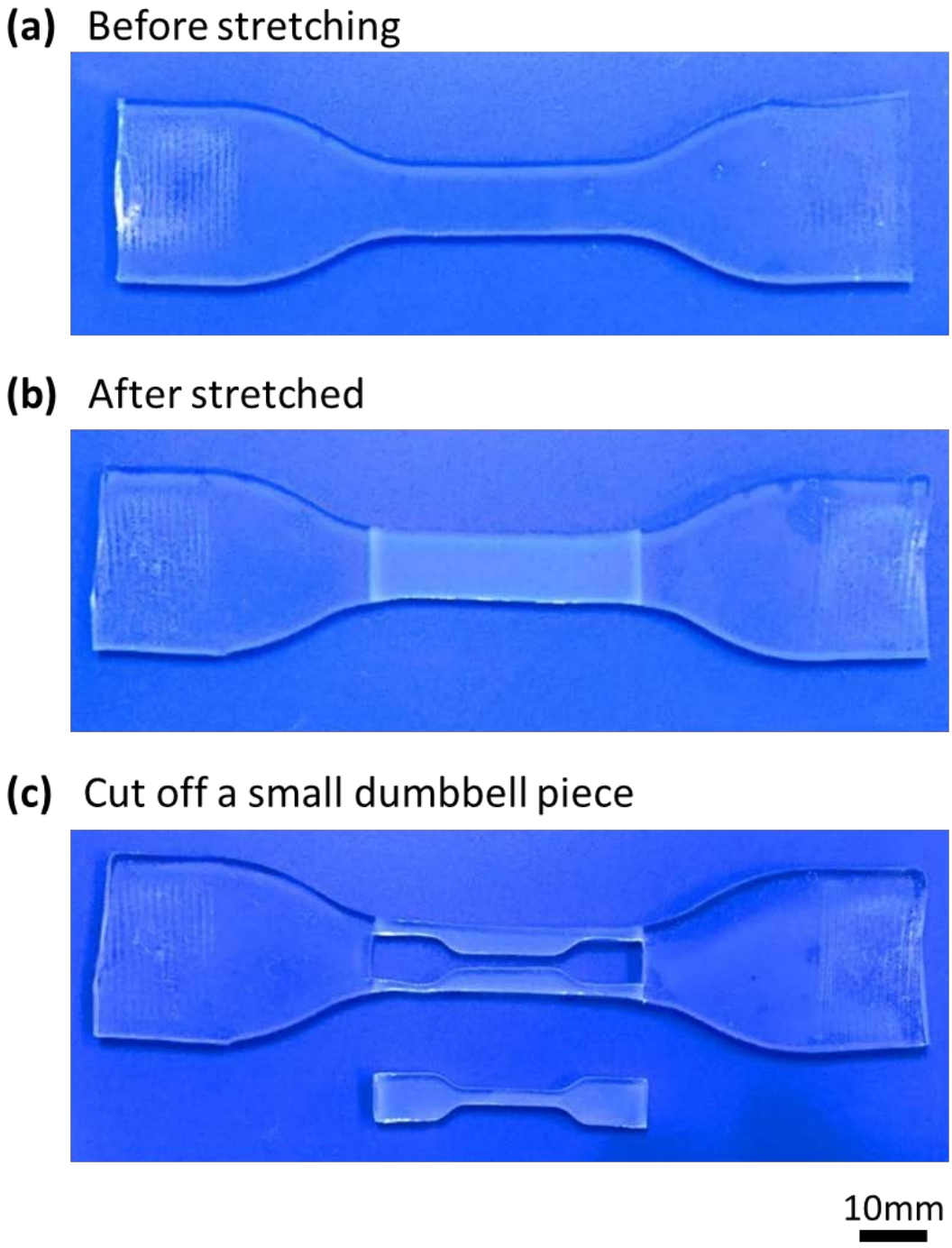

Figure 6-7. Photographic images of the result to explain the procedure for characterizing the self-strengthening due to mechanoradical polymerization in a pre-stretched (1-3/3-0.01) DN gel fed with 0.3 M NaAMPS and 0.3 M TADETA.

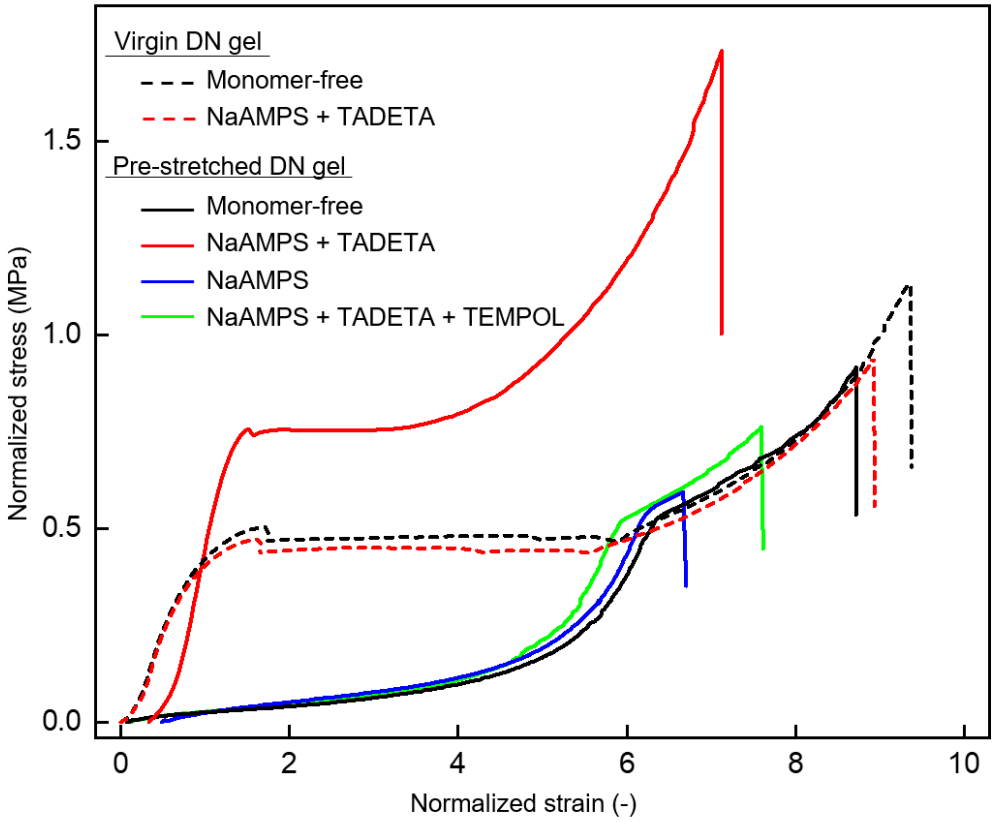

Figure 6-8. Stress–strain curves of virgin and pre-stretched (1-3/3-0.01) DN gels fed with or without NaAMPS and/or TADETA. The pre-stretch strain was $\varepsilon \approx 6$. Black curves ("Monomer-free"): neither NaAMPS nor TADETA was fed. Red curves ("NaAMPS + TADETA"): 0.3 M NaAMPS and 0.3 M TADETA were fed. Blue curve ("NaAMPS"): 1.2 M NaAMPS was fed without TADETA. Green curve ("NaAMPS + TADETA + TEMPOL"): 0.3 M NaAMPS, 0.3 M TADETA and 0.01 M TEMPOL (radical trapping agent) were fed. The stress and strain were normalized by residual strains induced by pre-stretching (see main text). This figure is from *Science* 363, 504–508 (2019) with modifications (changes of overall design including aspect ratio and notations of the key legends, and adding the data of green curve). Reprinted with permission from AAAS.

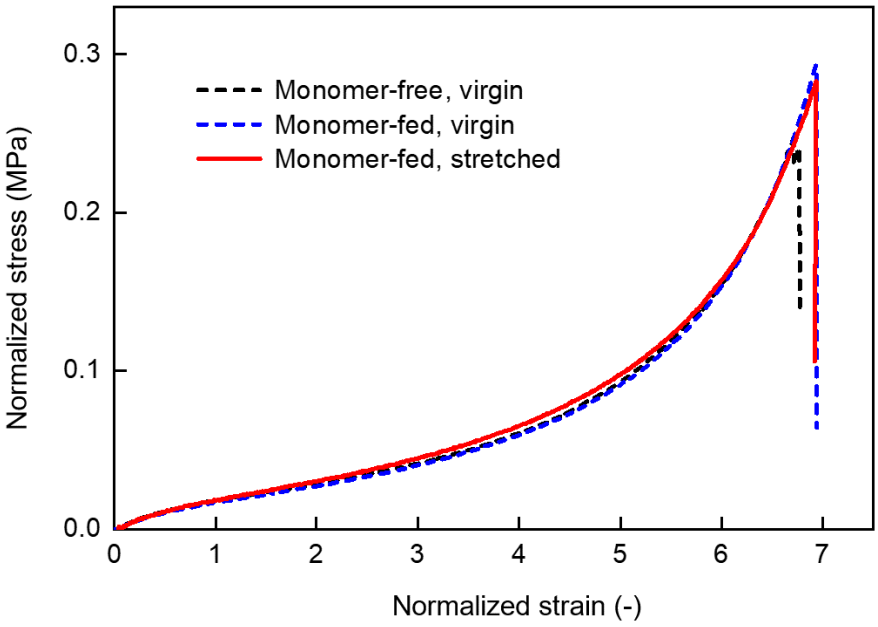

Figure 6-9. Stress–strain curves of the virgin and pre-stretched (3-0.01) PAAm SN gels fed with 0.3 M NaAMPS and 0.3 M TADETA. The pre-stretch strain was $\varepsilon \approx 4$. The stress and strain were normalized by residual strains induced by pre-stretching (see main text). Note that the residual strain of the pre-stretched SN gel was very small as approximately 4%. The data of the unstretched monomer-free (3-0.01) PAAm SN gel was also shown as a reference. This figure is from *Science* 363, 504–508 (2019). Reprinted with permission from AAAS.

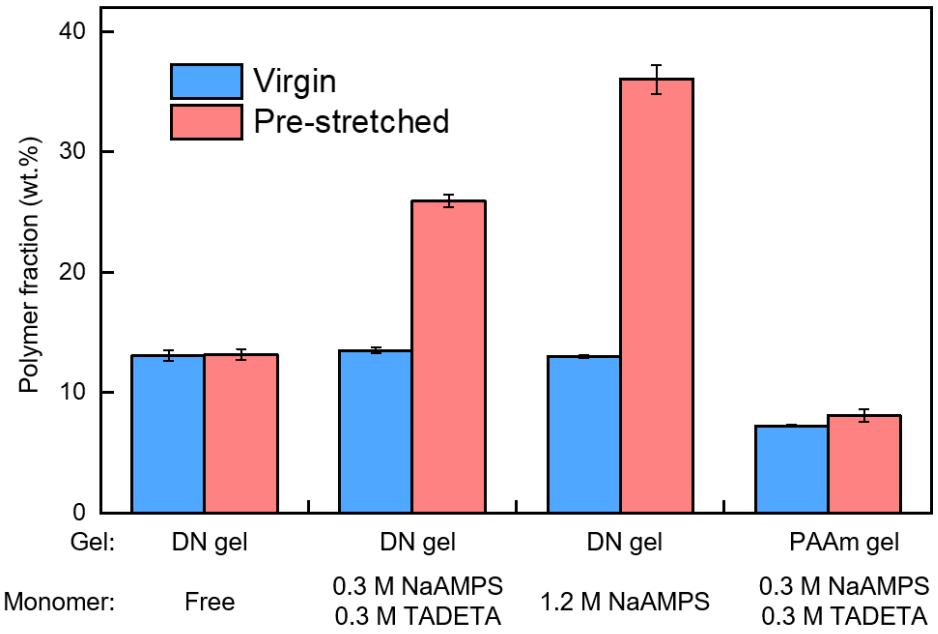

Figure 6-10. Polymer weight fraction in the virgin and pre-stretched (1-3/3-0.01) DN gel and (3-0.01) PAAm SN gels by the mechanoradical polymerization. Pre-stretch strains were $\varepsilon \approx 6$ for the DN gel and $\varepsilon \approx 4$ for the PAAm SN gel. The error bars represent standard deviations for three measurements. This figure is from *Science* 363, 504–508 (2019). The notations at the bottom are modified. Reprinted with permission from AAAS.

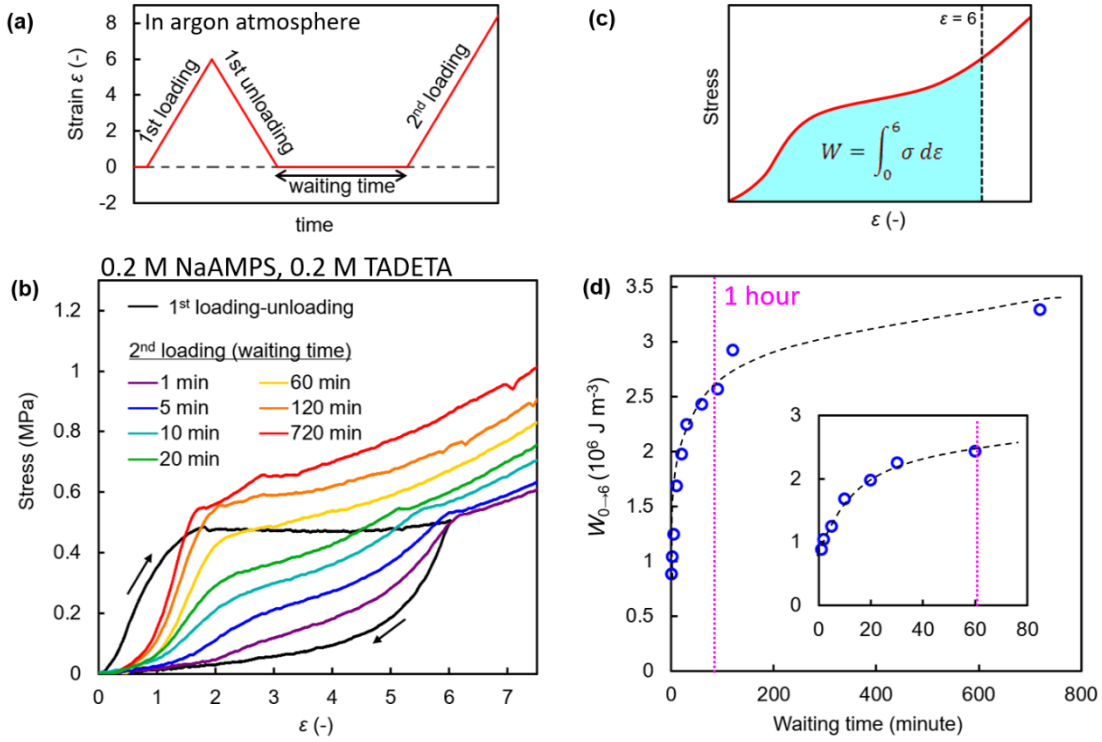

Figure 6-11. Kinetic investigation of mechanoradical strengthening (closed system, (1-3/3-0.01) DN gel fed with 0.2 M NaAMPS and 0.2 M TADETA). **(a)** Time profile of strain applied to the DN gel. **(b)** Stress-strain curves of 1st loading–unloading and 2nd loading with varied waiting times. **(c, d)** Quantitative analysis of the kinetics of mechanochemical strengthening in terms of work of extension from strain zero to pre-stretched strain.

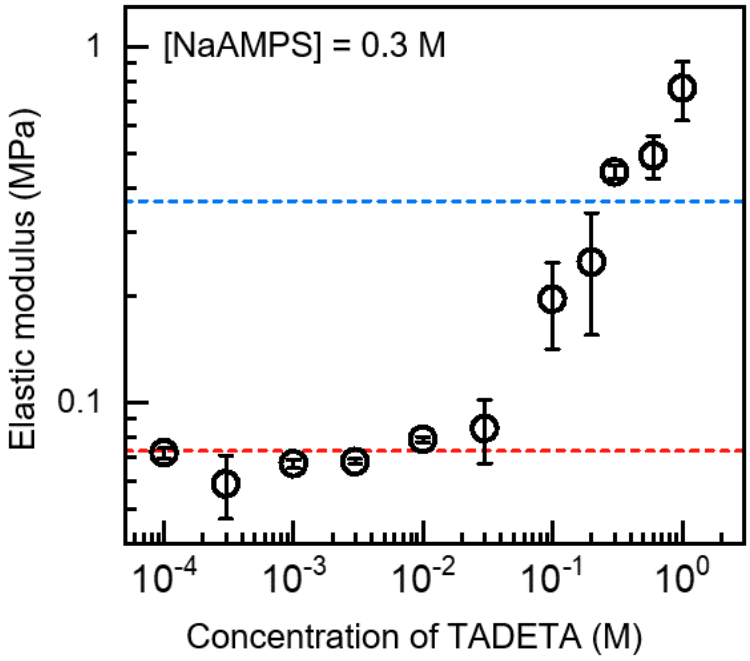

Figure 6-12. Elastic modulus of stretched (1-3/3-0.01) DN gels fed with NaAMPS (0.3 M) and various concentrations of TADETA. The pre-stretch strain was $\varepsilon \approx 6$. The modulus was measured with indentation test. The moduli of the virgin DN and stretched DN gels with no feeding of monomers are shown as blue (0.37 MPa) and red (0.07 MPa) dashed line, respectively. The error bars represent standard deviations for three measurements. This figure is from *Science* 363, 504–508 (2019). The notations are modified. Reprinted with permission from AAAS.

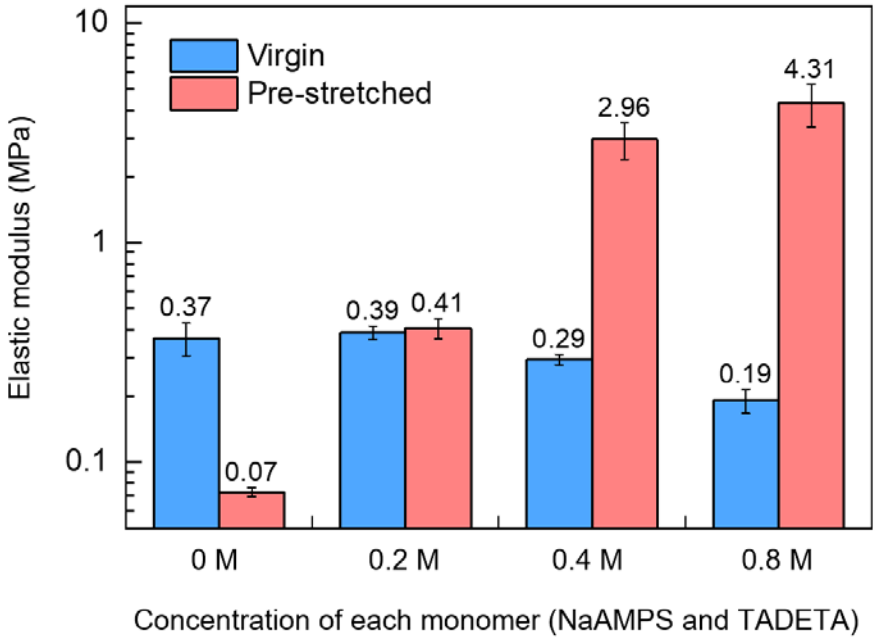

Figure 6-13. Elongation-triggered elastic modulus changes of DN gels fed with various concentrations of NaAMPS and TADETA in a 1:1 (mol/mol) composition. The pre-stretch strain was $\varepsilon \approx 6$. The modulus was measured with indentation test. The error bars represent standard deviations for three measurements. This figure is from *Science* 363, 504–508 (2019). The notations at the bottom are modified. Reprinted with permission from AAAS.

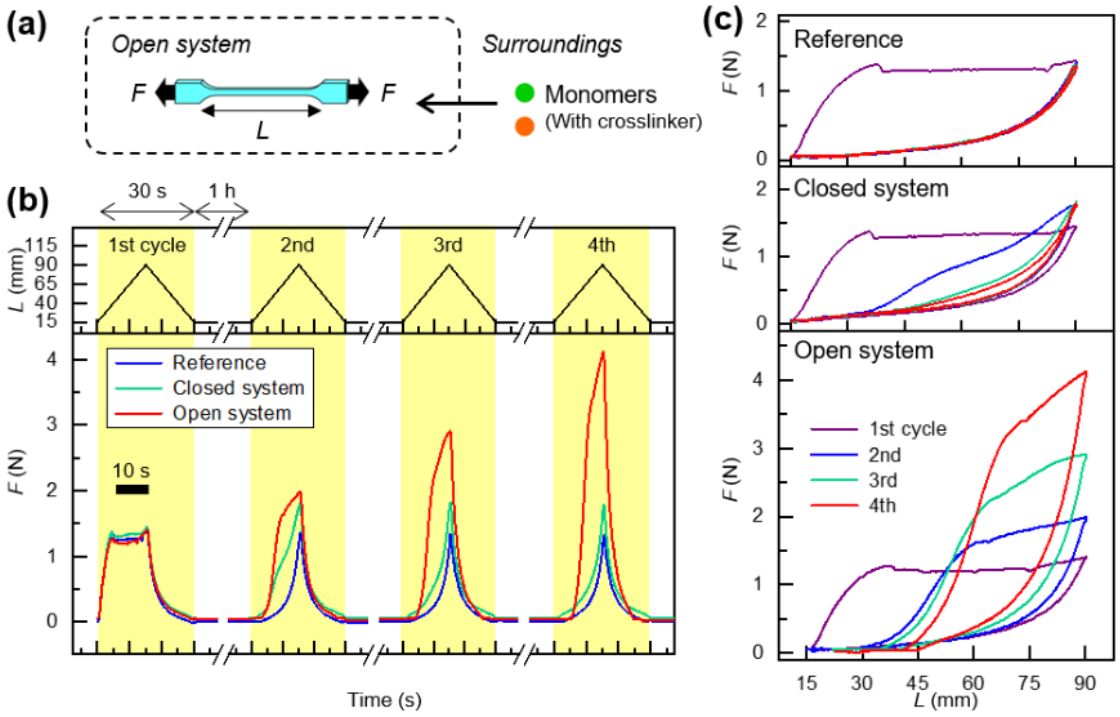

Figure 6-14. Repetitive stretching-triggered mechanical growth of DN gels. **(a)** Illustration of stretching a DN gel with a continuous monomer supply from surrounding solution, acting as an open system. The applied force and the gauge length are denoted by *F* and *L*, respectively. **(b)** Time profiles of the repetitive stretching of (1-3/3-0.01) DN gels (1 mm-thick) in terms of *L* and the required force *F*. The red, green and blue curves represent a (1-3/3-0.01) DN gel stretched in a monomer solution (open system), a (1-3/3-0.01) DN gel pre-fed with monomer and stretched in an argon atmosphere (closed system), and a (1-3/3-0.01) DN gel stretched in pure water (reference), respectively. **(c)** *F*–*L* curves to show the cyclic loading–unloading behavior. For the reference sample, all curves except the first loading curve overlap. An aqueous solution of 0.08 M NaAMPS and 0.08 M MBAA (crosslinker) were used in the experiment. This figure is from *Science* 363, 504–508 (2019). Reprinted with permission from AAAS.

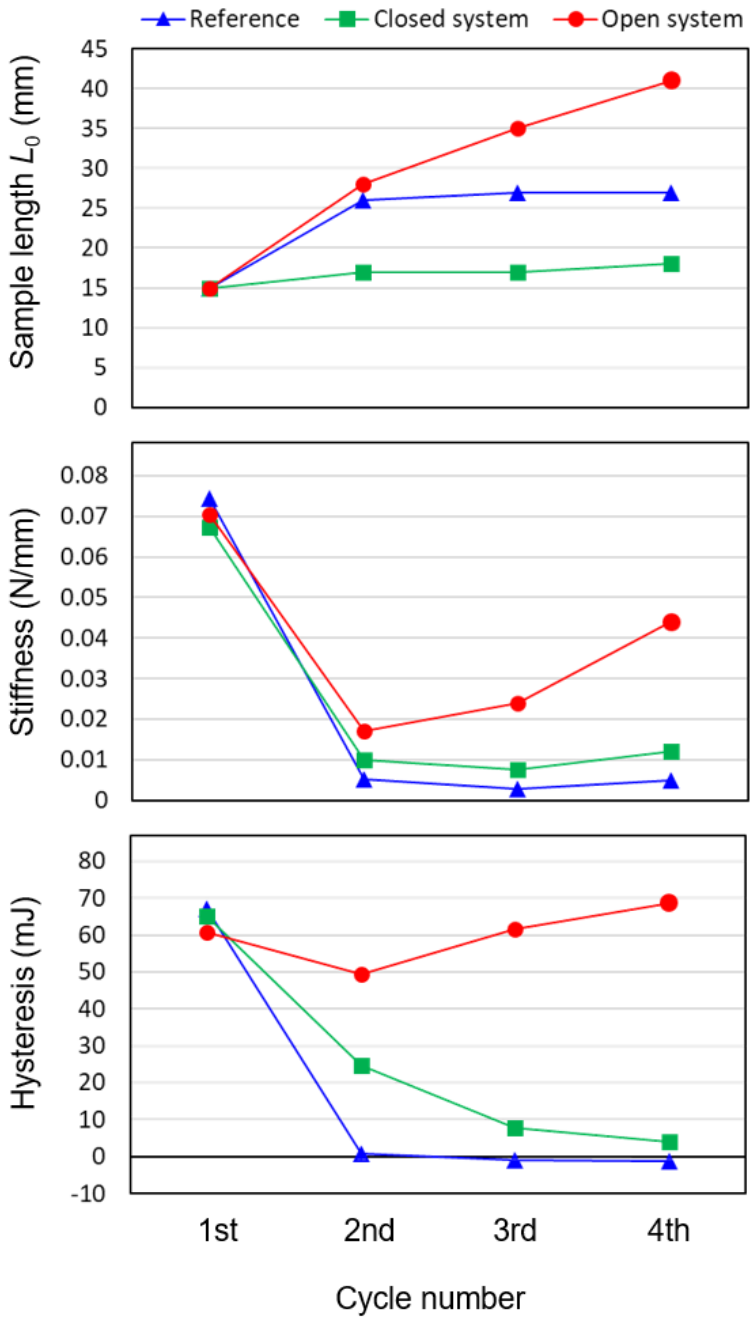

Figure 6-15. Sample load-free length, stiffness and mechanical hysteresis as the function of cycle number under the self-growing experiment. The data are obtained from analysis of the force–length curves in **Figure 6-14c**.

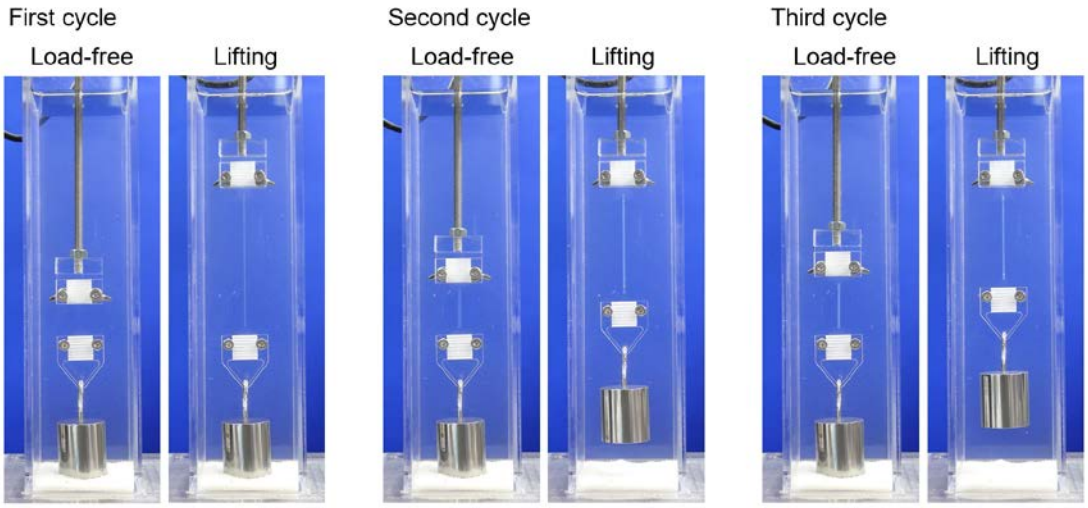

Figure 6-16. Optical images showing the growth on strength and length of a (1-3/3-0.01) DN gel by repetitive mechanical training. In a monomer aqueous solution containing 0.08 M NaAMPS and 0.08 M MBAA, a DN gel (15 mm gauge length, 2 mm width, 1.5 mm thickness) connected to a weight (200 g) was repeatedly lifted to a fixed height. The waiting time between two consecutive cycles was 1 h. This figure is from *Science* 363, 504–508 (2019). Reprinted with permission from AAAS.

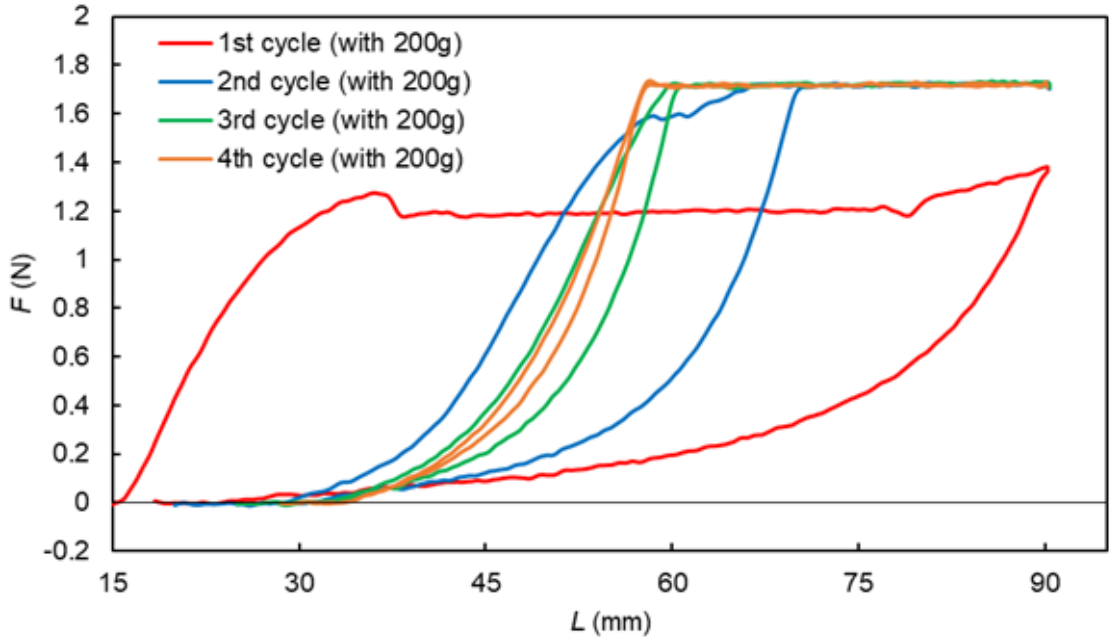

Figure 6-17. Force−length curve of the self-growing experiment corresponding to the photographic images shown in **Figure 6-16**. The force kept constant as ~1.7 N during the lifting of the weight (200 g) from the bottom.

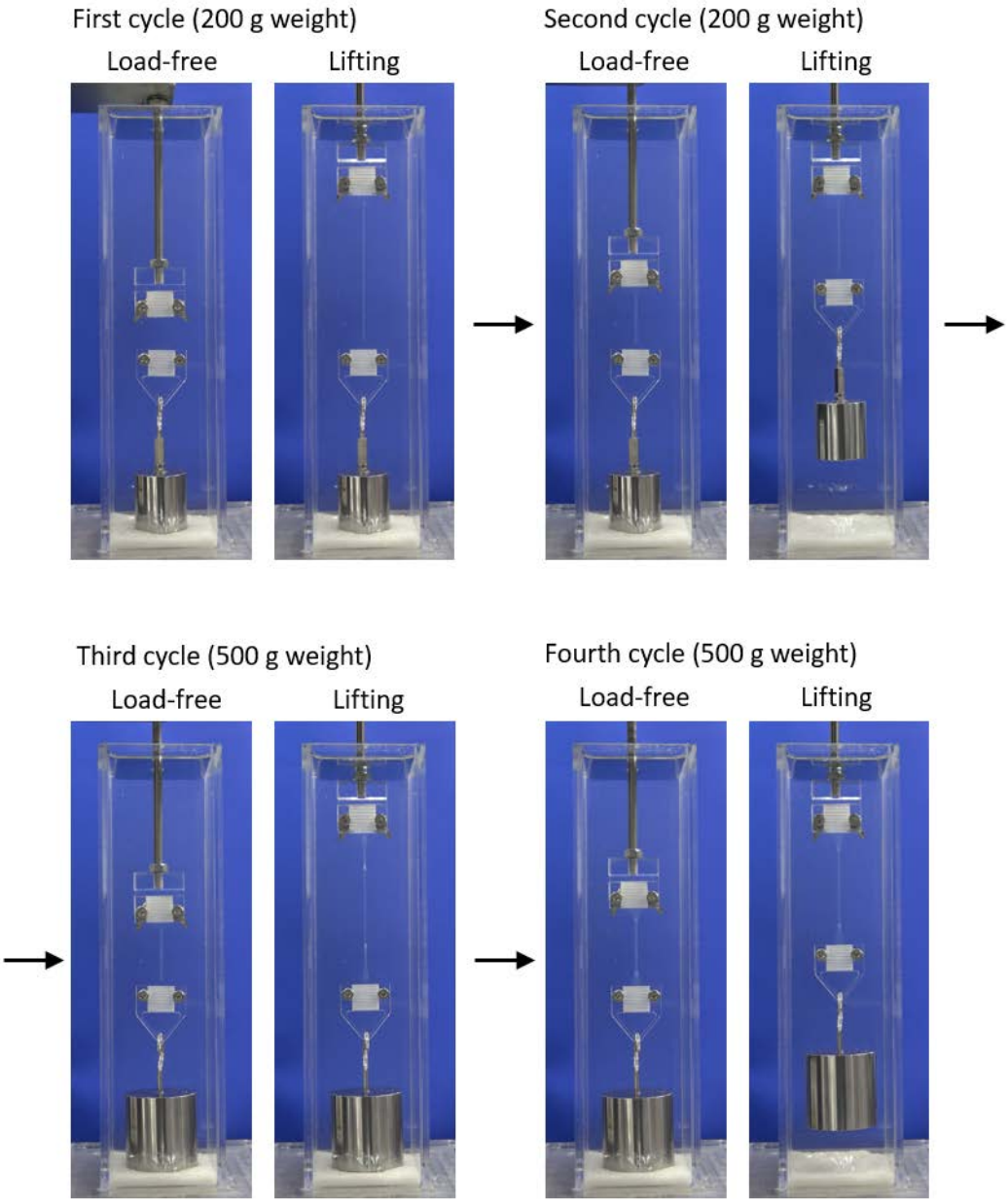

Figure 6-18. Optical images of the growth on strength and length of a (1-3/3-0.01) DN gel by repetitive mechanical training. In a monomer aqueous solution containing 0.3 M NaAMPS and 0.15 M MBAA, a DN gel (15 mm gauge length, 2 mm width, 1.5 mm thickness) connected to a weight was repeatedly lifted to a fixed height. The weight was 200 g for the first and second cycle, and 500 g for the fourth and fifth cycle. The waiting time between two consecutive cycles was 1 h except for that between second and third cycle (5 minutes).

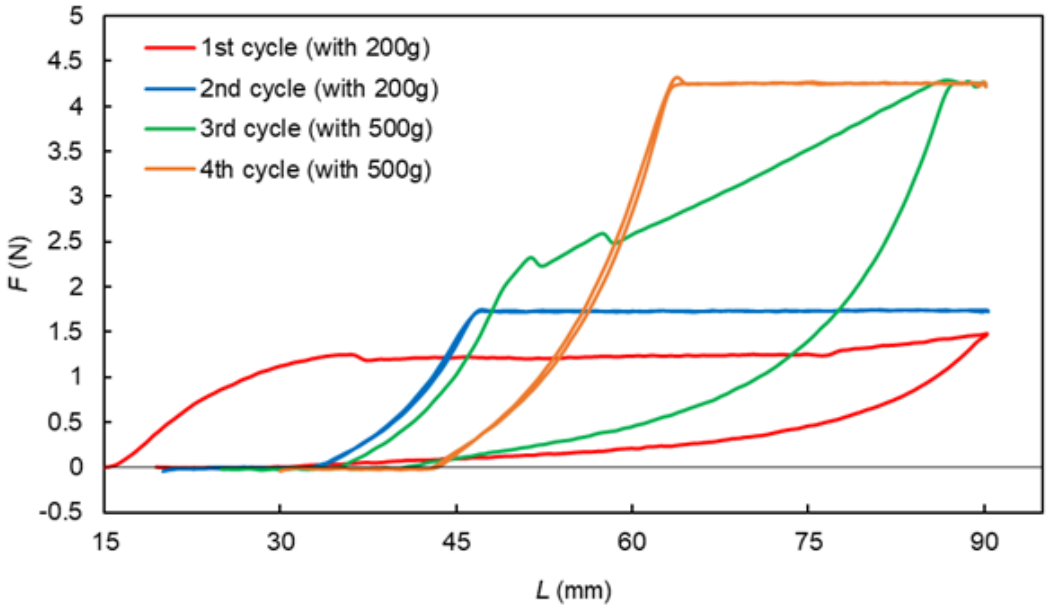

Figure 6-19. Force−length curve of the self-growing experiment corresponding to the photographic images shown in **Figure 6-18**. The force kept constant as ~1.7 N or ~4.3 N during the lifting of the weight (200 g or 500 g, respectively) from the bottom.

Chapter 7: Fabrication of Hybrid Double-Network Elastomers

7.1. Introduction

As described until **Chapter 6**, self-growing hydrogels that gain their strength and size in response to mechanical stressing has been created. In order to broaden potential applications of the self-growing materials, one direction is to apply the growing mechanism from hydrogels to the other materials. Although there are some criteria to achieve the self-growing property, the most critical thing is using materials that create abundant mechanoradicals. Therefore, elaborated network design like DN structure to effectively destruct the nanostructure to induce polymer chain scission is required to apply the self-growing mechanism found in this research.

In this chapter, a strategy to fabricate double-network elastomers with internal fracturing mechanism is proposed. Elastomers are soft and deformable elastic materials without containing solvent which are found ubiquitously in our daily life such as vehicle tires.[1–3] Whereas gels contain solvent so that the major application fields of the gels are usually limited in wet condition such as biomedical applications, elastomers can find broaden application in dried condition. Because elastomers are usually composed of soft polymer network similar as gels, the double-network structure having internal fracturing nature is expected to be straightforwardly applied in elastomers in order to create tough elastomer.

The creation of the DN elastomer is, however, still challenging due to the difficulty to create a contrasting two-network structure for the dried elastomer. According to systematic researches on DN hydrogels, the first and the second network must be brittle and stretchable, respectively, and the concentration of the first network must be much lower than that of the second network (the concentration ratio is 1:10 in typical) to yield

the *tough* DN gel.[4–6] To satisfy the requirement, a densely-crosslinked polyelectrolyte network, such as PNaAMPS network used in **Chapters 3−6**, is typically used as the first network to fabricate a DN hydrogel. Polyelectrolyte networks largely swell with water because of high osmotic pressure arising from the dissociated small counterions of polyelectrolytes.[7] The high swelling of the network induces triaxial prestretching of each polymer strand and dilution of the polymer concentration, resulting in a brittle gel. By synthesizing a concentrated and loosely-crosslinked second network in the brittle polyelectrolyte first network, a tough DN hydrogel is obtained.[4,8] When applying the tough DN system for elastomers, however, the polyelectrolyte approach is difficult to utilize because *elastic* polymers, rubbery state at room temperature which can be used in the second network of the DN elastomers, are usually low-polar polymers. Since ionic dissociation is occurred in polar environment such as in water, neither the low-polar polymers nor the corresponding monomers can not induce swelling of the polyelectrolyte network. Without using the high osmotic pressure of the polyelectrolyte, fabricating tough DN hydrogels and elastomers with showing large hysteresis and stretchability is difficult.[6,8–12] On elastomer, Ducrot et al. has shown that DN elastomer composed of two non-electrolyte polymer network is not so tough.[11] They demonstrated that a triple-network (TN) elastomer get toughen because the prestretching degree of the first network was extended; however, stretchability of the TN elastomer was still small (strain at break less than 200%) without showing yielding phenomenon compared to the tough DN hydrogels. Recently, they reported that quadruplet-network (QN) elastomer exhibits high stretchability with yielding phenomenon.[12] Although the QN elastomer is possibly adapted to our self-growing application, proposing another strategy to fabricate DN or multiple-network elastomer showing internal fracture is also valuable.

Herein, a polyelectrolyte approach to synthesize DN elastomers that exhibit high stretchability accompanying a large mechanical hysteresis is proposed. The idea is using a polar organic cosolvent that has high dielectric constant to fabricate a DN elastomer composed of polyelectrolyte first network and low-polar elastomeric second network. Polyelectrolyte gel highly swells in high dielectric polar solvent such as water because the dissociation of ionic compounds is mainly driven by the high dielectricity of the environment.[13–17] Therefore, if the high dielectric polar solvent is used for the solvent to synthesize the second network and the polyelectrolyte first network highly-swells in the solution, tough DN elastomer with contrasting network structure can be fabricated after removal of the solvent. To realize the idea, the major questions here are: (1) whether the low-polar monomer can be dissolved in the high dielectric solvent because such monomer is usually hardly soluble in water, (2) whether the polyelectrolyte network actually swell in the organic mixture, and (3) whether the resulting DN elastomer shows desired mechanical properties such as toughness and hysteresis. In this chapter, the questions are systematically investigated to leach fabrication of the DN elastomers.

7.2. Experiments

7.2.1. Materials

Deionized water (Milli-Q) was used as water. 2-Acrylamido-2-methylpropane sulfonic acid (AMPS) and 2-acrylamido-2-methylpropane sulfonic acid sodium salt (NaAMPS) were provided by Toagosei. *N*,*N'*-Methylenebisacrylamide (MBAA), 2-oxoglutaric acid, methanol, 1,4-dioxane, anisole, ethyl acetate, tetrahydrofuran, methyl isobutyl ketone, 2-methoxyethanol, cyclohexanone, ethanol, 2-ethoxyethanol, *N*-methylpyrrolidone, *N*,*N*-dimethylformamide, acetonitrile, ethylene glycol, dimethyl sulfoxide (DMSO), *N*-

methylformamide (NMF), 2,2'-azobis(isobutyronitrile) (AIBN), *p*-stylenesulfonic acid sodium salt (NaSS), acrylic acid (AAc), and 2-methoxyethyl acrylate (MTA) were purchased from Fujifilm Wako Pure Chemical Corporation. Propylene carbonate, *N*,*N*-dimethylacetamide, γ-butyl lactone, formamide, lithium chloride (LiCl), ethyl acrylate (EA), butyl acrylate (BA) and tetraethylene glycol diacrylate (4EGDA) were purchased from Tokyo Chemical Industry. Acetone and chloroform were purchased from Kanto Chemical. Polyethylene glycol diacrylate (PEGDA, average molecular weight 250 g/mol), acrylic acid sodium salt (NaAAc) and basic alumina were purchased from Sigma Aldrich. Tetramethyl ammonium ethyl acrylic chloride (ClAETMA) was provided by MT AquaPolymer. 2-(2-Ethoxyethoxy) ethyl acrylate (EEEA) was provided by Osaka Organic Chemical Industry. All the chemicals except for EA, BA and EEEA were used as received. For the use of polymerization, EA, BA, and EEEA were purified by passing through basic alumina before use. The abbreviations and chemical structures of some important chemical compounds used in this section are summarized in **Table 7-1**.

7.2.2. Measurement of dielectric constant of solvent and solution

Dielectric constant of solvents and solutions were measured with a commercial double cylinder type dielectric constant meter (Model 871, Nihon Rufuto Co.) at a frequency of 10 kHz at room temperature. The temperature of the liquid was measured individually. Calibration of the dielectric constant meter was carried out using air and deionized water.

7.2.3. Synthesis of polyelectrolyte gels for the first network

The synthetic procedure of the first network was well similar as that described in **section 3.2.2**. Aqueous solutions of C_1 (M) monomer, x_1 (mol%) MBAA as a crosslinker, and 1.0

mol% 2-oxoglutaric acid as a photo-induced radical initiator were prepared. The concentrations (mol%) of the initiator and crosslinker are the molar ratio with respect to the monomer. As the monomer, NaAMPS was mainly used; and NaAAc, NaSS, ClAETMA, AMPS and AAc were also used. On the synthesis of PNaAMPS gel, the concentrations of monomer and crosslinker were C_1 = 1.0 M and x_1 = 2−10 mol%, respectively. For synthesis of PNaAAc, PNaSS, PClAETMA and PAMPS gel, the concentrations were C_1 = 1.2 M and x_1 = 3 mol%, respectively. Each precursor solution containing monomer, crosslinker and initiator was moved to an argon glovebox (MBRAUN, oxygen concentration <100 ppm). Then, the solution was poured into a cuboid mold comprising two flat soda-lime glass plates (3-mm thickness, 10 cm × 10 cm) separated by a silicone rubber (0.5, 1.0 or 2.0 mm). Each solution in the mold was irradiated with UV light (365 nm, 4 mW cm^{-1}) from both sides for 8 hours to promote radical polymerization.

7.2.4. Measurement of swelling ratio of PNaAMPS gel in various solvent

The synthesized (1-3) PNaAMPS hydrogel (thickness at as-polymerized state t_0 = 1.0 mm) was cut into cylinder-shaped pieces (~6 mm radius). The gel pieces were immersed in methanol for more than 2 days to exchange the solvent in the gel from water to methanol. A swollen gel (~0.1 cm^3) with methanol was immersed in a solvent or solution (~100 mL) for 5 days. The volumetric swelling ratio, V/V_0, from the as-polymerized state to the swollen state was calculated under the assumption of the isotropic swelling:

$$V/V_0 = (t/t_0)^3 \qquad (7.1)$$

where t_0 and t are the thickness of the gel at as-polymerized state and swollen state, respectively.

7.2.5. Measurement of elastic shear modulus μ of (1-3) PNaAMPS gel swollen with solutions

The synthesized (1-3) PNaAMPS hydrogel, 2.0 mm-thick, was cut into cylinder shaped pieces (approximately 6 mm-diameter). The gel pieces were immersed in water or NMF for more than 3 days. The solvent choice (water or NMF) was corresponding to the solvent used in the following solution. Each gel piece (~1 cm^3) swollen in water or NMF was immersed in a solution (~100 mL) of LiCl in water, LiCl in NMF, or EA/NMF binary mixture for more than 5 days. The volumetric swelling ratio was calculated using **equation 7.1** described in **section 7.2.4**. Elastic modulus of each gel was measured by the indentation methods using a spherical indenter (1.0 mm radius) and commercial mechanical testing machine (Autograph AG-X 20kN, Shimadzu Co.) operating at a crosshead velocity of 1 mm min^{-1}. The modulus was determined by Hertzian equation for incompressible soft materials as described in **section 6.2.6**. In this chapter, elastic shear modulus μ was characterized instead of Young's modulus *E*, by using the relationship $E = 3\mu$ for incompressible isotropic materials.

7.2.6. Synthesis of PEA organogels and elastomers

The PEA organogels and elastomers were synthesized for preliminary experiment and control experiment. On the preliminary experiment, a solution of 45 wt.% EA, x_2 (mol%) PEGDA as a crosslinker, x_2 (mol%) AIBN as an initiator, and 55 wt.% NMF was prepared. Here x_2 was varied as 0.005, 0.01, 0.03 and 0.1 mol% that correspond to 0.006, 0.01, 0.03 and 0.11 wt.% for PEGDA and 0.004, 0.007, 0.02 and 0.07 wt.% for AIBN, respectively. Each precursor solution containing monomer, crosslinker and initiator was moved to an argon glovebox (MBRAUN, oxygen concentration <100 ppm). Then, the solution was

poured into a cuboid mold comprising two flat soda-lime glass plates (3-mm thickness, 10 cm × 10 cm) separated by a silicone rubber. Each solution in the mold was irradiated with UV light (365 nm, 4 mW cm^{-1}) from both sides for 9 hours to promote radical polymerization.

On the control experiment, a solution of 50 wt.% EA (~5.2 M), 0.2 wt.% 4EGDA (0.13 mol% to the monomer), 0.1 wt.% AIBN (0.12 mol% to the monomer) and 49.7 wt.% NMF was prepared. The precursor solution was irradiated with UV light in argon glovebox with same procedure above to proceed the polymerization.

7.2.7. Fabrication of DN elastomers

Here synthetic procedure for a PNaAMPS/PEA DN elastomer is described as a representative. The PNaAMPS/PEA DN elastomer composed of PNaAMPS first network and PEA second network is typically used in this research. PNaAMPS hydrogel sheet at as-polymerized state, 0.5 mm thick, was immersed in NMF for more than 3 days to exchange the solvent in the gel from water to NMF. The PNaAMPS gel swollen with NMF was immersed in second network precursor solution for 5 days. The second network precursor solution is composed of EA as monomer (weight fraction f_{EA} = 20–60 wt.%), 4EGDA as crosslinker (weight fraction f_c = 0.2 wt.%), AIBN as initiator (weight fraction f_i = 0.1wt.%) and NMF as solvent (weight fraction f_{NMF} (wt.%) = 100− f_{EA} − f_c − f_i). The second network in the swollen PNaAMPS network was synthesized using identical procedure described in **section 3.2.4**. Briefly, the PNaAMPS gel swollen with the second network precursor solution was sandwiched between glass plates and was irradiated UV light in argon glovebox for 9 hours. As the result, DN organogel was obtained. Afterwards, the synthesized DN organogels are immersed in acetone for more than 4 days to exchange

the solvent in the gel from NMF to acetone. The gel swollen with acetone was then stored *in vacuo* (<20 mbar) at room temperature for more than 5 days to remove the acetone, resulting a DN elastomer was obtained. Before mechanical characterization, the DN elastomer was stored under room condition (~25 ℃ and ~50% relative humidity). When the other DN elastomers were synthesized, same procedure was carried out. Note that only when the PNaAAc network was used as the first network, the as-polymerized PNaAAc hydrogel was first swollen in water for one day, and then immersed in NMF. This is because the gel would shrink if the as-polymerized hydrogels was directly immersed in NMF.

7.2.8. Characterization of volume fraction of each component

Volume fraction, ϕ, of each polymer component in the PNaAMPS/PEA DN elastomers and organogels were calculated. In this calculation, we put following assumptions: (1) the swelling and shrinking was isotropic so that volume change can be calculated from thickness change; (2) the specific density of each component was always identical even when surrounding environment (e.g. solvent) changed; (3) the PNaAMPS network virtually comprised only PNaAMPS (i.e., the amount of crosslinker and initiator was negligible compared to PNaAMPS main chain); (4) all NaAMPS monomers were incorporated into the first network (assuming 100% conversion and 0% sol fraction); and (5) there is no residual solvents in the dried elastomer. Using these assumptions, ϕ of each polymer component and solvent were calculated as:

$$\phi_{1\mathrm{st},0} = \frac{C_1 M_1}{\rho_{\mathrm{PNaAMPS}}} \left(\frac{1}{1000 - \frac{C_1 M_1}{\rho_{\mathrm{NaAMPS}}} + \frac{C_1 M_1}{\rho_{\mathrm{PNaAMPS}}}} \right) \qquad (7.2)$$

$$\phi_{1st,dry} = \phi_{1st,0}\left(\frac{t_{dry}}{t_0}\right)^{-3} \quad (7.3)$$

$$\phi_{2nd,dry} = 1 - \phi_{1st,dry} \quad (7.4)$$

$$\phi_{1st,gel} = \phi_{1st,dry}\left(\frac{t_{gel}}{t_{dry}}\right)^{-3} \quad (7.5)$$

$$\phi_{2nd,gel} = \phi_{2nd,dry}\left(\frac{t_{gel}}{t_{dry}}\right)^{-3} \quad (7.6)$$

$$\phi_{solvent,gel} = 1 - (\phi_{1st,gel} + \phi_{2nd,gel}) \quad (7.7)$$

where ϕ_{1st}, ϕ_{2nd}, and $\phi_{solvent}$ denote the volume fraction of the first and second network and solvent, respectively. The subscripted "0", "dry" and "gel" denote as-polymerized state of the first network, solvent-free dried elastomer state, and organogel state, respectively, and C_1, M_1, ρ_{NaAMPS}, $\rho_{PNaAMPS}$, and t denote the monomer concentration (1.0 M) in feed, molar mass of the NaAMPS (229.24 g mol^{-1}), specific density of NaAMPS (1.52 g cm^{-3}), PNaAMPS (1.74 g cm^{-3}),[18] and the thickness of the sample, respectively.

7.2.9. Uniaxial tensile test and the cyclic test

Tensile test was carried out similar as described in **sections 3.2.6** and **4.2.6**, but there are some differences such as specimen size and strain measurement protocol. Fabricated elastomers and gels, 0.4–1.3 mm thick, were cut into dumbbell-shaped pieces standardized to JIS K 6251-7 (12-mm gauge length and 2-mm width, **Figure 7-1**). Tensile test for each sample was carried out using the tensile tester (INSTRON 5965, Instron Co.) at the crosshead velocity of 100 mm min^{-1} corresponding to a nominal strain rate of ~0.1 s^{-1}. Nominal stress σ was calculated from measured force divided by original cross-sectional area vertical to the load. The elongation ratio, λ, was characterized as:

$$\lambda = 1 + D/L_0 \quad (7.8)$$

where D and L_0 are displacement length (D = 0 at the load free state) and the gauge length of the sample (L_0 = 12 mm), respectively. Note that the elongation ratio was characterized without using video extensometer that was used in **Chapters 3−6** because the stretchability of some DN elastomers are too large to be detected by the video extensometer. To characterize the Young's modulus of the DN elastomers from the σ–λ curve, the slope of the curve at small deformation regime ($1.01 < \lambda < 1.05$) was obtained by linear fitting. Note that the data around $1 < \lambda < 1.01$ was excluded because of the experimental noise due to inertia. Input mechanical energy density applied until material break, W_b, was calculated as:

$$W_b = \int_1^{\lambda_b} \sigma \, d\lambda \qquad (7.9)$$

where λ_b is the elongation ratio at break. True stress σ_T was calculated as $\sigma_T = \lambda\sigma$, assuming the elastomers are isotropic incompressible soft material. Cyclic tensile test was also performed using same experimental setup and condition described above.

For the tensile test of the dried PNaAMPS network, the as-polymerized (1-3) PNaAMPS gel (0.5 mm-thick) was cut into dumbbell-shaped pieces standardized to JIS K 6251-6 (25 mm gauge length and 4 mm width) and then dried under room condition (~25℃ and ~50% relative humidity) for 5 days. The tensile test of the dried sample (~15 mm gauge length, 2.4 mm width and 0.37 mm thickness) was performed with same procedure above.

7.2.10. Fracture test with single-edge notched geometry

Fracture test with single-edge notched specimen was carried out, similar to previous reports for rubbers, gels and multiple-network elastomers.[2,11,19,20] The elastomers were cut into cuboid-shaped pieces (7.8 mm width, ~70 mm length and 0.4–1.0 mm thickness).

On each sample, a notch (length c_0 = 2.0 ± 0.3 mm) was made in the middle of the strip of the material using a microtome razor blade (**Figure 7-2**). The length c_0 was individually measured for each sample. Two white dots were applied with a pen at the lower half of the specimen to measure the local displacement using video extensometer (AVE, Instron Co.) (**Figure 7-2**). The specimen was fixed between two clamps so that initial sample gauge length between the two clamps was 40 ± 2 mm. The sample was then stretched with a tensile tester (INSTRON 5965, Instron, Co.) at the crosshead velocity of 10 mm min^{-1} (nominal strain rate of 0.004 s^{-1}). During the stretching, force, displacement, and local deformation between the two dots were measured. The fracture energy G_c, which is the critical energy release rate at the initiation of crack propagation, was calculated as:

$$G_c = 2kW_c c_0 = \frac{6W_c c_0}{\lambda_c{}^{1/2}} \qquad (7.10)$$

where k, W_c and λ_c are the prefactor close to 3 that depends on elongation ratio,[19,20] critical strain-energy density in the material, critical elongation ratio, respectively. For the prefactor k, empirical factor $k = 3\lambda^{-1/2}$ that is commonly used was utilized.[2,11,20] For the critical point for W_c and λ_c is corresponding to the point where crack propagation was started under the extension (see **section 7.3.9**).

7.2.11. Fracture test with trouser shaped geometry

Tearing fracture test with a trouser-shaped specimen was carried out, similar to previous reports for rubbers and gels.[2,21–24] The sample (thickness t = 0.4–1.0 mm) was cut into trouser shape (full width 7.8 mm, each leg's width b = 3.9 mm) (**Figure 7-3**). Each leg was fixed to a separated clamp. Two white dots were applied with a pen to the lower leg of the sample to measure the local deformation of the leg by a non-contacting video extensometer (AVE, Instron Co.) (**Figure 7-3**). The sample was torn with a tensile tester

(INSTRON 5965, Instron Co.) at a crosshead velocity of 100 mm min^{-1}. Force, displacement, and the leg's local deformation were measured during the tearing. The tearing fracture energy T_c was calculated as:

$$T_c = \frac{2F_c\lambda_c}{t} - 2bW_c \qquad (7.11)$$

where F_c, λ_c and W_c are the average critical force, the average critical elongation ratio of the leg, and the average critical strain energy, respectively, during the crack propagation. The λ_c and W_c were measured by the σ–λ curve of the sample leg, where λ was measured using the displacement between two white dots observed by the video extensometer. The critical strain energy density W_c was assumed to be identical to the *input* strain energy density.

7.3. Results and Discussion

7.3.1. Swelling behavior of a PNaAMPS network in pure organic solvents

To confirm that the polyelectrolyte network can swell not only in water but also in organic media with high dielectric constant, swelling degree of the (1-3) PNaAMPS network in many, 23 kinds of, organic solvents with various dielectric constant ε_r were characterized. The solvents used here and their ε_r are summarized in **Table 7-2**. In this swelling experiment, (1-3) PNaAMPS gel synthesized as hydrogel was used. Since some organic solvents used here (chloroform, anisole, etc.) are not miscible with water, the hydrogel was first immersed in methanol to exchange the solvent in the gel from water to methanol that is miscible with any solvents used here. The PNaAMPS gel swelled in the methanol at the volumetric swelling ratio of V/V_0 = 7.4, indicating methanol is good (at least not bad) solvent for the PNaAMPS. Afterwards, the gel pieces are immersed in each various organic solvent or water. The results are summarized in **Figure 7-4** in terms of the

swelling ratio as the function of ε_r. (Some swelling data for (1-2.5) PNaAMPS gel and their photographical images are also shown in **Figure 7-5** as supplemental information.) It should be noted that the quantitative values of V/V_0 for gels with $V/V_0 < 4$ may not be accurate because V/V_0 was calculated from thickness change assuming homogeneous swelling but most of the gels characterized as $V/V_0 < 4$ collapsed and had curved inhomogeneous shapes and hard surface, indicating surface-skin layers formed due to the incompatibility of PNaAMPS with the solvent (see pictures in **Figure 7-5**). This restricted the homogeneous shrinking of the gel. On the other hand, the swollen gel with $V/V_0 > 4$ were observed to be homogeneously swollen. Therefore, the quantitative values of V/V_0 for the swollen gel ($V/V_0 > 4$) are considered as accurate, except for experimental errors on measuring thickness by caliper ($\lesssim$ 5% errors in thickness). As shown in **Figure 7-4** (blue squares), the PNaAMPS network substantially swells in high-dielectric solvents: i.e., ethylene glycol ($\varepsilon_r = 38$, $V/V_0 = 14$), dimethyl sulfoxide (DMSO, $\varepsilon_r = 47$, $V/V_0 = 13$), formamide ($\varepsilon_r = 111$, $V/V_0 = 16$) and *N*-methyl formamide (NMF, $\varepsilon_r = 182$, $V/V_0 = 18$) as well as in water ($\varepsilon_r = 78$, $V/V_0 = 16$). On the other hand, the PNaAMPS network collapsed in organic solvents having low ε_r. Clear boundary was observed at around $\varepsilon_r = 40$, even though we can observe two exceptions: 2-methoxy ethanol ($\varepsilon_r = 17$, $V/V_0 = 4.7$) and propylene carbonate ($\varepsilon_r = 66$, collapsed). In previous researches, similar volume transition with ε_r has also been observed for other polyelectrolyte networks such as alkali-metal Poly(acrylic acid) gel, quaternized poly(4-vinylpyridine) gel and alkali-metal poly(styrene sulfonate) gel, of which the transition values of ε_r typically vary from 20 to 70.[15,16,25] The transition value depends on the interaction of solvent with counterions or polymer backbones,[15,16,25] which may explain the two exceptions in the result here. According to the result, we found that polyelectrolyte networks can swell highly in

organic solvents with ε_r that is higher than the critical values.

7.3.2. Miscibility of high dielectric solvent with a monomer for the second network

To select the appropriate high dielectric solvent, simple miscibility test was carried out. As a model system, the author selected ethyl acrylate (EA) as a monomer for the second network. The corresponding polymer poly(ethyl acrylate) (PEA) is rubbery polymer of which glass transition temperature is enough lower than room temperature (approximately −20°C).[11,26,27] Considering the result in **section 7.3.1**, DMSO (ε_r = 47), formamide (ε_r = 111), NMF (ε_r = 182) and water (ε_r = 78) were chosen to check the miscibility with EA. As the result, EA was not arbitrarily miscible with formamide and water because EA is hydrophobic low polar molecule; whereas EA was miscible with DMSO and NMF at arbitrarily ratio. The important finding here is that NMF was miscible with low-polar EA even though the ε_r of NMF is quite high as 182 that is much higher than ε_r of water (78). The other solvents such as *N*-methylpropioneamide (ε_r = 172) may also be used because it seems to have better compatibility with organic compounds considering the molecular structure. However, considering current commercial availability and price, NMF seems to be the best solvent to be investigated. Therefore, I used NMF as an appropriate solvent in this work.

7.3.3. Swelling behavior of a PNaAMPS network in EA/NMF binary mixture

To achieve the purpose of my research, polyelectrolyte network has to swell highly in the mixture of monomer for rubbery polymer and high dielectric solvent. As the model system, swelling behavior of a PNaAMPS network in EA/NMF binary mixture was investigated. For comparison, the swelling behavior in EA/DMSO binary mixture was

also characterized. The result of the swelling ratio as the function of weight fraction of EA, f_{EA}, is shown in **Figure 7-6**. The PNaAMPS highly swelled as $V/V_0 > 10$ when f_{EA} was small. The swelling ratio was gradually decreased with the f_{EA}, and the volume transition was observed at around f_{EA} = 70 wt.% for EA/NMF and f_{EA} = 35 wt.% for EA/DMSO. At the same f_{EA}, the swelling ratio in NMF is higher than that in DMSO. These results are because NMF has higher ε_r than DMSO. Hence, to achieve the wide range applicability of the EA concentration, NMF is better than DMSO.

To consider the volume transition for EA/NMF binary mixture, the dielectric constant ε_r of the binary mixture was measured by commercial dielectric constant meter. The ε_r of the pure EA was quite low as 5.8 which is comparable with chloroform (4.8) and ethyl acetate (6.0). As shown in **Figure 7-7**, ε_r of the dielectric constant decreased monotonically with increasing the EA weight fraction. The ε_r kept high value even at relatively high EA concentration, for example, ε_r = 70.6 for f_{EA} = 50 wt.% which is comparable with pure water. The plots do not behave linear relationship, which is usually observed for the ε_r of binary mixtures.[28,29] With using the measured ε_r values, the swelling ratio in EA/NMF binary mixture was plotted as a function of the ε_r (**Figure 7-4**, red circles). The transition value was observed around $\varepsilon_r \approx 40$ that is corresponding to the data for pure solvents (blue squares). The ε_r of EA/DMSO binary mixtures was not measured; however, we can briefly consider as follows. Although there are various equations to predict the dielectric constant of binary mixture,[28,29] one of the simplest equations to predict is the simple mixing law:

$$\varepsilon_{r,ave} = \phi_A \varepsilon_{r,A} + \phi_B \varepsilon_B \qquad (7.12)$$

where ϕ is the volume fraction, and the subscripts A and B are the components ($\phi_A + \phi_B = 1$). For the transition point $f_{EA} \approx 30$ wt.% ($f_{DMSO} \approx 70$ wt.%) on the EA/DMSO binary

mixture, the weight-averaged dielectric constant is close to the critical value 40:

$$\varepsilon_{r,ave} \approx \phi_{DMSO}\varepsilon_{r,DMSO} + \phi_{EA}\varepsilon_{r,EA} \approx 34 \quad (7.13)$$

$$\left(\phi_{DMSO} \approx \frac{f_{DMSO}/\rho_{DMSO}}{f_{DMSO}/\rho_{DMSO} + f_{EA}/\rho_{EA}} \ , \phi_{EA} = 1 - \phi_{DMSO}\right) \quad (7.14)$$

where ρ is the specific density of each component (ρ_{DMSO} = 1.00, ρ_{EA} = 0.92). The result indicates that the critical concentration to determine the swelling/collapse transition of the polyelectrolyte gel is mainly controlled by the dielectric constant even for the mixture solvent.

7.3.4. Effect of salt on swelling, and elastic modulus of the swollen gels

To confirm that the swelling of PNaAMPS gel in NMF results from the osmotic pressure of dissociated counter ions of polyelectrolyte, the swelling behavior of PNaAMPS gels in NMF solution containing simple salt (LiCl) was investigated. Swelling ratios of the gel as the function of the concentration of LiCl are shown in **Figure 7-8**. Swelling ratio of the PNaAMPS gel decreased with the LiCl concentration both for NMF and aqueous solution. Note that all the gels were homogeneously shrunk (i.e. not collapsed with curved shape) and transparent. For polyelectrolyte gel, the osmotic pressure from the dissociated counter ions of polyelectrolyte is suppressed in salt solution because of Donnan equilibrium, which leads to deswelling of the polyelectrolyte gels.[30] Therefore, the result is an evidence that the high swelling of the gel in NMF originates from the high osmotic pressure caused by dissociation of the counter ions of polyelectrolyte.

For the highly swollen polyelectrolyte gel accompanying with dissociation of counter ions, stiff elastic modulus is often observed because of the pre-stretching of the polymer strands. To see the effect, shear moduli, μ, of the PNaAMPS gels in NMF with salt, in EA/NMF binary mixtures, and in water with salt were characterized. As the result,

a master curve regardless of the solvent was observed for the swelling ratio V/V_0 and the modulus μ (**Figure 7-9a**). Specifically, the modulus moderately decreases and then increases with the high swelling. Even though the polymer concentration is highly diluted (more than 1/10) by swelling, the modulus of highly swollen gels (for $V/V_0 > 10$, μ > 18 kPa) is higher than that of the as-polymerized gel (μ = 14 kPa at $V/V_0 = 1$), which is the typical observation for the densely crosslinked polyelectrolyte gels. The swelling-induced stiffening of gels was also observed in the EA/NMF binary mixtures at $f_{EA} \leq 60$ wt.% (green triangles in **Figure 7-9a**), implying the counter ions were also dissociated in the EA/NMF binary mixtures.

Here, the chain stiffening is quantitatively discussed using some reported considerations. In general, the modulus of gel (μ) is given as the product of the number density of elastically effective polymer strands (ν) and the average energy per strand (W_{strand}),[31]

$$\mu \cong \nu W_{\mathrm{strand}} \tag{7.15}$$

The strands density ν is inversely proportional to the volumetric swelling ratio, $\nu \sim (V/V_0)^{-1}$. For the Gaussian chain (flexible chain), W_{strand} is proportional to $(V/V_0)^{2/3}$, so that the μ of the soft network with Gaussian chain is proportional to $(V/V_0)^{-1/3}$.[32,33] The relation is observed in **Figure 7-9a** at the swelling-induced softening region ($V/V_0 < 4$). Hence, the increase of the modulus by swelling ($V/V_0 > 10$) indicates that the network strands become stiff non-Gaussian chains that are closed to their stretching limit.[34–36] The average stored elastic energy in the pre-stretched strand (W_{strand}) normalized to that of the as-polymerized state ($W_{strand,0}$) is described as

$$\frac{W_{\mathrm{strand}}}{W_{\mathrm{strand},0}} \cong \frac{\mu}{\mu_0}\frac{\nu_0}{\nu} = \frac{\mu}{\mu_0}\frac{V}{V_0} \tag{7.16}$$

Assuming an affine deformation, the average end-to-end distance of the strand (R) relative

to that of the as-polymerized state (R_0), is[31,32]

$$\frac{R}{R_0} \cong \left(\frac{V}{V_0}\right)^{\frac{1}{3}} \tag{7.17}$$

The correlation of average stored elastic energy of the pre-stretched strand and the average end-to-end distance of the strand is plotted in **Figure 7-9b**. When the R/R_0 is small ($R/R_0 < 1.6$), W_{strand} is proportional to $(R/R_0)^2$ that corresponds to the Gaussian chain regime. At large R/R_0, the deviation from the Gaussian regime was observed. At larger swelling state ($R/R_0 > 2.6$), W_{strand} is scaled to R/R_0 with a strong experimental power exponent ~11, and reached 100-fold larger than $W_{strand,0}$. These transition points ($R/R_0 \approx$ 1.6 and 2.6) are roughly corresponding to the deviation from neo-Hookean regime and showing the strain hardening region, respectively, observed in the stress−strain curve for the uniaxial stretching test of the as-prepared (1-3) PNaAMPS gel (see **Figure 4-19**, R/R_0 = 1.6 and 2.6 corresponding to strain ε = 0.6 and 1.6, respectively, for uniaxial stretching direction).

Nevertheless, the high swelling of the network brings low extensibility and dilution of the first network even in the EA/NMF binary mixtures, which are required to obtain the contrasting DN structure.

7.3.5. Compatibility of PEA with NMF

Before synthesis of DN elastomers, I checked the compatibility of PEA with NMF, and appropriate condition (e.g. crosslinker concentration) to synthesize second network. As preliminary experiment, 45 wt.% (approximately 4.3 M) EA was polymerized in NMF with 0.005–0.1 mol% crosslinker with respect to the monomer. At the crosslinker concentration of 0.005−0.03 mol% that is normal condition for the second network of

stretchable DN hydrogels, the solution did not form gel but viscous liquid was obtained, suggesting the crosslinker concentration was not enough to form the percolated network. The result implies that effectiveness of radical polymerization in NMF is poorer than in water. Meanwhile, when 0.1 mol% crosslinker concentration was used, a gel exhibiting high stretchability (elongation at break >1000%) was obtained. Because the gel was transparent, PEA seems to have good compatibility with NMF. Considering the high-stretchable second network is appropriate for the second network of DN hydrogels, the author determined that the crosslinker concentration at around ~0.1 mol% is the good condition for the second network synthesis with NMF solvent for the DN elastomer.

Using the obtained PEA organogel, the swelling property of the gel in organic solvents was investigated to find the good solvent for the PEA and to check the not only EA monomer but also PEA polymer has good compatibility with NMF. As shown in **Figure 7-10**, The PEA was largely swollen in low-polar solvents except for hexane. The PEA organogel was also swollen well in NMF, suggesting NMF is a good solvent for PEA, even though the swelling ratio is not as high as that in low-polar solvent.

7.3.6. Synthesis and characterization of a PNaAMPS/PEA DN organogel

Next, a DN organogel possessing the PNaAMPS first network and the poly(ethylacrylate) (PEA) second network was synthesized using NMF as a solvent. The NMF-swollen PNaAMPS gel (crosslinking density of 3 mol% with respect to the monomer) was immersed in a mixture of EA (f_{EA} = 50 wt.%) and NMF containing crosslinker (4EGDA, concentration f_c = 0.2 wt.% corresponding to 0.13 mol% with respect to the monomer) and AIBN initiator (0.1 wt.%) to reach a swelling equilibrium. Then EA was polymerized into a polymer network by a free-radical polymerization in the highly-prestretched

PNaAMPS network. Thus-obtained as-prepared DN organogel containing NMF solvent is transparent, implying a homogeneous structure at the scales larger than several hundreds of nanometers. This is because NMF worked as a cosolvent for PNaAMPS and PEA.

Uniaxial tensile test of the as-polymerized DN organogel and corresponding SN organogels was conducted. Note that the DN organogel and PEA organogel are as-polymerized state and PNaAMPS SN gel are swollen state in NMF containing 0.04 M LiCl, so that the concentration of each polymer component in the gels are approximately identical. As observed in **Figure 7-11**, the DN organogel exhibits enhanced mechanical properties compared to single-network (SN) organogels. The DN organogel shows a yielding phenomenon (elongation ratio and stress at yield $\lambda_y = 4.1$ and $\sigma_y = 0.84$ MPa) and high stretchability (elongation ratio at break $\lambda_b = 9$) accompanying with strain hardening ($\lambda > 7$), which are the features of DN hydrogels with high toughness.[5,37,38]

At the synthetic condition, the essential requirements for toughening DN gel are achieved via prestretching of the first network. First, the first network is much less extensible than the second network ($\lambda_b \approx 1.7$ for PNaAMPS SN gel and $\lambda_b \approx 17$ for PEA SN gel). Second, the first network is highly diluted compared to the second network. The volume fraction, ϕ, of the first and second networks are $\phi_{1st} = 1.3$ vol% and $\phi_{2nd} = 37$ vol%, respectively, meaning that the volume of the second network is 30-fold higher than the first network. As the result, the DN organogels showed excellent mechanical property similar to DN hydrogels.

7.3.7. Fabrication and uniaxial tensile test of a PNaAMPS/PEA DN elastomer

A hybrid DN elastomer was subsequently fabricated by removing the solvent from the

DN organogel. To remove the NMF and some unreacted molecules in the organogel, the DN organogel was first immersed in acetone that is mixable to NMF and a good solvent for PEA (see **section 7.3.5**), so that the solvent in the organogel was exchanged from NMF for acetone. Then, the sample was stored under a vacuum (<20 mbar for more than 5 days) to remove the acetone from the organogel. All or most of acetone was expected to be removed since acetone is volatile solvent (boiling point of 56^{o}C at 1000 mbar) and the vacuuming pressure is much lower than the vapor pressure of pure acetone (308 mbar at 25^{o}C). Because only solvent was removed, the volume fractions, ϕ, of the first and second networks in the DN elastomer are ϕ_{1st} = 3 vol% and ϕ_{2nd} = 97 vol%, respectively, maintaining the same volume ratio of the two networks in the DN organogel (ϕ_{1st} = 1.3 vol% and ϕ_{2nd} = 37 vol%, respectively). It is reasonable to consider that the hydrophilic PNaAMPS is poorly mixable with hydrophobic low polar PEA; however, the dried DN elastomer is transparent observed with the naked eye (**Figure 7-12**), suggesting the DN elastomer has homogeneous structure at larger than several 100s nm scale. It is expected that macroscopic phase separation is suppressed by the topologically interpenetrated structure of the two networks at the network scale (typically from several to tens of nanometers).

The nominal stress (σ)–elongation ratio (λ) curves on the uniaxial tensile test of the DN elastomer and its individual components at dried state are shown in **Figure 7-13**. The experimental condition was kept as room temperature at ~50% relative humidity because polyelectrolyte may absorb fraction of water molecules from air which depends on the humidity. Like DN organogel discussed above and DN hydrogels, the DN elastomer exhibits excellent mechanical behavior, compared to the single components. The DN elastomer exhibits clear yielding phenomenon at λ = 5.3 and a strong strain

hardening from $\lambda \approx 10$ to the break point ($\lambda_b = 20$ and $\sigma_b = 4.9$ MPa). The σ–λ curve of the DN elastomer is weakly dependent on the stretch velocity (**Figure 7-14**). In addition, it should be noted that the solvent-free PNaAMPS SN polymer is in a glassy state at room temperature.[39] The maximum stress, 28 MPa, is larger than DN elastomer because glassy polymer is usually stronger than stretchable elastomer. However, considering the volume fraction of the first network in the DN elastomer ($\phi_{1st} = 3$ vol%), the stress increase from PEA SN elastomer to DN elastomer is still surprising.

7.3.8. Cyclic tensile test of a PNaAMPS/PEA DN elastomer to confirm internal fracturing

Because the concept of DN elastomers is based on conventional DN hydrogels, it is naturally expected that the toughening mechanism is based on mechanical energy dissipation by covalent bonds scission, as observed in DN hydrogels. Such internal fracturing is crucially important character to achieve the self-growing behavior discussed until the previous chapter. To confirm the internal fracturing, cyclic tensile test of the DN elastomer was performed. The applied λ as a function of time, and the resulting stress response as the function of λ, are shown in **Figures 7-15a** and **b**, respectively. As expected, the DN elastomer exhibits large mechanical hysteresis in its loading and unloading curves. The shape of cyclic σ–λ curve is similar to that observed on conventional DN hydrogels (**Figure 4-15** and references 37 and 40). When carefully observed, the hysteresis of the DN elastomer was slightly recovered on its reloading curve compared to previous unloading curve, which is different from irreversible hysteresis observed in DN hydrogels.[37,41] This is probably due to intrinsic viscoelasticity of PEA matrix and/or possible nanoscopic aggregation structure of PNaAMPS chains surrounded by PEA. As

the evidence of the former reason, PEA SN elastomer also exhibit hysteresis at the experimental condition at the strain rate of ~0.1 s^{-1} (**Figure 7-15c**). For the latter reason, even though we have confirmed the possible homogeneous microstructure (> 100s nm scale) by the visible transparency, nanoscopic phase separation (< 100s nm) is still unvalidated. These two expected reasons should be deeply investigated in the future to understand the partial recovery of the hysteresis which is different from DN hydrogels. Nevertheless, most of the hysteresis in the largely stretched DN elastomer was not recovered even after waiting for 1 week (**Figure 7-16**), hence the observed mechanical hysteresis essentially originates from the internal fracturing of the first network strands. Therefore, mechanoradicals are expected to be generated in the invented DN elastomers as well as DN hydrogels during its deformation.

7.3.9. Toughness (crack resistance) of a PNaAMPS/PEA DN elastomer

To confirm the toughening effect on the elastomer, fracture test was performed for the PNaAMPS/PEA DN elastomer. Two individual methods, single-edge notched fracture test and trouser-shaped tearing test, were performed. As shown in the method **section 7.2.10**, the fracture energy characterized by single-edge notched fracture test, G_c, can be characterized as:

$$G_c = \frac{6W_c c_0}{\lambda_c{}^{1/2}} \qquad (7.10)\ \text{reproduced}$$

where c_0, W_c and λ_c are the inserted notch length, critical strain-energy density in the material and critical elongation ratio, respectively. The *critical* point for W_c and λ_c corresponds to the point where crack propagation starts under the extension. The sample geometry has already shown in **Figure 7-2**. The σ–λ curve of the PNaAMPS/PEA DN elastomers with and without notch are shown in **Figure 7-17a**. In the experiment, the

critical point where the crack propagation starts was difficult to detect precisely because the difference between crack opening (deformation) and crack propagation is not clear. Thus, I assumed that the point giving maximum force was the critical point (**Figure 7-17b**). In original papers proposing the single-edge notched fracture test,[19,20] W_c was characterized by stress−strain curve of un-notched sample. In my experiment, W_c was measured from the σ–λ curve of the *unnotched region* of the *notched sample*, where the elongation ratio, λ, was corrected via displacement of the two dots on the sample, in order to reduce the number of the testing samples. As shown in **Figure 7-17a**, the σ–λ curve of the unnotched region of the notched sample was nearly identical to that of the unnotched sample. In fact, the W_c value measured from the notched sample was ~10% smaller than that from the unnotched sample. Considering the G_c characterization here includes some assumptions such as the prefacter $3\lambda_c^{-1/2}$ in the equation and using *input* energy density for the W_c, the 10% error is relatively small. Using the experimental data and equation shown above, the fracture energy by single-edge notched testing, G_c, of the PNaAMPS/PEA DN elastomer was characterized as 4.7 kJ m^{-2}, which is six-fold higher than the PEA SN elastomer (0.8 kJ m^{-2}).

Fracture energy obtained from trouser-shaped specimen, T_c, was also characterized. The force−displacement curve under the tearing for the PNaAMPS/PEA DN elastomer is shown in **Figure 7-18**. Stick-slip like fracturing was observed for this sample. Although steady fracture is ideally desired to characterize the tearing fracture energy, T_c can be calculated using the average force during the crack propagation. As described in method **section 7.2.11**, the tearing fracture energy by trouser-shaped specimen, T_c, can be calculated as:

$$T_c = \frac{2F_c\lambda_c}{t} - 2bW_c \qquad (7.11)\ \text{reproduced}$$

where F_c, λ_c, b, and W_c are the average critical force, the average critical elongation ratio of the leg, leg's width, and the average critical strain energy, respectively, during the crack propagation. This is the original equation proposed in 1953.[19] If leg's deformation is negligibly small ($\lambda_c \approx 1$), and the input energy to the leg would be also small ($W_c \approx 0$), therefore, an approximated equation:

$$T_c \approx \frac{2F_c}{t} \qquad (7.18)$$

has been also used for the T_c characterization.[2,21,22] However, observing at the stress−strain behavior at the sample leg, $\lambda_c \approx 2.1$ was observed for this sample (**Figure 7-19**). Therefore, it is desired to use the original equation without approximation. If a sample with wider legs or thinner sample was used, λ_c would be close to 1. By using the original equation (equation (7.11)), the tearing fracture energy T_c of the PNaAMPS/PEA DN elastomer was characterized as 12.0 kJ m^{-2}. Note that each component in the equation was determined as $2F_c/t$ = 7.6 kJ m^{-2}, λ_c = 2.2 and $2bW_c$ = 4.5 kJ m^{-2}. The tearing fracture energy T_c =12.0 kJ/m^2 is quite larger than single-edge notched fracture energy G_c (4.7 kJ m^{-2}), which will be discussed in **section 7.3.11**.

7.3.10. Mechanical properties of PNaAMPS/PEA DN elastomers with various formulations under uniaxial tensile test

Next, PNaAMPS/PEA DN elastomers with various formulation were synthesized by changing the feed composition of monomer or crosslinker. The effect of DN elastomer formulation on the resulting mechanical properties was systematically investigated. First, the crosslinker concentration of the first network, x_1, was varied from 2 to 10 mol% with respect to the monomer concentration (1.0 M), whereas the composition of the precursor solution of the second network was fixed (monomer (EA) and crosslinker (4EGDA)

concentration of f_{EA} = 50 wt.% and f_c = 0.2 wt.%, respectively). The σ–λ curves and parameters including volume fraction of each component and resulting mechanical properties of the DN elastomers are shown in **Figure 7-20a** and **Table 7-3**, respectively. The volume fraction of the first network ϕ_{1st} increased with x_1, because the high crosslinking density of the first network suppressed the swelling ability of the PNaAMPS network in the EA/NMF binary mixture. The σ–λ curves are obviously different with the x_1. The elastic modulus and yielding stress and/or stress at break increased with the increase of x_1. The stretchability decreases at large x_1 (> 4 mol%) and the distinct yielding behavior disappears at x_1 = 8 and 10 mol%. These results on the x_1-effect correspond to that on the conventional DN gels.[5] Specifically on the stretchability, for DN gel, the contrast of the first and second networks must be enough high to show yielding and stretchable behavior. The same tendency is found in the DN elastomers: the highly stretchable samples exhibiting a large stress plateau after yielding have a high concentration contrast (ϕ_{1st}/ϕ_{2nd} = 0.02–0.08 for x_1 = 2–6 mol%), whereas low stretchable samples has relatively low contrast (ϕ_{1st}/ϕ_{2nd} > 0.11 for x_1 = 8 and 10 mol%).

I also synthesized various DN elastomers from different monomer concentrations for the second network, f_{EA} = 20–60 wt.%, while the same PNaAMPS first network (x = 3 mol%) was used (**Figure 7-20b** and **Table 7-3**). The concentration of the second network crosslinker was kept constant at f_c = 0.2 wt.%. At higher f_{EA}, lower ϕ_{1st} was yielded because of the increase in the concentration of the second network monomer in-feed. Thus, the yielding stress decreased at higher f_{EA}. All samples showed yielding. All samples except for the sample of f_{EA} = 20 wt.% showed high stretchability accompanying with strain hardening. The low stretchability of the sample of f_{EA} = 20 wt.% is because of the relatively low contrast of the two networks (ϕ_{1st}/ϕ_{2nd} = 0.08). The

strain hardening of the samples (f_{EA} > 30 wt.%) was steeper with an increase of f_{EA} (**Figure 7-20b**). Since such steepness difference is hardly observed in the samples with varied x_1 (= 2–4) and fixed f_{EA} (**Figure 7-20a**), the steepness difference possibly originates in the second network. In general, the steepness of the strain hardening of soft network polymers (rubbers and gels) is enhanced by the crosslinking density.[1,2] For the DN elastomers, the crosslinker concentration in feed of the second network, f_c, was kept constant (f_c = 0.2 wt.%). Therefore, the crosslinker concentration (weight fraction) in the DN elastomer after removing the solvent corresponds to $f_c/(f_c+f_{EA})$. Because $f_c/(f_c+f_{EA})$ decreases with the increase of the f_{EA}, the concentration of chemical crosslinker does not explain the steepness difference. However, it is reasonable to consider for the soft elastomeric networks that the crosslinking density is strongly affected by the effective crosslinking of the trapped entanglements of the second network strands, which increases with the polymer concentration at the second network synthesis. Therefore, the trapped entanglement density increases with increasing of the f_{EA}, which would affect to the steepness difference. The argument also implies that the entanglement density is more dominant than chemical crosslinking density for the soft second network.

Here, the concentration contrast, ϕ_{1st}/ϕ_{2nd}, is focused. The effect of ϕ_{1st}/ϕ_{2nd} on the stretchability and strengths were summarized in **Figures 7-21a** and **b**, respectively. The elongation at break, λ_b, decreases with increase of ϕ_{1st}/ϕ_{2nd}, especially at ϕ_{1st}/ϕ_{2nd} > 0.06. Furthermore, at ϕ_{1st}/ϕ_{2nd} > 0.1, λ_b becomes much smaller without showing the yielding. The yield stress σ_y and the stress at break σ_b increase with ϕ_{1st}/ϕ_{2nd}. These results indicate that concentration contrast is the dominant parameter to obtain the DN elastomers showing yielding and high stretchability (λ_b ~ 20). Because the systematic research on DN hydrogels indicated that the strand number density of the two networks should be

considered as the essential criterion to show the yielding,[5] the concentration criteria found here ($\phi_{1st}/\phi_{2nd} > 0.06$–$0.1$) may depend on crosslinking density of the two networks. However, because similar value of ϕ_{1st}/ϕ_{2nd} criteria are also found for DN hydrogels and multiple network elastomers,[5,12] so that the quantity can be used as a practical experimental guide to optimize the contrasting structure of the DN system.

7.3.11. Fracture energy of PNaAMPS/PEA DN elastomers with various formulations

Fracture energies of all ten DN elastomers were also characterized using two individual methods described in **section 7.3.9**. First, the fracture toughness G_c using single-edge notched geometry was characterized. Typical stress−deformation ratio curves of the notched samples are shown in **Figure 7-22**. The G_c ranges around 3–9 kJ m^{-2}. The sample with $\phi_{1st}/\phi_{2nd} \approx 0.08$ exhibiting distinct yielding and no strain hardening shows the highest G_c (**Figure 7-21c**), which contrasts the strengths (i.e., stresses at yield and break, σ_y and σ_b) that monotonically increase with ϕ_{1st}/ϕ_{2nd} (**Figure 7-21b**). The fracture toughness by a tearing test with a trouser-shaped geometry was also characterized. Typical normalized force–displacement curves on the tearing experiment are shown in **Figure 7-23**. Most samples showed stick-slip phenomenon. The tearing fracture energy, T_c, of the ten DN elastomers ranges from 8 to 14 kJ m^{-2}, higher than that measured by a single-edge notched geometry (around 3–9 kJ m^{-2}), especially for the samples showing yielding and strain hardening. The G_c and T_c of the samples are summarized in **Figure 7-21c** as the function of ϕ_{1st}/ϕ_{2nd}. The volume ratio to give highest toughness shifts slightly from $\phi_{1st}/\phi_{2nd} \approx 0.08$ for G_c to $\phi_{1st}/\phi_{2nd} \approx 0.06$ for T_c.

There are several expected reasons for the differences between G_c and T_c. The intrinsic fracture energy should depend on the local strain rate at the crack tip, that is

different between testing speed and geometry.[22,23,43–45] Both equations characterizing G_c and T_c (see **sections 7.2.10, 7.2.11** and **7.3.9**) contain the critical elastic stored energy (W_c) in the bulk elastomer, which is rather complicated for elastomers showing mechanical hysteresis.[19,44] The equation characterizing G_c contains an empirical factor of $3\lambda^{-1/2}$ that is not validated for our DN elastomers.[2,20] Therefore, the small difference within a numerical factor of the characterized fracture energies of soft materials is less meaningful, especially when different testing methods are conducted. Even so, the fracture energy of the DN elastomers is in the order of 10^3–10^4 J m^{-2}, which is comparable to conventional tough elastomers such as unfilled natural rubbers, filled synthetic elastomers, and triple-network elastomers.[11,23,45,46]

7.3.12. DN elastomers with various polymer combinations

The concept to synthesize the DN elastomer composed of polyelectrolyte first network and low-polar elastomeric second network using high dielectric solvent is possibly applied to various combinations of polymer species. In this section, various chemical structures of polymer are tested to fabricate DN elastomers. Five kinds of polyelectrolyte first networks were synthesized from five monomers: *p*-styrene sulfonic acid sodium salt (NaSS), acrylic acid sodium salt (NaAAc), 2-acryloxyethyl trimethylammonium chloride (ClAETMA), acrylic acid (AAc), and 2-acrylamido-2-methylpropane sulfonic acid (AMPS) (**Figure 7-24a**). The resulting polymers are denoted as PNaSS, PNaAAc, PClAETMA, PAAc, and PAMPS, respectively. For the second network, three kinds of polymers are tested, synthesized from butyl acrylate (BA), 2-methoxyethyl acrylate (MTA), and 2-(2-ethoxyethoxy)ethyl acrylate (EEEA) (**Figure 7-24b**). The resulting polymers are denoted as PBA, PMTA, and PEEEA, respectively. These second network

polymers are rubbery state at room temperature.

First, swelling ability of these polyelectrolyte networks in NMF and EA/NMF (50:50 w/w) binary mixture, and of a PNaAMPS network in binary mixtures of NMF and the monomer for the second network (BA, MTA or EEEA) were investigated. As shown in **Figure 7-24c**, the swelling ratios of the polyelectrolyte networks with metal counter ions (PNaSS and PNaAAc) and chloride counter ion (PClAETMA) in NMF and EA/NMF binary mixtures were as high as those in water, suggesting the counter ions are dissociated in NMF and EA/NMF binary mixtures. The polyelectrolyte networks of polyacids (PAMPS and PAAc) with proton counter ions also showed high swelling ratio in NMF and EA/NMF binary mixtures, suggesting the dissociation of protons in the solvents. It should be noted that the PAAc hardly swelled in water ($V/V_0 = 2$). Since the PAAc is weak acid of which the pK_a in water is 5,[47] the most protons are probably not dissociated in the hydrogel. On the contrary, the PAAc network highly swelled in NMF, suggesting much larger number of protons of PAAc were dissociated in NMF. This may be owing to the proton-accepting ability of NMF.[13] In addition to the dissociation degree of protons, the other possibility to explain the large difference roots in the hydrogen bonding. Carboxylic acid group of PAAc may form dimer with hydrogen bond in water, which may be weakened or destroyed by the NMF with amide bond. Nevertheless, the high-swelling ratio of densely crosslinked PAAc gel in NMF suggests some protons of PAAc is dissociated in the NMF environment.

Swelling ability of a PNaAMPS network in binary mixtures (50:50 w/w) of NMF and the monomer (BA, MTA, or EEEA) was also characterized. The measured dielectric constant ε_r of the binary mixtures are shown in **Table 7-2**. In the all binary mixtures, PNaAMPS network was highly swollen comparable to that in water (**Figure 7-24d**).

Next, DN elastomers comprising polyelectrolyte (PNaSS, PNaAAc, PClAETMA, PAAc, or PAMPS) first network and PEA second network, and comprising PNaAMPS first network and elastomeric polyacrylate (PBA, PMTA or PEEEA) second network were fabricated using same procedure. Only when the PNaAMPS/PBA DN organogel containing NMF was fabricated, the gel was slightly opaque, suggesting PBA is bit incompatible with NMF. After drying, all DN elastomers are transparent. The stress–strain curves of the DN elastomers are shown in **Figure 7-25**. All DN elastomers showed yielding phenomenon, and most of the elastomers show a strain hardening and high extensibility (λ_b > 10). Note that the mechanical properties and swelling ratio observed above are not only depend on chemical feature of side-chain group of the polymer but also affected by the different architecture of the network, because the kinetics of the free-radical polymerization and the reactivity ratio between the monomer and the crosslinker (MBAA) is different. According to the results, the fabrication strategy for DN elastomers using dielectric solvent can be widely applied for various polyelectrolyte first network and elastomeric second network combination.

7.4. Conclusion

In this chapter, a procedure to fabricate tough and stretchable DN elastomers is proposed and the results are systematically discussed. By using high-dielectric organic solvent (e.g. NMF), DN elastomer composed of contrasting two-network structure of a pre-stretched brittle polyelectrolyte first network (e.g. PNaAMPS network) and a stretchable elastomeric low polar second network (e.g. PEA network) was fabricated. The DN elastomers exhibit high strength (~5 MPa nominal stress and ~100 MPa true stress at break), large stretchability (~2000%) and high fracture toughness (~10^4 J m^{-2}). Similar to

the DN hydrogels, the DN elastomer shows large irreversible fraction of mechanical hysteresis, suggesting internal fracturing occurred in the DN elastomers. Therefore, self-strengthening or self-growing property will be possibly given to the DN elastomers.

References

(1) L. R. G. Treloar, The Physics of Rubber Elasticity, 3rd ed. (Oxford University Press: New York, 2005).

(2) A. N. Gent, Engineering with Rubber, 3rd ed. (Hanser: Munich, 2012).

(3) C. Creton. 50th anniversary perspective: Networks and gels: Soft but dynamic and tough. *Macromolecules* **50,** 8297–8316 (2017).

(4) J. P. Gong, Why are double network hydrogels so tough? *Soft Matter* **6,** 2583–2590 (2010).

(5) S. Ahmed, T. Nakajima, T. Kurokawa, M. A. Haque, J. P. Gong, Brittle–ductile transition of double network hydrogels: Mechanical balance of two networks as the key factor. *Polymer* **55,** 914–923 (2014).

(6) T. Nakajima, H. Sato, Y. Zhao, S. Kawahara, T. Kurokawa, K. Sugahara, J. P. Gong, A universal molecular stent method to toughen any hydrogels based on double network concept. *Adv. Funct. Mater*. **22,** 4426–4432 (2012).

(7) R. S. Harland, R. K. Prud'homme, Polyelectrolyte Gels (American Chemical Society: Washington DC, 1992).

(8) J. P. Gong, Y. Katsuyama, T. Kurokawa, Y. Osada, Double-network hydrogels with extremely high mechanical strength. *Adv. Mater.* **15,** 1155–1158 (2003).

(9) S. S. Es-haghi, R. A. Weiss, Fabrication of tough hydrogels from chemically cross-linked multiple neutral networks. *Macromolecules* **49,** 8980–8987 (2016).

(10) A. Argun, V. Can, U. Altun, O. Okay, Nonionic double and triple network hydrogels of high mechanical strength. *Macromolecules* **47,** 6430–6440 (2014).

(11) E. Ducrot,Y. Chen, M. Bulters, R. P. Sijbesma, C. Creton, Toughening elastomers with sacrificial bonds and watching them break. *Science* **344,** 186–189 (2014).

(12) P. Millereau, E. Ducrot, J. M. Clough, M. E. Wiseman, H. R. Brown, R. P. Sijbesma, C. Creton, Mechanics of elastomeric molecular composites. *Proc. Natl. Acad. Sci. USA* **115,** 9110–9115 (2018).

(13) Izutsu, K. Electrochemistry in Nonaqueous Solutions, 2nd ed. (Wiley–VCH: Weinheim, 2009).

(14) A. R. Khokhlov, E. Y. Kramarenko, Polyelectrolyte/ionomer behavior in polymer gel collapse. *Macromol. Theory Simul.* **3,** 45–59 (1994).

(15) D. Kawaguchi, M. Satoh, Swelling behavior of partially quaternized poly(4-vinylpyridine) gels in water/organic solvent mixtures. *Macromolecules* **32,** 7828–7835 (1999).

(16) Y. Nishiyama, M. Satoh, Solvent- and counterion- specific swelling behavior of poly(acrylic acid) gels. *J. Poly. Sci. B Polym. Phys.* **38,** 2791–2800 (2000).

(17) K. Kabiri, M. J. Zohuriaan-Mehr, H. Mirzadeh, M. Kheirabadi, Solvent-, ion- and pH-specific swelling of poly(2-acrylamido-2-methylpropane sulfonic acid) superabsorbing gels. *J. Polym. Res.* **17,** 203–212 (2010).

(18) J.-M. Corpart, J. Selb, F. Candau, Characterization of high charge density ampholytic copolymers prepared by microemulsion polymerization. *Polymer* **34,** 3873–3886 (1993).

(19) R. S. Rivlin, A. G. Thomas, Rupture of rubber. I. Characteristic energy for tearing. *J. Polym. Sci.* **10,** 291–318 (1953).

(20) H. W. Greensmith, Rupture of rubber. X. The change in stored energy on making a small cut in a test piece held in simple extension. *J. Appl. Polym. Sci.* **7,** 993–1002 (1963).

(21) H. W. Greensmith, A. G. Thomas, Rupture of rubber. III. Determination of tear properties. *J. Polym. Sci.* **18,** 189–200 (1955).

(22) A. N. Gent, Adhesion and strength of viscoelastic solids. Is there a relationship between adhesion and bulk properties? *Langmuir* **12,** 4492–4496 (1996).

(23) K. Sakulkaew, A. G. Thomas, J. J. C. Busfield, The effect of the rate of strain on tearing in rubber. *Polym. Test.* **30,** 163–172 (2011).

(24) Y. Akagi, H. Sakurai, J. P. Gong, U.-I. Chung, T. Sakai, Fracture energy of polymer gels with controlled network structures. *J. Chem. Phys.* **139,** 144905 (2013).

(25) Y. Fukunaga, M. Hayashi, M. Satoh, Specific swelling behaviors of alkali-metal poly(styrene sulfonate) gels in aqueous solvent mixtures. *J. Poly. Sci. B Polym. Phys.* **45,** 1166–1175 (2007).

(26) U. Gaur, S. Lau, B. B. Wunderlich, B. Wunderlich, Heat capacity and other thermodynamic properties of linear macromolecules VI. Acrylic polymers. *J. Phys. Chem. Ref. Data* **11,** 1065–1089 (1982).

(27) L. Andreozzi, V. Castelvetro, M. Faetti, M. Giordano, F. Zulli, Rheological and thermal properties of narrow distribution poly(ethyl acrylate)s. *Macromolecules* **39,** 1880–1889 (2006).

(28) A. Jouyban, S.Soltanpour, H.-K. Chan, A simple relationship between dielectric constant of mixed solvents with solvent composition and temperature. *Int. J. Pharm.* **269,** 353–360 (2004).

(29) A. V. Goncharenko, V. Z. Lozovski, E. F. Venger, Lichtenecker's equation:

applicability and limitations. *Optics Commun.* **174,** 19–32 (2000).

(30) J. Ricka, T. Tanaka, Swelling of ionic gels: Quantitative performance of the Donnan theory. *Macromolecules* **17,** 2916–2921 (1984).

(31) M. Rubinstein, R. H. Colby, A. V. Dobrynin, J.-F. Joanny, Elastic modulus and equilibrium swelling of polyelectrolyte gels. *Macromolecules* **29,** 398–406 (1996).

(32) S. P. Obukhov, M. Rubinstein, R. H. Colby, Network modulus and superelasticity. *Macromolecules* **27,** 3191–3198 (1994).

(33) T. Sakai, M. Kurakazu, Y. Akagi, M. Shibayama, U.-I. Chung, Effect of swelling and deswelling on the elasticity of polymer networks in the dilute to semi-dilute region. *Soft Matter* **8,** 2730–2736 (2012).

(34) N. Gundogan, D. Melekaslan, O. Okay, Rubber elasticity of poly(*N*-isopropylacrylamide) gels at various charge densities. *Macromolecules* **35,** 5616–5622 (2002).

(35) J. Li, Z. Suo, J. J. Vlassak, A model of ideal elastomeric gels for polyelectrolyte gels. *Soft Matter* **10,** 2582–2590 (2014).

(36) K. Hoshino, T. Nakajima, T. Matsuda, T. Sakai, J. P. Gong, Network elasticity of a model hydrogel as a function of swelling ratio: from shrinking to extreme swelling states. *Soft Matter*, **14,** 9693–9701 (2018).

(37) Y.-H. Na, Y. Tanaka, Y. Kawauchi, H. Furukawa, T. Sumiyoshi, J. P. Gong, Y. Osada, Necking phenomenon of double-network gels. *Macromolecules* **39,** 4641–4645 (2006).

(38) T. Matsuda, T. Nakajima, Y. Fukuda, W. Hong, T. Sakai, T. Kurokawa, U. Chung, J. P. Gong, Yielding criteria of double network hydrogels. *Macromolecules* **49,** 1865–1872 (2016).

(39) S. C. Yeo, A. Eisenberg, Effect of ion placement and structure on properties of plasticized polyelectrolytes. *J. Macromol. Sci. B Phys.* **13,** 441–484 (1977).

(40) T. Nakajima, T. Kurokawa, S. Ahmed, W.-L. Wu, J. P. Gong, Characterization of internal fracture process of double network hydrogels under uniaxial elongation. *Soft Matter* **9,** 1955–1966 (2013).

(41) R. E. Webber, C. Creton, H. R. Brown, J. P. Gong, Large strain hysteresis and Mullins effect of tough double-network hydrogels. *Macromolecules* **40,** 2919–2927 (2007).

(42) M. Rubinstein, R. H. Colby, Polymer Physics (Oxford University Press: Oxford 2003).

(43) Q. M. Yu, Y. Tanaka, H. Furukawa, T. Kurokawa, J. P. Gong, Direct observation of damage zone around crack tips in double-network gels. *Macromolecules* **42,** 3852–3855 (2009).

(44) K. Mayumi, J. Guo, T. Narita, C. Y. Hui, C. Creton, Fracture of dual crosslink gels with permanent and transient crosslinks. *Extreme Mech. Lett.* **6,** 52–59 (2016).

(45) Y. Morishita, K. Tsunoda, K. Urayama, Velocity transition in the crack growth dynamics of filled elastomers: Contributions of nonlinear viscoelasticity. *Phys. Rev. E.* **93,** 043001 (2016).

(46) M. Morton, Rubber Technology, 3rd ed. (Springer: Berlin, 1999).

(47) H. G. Spencer, A note on dissociation constants of polycarboxylic acids. *J. Polym. Sci.* **56,** S25–S28 (1962).

(48) J. A. Riddick, W. B. Bunger, Organic Solvents: Physical Properties and Methods of Purification, 3rd ed. (Wiley-intersciene: New York, 1971).

(49) Y. Marcus, Ion Solvation (Wiley: New York, 1985).

Figures and Tables

Table 7-1. Abbreviations and structures of some chemical compounds used in this chapter.

Chemical name	Abbreviation	Chemical structure
(2-Acrylamido-2-methylpropanesulfonic acid) sodium salt	NaAMPS	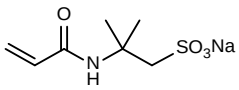
Poly(2-acrylamido-2-methylpropanesulfonic acid) sodium salt	PNaAMPS	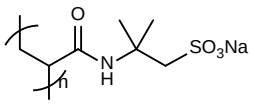
N,N′-Methylenebisacrylamide	MBAA	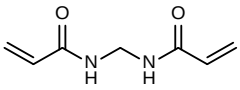
Ethyl acrylate	EA	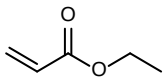
Poly(ethyl acrylate)	PEA	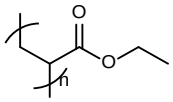
Poly(ethyleneglycol) diacrylate (average molecular weight 250, $n \approx 3$)	PEGDA	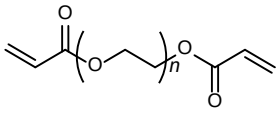
Tetraethyleneglycol diacrylate	4EGDA	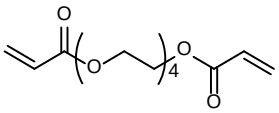
2,2'-Azobis(isobutyronitrile)	AIBN	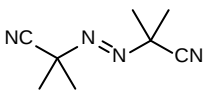
N-Methylformamide	NMF	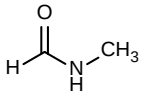
Dimethyl sulfoxide	DMSO	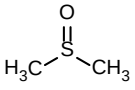

Table 7-1. Cont'd

Chemical name	Abbreviation	Chemical structure
p-Stylenesulfonic acid sodium salt	NaSS	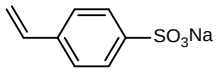
Acrylic acid sodium salt	NaAAc	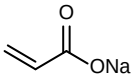
Acrylic acid	AAc	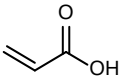
Tetramethyl ammonium ethyl acrylic chloride	ClAETMA	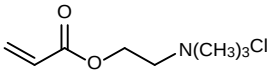
2-Acrylamido-2-methylpropane sulfonic acid	AMPS	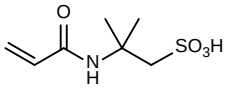
Butyl acrylate	BA	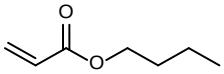
2-Methoxyethyl acrylate	MTA	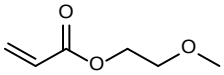
2-(2-Ethoxyethoxy) ethyl acrylate	EEEA	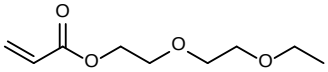

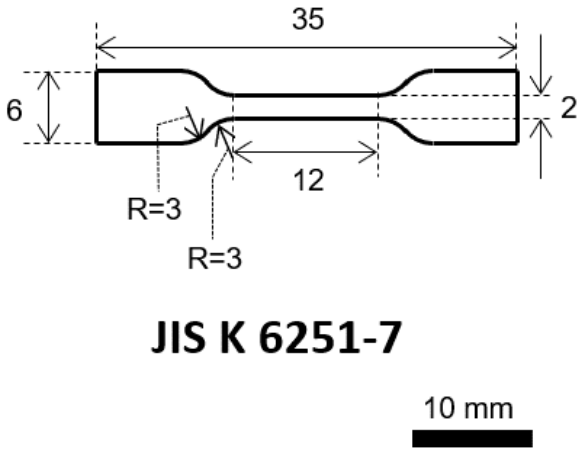

Figure 7-1. Dumbbell shape (JIS K 6251-7 standard) used in this chapter for tensile experiment.

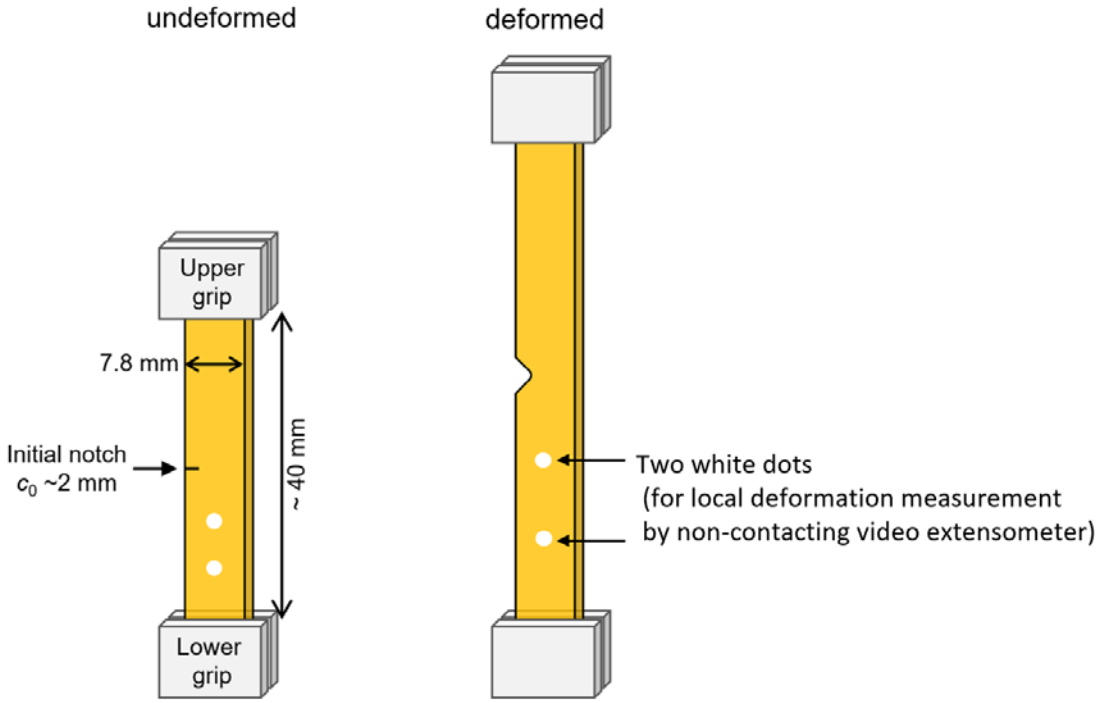

Figure 7-2. Experimental setup of fracture test with single-edge notched geometry. Elongation ratio of un-notched region was measured by non-contacting video extensometer. Reprinted with permission from *Chemistry of Materials* 31, 3766–3776 (2019). Copyright 2019 American Chemical Society.

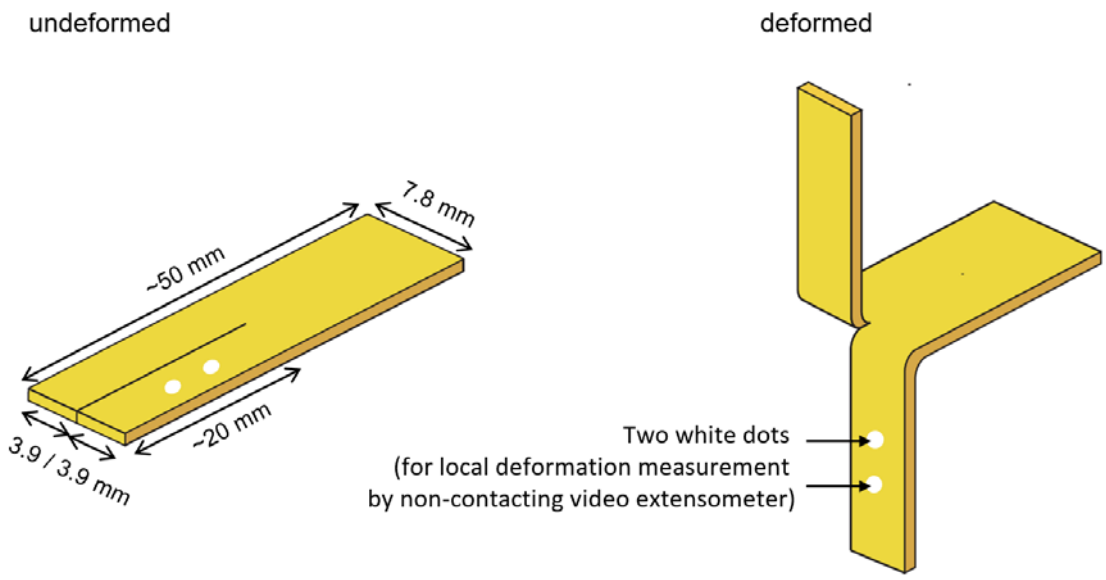

Figure 7-3. Experimental setup of fracture test with a trouser-shaped specimen. The elongation ratio of the lower leg was measured by non-contacting video extensometer. Reprinted with permission from *Chemistry of Materials* 31, 3766–3776 (2019). Copyright 2019 American Chemical Society.

Table 7-2. Solvents and solutions used in swelling experiment and their dielectric constants. Reprinted with permission from *Chemistry of Materials* 31, 3766–3776 (2019). Copyright 2019 American Chemical Society.

Solvent	Dielectric constant[a] ε_r [-] (temperature [°C])		Monomer solution	Dielectric constant[c] ε_r [-] (temperature [°C])	
dioxane	2.209	(25)	EA	5.83	(25.0)
anisole	4.33	(25)	EA:NMF 90:10(w/w)	13.52	(23.5)
chloroform	4.806	(20)	EA:NMF 80:20(w/w)	24.6	(23.4)
ethyl acetate	6.02	(25)	EA:NMF 70:30(w/w)	38.4	(23.6)
tetrahydrofuran	7.58	(25)	EA:NMF 60:40(w/w)	53.4	(24.1)
methyl isobutyl ketone	13.11	(20)	EA:NMF 50:50(w/w)	70.6	(24.8)
2-methoxyethanol	16.93	(25)	EA:NMF 40:60(w/w)	90.0	(24.4)
cyclohexanone	18.3	(20)	EA:NMF 30:70(w/w)	111.8	(24.8)
acetone	20.70	(25)	EA:NMF 20:80(w/w)	136.4	(24.6)
ethanol	24.55	(25)	EA:NMF 10:90(w/w)	163.0	(24.8)
2-ethoxyethanol	29.6	(24)			
N-methylpyrrolidone	32.0	(25)	BA	5.06	(25.3)
methanol	32.70	(25)	BA:NMF 50:50(w/w)	73.4	(24.0)
N,N-dimethylformamide	36.71	(25)			
acetonitrile	37.5	(20)	2-MTA	7.80	(25.6)
ethylene glycol	37.7	(25)	MTA:NMF 50:50(w/w)	71.6	(25.1)
N,N-dimethylacetamide	37.78	(25)			
γ-butyl lactone	39	(20)	EEEA	7.65	(25.0)
dimethyl sulfoxide (DMSO)	46.68	(25)	EEEA:NMF 50:50(w/w)	75.7	(25.0)
propylene carbonate[b]	66.1	(25)			
water	78.39	(25)			
formamide	111.0	(20)			
N-methylformamide (NMF)	182.4	(25)			

[a]Reference 48 except for b; [b]reference 49; [c]measured values.

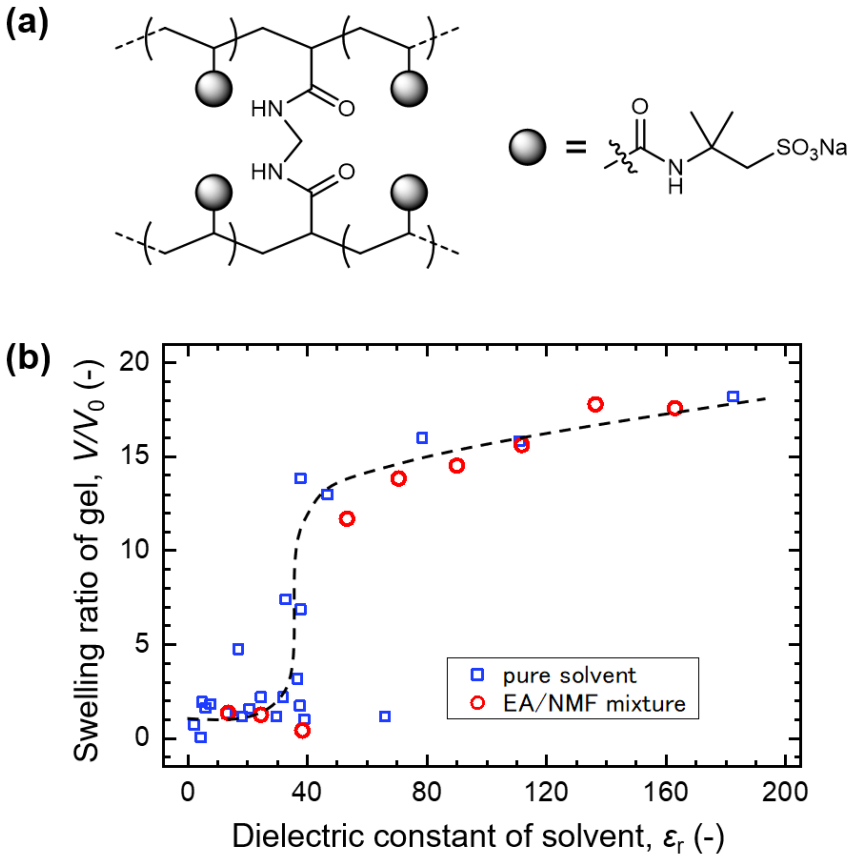

Figure 7-4. (a) Chemical structure of PNaAMPS network crosslinked by MBAA. **(b)** Swelling ratio (V/V_0) of (1-3) PNaAMPS gel in various solvents (blue squares) or in EA/NMF binary mixtures (red circles), as a function of the dielectric constant of the solvents (ε_r) (see **Table 7-2** for the solvents used here and their values of ε_r). Note that the values of V/V_0 for collapsed gel ($V/V_0 < 4$) are not quantitatively accurate (see main text **section 7.3.1**). The dashed line is a guide for the eyes. Reprinted with permission from *Chemistry of Materials* 31, 3766–3776 (2019). Copyright 2019 American Chemical Society.

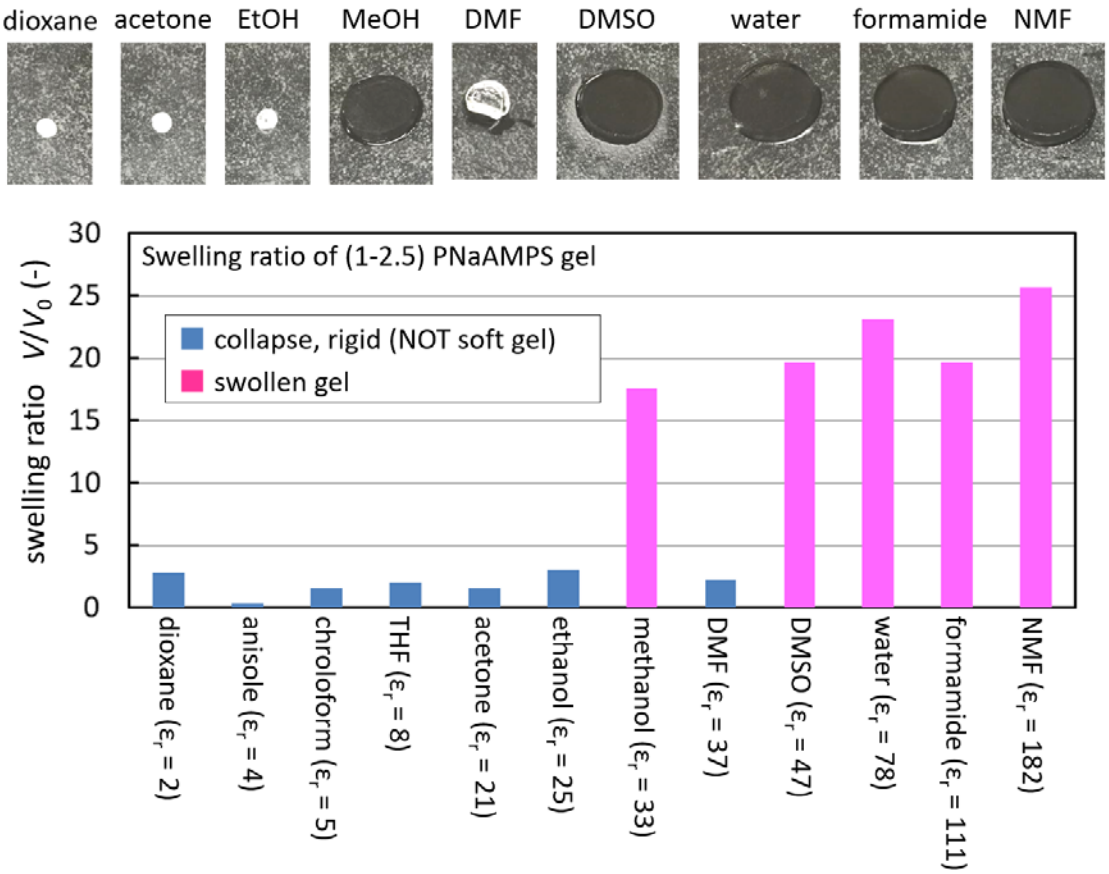

Figure 7-5. Photographic images and swelling ratio of (1-2.5) PNaAMPS gel in various solvents as the supplementary results.

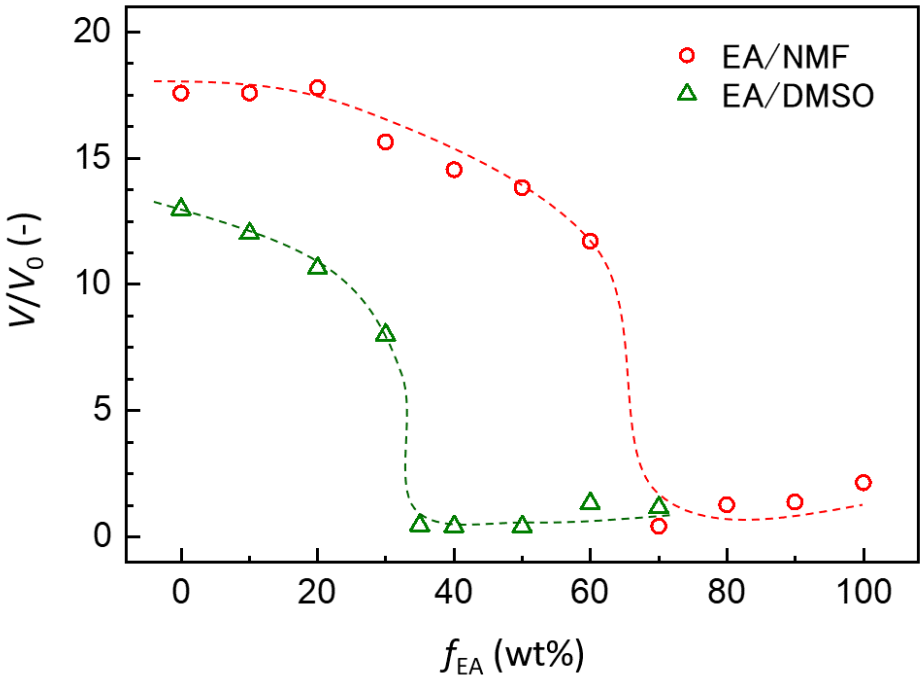

Figure 7-6. Swelling ratio (V/V_0) of (1-3) PNaAMPS gel in EA/NMF (red circles) or EA/DMSO (green triangles) binary mixtures, as a function of the weight fraction of EA (f_{EA}). For collapsed gels ($V/V_0 < 4$), the values of V/V_0 are inaccurate (see main text **section 7.3.1**). The dashed line is a guide for the eyes. Reprinted with permission from *Chemistry of Materials* 31, 3766–3776 (2019). Copyright 2019 American Chemical Society.

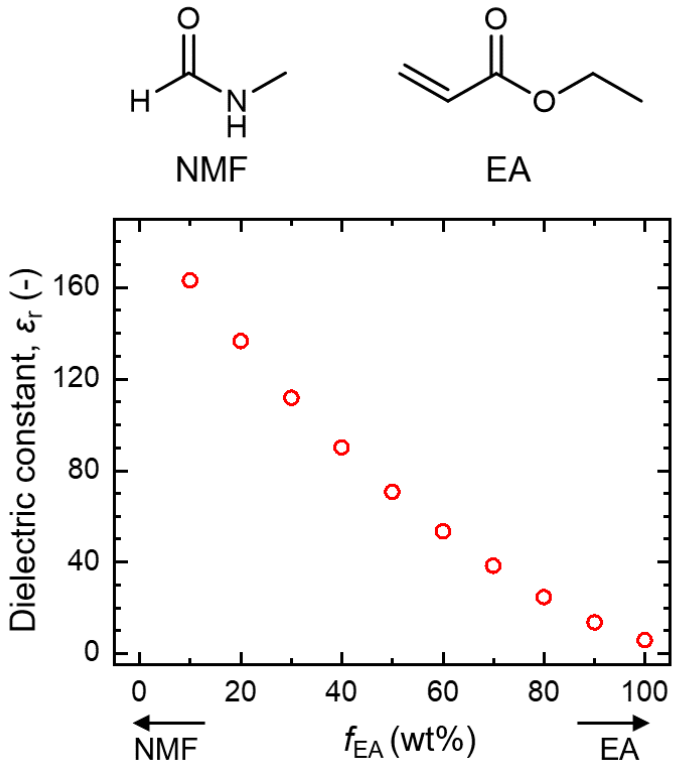

Figure 7-7. Dielectric constant of EA/NMF binary mixture at 24.2±0.8℃, as a function of the weight fraction of EA (f_{EA}) in the mixture. The chemical structures of NMF and EA are also shown (top). Reprinted with permission from *Chemistry of Materials* 31, 3766–3776 (2019). Copyright 2019 American Chemical Society.

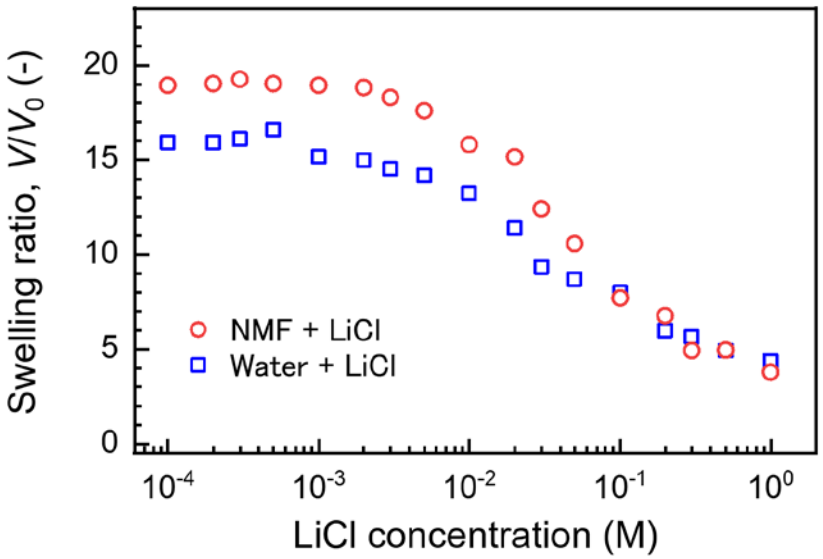

Figure 7-8. Swelling ratio of (1-3) PNaAMPS gel in LiCl salt solution in water or NMF, as a function of the LiCl concentration. Reprinted with permission from *Chemistry of Materials* 31, 3766–3776 (2019). Copyright 2019 American Chemical Society.

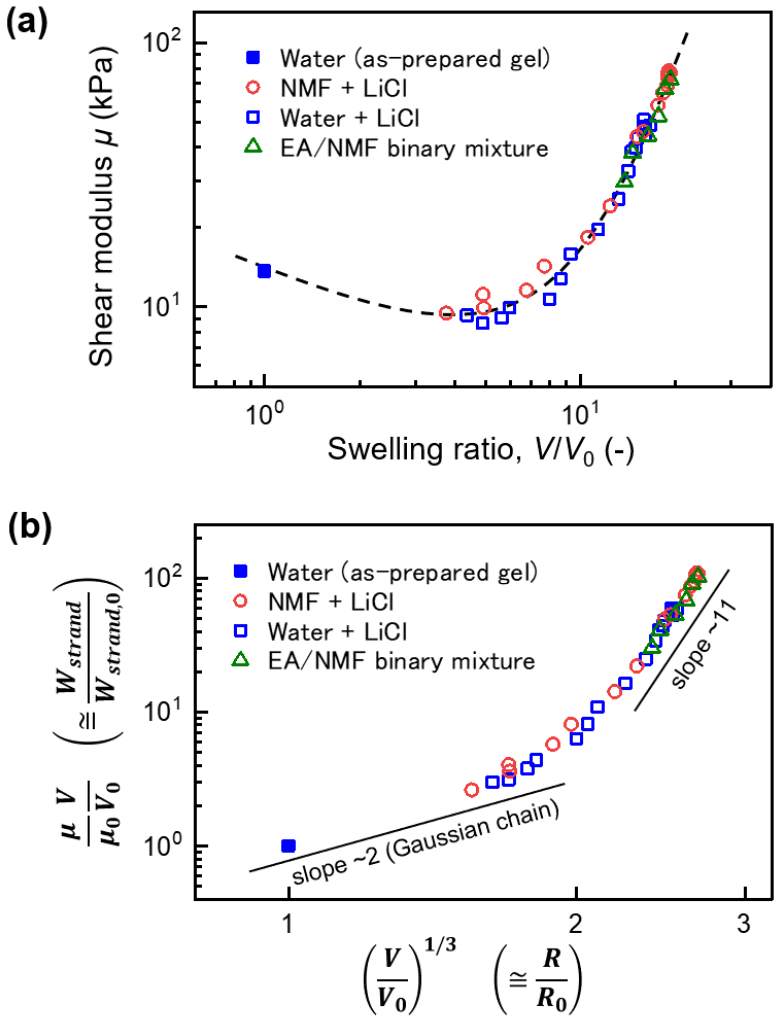

Figure 7-9. (a) Shear moduli of the PNaAMPS gels swollen in LiCl salt solution in water or NMF, or binary mixture of EA/NMF (f_{EA} = 10, 20, 30, 40, 50, and 60 wt.%), as a function of the swelling ratio. The dashed lines are guides for the eyes. **(b)** Normalized average stored elastic energy per strand as a function of normalized average strand length between crosslinking points. The thin solid lines are guides for the scaling exponents. Reprinted with permission from *Chemistry of Materials* 31, 3766–3776 (2019). Copyright 2019 American Chemical Society.

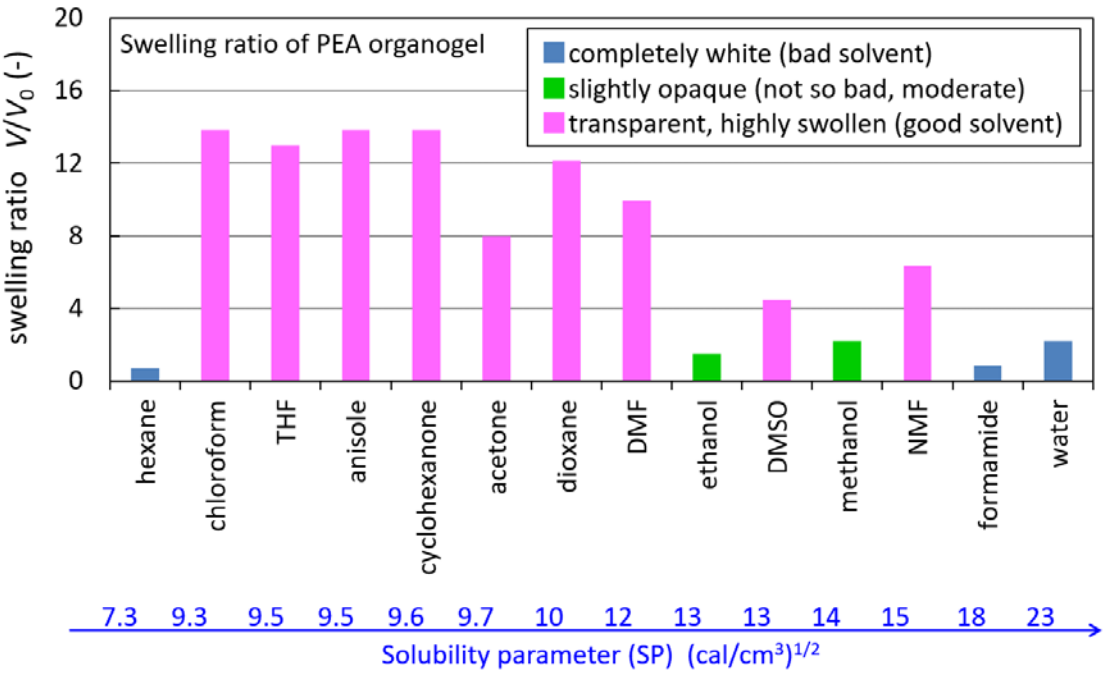

Figure 7-10. Swelling ratio of PEA gel in various solvents. The PEA gel was synthesized from 45 wt.% EA, 0.11 wt.% PEGDA (0.1 mol% to EA), 0.07 wt.% AIBN (0.1 mol% to EA) and 55 wt.% NMF.

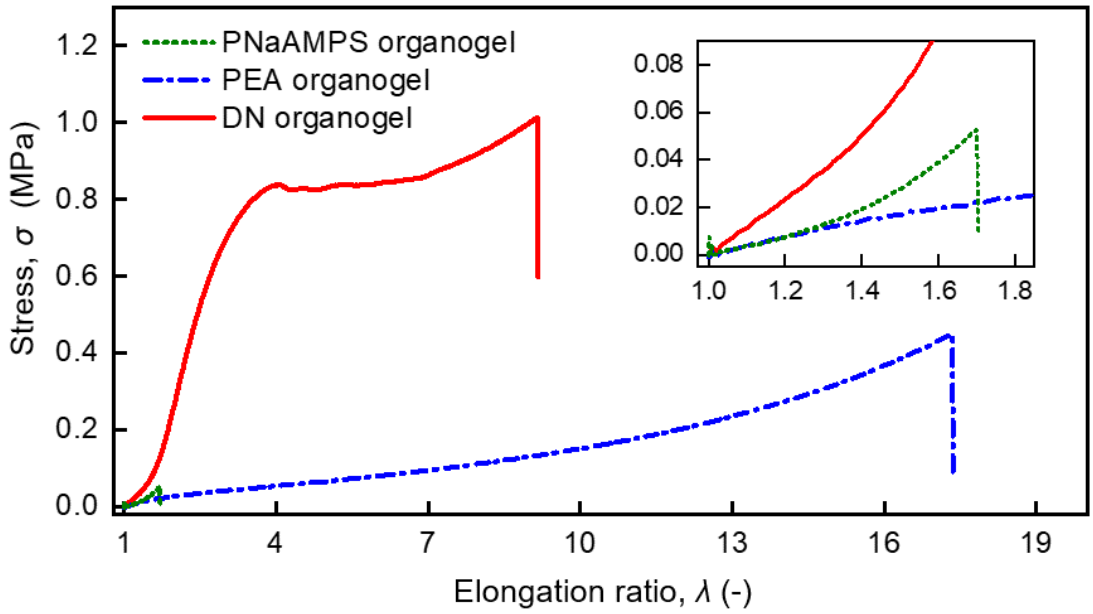

Figure 7-11. Typical tensile stress–elongation ratio curves of a PNaAMPS SN, a PEA SN, and a PNaAMPS/PEA DN organogel containing NMF solvent. The PNaAMPS SN gel is swollen in an NMF solution containing 0.04 M LiCl to have the same volume fraction of PNaAMPS in the SN organogel as in the DN organogel. The DN gel and the PEA SN gel were in as-synthesized state with virtually identical volume fraction of PEA. Reprinted with permission from *Chemistry of Materials* 31, 3766–3776 (2019). Copyright 2019 American Chemical Society.

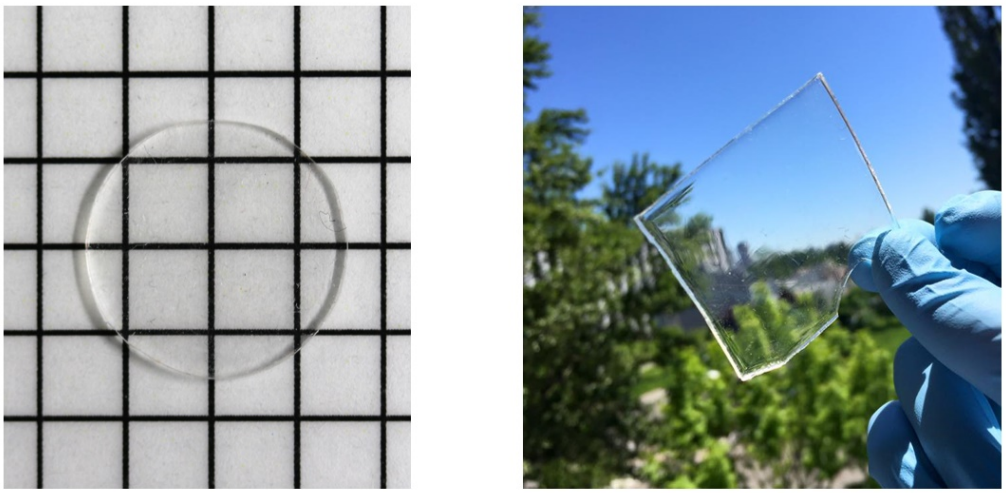

Figure 7-12. Optical images of a PNaAPMS/PEA DN elastomer after removing of NMF. Left figure is reprinted with permission from *Chemistry of Materials* 31, 3766–3776 (2019). Copyright 2019 American Chemical Society.

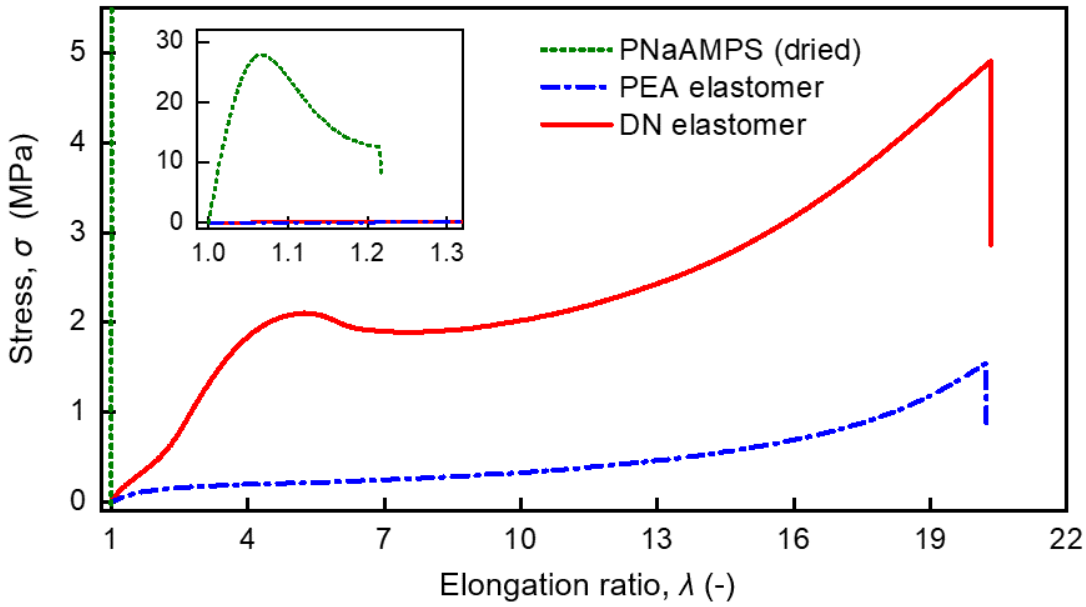

Figure 7-13. Typical tensile stress–elongation ratio curves of a solvent-free (1-3) PNaAMPS SN polymer, a PEA SN elastomer, and a DN elastomer. In the experiment depicted in this figure, the crosslinker concentration of the first network, x_1 = 3 mol%, and the monomer concentration of the second network, f_{EA} = 50 wt.%, were selected. The nominal strain rate was ~0.1 s^{-1}. Reprinted with permission from *Chemistry of Materials* 31, 3766–3776 (2019). Copyright 2019 American Chemical Society.

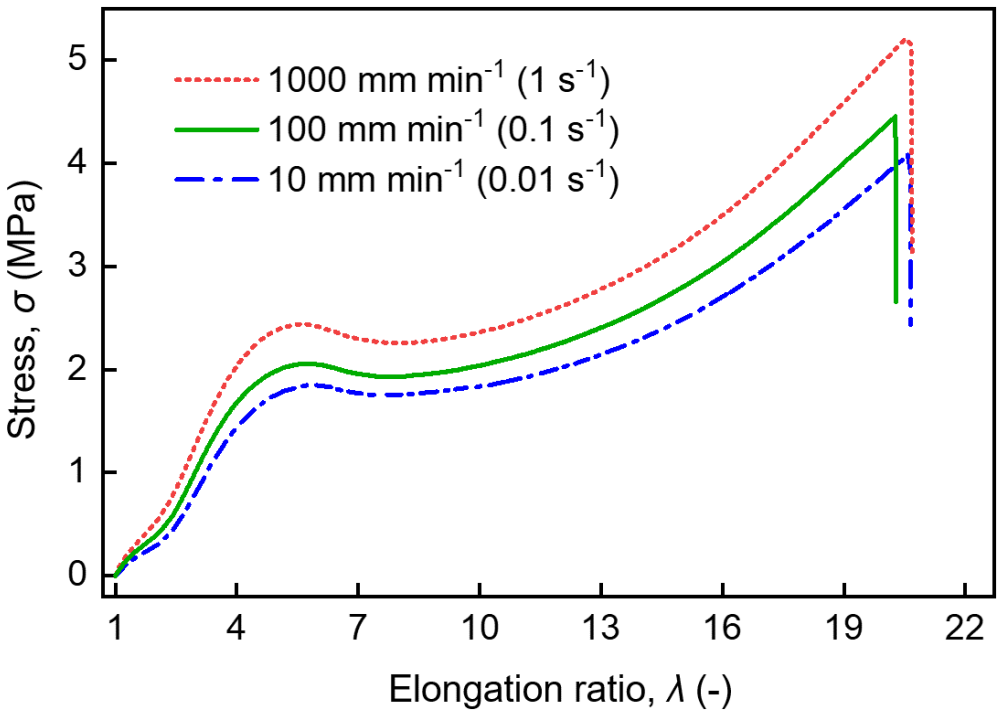

Figure 7-14. Dependence of the strain rate for the tensile stress–elongation ratio curves of a DN elastomer (x_1 = 3 mol% and f_{EA} = 50 wt.%). Reprinted with permission from *Chemistry of Materials* 31, 3766–3776 (2019). Copyright 2019 American Chemical Society.

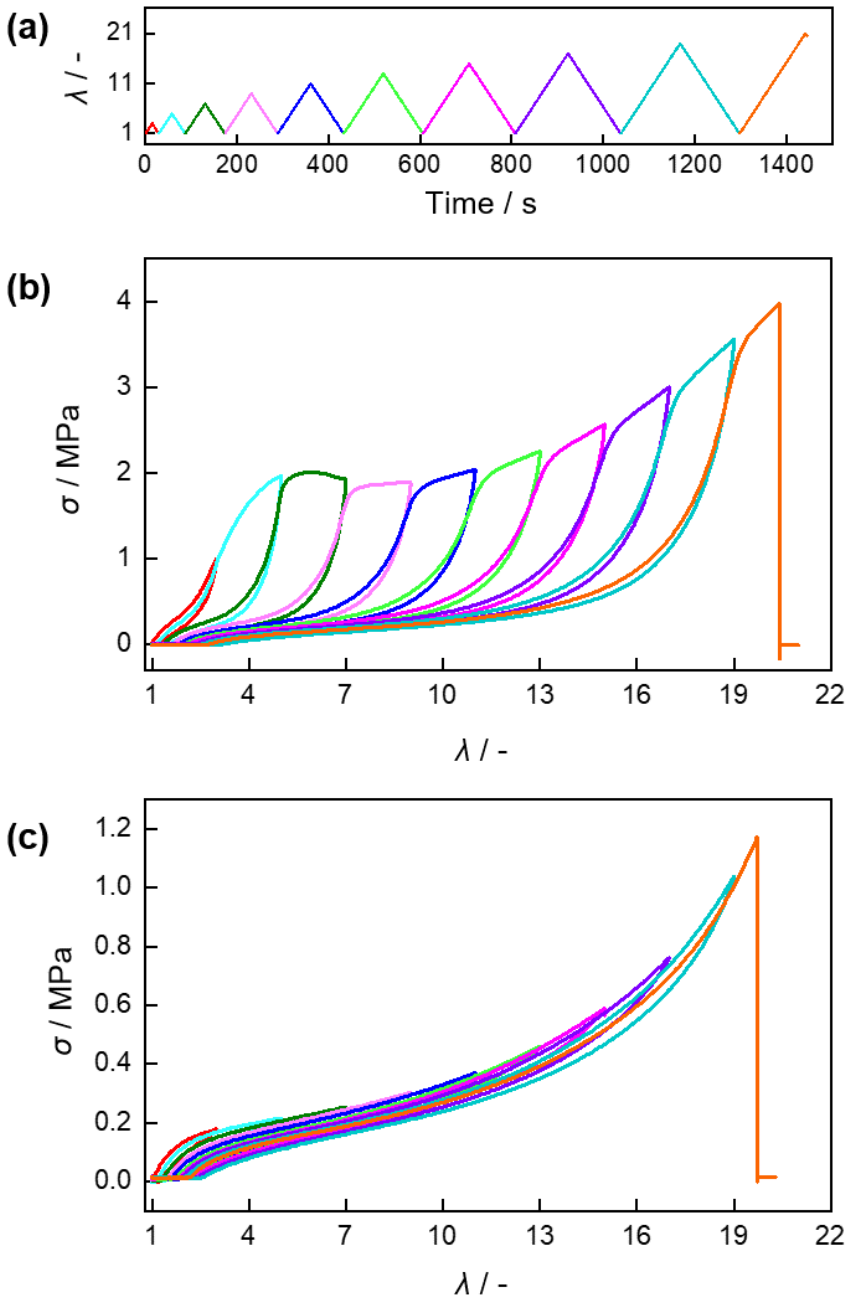

Figure 7-15. Cyclic tensile test of a DN elastomer and PEA SN elastomer. **(a)** Applied elongation ratio as a function of time at the nominal strain rate of ~0.1 s^{-1}. Cyclic tensile stress–elongation ratio curves of **(b)** a DN elastomer (x_1 = 3 mol% and f_{EA} = 50 wt.%) and **(c)** a PEA SN elastomer (f_{EA} = 50 wt.%). **(a)** and **(b)** are reprinted with permission from *Chemistry of Materials* 31, 3766–3776 (2019). Copyright 2019 American Chemical Society.

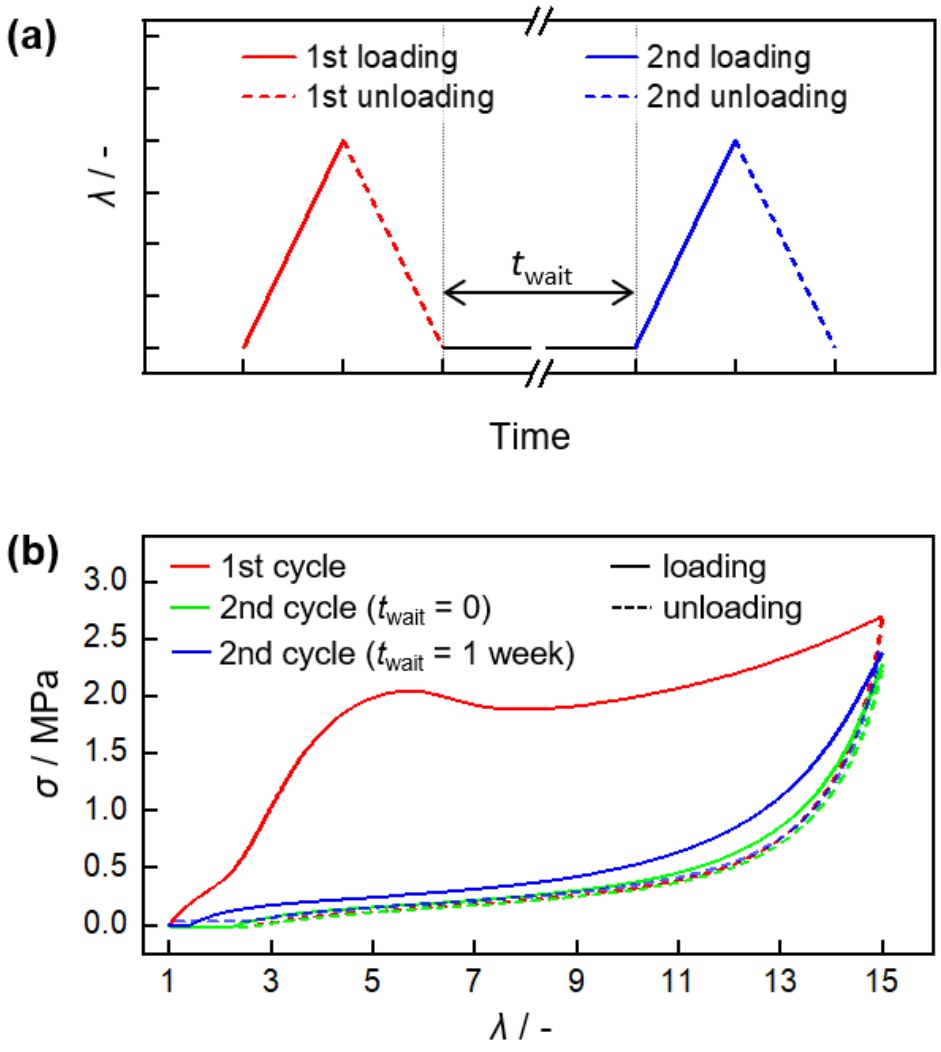

Figure 7-16. Cyclic tensile test of a DN elastomer (x_1 = 3 mol% and f_{EA} = 50 wt.%) with different waiting time.

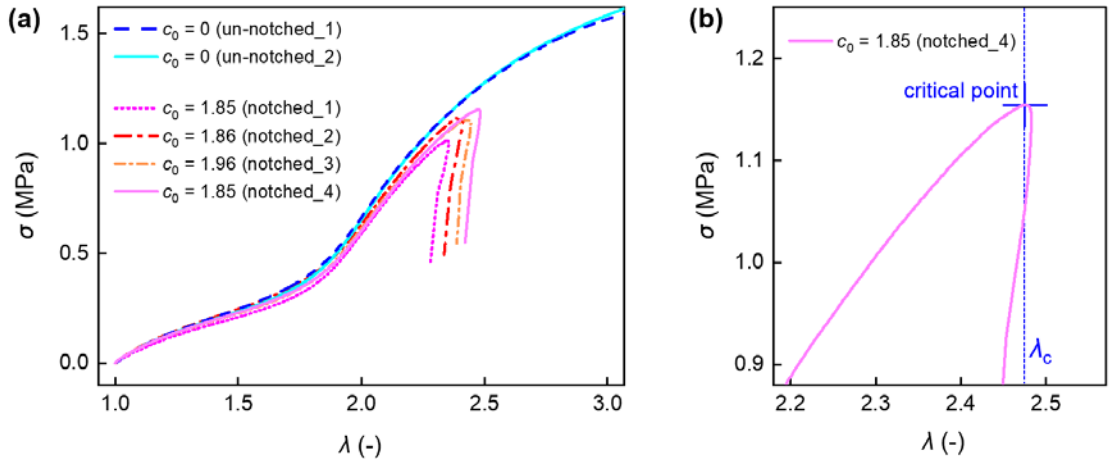

Figure 7-17. Typical result of stress–elongation ratio curves of fracture test with single-edge notched geometry. **(a)** The stress–elongation ratio curves of a DN elastomer (x_1 = 3 mol% and f_{EA} = 50 wt.%) with (number of samples n = 4) and without (n = 2) crack. The elongation ratio was measured on un-notched region of the sample by non-contacting video extensometer. **(b)** Expanded view of a typical result around critical point of the crack initiation. The deformation speed was 10 mm min^{-1}. Reprinted with permission from *Chemistry of Materials* 31, 3766–3776 (2019). Copyright 2019 American Chemical Society.

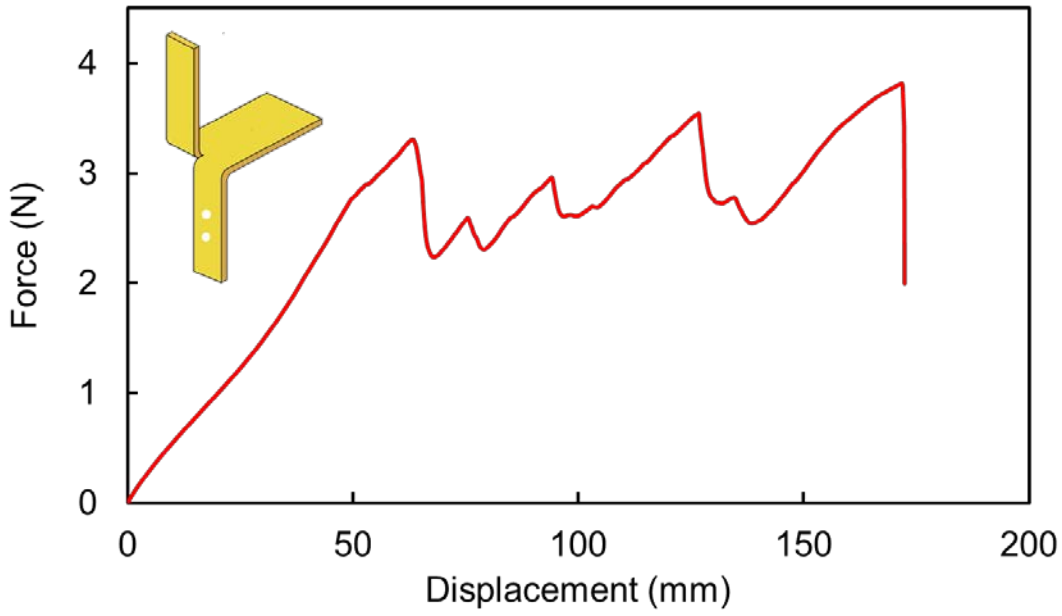

Figure 7-18. Typical force–displacement curve of the trouser-shaped tearing test of a DN elastomer (x_1 = 3 mol% and f_{EA} = 50 wt.%). The deformation speed was 100 mm min^{-1}.

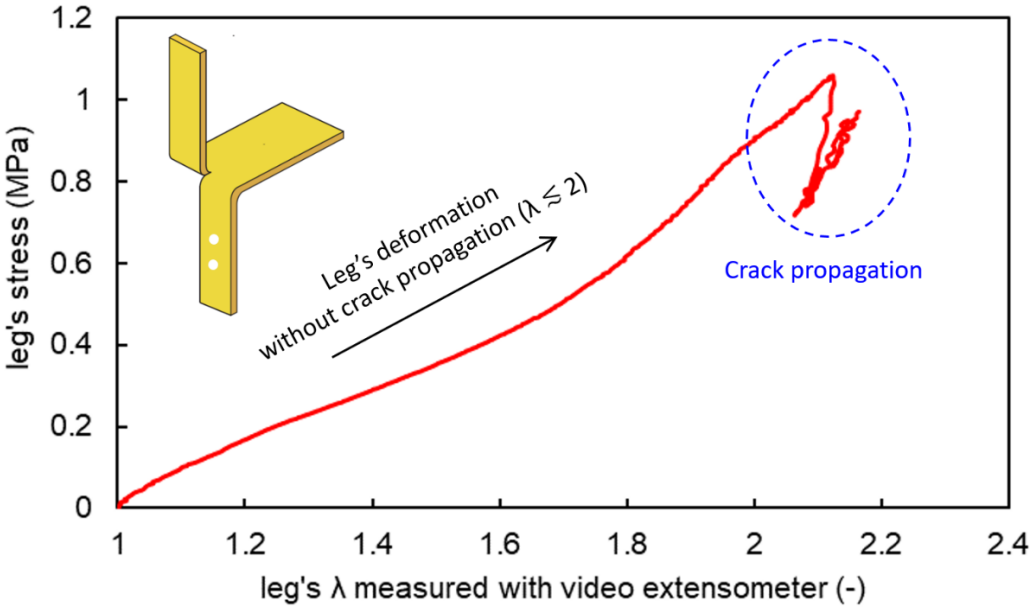

Figure 7-19. Typical stress–strain curve of the leg under the trouser-shaped tearing test of a DN elastomer (x_1 = 3 mol% and f_{EA} = 50 wt.%). The deformation speed was 100 mm min^{-1}.

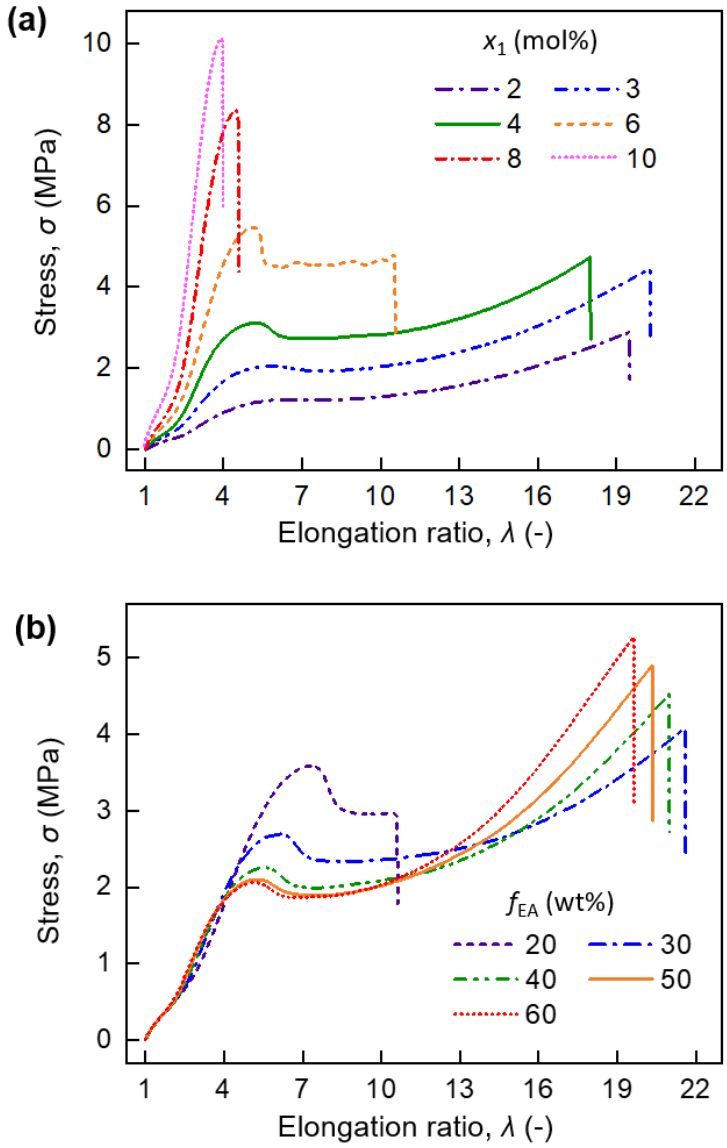

Figure 7-20. (a) Typical tensile σ–λ curves of PNaAMPS/PEA DN elastomers with various feed concentrations of crosslinker of the first network, x_1 = 2, 3, 4, 6, 8 and 10 mol%. The feed concentrations of monomer of the second network were fixed as f_{EA} = 50 wt.%. **(b)** Typical tensile σ–λ curves of PNaAMPS/PEA DN elastomers with various feed concentration of monomer of second network, f_{EA} = 20, 30, 40, 50 and 60 wt.%. The feed concentrations of crosslinker of the first network were fixed as x_1 = 3 mol%. Reprinted with permission from *Chemistry of Materials* 31, 3766–3776 (2019). Copyright 2019 American Chemical Society.

Table 7-3. Compositions and mechanical properties of the PEA SN and PNaAMPS/PEA DN elastomers. Reprinted with permission from *Chemistry of Materials* 31, 3766–3776 (2019). Copyright 2019 American Chemical Society.

	ϕ_{1st} (vol%)	ϕ_{2nd} (vol%)	ϕ_{1st}/ϕ_{2nd} (-)	E (MPa)	λ_y (-)	σ_y (MPa)	λ_b (-)	σ_b (MPa)	$\sigma_{T,b}$ (MPa)	W_b (MJ m^{-3})	G_c (kJ m^{-2})	T_c (kJ m^{-2})
PEA SN	0	100	0	0.3	-	-	20	1.4	29	9	0.8	3.4
DN2/50	2	98	0.02	0.4	5.4	1.3	19	2.8	53	28	3.4	10.2
DN3/50	3	97	0.03	0.8	5.3	2.1	21	4.8	98	46	4.7	12.0
DN4/50	4	96	0.05	1.2	5.2	3.1	18	5.1	94	52	6.4	12.7
DN6/50	7	93	0.08	2.1	4.5	5.3	13	5.0	66	48	8.1	11.0
DN8/50	10	90	0.11	5.4	4.7	8.5	5	6.6	34	21	7.5	9.8
DN10/50	12	88	0.14	10.2	-	-	4	11.5	47	20	7.2	8.4
DN3/20	7	93	0.08	0.8	7.4	3.6	10	3.0	31	21	9.0	12.0
DN3/30	5	95	0.05	0.8	6.0	2.7	20	3.7	74	45	6.1	13.6
DN3/40	4	96	0.04	0.7	5.5	2.2	20	4.3	89	45	5.3	12.7
DN3/60	3	97	0.03	0.8	5.2	2.0	17	4.0	70	35	4.0	11.0

In sample code DNx_1/f_{EA}, x_1 and f_{EA} denote the feed crosslinker concentration with respect to the monomer (mol%) of the PNaAMPS first network and the feed monomer concentration (wt.%) of the PEA second network, respectively. The resulting volume fractions of the first and second network in the DN elastomers (ϕ_{1st} and ϕ_{2nd}, respectively) and the ratio (ϕ_{1st}/ϕ_{2nd}), Young's modulus (E), elongation ratio and nominal stress at yield (λ_y and σ_y, respectively), elongation ratio, nominal stress, true stress and input energy density at break (λ_b, σ_b, $\sigma_{T,b}$ and W_b, respectively), fracture energies characterized by single-edge notched geometry (G_c) and trouser-shaped tearing (T_c) are summarized. All values except for φ_{1st}, φ_{2nd} and $\varphi_{1st}/\varphi_{2nd}$ are average values among three measurements.

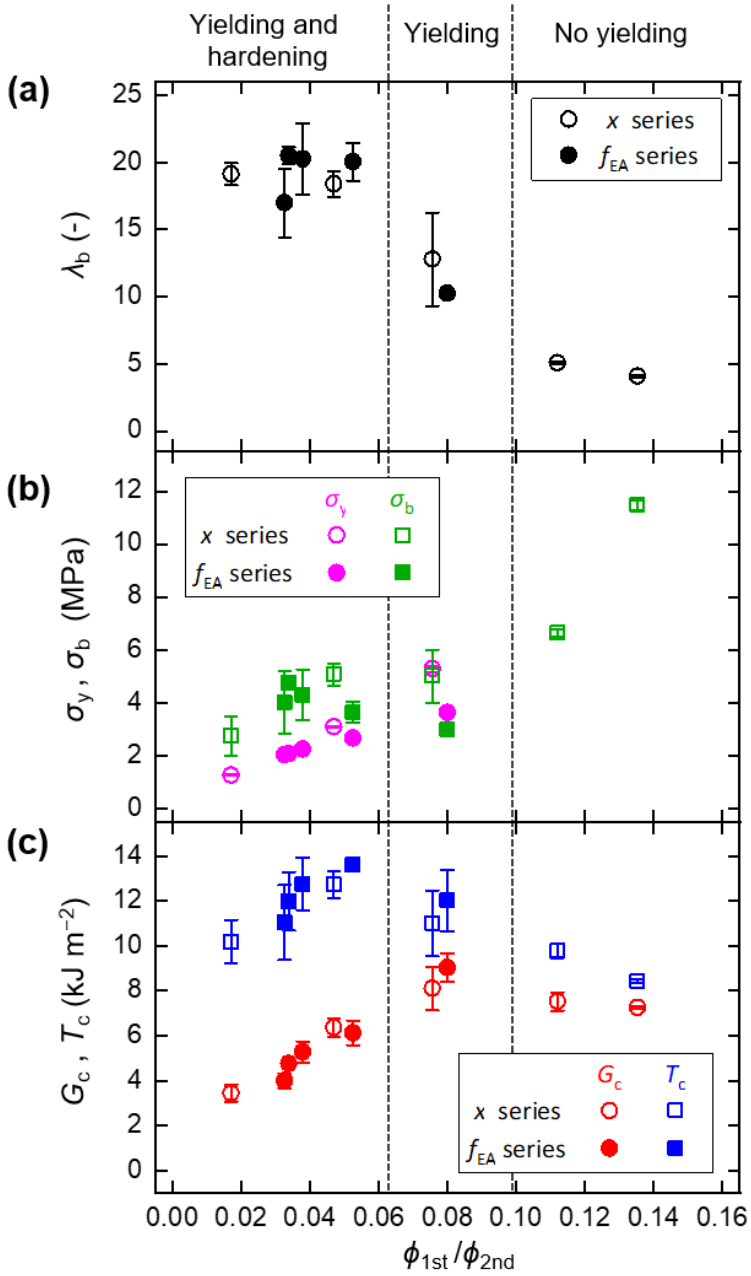

Figure 7-21. (a) Elongation ratio at break λ_b; **(b)** stresses at yield σ_y and break σ_b; **(c)** fracture energies characterized by single-edge notched geometry G_c and by trouser tearing geometry T_c of the DN elastomers as a function of the volume ratio of the first network to the second network, ϕ_{1st}/ϕ_{2nd}. The error bars are standard deviations on three measurements. Reprinted with permission from *Chemistry of Materials* 31, 3766–3776 (2019). Copyright 2019 American Chemical Society.

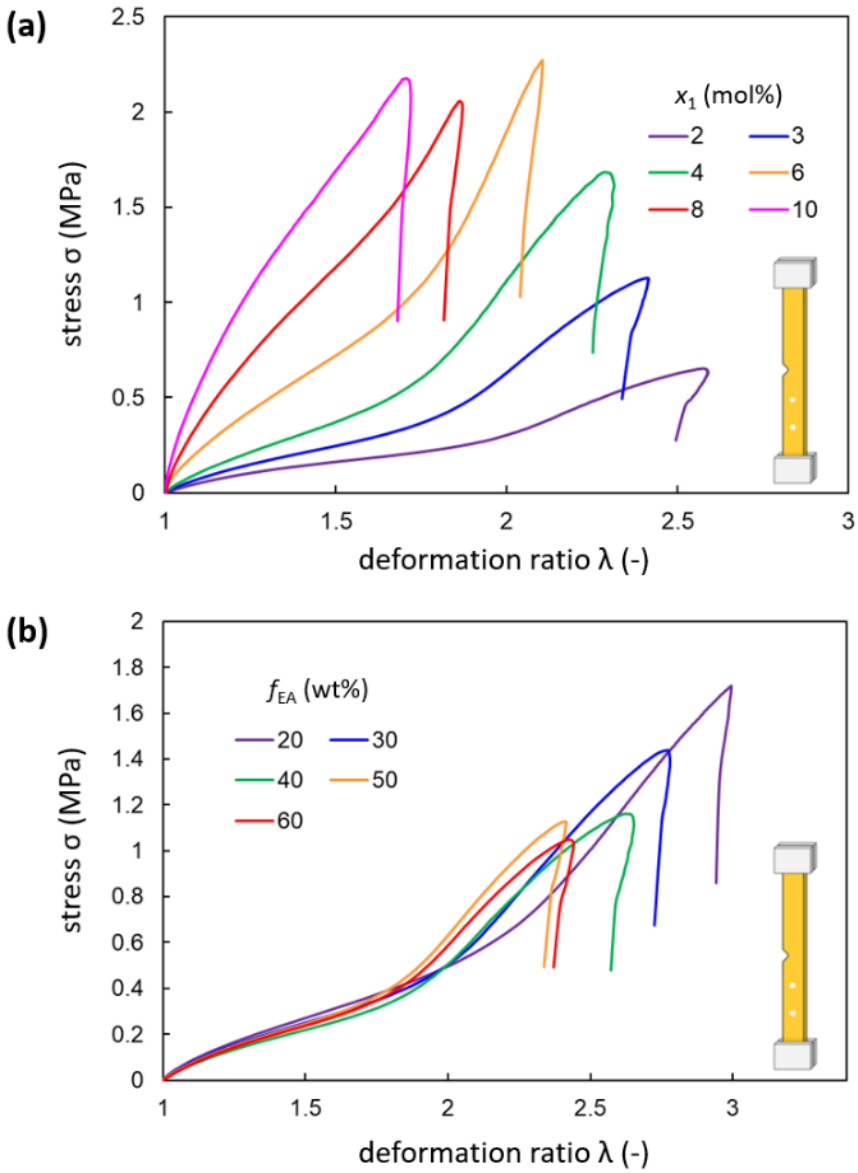

Figure 7-22. Typical stress–deformation ratio curves of un-notched region of the notched sample in the single-edge notched fracture test of the DN elastomers. **(a)** x_1 is varied as 2, 3, 4, 6, 8 and 10 mol%; and f_{EA} is fixed as 50 wt.%. **(b)** x_1 is fixed as 3 mol%; and f_{EA} is varied as 20, 30, 40, 50 and 60 wt.%. The deformation speed was 10 mm min^{-1}.

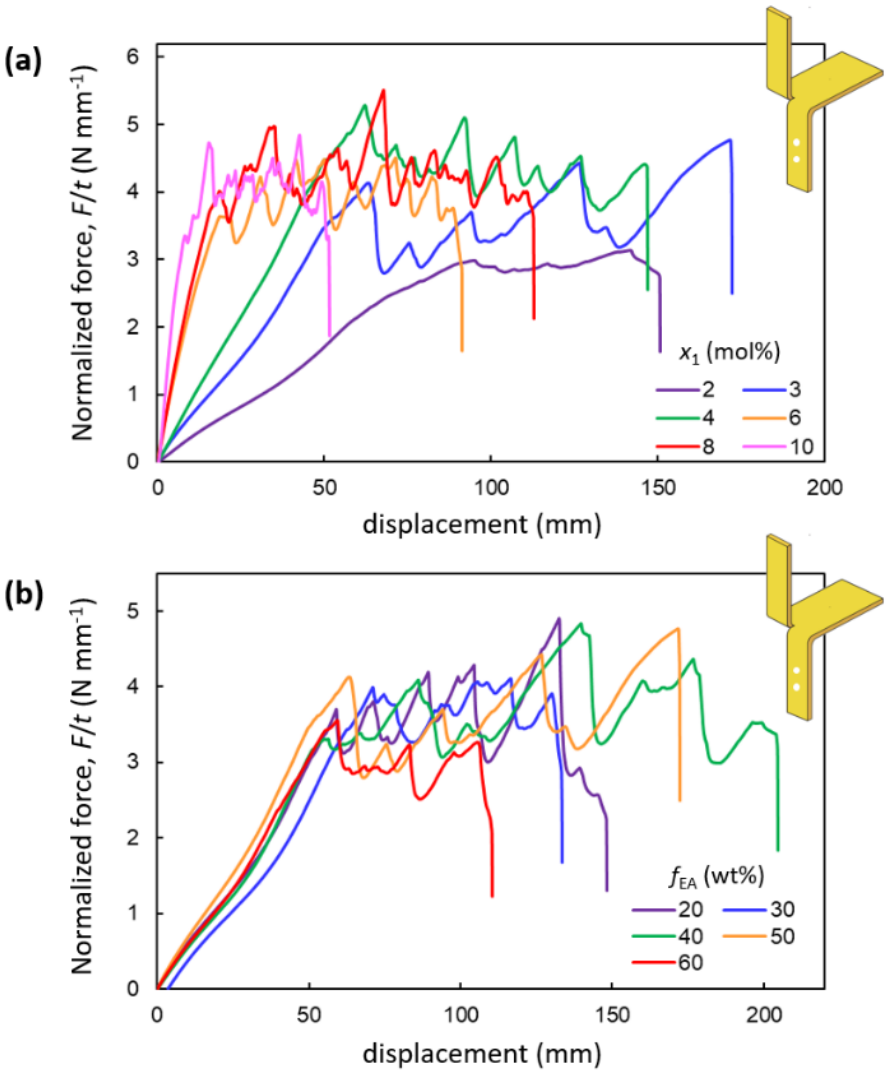

Figure 7-23. Typical normalized force–displacement curves of the trouser-shaped tearing fracture test of the DN elastomers. The force was normalized by the sample thickness. **(a)** x_1 is varied as 2, 3, 4, 6, 8 and 10 mol%; and f_{EA} is fixed as 50 wt.%. **(b)** x_1 is fixed as 3 mol%; and f_{EA} is varied as 20, 30, 40, 50 and 60 wt.%. The deformation speed was 100 mm min^{-1}.

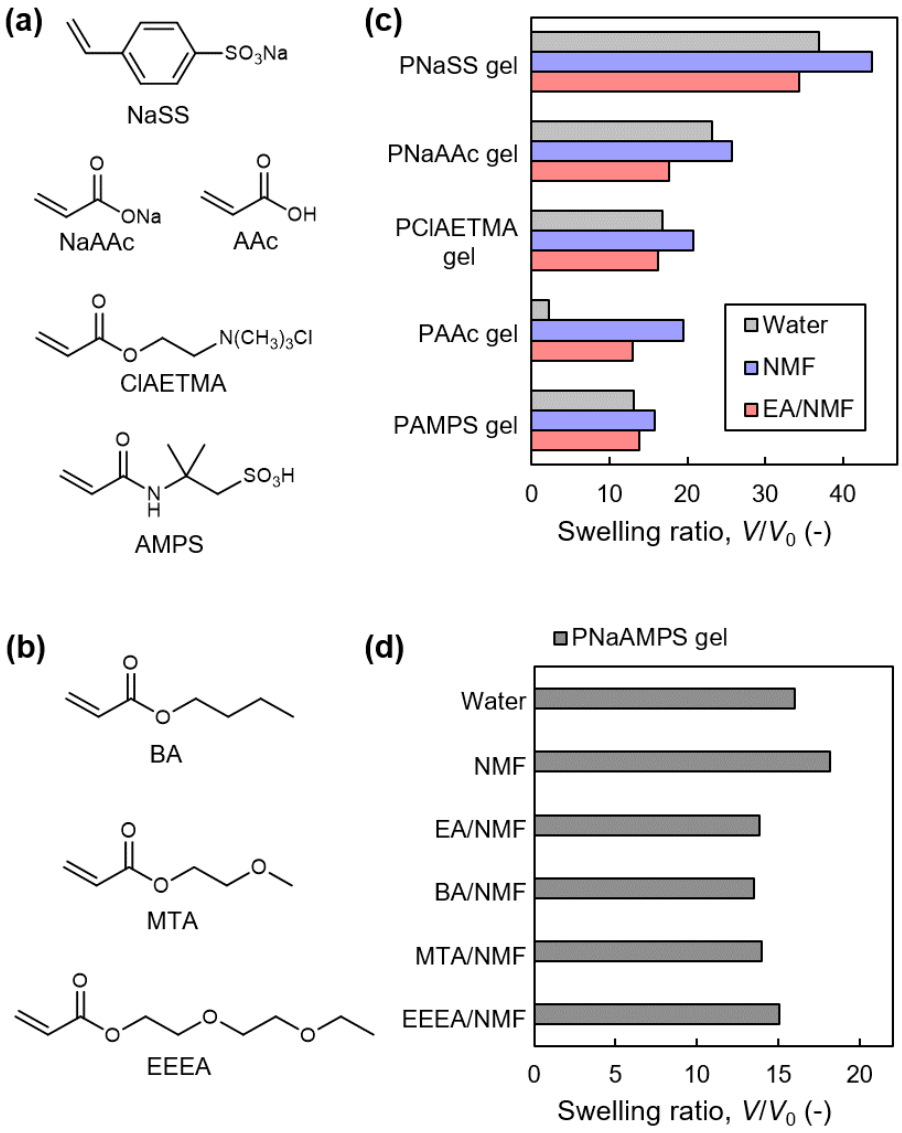

Figure 7-24. Chemical structures of monomers for **(a)** polyelectrolytes as the first networks and **(b)** elastomeric polyacrylates as the second networks. **(c)** Swelling ratio of the polyelectrolyte gels in water, NMF, and EA/NMF binary mixtures (50:50 w/w). **(d)** Swelling ratio of the PNaAMPS gels in water, NMF, and monomer/NMF binary mixtures (50:50 w/w). Reprinted with permission from *Chemistry of Materials* 31, 3766–3776 (2019). Copyright 2019 American Chemical Society.

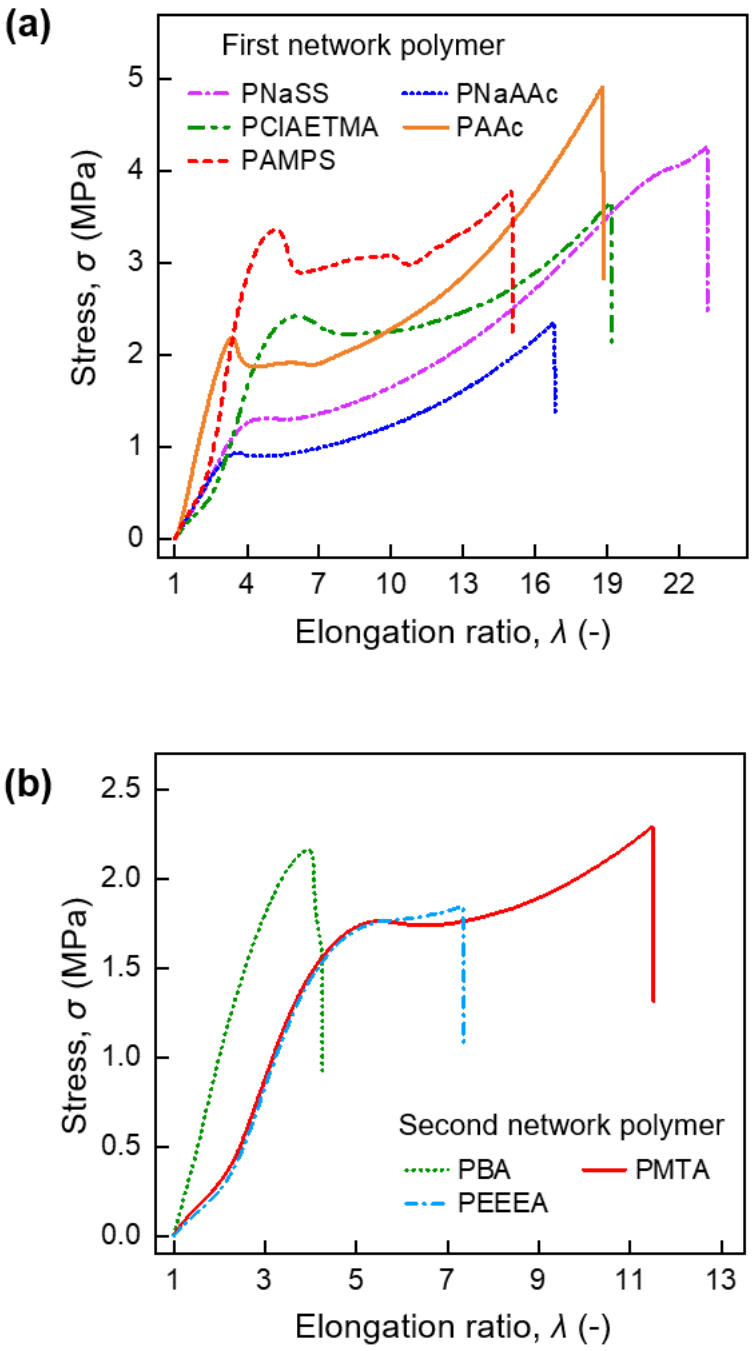

Figure 7-25. Tensile σ–λ curves of DN elastomers with various chemical structure of the networks. **(a)** DN elastomers with polyelectrolytes and PEA; and **(b)** DN elastomers with PNaAMPS and elastomeric poly-acrylates. Reprinted with permission from *Chemistry of Materials* 31, 3766–3776 (2019). Copyright 2019 American Chemical Society.

Chapter 8: General Conclusion and Outlook

Inspired by mechanoresponsive biological tissues, I developed a self-growing hydrogel that repetitively grows in size and strength in response to mechanical activation through an efficient mechanoradical polymerization. This dissertation has described the essential issues and solution to realize the self-growing property through mechanochemical transduction.

At first, I carefully considered the current stream of the materials science especially on mechanochemistry. Given the progress and difficulty on the self-strengthening materials, I focused on an essential issue on this research; that is, efficiency of the mechanochemical reaction in bulk materials. To achieve the efficient reaction, a DN gel was used for the candidate material to achieve the self-growing property because the DN gel contains a lot of solvent, and a lot of polymer strands are fractured during the deformation of the gel, suggesting plenty of mechanoradicals are generated in the gel.

To confirm the mechanoradical generation, Ferrous ion oxidation triggered by mechanoradicals is performed. An explicit result was found: ~10^{-5} M (≈10^{22} m^{-3}) of mechanoradicals are generated in the stretched DN gel, which is 10 times or more higher than conventional SN hydrogels. I also found that approximately 10% of the first network strands may be broken when a DN gel was largely stretched.

Because plenty of mechanoradicals are indeed generated in the DN gels, highly efficient mechanoradical polymerization can be performed in the DN gels fed with monomer. Once large amount of crosslinker was added as well as monomer, distinct self-stiffening and self-strengthening induced by mechanical stress were achieved, for example, modulus was 23 times increased by the stretching. Furthermore, when the

monomer was continuously supplied to the DN gels, the gel showed repetitive growing phenomena in size and strength. In addition, as exemplified by stress induced NIPAAm polymerization at local position, diverse functions can be imparted on demand by applying programmed mechanical stimuli when appropriate functional monomer was supplied.

To expand the concept found above, I have created a DN elastomer composed of polyelectrolyte first network and rubbery hydrophobic second network without solvent. Even though it does not contain solvent, the large amount of internal fracture was observed on the mechanical testing, which will enable self-strengthening/growing property using mechanoradicals.

The advantage of using the DN gel would be not limited for the mechanoradical generator, but many types of rupture-triggered mechanochemical transduction with various polymer mechanochemistry may be also applied to the DN gels for diverse force-initiated or -catalyzed reactions. Even though oxygen typically inhibits a radical polymerization, such mechanocatalyzed/initiated polymerizations or using oxygen tolerant technologies will enables widespread applications. This concept could be applied to develop novel damage- and fatigue-tolerant structural materials that evolve spontaneously to adapt to their local mechanical environments or strengthen selectively at highly stressed regions. New functions, such as spatially programmed temperature and/or pH tunability, redox capacity, electrical conductivity, and biological affinity, could be gained with the application of mechanical stimuli during use or fabrication. To apply such self-growing DN systems for practical use, the reactant supply should be designed in more sophisticated ways. For example, a DN gel with vascular-like microfluidic

channels would enable the supply of monomers to desired locations at required times on demand. Such materials have potential applications and implementations in various fields, such as intelligent soft robots that are not only robust but also grow to acquire specific strength, functions and shape to adapt to biased mechanical stimuli or in response to educational mechanical training.

This dissertation has opened a brand-new concept of a material that *actively* uses the mechanical force to adapt, strengthen and grow itself. I believe such new material concept will positively change our lives.

List of Publications

Original papers related to doctoral dissertation

1. Takahiro Matsuda, Runa Kawakami, Ryo Namba, Tasuku Nakajima, and Jian Ping Gong, “Mechanoresponsive Self-growing Hydrogels Inspired by Muscle Training.” *Science* **363,** 504–508 (2019).

2. Takahiro Matsuda, Tasuku Nakajima, and Jian Ping Gong, “Fabrication of Tough and Stretchable Hybrid Double-Network Elastomers Using Ionic Dissociation of Polyelectrolyte in Nonaqueous Media.” *Chemistry of Materials* **31,** 3766–3776 (2019).

Other original papers

3. Takahiro Matsuda, Tasuku Nakajima, Yuki Fukuda, Wei Hong, Takamasa Sakai, Takayuki Kurokawa, Ung-il Chung, and Jian Ping Gong, “Yielding Criteria of Double Network Hydrogels.” *Macromolecules* **49,** 1865–1872 (2016).

4. Thanh-Tam Mai, Takahiro Matsuda, Tasuku Nakajima, Jian Ping Gong, and Kenji Urayama, “Distinctive Characteristics of Internal Fracture in Tough Double Network Hydrogels Revealed by Various Modes of Stretching.” *Macromolecules* **51,** 5245–5257 (2018).

5. Ken-ichi Hoshino, Tasuku Nakajima, Takahiro Matsuda, Takamasa Sakai, and Jian Ping Gong, “Network Elasticity of a Model Hydrogel as a Function of Swelling

Ratio: from Shrinking to Extreme Swelling States." *Soft Matter* **14,** 9693–9701 (2018).

6. Thanh-Tam Mai, Takahiro Matsuda, Tasuku Nakajima, Jian Ping Gong, and Kenji Urayama, "Damage Cross-effect and Anisotropy in Tough Double Network Hydrogels Revealed by Biaxial Stretching." *Soft Matter* **15,** 3719–3732 (2019).

7. Joji Murai, Tasuku Nakajima, Takahiro Matsuda, Katsuhiko Tsunoda, Takayuki Nonoyama, Takayuki Kurokawa, and Jian Ping Gong, "Tough Double Network Elastomers Reinforced by the Amorphous Cellulose Network." *Polymer* **178,** 121686 (2019).

8. Honglei Guo, Wei Hong, Takayuki Kurokawa, Takahiro Matsuda, Zi Liang Wu, Tasuku Nakajima, Masakazu Takahata, Taolin Sun, Ping Rao, and Jian Ping Gong, "Internal Damage Evolution in Double-Network Hydrogels Studied by Microelectrode Technique." *Macromolecules* **52,** 7114–7122 (2019).

9. Tasuku Nakajima, Yuhei Ozaki, Ryo Namba, Kuim Ota, Yuki Maida, Takahiro Matsuda, Takayuki Kurokawa, and Jian Ping Gong, "Tough Double-Network Gels and Elastomers from the Nonprestretched First Network." *ACS Macro Letters* **8,** 1407–1412 (2019).

Other written works

10. 松田昂大、中島祐、龔剣萍：「鍛えて成長するゲル ―破壊による創造の材料

科学一 」*現代化学 (Chemistry Today)*、2019 年 8 月号, No. 581, pp. 53–57 (2019).

11. 松田昂大：「「鍛えて成長する材料」：力で共有結合を切断するとどうなる？そしてどう使う？」 *Chem-Station*, 1st March 2019, https://www.chem-station.com/blog/2019/02/mself-growinghydrogels.html

Presentations in conferences related to doctoral dissertation

1. ○Takahiro Matsuda, Tasuku Nakajima, Takayuki Nonoyama, Takayuki Kurokawa, Jian Ping Gong, “Fracture Induced Mechanochemical Reactions in Double Network Hydrogels.” IUPAC 11th International Conference on Advanced Polymers via Macromolecular Engineering (APME2015), Yokohama (Japan), October 18–22, 2015 (Poster).

2. ○Takahiro Matsuda, Tasuku Nakajima, Jian Ping Gong, “Mechanochemical Reactions in Double Network Hydrogels Induced by Polymer Chain Scission” The First International Symposium on Advanced Soft Matter, Sapporo (Japan), June 13–15, 2016 (Poster).

3. ○Takahiro Matsuda, Runa Kawakami, Tasuku Nakajima, Takayuki Kurokawa, Takayuki Nonoyama, Jian Ping Gong「高分子鎖破断が誘起する化学反応：ダブルネットワークゲルの内部破壊の可視・定量化」平成 28 年度未踏科学サマー道場, Kashiwa (Japan), August 18, 2016 (Poster).

4. ○Takahiro Matsuda, Tasuku Nakajima, Takayuki Kurokawa, Jian Ping Gong「高分子鎖破断が誘起するメカノケミカル反応－ダブルネットワークゲルの新展開－」第 51 回高分子学会北海道支部研究発表会, Sapporo (Japan), January 19, 2017 (Poster).

5. ○Takahiro Matsuda, Tasuku Nakajima, Takayuki Kurokawa, Jian Ping Gong, “Mechanical Stress Triggers Productive Mechanochemical Reactions in Double Network gels.” GelSympo2017, Chiba (Japan), March 6–9, 2017 (Poster).

6. ○Takahiro Matsuda, Runa Kawakami, Ryo Namba, Tasuku Nakajima, Takayuki Kurokawa, Jian Ping Gong, “Mechanoradical-Triggered Productive Mechanochemical Reactions in Double Network Gels.” Gordon Research Seminar on the Science of Adhesion, South Hadley (MA, USA) July 22–23, 2017 (Poster).

7. ○Takahiro Matsuda, Runa Kawakami, Ryo Namba, Tasuku Nakajima, Takayuki Kurokawa, Jian Ping Gong, “Mechanoradical-Triggered Productive Mechanochemical Reactions in Double Network Gels.” Gordon Research Conference on the Science of Adhesion, South Hadley (MA, USA) July 23–28, 2017 (Poster).

8. ○Takahiro Matsuda, Runa Kawakami, Ryo Namba, Tasuku Nakajima, Jian Ping Gong,「高分子鎖破断が誘起する化学反応：ダブルネットワークゲルの新展

開」第 66 回高分子討論会, Matsuyama (Japan), September 21, 2017 (Poster).

9. ○Takahiro Matsuda, Runa Kawakami, Ryo Namba, Tasuku Nakajima, Jian Ping Gong,「ＤＮゲルの高分子鎖破断が誘起する化学反応」ゲルワークショップイン松山, Matsuyama (Japan), September 22, 2017 (Poster).

10. ○Takahiro Matsuda, Runa Kawakami, Ryo Namba, Tasuku Nakajima, Jian Ping Gong,「力学刺激が誘起する DN ゲルの機能転換：内部破壊が鍵となる高分子鎖破断ラジカルの活用」第 29 回高分子ゲル研究討論会, Tokyo (Japan), January 11–12, 2018 (Oral).

11. ○Takahiro Matsuda, Runa Kawakami, Ryo Namba, Tasuku Nakajima, Jian Ping Gong, “Mechano-induced network remodeling of a hydrogel via mechanoradical polymerization.” The 2nd Conference on Multiscale Mechanochemistry and Mechanobiology (MechanoChemBio2019), Montreal (Canada), July 29–31, 2019 (Poster).

12. ○Takahiro Matsuda, Tasuku Nakajima, Jian Ping Gong, 「高分子電解質ゲルの高膨潤を利用した強靭・高伸長性ＤＮエラストマーの創製と力学物性評価」第 68 回高分子討論会, Fukui (Japan), September 25–27, 2019 (Poster).

Presentations in conferences (others)

13. ○Takahiro Matsuda, Tasuku Nakajima, Takayuki Kuroakwa, Takayuki Nonoyama, Takamasa Sakai, Ung-il Chung, Jian Ping Gong,「ダブルネットワークゲルの降伏メカニズムの解明」第 64 回高分子学会年次大会, Sapporo (Japan), May 27–29, 2015 (Poster).

14. ○Takahiro Masuda, Tatiana B. Kouznetsova, Tasuku Nakajima, Takamasa Sakai, Takayuki Kurokawa, Steven L. Craig, Jian Ping Gong, 「ダブルネットワークゲルの力学挙動から読み解く高分子鎖の極限伸長特性」第 65 回高分子討論会, Yokohama (Japan), September 14, 2016 (Oral).

15. ○Takahiro Masuda, Tasuku Nakajima, Takamasa Sakai, Takayuki Kurokawa, Jian Ping Gong,「ＤＮゲルの降伏メカニズムの解明」ゲルワークショップインお台場, Tokyo (Japan), September 17, 2016 (Poster).

16. ○Takahiro Matsuda, Luna Kawakami, Tasuku Nakajima, Takayuki Kurokawa, Takayuki Nonoyama, Jian Ping Gong, “Visualization of the Internal Fracture around the Crack Tip of Tough Double Network Hydrogels.” International Rubber Conference (IRC2016), Kitakyushu (Japan), October 24–28, 2016 (Oral).

17. ○Takahiro Matsuda, Tatiana B. Kouznetsova, Tasuku Nakajima, Takamasa Sakai, Takayuki Kurokawa, Stephen L. Craig, Jian Ping Gong “Extracting Mechanical

Properties of Fully-Extended Polymer Chains from DN Gels.” APS March Meeting 2017, New Orleans (LA, USA), March 16, 2017 (Oral).

18. ○Takahiro Matsuda, Tatiana B. Kouznetsova, Tasuku Nakajima, Takamasa Sakai, Takayuki Kurokawa, Stephen L. Craig, Jian Ping Gong “Mechanical Fingerprint of Fully-Stretched Polymer Chains: From Tough DN gels to Single Molecular Chain.” International Symposium on Advanced Soft Matter, Sapporo (Japan), August 7–8, 2017 (Poster).

Presentations in conferences related to doctoral dissertation (presented by co-authors)

19. Takahiro Matsuda, ○Tasuku Nakajima, Ryo Namba, Jian Ping Gong, 「変形誘起ラジカル重合による「鍛えると強くなる」ダブルネットワークゲルの創製」第 67 回高分子討論会, Sapporo, September 12, 2018 (Oral).

20. Takahiro Matsuda, Ryo Namba, Tasuku Nakajima, ○Jian Ping Gong, “Self-growing double network hydrogels by repetitive mechanical training.” 6th International Symposium Frontiers in Polymer Science, Budapest (Hungary), May 8, 2019 (Plenary Lecture).

21. Takahiro Matsuda, ○Tasuku Nakajima, Ryo Namba, Jian Ping Gong, 「筋肉のように力学負荷によって成長するダブルネットワークゲルの創製」第 68 回高分

子学会年次大会、Osaka (Japan), May 30, 2019 (Oral).

22. Takahiro Matsuda, Ryo Namba, Tasuku Nakajima, ○Jian Ping Gong, “Self-growing hydrogels by repetitive mechanical training.” The 3rd International Symposium for Advanced Gel Materials & Soft Matters, Xi'an (China), June 14–17, 2019 (Invited Lecture).

Presentations in conferences (other reports contributed as a co-author)

Fifty-one presentations made by Tasuku Nakajima, Ken-ichi Hoshino, Runa Kawakami, Ryo Namba, Yukiko Takahashi, Tomoko Yamazaki, Chika Imaoka, Shotaro Namiki, Zheng Yong, Tsutomu Indei, Zhang Ye, Akira Tanaka, Hiroki Koike, or Chengtao Yu (detail descriptions are not shown here).

Acknowledgement

This research on this dissertation has been carried out in the Laboratory of Soft and Wet Matter (LSW), Graduate School of Life Science, Hokkaido University, Japan, supervised by Professor Jian Ping Gong. Associate examiners are Professor Takayuki Kurokawa, Professor Tamiki Komatsuzaki and Associated Professor Tasuku Nakajima.

I greatly appreciate the excellent and warmful support of my respected supervisors Professor Jian Ping Gong and Associated Professor Tasuku Nakajima. Through a lot of discussions with them, I could construct the ground-breaking concept of this research. These professors also prompted and supported my fighting spirit for conducting experiments and writing papers through many years.

As well as the supervisors, I am grateful to Runa Kawakami and Ryo Namba who were the junior students and are the key collaborators of my research. Discussions and trial-and-error processes with them, their ideas and results helped me a lot to understand the fundamentals of the mechanochemistry of DN gels and to conceive the idea of self-growing DN system, all of which pushed me to the higher level.

I would like to thank Professor Kurokawa Takayuki, Assistant Professors Takayuki Nonoyama, Daniel Rudolf King and Tao Lin Sun, who all are excellent professors in our laboratory “LSW”, for their scientific comments, research life advices and improving my English. Other many members in LSW, more than a hundred people including alumni and secretaries (Ms. Hasegawa, Ms. Okubo and Ms. Kato), also supported me a lot to work on, devote and advance my project and research/daily life.

During my Ph.D., I had fruitful research experiences with many professors and researchers. I also would like to express my thanks to Professor Stephen L. Craig in Duke

University for accepting my internship and supervising me in Duke in which I learned a lot about mechanochemistry, which helped me to construct this research; Professor Takamasa Sakai in Tokyo University for his kind help through any discussions and chats. I also thank Professor Okazaki Susumu and Assistant Professor Kazushi Fujimoto in Nagoya University for giving me a research experience on computational chemistry; Dr. Markus Bulters and Dr. Robert Janssen in DSM for giving me a fantastic internship experience in the Netherlands; Professor Kenji Urayama in Kyoto Institute of Technology, with whom I contributed papers, for constructive discussions.

I thank Fujifilm, Toagosei, MT AquaPolymer and Osaka Organic Chemical Industry for providing chemical materials. I especially thank Mr. Atsushi Sugasaki, Mr. Tatsuya Susuki and Ms. Hatsune Sakata of Fujifilm Corporation for arrangement to provide new water-soluble crosslinkers and having discussions.

This research was partially funded by JSPS KAKENHI Grant JP17H06144 as my Research Fellowship for Young Scientists. I appreciate the financial support.

Finally, I wish to express my special thanks to my late father, my mother and my sister for their love, support and encouragement. This dissertation is dedicated to them.

Takahiro Matsuda

22nd November 2019